

Oxidative Ring-Opening of Aromatics

by

Natalia Montoya Sanchez

A thesis submitted in partial fulfillment of the requirements for the degree of

Doctor of Philosophy

in

Chemical Engineering

Department of Chemical and Materials Engineering

University of Alberta

Abstract

The increased production of heavy and extra-heavy oils has changed the quality of the feedstocks processed in refineries. Conversion of heavier aromatic-rich materials using traditional upgrading technologies is possible but modifications are needed. There is a growing interest from industry and academia to develop new approaches to deal with the upgrading of heavier oils. The objective of this work was to explore a new conversion strategy: oxidative ring-opening of multinuclear aromatics.

The oxidative ring-opening strategy refers to the oxidation of multinuclear aromatics using oxygen (in air) as oxidant to produce ring-opened hydrocarbons products that do not contain oxygen. This concept involves three steps: *(i)* oxidation of multinuclear aromatics to produce quinonoids, *(ii)* further oxidation and ring-opening to produce aromatic carboxylic acid species, and *(iii)* decarboxylation of aromatic carboxylic acids to yield the ring-opened product. Ultimately, the structure of the multinuclear aromatic feed is simplified and the H:C ratio of the product increased. The conversion chemistry of the individual steps was investigated.

The oxidation chemistry of atoms that are part of an aromatic ring using air as oxidant was reviewed. Emphasis was placed on reactions leading to selective cleavage of C–C bonds as well as on competing non-selective oxidation reactions. The application of the Clar-formalism to multinuclear aromatics guided the discussion of fundamental aspects of aromatic oxidation. The need to adopt a catalytic approach for the oxidative ring-opening of multinuclear aromatics became evident.

Patent literature dealing with air oxidation of heavy feedstocks was also reviewed. Claims stating that the non-catalytic low-temperature oxidation of asphaltenes is able to produce liquid products of petrochemical value were found; their validity was questioned and explored in a concise experimental study. Under all conditions studied, little asphaltenes oxidative degradation was observed. No increase in the yield of the maltenes fraction took place. These observations were consistent with expectations based on free radical oxidation fundamentals.

The oxidation of multinuclear aromatic model compounds over metal oxide catalysts was studied. Liquid-phase autoxidation and catalytic oxidation of anthracene and 9,10-anthraquinone in the presence of V_2O_5 , MoO_3 , Fe_2O_3 , and NiO were conducted. It was confirmed that catalytic oxidation of both compounds took place by transfer of lattice oxygen from V_2O_5 and that catalytic oxidation led to ring-opening. The contribution of thermal cracking and the competition of ring-opening and ring-closing reactions affected the selectivity towards ring-opened products.

Effective removal of the carboxylic acid functionality, rejecting the carbon as CO_2 , is necessary to produce ring-opened hydrocarbons. Thermal decomposition of aromatic carboxylic acids produced by the oxidative ring-opening of multinuclear aromatics was studied in order to understand how to manipulate the reaction selectivity. Analysis of the reaction network showed that ketonization and dehydration, i.e., undesirable ring-closing reactions, competed with decarboxylation. Two strategies to limit the contribution of the ring-closing reactions were suggested: (i) carboxylic acid decomposition using a catalyst that favors decarboxylation to produce CO_2 , and (ii) decomposition in the presence of water to suppress reactions involving dehydration.

Catalytic decomposition of aromatic carboxylic acids was studied using metal carboxylates as catalytic surrogates. The study of zinc biphenyl carboxylates demonstrated the potential selectivity benefit of catalytic decomposition over thermal decomposition. It also highlighted possible changes in the temperature and chemistry of decomposition depending on the metal used to facilitate the decarboxylation reaction. Selected alkali, alkaline earth, and transition metals were investigated. The base knowledge for the catalytic behavior of specific metals was expanded (empirical contribution). The need for a systematic approach to predict which materials are suitable for carboxylic acid decarboxylation became evident.

Decomposition of aromatic carboxylic acids in the presence of water was investigated. Production of ring-opened products was favored indicating the beneficial effect of water on the reaction selectivity. The latter was found to be sensitive to the mass transport of water. For the overall oxidative ring-opening process, this finding emphasized that the success of the strategy relies not only on the conversion chemistry but also on the reaction engineering.

The critical review of the literature on aromatic oxidation in combination with experimental work on the oxidation of multinuclear aromatics and the decarboxylation of aromatic carboxylic acids contributed to the advancement of the oxidative ring-opening concept.

Keywords: Aromatic oxidation, asphaltene oxidation, metal oxide catalysis, carboxylic acid decomposition, decarboxylation, metal carboxylates, multinuclear aromatic ring-opening.

Preface

(Mandatory due to collaborative work)

Chapter 2 of this thesis was accepted for publication in *Applied Petrochemical Research* as “Montoya Sánchez, N.; De Klerk, A. Autoxidation of Aromatics: A Review”. I was responsible for concept formation, data collection and interpretation as well as manuscript composition; I was also the corresponding author. Arno de Klerk acted as the supervisory author and was involved in the concept formation, data interpretation and manuscript composition.

Chapter 3 of this thesis was published as “Montoya Sánchez, N.; De Klerk, A. Low-temperature oxidative asphaltenes liquefaction for petrochemicals: fact or fiction? *Appl. Petrochem. Res.* **2016**, 6, 97-106”. I was responsible for concept formation, experimental design, data collection and analysis as well as manuscript composition; I was also the corresponding author. Dominic Lung Ming Lim and Jui Hua Tan assisted with data collection and initial interpretation. They conducted their term projects for CME 458 - Special Project Course, under my guidance. Arno de Klerk acted as the supervisory author and was involved in the concept formation, data interpretation and manuscript composition.

Chapter 4 of this thesis was published as “Montoya Sánchez, N.; De Klerk, A. Oxidative ring-opening over metal oxides. *Prepr. Pap.-Am. Chem. Soc., Div. Energy Fuels* **2014**, 59(2), 558-561”. I was responsible for concept formation, experimental design, data collection and analysis as well as manuscript composition. I was also responsible for presenting this paper at the conference. Arno de Klerk acted as the supervisory author and was involved in the concept formation, data interpretation and manuscript composition.

Chapter 5 of this thesis was published as “Montoya Sánchez, N.; De Klerk, A. Oxidative ring-opening of aromatics: Decomposition of biphenyl carboxylic acids and zinc biphenyl carboxylates. *Energy Fuels* **2015**, 29, 7910-7922”. I was responsible for concept formation, experimental design, data collection and analysis as well as manuscript composition. Arno de Klerk acted as the supervisory author and was involved in the concept formation, data interpretation and manuscript composition.

Chapter 6 of this thesis was published as “Montoya Sánchez, N.; De Klerk, A. Oxidative ring-opening of aromatics: Effect of Water on Reaction Selectivity. *Prepr. Pap.-Am. Chem. Soc., Div. Energy Fuels* **2016**, *61* (1) 489-492”. I was responsible for concept formation, experimental design, data collection and analysis as well as manuscript composition. I was also responsible for presenting this paper at the conference. Rena Feng assisted with data collection and initial interpretation. She conducted her term project for CME 458 - Special Project Course, under my guidance. Arno de Klerk acted as the supervisory author and was involved in the concept formation, data interpretation and manuscript composition.

Chapter 7 of this thesis was published as “Montoya Sánchez, N.; De Klerk, A. Oxidative ring-opening of aromatics: Thermochemistry of sodium, potassium and magnesium biphenyl carboxylates. *Thermochim. Acta* **2016**, *645*, 31-42”. I was responsible for concept formation, experimental design, data collection and analysis as well as manuscript composition; I was also the corresponding author. Javier Castillo and Nazim Nagizada assisted with data collection and initial interpretation. I was responsible for their training in laboratory techniques, e.g. infrared spectroscopy, thermal analysis, gas chromatography. Arno de Klerk acted as the supervisory author and was involved in the concept formation, data interpretation and manuscript composition.

Chapter 8 of this thesis was published as “Montoya Sánchez, N.; De Klerk, A. Oxidative ring-opening of aromatics: Thermochemistry of iron, copper and cobalt biphenyl carboxylates. *Thermochim. Acta* **2018**, *662*, 23-40”. I was responsible for concept formation, experimental design, data collection and analysis as well as manuscript composition; I was also the corresponding author. Yohana Páez and Giselle Uzcátegui assisted with data collection and initial interpretation. I was responsible for their training in laboratory techniques, e.g. infrared spectroscopy, thermal analysis, gas chromatography. Arno de Klerk acted as the supervisory author and was involved in the concept formation, data interpretation and manuscript composition.

*To Jose,
my parents, and my little sister for always believing in me.*

Acknowledgments

I want to express my sincere gratitude to my supervisor Dr. Arno de Klerk. I really appreciated your guidance, support, encouragement, and patience during these years. I enjoyed all of our conversations. Thank you for sharing with me your thoughts about science and, more importantly about life. I feel very fortunate to have had the opportunity to work with you.

I want to thank my research group friends and colleagues for your insights, your stories, your jokes and your silly comments. I am really glad I got to meet so many wonderful people. You made my time here a valuable experience. I want to especially thank Yohana for always cheering me up and for being there along the way, Lina for putting a smile in my face, especially during difficult times, and for always being willing to help me, Cloribel for all the advice and for giving me the final push when I got stuck, and Giselle for listening to me and for discussing with me when I needed it. Thank you for the support. I treasured your friendship.

I want to thank my friend Yoshi for listening to all my stories, the happy and the not so happy ones. Your phone calls always made a difference.

I want to thank my parents and my little sister for believing in me and for supporting my decisions.

I want to thank Jose for all the love, encouragement, understanding and support. Thank you for all the adventures and for being there for me. This experience would have not been the same without you.

I would also like to thank the Canadian Centre for Clean Coal/Carbon and Mineral Processing Technology (C⁵MPT) for the financial support.

CONTENTS

1. Introduction	1
1.1 Background	1
1.2 Objective	3
1.3 Scope	3
1.4 References	5
2. Autoxidation of Aromatics: A Review	7
2.1 Introduction	8
2.2 Oxidation of Aromatic Hydrocarbons	10
2.2.1 Benzene Oxidation	11
2.2.2 Naphthalene Oxidation	16
2.2.3 Anthracene and Phenanthrene Oxidation	19
2.2.4 Reactor Engineering	25
2.3 Oxidation of Heterocyclic Aromatics	28
2.3.1 Oxidation of Aromatic S-heterocyclic Compounds	30
2.3.2 Oxidation of Aromatic N-heterocyclic Compounds	34
2.3.3 Oxidation of Aromatic O-heterocyclic Compounds	37
2.4 Discussion	39
2.4.1 Reactivity of Aromatic Hydrocarbons towards Oxidation	39
2.4.2 Reactivity of Oxygen towards Heterocyclic Aromatics	45
2.4.3 Catalysis in Aromatic Oxidation	46
2.4.4 Implications for Industrial Use	48
2.5 Conclusions	50
2.6 References	52
3. Low Temperature Oxidative Asphaltenes Liquefaction for Petrochemicals: Fact or Fiction?	61
3.1 Introduction	62

3.2	Experimental Section	63
3.2.1	Materials	63
3.2.2	Procedure and Equipment.....	65
3.2.3	Analysis	66
3.3	Results.....	68
3.3.1	Low-Temperature Dry Autoxidation of Asphaltenes.....	68
3.3.2	Low-Temperature Water-Assisted Oxidation of Asphaltenes.....	73
3.4	Discussion.....	76
3.4.1	Benefits from Oxidation	76
3.4.2	Oxidation Selectivity	77
3.4.3	Heating Effects on Asphaltenes Content.....	80
3.5	Conclusions.....	81
3.6	References.....	82
4.	Oxidative Ring-Opening over Metal Oxide Catalysts	85
4.1	Introduction.....	86
4.2	Experimental Section	87
4.2.1	Materials	87
4.2.2	Equipment and Procedure.....	87
4.2.3	Analysis	88
4.3	Results and Discussion	89
4.3.1	Autoxidation of Anthracene	89
4.3.2	Catalytic Oxidation of Anthracene	91
4.3.3	Autoxidation of Anthraquinone.....	93
4.3.4	Catalytic Oxidation of Anthraquinone	94
4.3.5	Product Characterization	95
4.4	Conclusions.....	98
4.5	References.....	99

5. Oxidative Ring-Opening of Aromatics: Decomposition of Biphenyl Carboxylic Acids and Zinc Biphenyl Carboxylates	101
5.1 Introduction.....	102
5.2 Experimental Section.....	104
5.2.1 Materials	104
5.2.2 Synthesis of Zinc Carboxylates.....	104
5.2.3 Equipment and Procedure.....	105
5.2.4 Analyses.....	105
5.2.5 Calculations	108
5.3 Results and Discussion	108
5.3.1 Thermal Decomposition of Aromatic Carboxylic Acids.....	108
5.3.1.1 Product Characterization.....	108
5.3.1.2 Reaction Network	113
5.3.1.3 Thermal Decomposition Selectivity.....	118
5.3.2 Catalytic Decomposition of Aromatic Carboxylic Acids.....	119
5.3.2.1 Metal Carboxylates as Catalytic Surrogates	119
5.3.2.2 Catalyst Selection for Carboxylic Acid Decomposition.....	120
5.3.2.3 Infrared Spectroscopy of Zinc Carboxylates	121
5.3.2.4 Thermal Analysis of Zinc Carboxylates	122
5.3.2.4.1 Zinc(II) Bphenyl-2,2'-dicarboxylate.....	123
5.3.2.4.2 Zinc(II) Bphenyl-2-carboxylate	126
5.3.3 Decarboxylation Selectivity during the Decomposition of Zinc Carboxylates	127
5.4 Conclusions.....	129
5.5 References.....	132
6. Oxidative Ring-opening of Aromatics: Effect of Water on Reaction Selectivity	136
6.1 Introduction.....	137
6.2 Experimental Section.....	138
6.2.1 Materials	138

6.2.2	Equipment and Procedure.....	138
6.2.2.1	Procedure I.....	139
6.2.2.2	Procedure II.....	139
6.2.2.3	Procedure III.....	140
6.2.3	Analyses.....	140
6.3	Results.....	141
6.3.1	Product Characterization.....	141
6.3.2	Selectivity of Reaction.....	141
6.3.2.1	Procedure I Reactions.....	142
6.3.2.2	Procedure II Reactions.....	143
6.3.2.3	Procedure III Reactions.....	145
6.4	Discussion.....	146
6.4.1	Effect of Water on Reaction Selectivity.....	146
6.4.2	Variability in Selectivity due to Water.....	148
6.5	Conclusions.....	149
6.6	References.....	150
7.	Oxidative Ring-Opening of Aromatics: Thermochemistry of Sodium, Potassium and Magnesium Biphenyl Carboxylates	151
7.1	Introduction.....	152
7.2	Experimental Section.....	153
7.2.1	Materials.....	153
7.2.2	Synthesis of Metal Carboxylates.....	154
7.2.3	Equipment and Procedure.....	156
7.2.4	Calculations.....	158
7.3	Results and Discussion.....	158
7.3.1	Infrared Spectroscopy.....	158
7.3.2	¹ H NMR Analysis.....	162
7.3.3	Sodium Biphenyl-2,2'-dicarboxylate.....	162
7.3.4	Potassium Biphenyl-2,2'-dicarboxylate.....	172

7.3.5	Magnesium Biphenyl-2,2'-dicarboxylate	177
7.3.6	Thermal Stability of Alkali and Alkaline Earth Biphenyl Metal Carboxylates	180
7.3.7	Generalization of Metal Carboxylates Decomposition Results.....	181
7.4	Conclusions.....	182
7.5	References.....	184
8.	Oxidative Ring-Opening of Aromatics: Thermochemistry of Iron, Copper and Cobalt Biphenyl Carboxylates	186
8.1	Introduction.....	187
8.2	Experimental Section	189
8.2.1	Materials	189
8.2.2	Synthesis of Metal Carboxylates	190
8.2.3	Equipment and Procedure.....	191
8.2.3.1	Characterization of Metal Carboxylates	191
8.2.3.2	Thermal Analysis	193
8.2.4	Calculations	195
8.3	Results and discussion	195
8.3.1	Characterization of Metal Carboxylates	195
8.3.1.1	Infrared Spectroscopy	195
8.3.1.1.1	Synthesis of Metal Carboxylates.....	195
8.3.1.1.2	Nature of the Carboxylate Bonding	198
8.3.1.2	Purity of Metal Carboxylates	200
8.3.1.3	Scanning Electron Microscopy	201
8.3.1.4	Elemental Analysis	201
8.3.1.5	Metal Content.....	203
8.3.1.6	Remarks	205
8.3.2	Thermochemistry of Metal Carboxylates	206
8.3.2.1	Thermochemistry of Iron Biphenyl-2,2'-Dicarboxylate.....	206
8.3.2.2	Thermochemistry of Copper (II) Biphenyl-2,2'-Dicarboxylate and Copper Biphenyl-2-Carboxylate	213

8.3.2.2.1	Decomposition of Copper (II) Biphenyl-2,2'-Dicarboxylate	214
8.3.2.2.2	Decomposition of Copper (II) Biphenyl-2-Carboxylate	217
8.3.2.2.3	Comparison of the Decomposition of the Copper Carboxylates	219
8.3.2.2.4	Decomposition Chemistry of Copper Carboxylates	223
8.3.2.3	Thermochemistry of Cobalt Biphenyl-2,2'-Dicarboxylate and Cobalt Biphenyl-2-Carboxylate	224
8.3.2.3.1	Decomposition of Cobalt Biphenyl-2,2'-Dicarboxylate	225
8.3.2.3.2	Decomposition of Cobalt Biphenyl-2-Carboxylate	229
8.3.2.4	Thermal Stability of Transition Metal Carboxylates	232
8.4	Conclusions	233
8.5	References	235
9.	CONCLUSIONS	237
9.1	Introduction	237
9.2	Significance, Major Conclusions and Insights	237
9.3	Recommended Work	241
9.3.1	Future Work on Process Development of Oxidative Ring-Opening of Multinuclear Aromatics	241
9.3.2	Future Work on Selective Decarboxylation Catalysis	242
9.4	Presentations and Publications	243
9.5	References	244
	REFERENCES	246
	APPENDIXES	261
	APPENDIX A	261
	APPENDIX B	263
B.1.	Chromatograms of decomposition products	263
	APPENDIX C	266
C.1.	Purity of metal carboxylates	266
C.2.	Scanning Electron Microscopy Analysis of Biphenyl Transition Metal Carboxylates	269

C.3. Elemental Analysis - Sample Calculation.....	274
C.4. X-ray diffraction (XRD) analysis for the residues of decomposition in air atmosphere of the biphenyl transition metal carboxylates	276
C.5. Infrared analysis of the gases evolved during thermal analysis of the synthesized metal carboxylates	280
C.6. DSC-microscopy of cobalt biphenyl-2-carboxylate	281

TABLES

Table 2.1. Common oxidants for liquid phase oxidation	9
Table 2.2. Catalytic oxidation of benzene: kinetics	15
Table 2.3. Heat evolved during aromatic oxidation	27
Table 2.4. Desulfurization of model mixtures and industrial feedstocks by liquid phase oxidation with air	32
Table 3.1. Properties of asphaltenes from industrial C ₅ solvent deasphalting process	64
Table 3.2. Relative peak intensities of absorptions at different regions of the IR spectra for oxidized asphaltenes	70
Table 3.3. Micro carbon residue data for raw asphaltenes, oxidized asphaltenes, and asphaltenes heated in nitrogen atmosphere for 16 h.....	72
Table 3.4. Asphaltene and micro carbon residue data for unreacted asphaltenes and asphaltenes heated at low temperature in air and moist air atmospheres for different reaction times.....	73
Table 3.5. Relative peak intensities of absorptions at different regions of the IR spectra for the total oxidized products after oxidation using moist air at 52 °C.....	74
Table 4.1. Main Thermal Events found in HP–DSC Analyses for the Autoxidation of Anthracene	90
Table 4.2. Main Thermal Events found in HP–DSC Analysis for the Catalytic Oxidation of Anthracene	91
Table 4.3. Main Thermal Events found in HP–DSC Analyses for the Autoxidation of Anthraquinone.....	93
Table 4.4. Main Thermal Events According to HP-DSC Analysis for the Catalytic Oxidation of Anthraquinone.....	94
Table 4.5. Compounds Identified through GC–MS for Catalytic Oxidation of Anthraquinone..	97
Table 5.1. Products from decomposition reactions identified by GC-MS analysis	110
Table 5.2. Chemical Structure of the Products from Decomposition Reactions Identified by Gas Chromatography-Mass Spectroscopy (GC-MS)	111
Table 5.3. Relative abundance of the reaction products from thermal decomposition of aromatic carboxylic acids	112

Table 5.4. Thermal decomposition of zinc carboxylates studied by DSC and TGA analyses...	123
Table 5.5. Relative Abundance of the Reaction Products from Thermal Decomposition of Zinc Carboxylates	128
Table 6.1. Average Relative Ratio of Biphenyl to Fluorenone from Thermal Decomposition of Biphenyl-2-carboxylic Acid.....	142
Table 7.1. Commercially available chemicals employed in this study	154
Table 7.2. Chemicals synthesized in this study.....	155
Table 7.3. Characteristic stretching vibrations in the infrared spectra for the synthesized metal biphenyl-2,2'-dicarboxylates.....	159
Table 7.4. Thermal decomposition and mass loss profile of the synthesized biphenyl-2,2'-carboxylic acid salts studied by TGA and TGA-FTIR analyses.....	164
Table 7.5. Thermal decomposition of the synthesized biphenyl-2,2'-carboxylic acid salts studied by DSC analysis.....	165
Table 7.6. Mass loss of the synthesized biphenyl-2,2'-carboxylic acid salts after decomposition determined by TGA and calculated according to the expected inorganic residue.....	172
Table 8.1. Chemicals employed in this study.....	189
Table 8.2. Strong carboxylate stretching vibrations in the infrared spectra of the synthesized metal carboxylates	196
Table 8.3. Fractional purity of the synthesized metal carboxylates	200
Table 8.4. Elemental composition of the synthesized metal carboxylates.....	202
Table 8.5. Metal content of the synthesized metal carboxylates.....	204
Table 8.6. Thermal decomposition and mass loss profile of the synthesized metal carboxylates studied by TGA and TGA-FTIR analyses	208
Table 8.7. Thermal decomposition of the synthesized metal carboxylates studied by DSC analysis.....	209
Table A.1. Reaction stoichiometry for the catalytic oxidation of anthracene.....	261
Table C.1. Purity and contaminants of the synthesized metal carboxylates	266
Table C.2. Results from elemental analysis of the copper biphenyl-2-carboxylate	275
Table C.3. Elemental composition (adjusted) of the copper biphenyl-2-carboxylate	275

FIGURES

Figure 2.1. Examples of aromatic oxidation involving (a) non-cleavage of the aromatic ring, (b) cleavage of the aromatic ring, and (c) oxidation of the side chains attached to the aromatic ring	11
Figure 2.2. Benzene oxidation reaction scheme	12
Figure 2.3. Naphthalene oxidation reaction scheme	17
Figure 2.4. Catalytic hydrogen peroxide production through the anthraquinone process	20
Figure 2.5. Vapor-phase oxidation of anthracene	21
Figure 2.6. Phenanthrene oxidation reaction scheme	23
Figure 2.7. Ruhrol-Lurgi process for production of maleic anhydride by benzene oxidation	26
Figure 2.8. Examples of heteroaromatic oxidation involving (a) carbon oxidation without the cleavage of the aromatic rings, (b) heteroatom oxidation without the cleavage of the aromatic rings, (c) cleavage of carbon-carbon bonds of the aromatic rings, (d) cleavage of carbon-heteroatom bonds of the heterocyclic aromatic rings, (e) oxidation of the side chains attached to the aromatic rings	29
Figure 2.9. Examples of heterocyclic aromatic compounds	31
Figure 2.10. Oxidation of sulfur compounds by oxygen in air, as illustrated by the oxidation of thiophene	31
Figure 2.11. Oxidation of pyrrolic compounds by oxygen in air, as illustrated by the oxidation of 2,5-dimethylpyrrole	36
Figure 2.12. Oxidation of furan with air as oxidant	38
Figure 2.13. Oxidation of furan and furan derivatives using V_2O_5 as catalyst and air as oxidant	38
Figure 2.14. Types of aromatic rings according to Clar's π -sextet	40
Figure 2.15. Clar formalism applied to aromatic compounds having three fused rings	42
Figure 2.16. Pre-oxidative behavior of (a) perinaphthyl, (b) phenanthrene and (c) anthracene	43
Figure 2.17. Types of diones obtained by oxidation of multinuclear aromatics	48
Figure 3.1. Experimental setup for asphaltenes oxidation with (a) dry air and (b) moist air	65
Figure 3.2. Asphaltenes content of the products obtained by heating asphaltenes feed in air and nitrogen atmospheres for 16 h at 45, 55, 86, and 100 °C	68

Figure 3.3. Infrared spectra of the raw asphaltenes and the total oxidized product after 16 h oxidation at 45, 56, 86, and 100 °C	70
Figure 3.4. Infrared spectra of the maltenes fraction separated from of the oxidized products obtained after 16 h oxidation at 45, 56, 86, and 100 °C	72
Figure 3.5. Infrared spectra of raw asphaltenes feed and total oxidized product after wet air oxidation at 52 °C for 2, 4 and 8 h respectively	74
Figure 3.6. Asphaltene content of the products obtained by heating asphaltenes for 2 h at 52 and 100 °C, under air and moist air atmosphere	75
Figure 3.7. Reaction pathway explaining ester formation during low temperature autoxidation of cycloalkane containing feed materials, as illustrated by the oxidation of indan	79
Figure 4.1. Autoxidation of phenanthracene to illustrate the concept of oxidative ring-opening	86
Figure 4.2. GC-MS analysis of products obtained by conversion of anthraquinone (no V ₂ O ₅) at 430 °C, 4 MPa N ₂ for 1 h	96
Figure 4.3. GC-MS analysis of products obtained by conversion of anthraquinone with V ₂ O ₅ at 430 °C, 4 MPa N ₂ for 1 h	96
Figure 5.1. Autoxidation of phenanthrene to illustrate the concept of oxidative ring-opening.	102
Figure 5.2. Chromatogram of biphenyl-2-carboxylic acid decomposition products after 20 min reaction under 4 MPa N ₂ pressure at (a) 350 °C, and (b) 385 °C	113
Figure 5.3. Reaction network for thermal decomposition of biphenyl-2-carboxylic acid under inert atmosphere	114
Figure 5.4. Reaction network for thermal decomposition of biphenyl-2,2'-dicarboxylic acid under inert atmosphere	116
Figure 5.5. Electron impact mass spectrum of compound tentatively identified as dibenzo[<i>a,c</i>]cycloheptene-5,6,7-trione	117
Figure 5.6. Infrared spectrum of (a) zinc(II) biphenyl-2,2'-dicarboxylate, and (b) zinc(II) biphenyl-2-carboxylate	121
Figure 5.7. DSC heat flow signal and TGA mass loss data for decomposition of zinc(II) biphenyl-2,2'-dicarboxylate under inert atmosphere	124
Figure 5.8. Infrared spectra of the gases evolved from the zinc(II) biphenyl-2,2'-dicarboxylate TGA-FTIR analysis	126

Figure 5.9. DSC heat flow signal and TGA mass loss data for decomposition of zinc(II) biphenyl-2-carboxylate under inert atmosphere	127
Figure 6.1. Main and competing reaction pathways for decomposition of biphenyl-2-carboxylic acid	137
Figure 6.2. Effect of water on reaction selectivity for reactions performed using Procedure I. 143	
Figure 6.3. Effect of water on reaction selectivity for reactions performed using Procedure II (hollow markers) and Procedure I (solid markers)	144
Figure 6.4. Effect of water on reaction selectivity for reactions performed using Procedure III (hollow markers). The results of the blank experiments without water (solid markers) are also shown	146
Figure 6.5. Mechanism and transition states for the thermal decomposition of acetic acid with and without water present	147
Figure 7.1. Infrared spectra of (a) biphenyl-2,2'-dicarboxylic acid, and (b) sodium, (c) potassium and (d) magnesium biphenyl-2,2'-dicarboxylates. A: O–H stretching; B: $\nu_{as}(C=O)$ stretching; C: O–H bending; D: C–O stretching; E, I, M: OH stretching for lattice water; F, J, N: HOH bending for lattice water; G, K, O, P: $\nu_{as}(CO_2^-)$ stretching; H, L, Q, R: $\nu_s(CO_2^-)$ stretching.....	160
Figure 7.2. TGA mass loss profile (collected with Mettler Toledo TGA/DSC1 system) and DSC heat flow signal for decomposition of sodium biphenyl-2,2'-dicarboxylate	163
Figure 7.3. Infrared spectra of the gaseous products evolved during thermal analysis of the sodium biphenyl-2,2'-dicarboxylate	166
Figure 7.4. Infrared spectra of the (a) gas product evolved during heating of the sodium biphenyl-2,2'-dicarboxylate at 200 °C, and (b) liquid formic acid at room temperature	167
Figure 7.5. Possible reaction pathway leading to formic acid formation during decomposition of sodium biphenyl-2,2'-dicarboxylate.....	168
Figure 7.6. Infrared spectra of the solid residue obtained after DSC analysis of the sodium biphenyl-2,2'-dicarboxylate.....	169
Figure 7.7. Infrared spectrum of the (a) solid residue obtained after thermal decomposition of the sodium biphenyl-2,2'-dicarboxylate when heated to 600 °C, (b) sodium carbonate.....	171
Figure 7.8. TGA mass loss profile (collected with Mettler Toledo TGA/DSC1 system) and DSC heat flow signal for decomposition of potassium biphenyl-2,2'-dicarboxylate	173

Figure 7.9. DSC-microscopy images of the potassium biphenyl-2,2'-dicarboxylate: solid (left) and liquid phase formed during transition <i>iii</i> (right).....	174
Figure 7.10. Infrared spectra of the solid residue obtained after DSC analysis of the potassium biphenyl-2,2'-dicarboxylate.....	175
Figure 7.11. Infrared spectrum of the (a) solid residue obtained after thermal decomposition of the potassium biphenyl-2,2'-dicarboxylate when heated to 600 °C, (b) potassium carbonate, (c) potassium bicarbonate.....	176
Figure 7.12. TGA mass loss profile (collected with Mettler Toledo TGA/DSC1 system) and DSC heat flow signal for decomposition of magnesium biphenyl-2,2'-dicarboxylate	178
Figure 7.13. Infrared spectra of the solid residue obtained after DSC analysis of the magnesium biphenyl-2,2'-dicarboxylate.....	179
Figure 8.1. Dominant decomposition pathways of biphenyl-2,2'-dicarboxylic acid and zinc biphenyl-2,2'-dicarboxylate at around 380 °C	187
Figure 8.2. Infrared spectra of (a) biphenyl-2,2'-dicarboxylic acid, (b) iron, (c) cobalt, (d) and copper biphenyl-2,2'-dicarboxylates, (e) biphenyl-2-carboxylic acid, (f) cobalt, and (g) copper biphenyl-2-carboxylates. A, a: O–H stretching; B, b: $\nu_{as}(C=O)$ stretching; C, c: O–H bending; D, d: C–O stretching; E, J, O, e: OH stretching for lattice water; F, K, P, f: HOH bending for lattice water; G, H, L, M, Q, R, g, h, j, k: $\nu_{as}(CO_2^-)$ stretching; I, N, S, i, l: $\nu_s(CO_2^-)$ stretching.....	197
Figure 8.3. Bonding configurations for metal carboxylates.....	198
Figure 8.4. TGA mass loss profile and DSC signal for decomposition of iron biphenyl-2,2'-dicarboxylate.....	207
Figure 8.5. Infrared spectra of the gaseous products evolved during thermogravimetric analysis of the iron biphenyl-2,2'-dicarboxylate	210
Figure 8.6. Infrared spectra of (a) gases evolved during heating of the iron biphenyl-2,2'-dicarboxylate at 385 °C, (b) gas phase fluorenone, and (c) gas phase biphenyl.....	211
Figure 8.7. Infrared spectra of the solid residue obtained after DSC analysis of the iron biphenyl-2,2'-dicarboxylate to different temperatures.....	212
Figure 8.8. TGA mass loss profile and DSC signal for decomposition of (a) copper (II) biphenyl-2,2'-dicarboxylate (b) copper (II) biphenyl-2-carboxylate	214

Figure 8.9. Infrared spectra of (a) the gases evolved during heating of the copper (II) biphenyl-2,2'-dicarboxylate at 281 °C, and (b) vapor phase benzoic acid at 160 °C (c) gas phase fluorenone, and (c) gas phase biphenyl.....	217
Figure 8.10. Infrared spectra of (a) the gases evolved during heating of the copper (II) biphenyl-2,2'-dicarboxylate at 281 °C, and (b) vapor phase benzoic acid at 160 °C (c) gas phase fluorenone, and (c) gas phase biphenyl.....	220
Figure 8.11. Infrared spectra of the solid residue left after heating the (a) copper (II) biphenyl-2,2'-carboxylate (b) copper (II) biphenyl-2-carboxylate.....	221
Figure 8.12. Possible reaction pathway leading copper reduction during decomposition of copper (II) biphenyl-2,2'-dicarboxylate.....	223
Figure 8.13. TGA mass loss profile and DSC signal for decomposition of (a) cobalt biphenyl-2,2'-dicarboxylate (b) cobalt biphenyl-2-carboxylate	224
Figure 8.14. Infrared spectra of the gases evolved during heating of the cobalt biphenyl-2,2'-dicarboxylate (a) 430 °C, (b) 550 °C, as well as (c) gas phase fluorenone, and (d) gas phase biphenyl.....	226
Figure 8.15. Possible reaction pathway leading fluorenone during decomposition of cobalt biphenyl-2,2'-dicarboxylate.....	227
Figure 8.16. Infrared spectra of the solid residue obtained after DSC analysis of the (a) cobalt biphenyl-2,2'-dicarboxylate, (b) cobalt biphenyl-2-carboxylate.....	228
Figure 8.17. DSC-microscopy images of cobalt biphenyl-2-carboxylate to show the solid (up-left), transition <i>ii</i> (up-right), transition <i>iii</i> (bottom-left) and transition <i>iv</i> (bottom-right)	230
Figure B.1. Chromatogram of biphenyl-2,2'-dicarboxylic acid decomposition products after reaction at 4MPa of nitrogen, during 20 min at (a) 340 °C, and (b) 400 °C.....	263
Figure B.2. Chromatogram of zinc(II) biphenyl-2,2'-dicarboxylate decomposition products after reaction under nitrogen atmosphere at (a) 263 °C, (b) 380 °C, and (c) 435 °C	264
Figure B.3. Chromatogram of zinc(II) biphenyl-2-carboxylate decomposition products after reaction under nitrogen atmosphere at (a) 350 °C, and (b) 390 °C.....	265
Figure C.1. Calibration curve to estimate purity of biphenyl-2,2'-dicarboxylates.....	267
Figure C.2. Calibration curve to estimate purity of biphenyl-2-carboxylates	267
Figure C.3. SEM micrograph of iron biphenyl-2,2'-dicarboxylate	269
Figure C.4. SEM micrograph of copper biphenyl-2,2'-dicarboxylate.....	270

Figure C.5. SEM micrograph of cobalt biphenyl-2,2'-dicarboxylate.....	271
Figure C.6. SEM micrograph of copper biphenyl-2-carboxylate	272
Figure C.7. SEM micrograph of cobalt biphenyl-2-carboxylate	273
Figure C.8. Backscattered electron micrograph of copper biphenyl-2-carboxylate with points of microanalysis indicated (3_1: Copper hydroxide, 3_2: Copper biphenyl-2-carboxylate).....	274
Figure C.9. XRD pattern of the residue of decomposition of the iron biphenyl-2,2'-dicarboxylate after heating in air atmosphere to 900 °C for 2 hours	276
Figure C.10. XRD pattern of (a) the residue of decomposition of the copper biphenyl-2,2'-dicarboxylate after heating in air atmosphere to 900 °C for 2 hours (b) copper (II) oxide	277
Figure C.11. XRD pattern of (a) the residue of decomposition of the cobalt biphenyl-2,2'-dicarboxylate after heating in air atmosphere to 900 °C for 2 hours (b) Cobalt (II,III) oxide....	278
Figure C.12. XRD pattern of the residue of decomposition of the cobalt biphenyl-2-carboxylate after heating in air atmosphere to 900 °C for 2 hours	279
Figure C.13. XRD pattern of the residue of decomposition of the copper biphenyl-2-carboxylate after heating in air atmosphere to 900 °C for 2 hours	279
Figure C.14. Infrared spectra of (a) gases evolved during heating of the iron biphenyl-2,2'-dicarboxylate to 205 °C, and (b) gas phase tetrahydrofuran.....	280
Figure C.15. Infrared spectra of (a) the gases evolved during heating of the copper (II) biphenyl-2,2'-dicarboxylate at 186 °C, and (b) gas phase ethanol.....	280
Figure C.16. DSC-microscopy of cobalt biphenyl-2-carboxylate to show transition <i>iii</i> after...	281

1. Introduction

1.1 Background

The demand for transportation fuels and petrochemicals products has rapidly grown in recent years and it is expected to continue growing in future [1]. Moreover, the reserves of conventional light crude oils are depleting. Hence, there has been a sharp increase in the heavy and extra-heavy crude oils exploration and production [2]. Refineries are required to meet the market demand for high quality products, with increasingly more stringent regulations, using heavy feedstocks of lower quality and reduced yield of light fractions, which also are more expensive to produce [2]. This situation poses a significant challenge for the oil industry.

Reservoirs of heavy and extra-heavy oils as well as deposits of oil sands are distributed all around the world. Production of these resources is anticipated to overtake production of conventional crude oil and is expected to become the main source of oil. Resources of extra-heavy oil in Venezuela and oilsands bitumen in Canada are of particular importance [1][3]. On one hand, Venezuela owns the world's largest deposit of extra-heavy crude oil, which contains approximately 2450 billion barrels of crude oil. Close to 14 billion barrels have been recovered and ~ 59 billion barrels can still be recovered using the current technology [4]. On the other hand, Canada has the world's largest deposit of oilsands. It contains approximately 2400 billion barrels of bitumen, from which about 5 billion barrels have been recovered and ~ 174 billion barrels are expected to be recovered [4].

The complex chemical nature of these heavy feedstocks makes them difficult to produce and upgrade. Compared to light crude oils, these heavy materials are characterized by high density (low API gravity), high viscosity and high content of sulfur, nitrogen and metals. Furthermore, they are hydrogen deficient, have a significant content of multinuclear aromatics as well as a significant carbon residue value [1]. Also, they have a substantial content of non-distillable, high molecular weight materials, including a high content of asphaltenes (paraffin insoluble compounds) [1][4]. Asphaltenes is considered one of the most problematic constituents during

upgrading operations because they are considered the main cause of catalyst deactivation and coke formation [2]. Asphaltene content lowers the economic value of a crude oil and is a major operational concern [5].

A number of technologies have been developed over the years to deal with heavy oil and bitumen upgrading. Thermal processes, e.g. visbreaking or coking, allow for redistributing the hydrogen among the components to modify the hydrogen-to-carbon (H:C) ratio of the products. Fractions with both an increased and decreased H:C ratio are obtained [1]. The latter is known as “coke”, although it should rather be called carbonaceous deposits. These processes are used at industrial scale and are usually selected when the quality of the feed is low and it is not appropriate for catalytic processes [6]. On the other hand, the addition of hydrogen is also an option. Hydroprocessing requires an external source of hydrogen and a catalyst. This process yields a series of products with an overall increase of the H:C ratio. The yield of liquid fractions is higher in hydroprocessing than in visbreaking or coking processes [6].

The characteristics of the feedstocks to be processed and the products finally obtained as well as the operating conditions are different among upgrading technologies. Hydroprocessing is attractive because of the increased yield in liquid products of high quality. However, the need to use catalysts, an external source of hydrogen and high-pressure equipment make this type of operation very expensive. Typical, residue hydroconversion processes operate at temperatures around 340–450 °C and pressures between 10–17 MPa [7]. In addition, hydroprocessing of highly aromatic materials is subject to demanding thermodynamic constraints. Aromatics are more stable as aromatics at hydroconversion temperatures than they are as hydrogenated products. On the other hand, thermal processes operate at lower pressure but require even higher temperatures. Depending on the technology, coking processes operate in a temperature range between 485–540 °C [7]. The yield of coke and gas products for thermal processes is high; whereas, the yield to liquid products is low [2]. Multinuclear aromatics are more likely to form coke than they are to crack to give lighter products.

It is clear that in future heavy aromatic-rich materials will become a regular feedstock for refineries. Traditional upgrading processes require modifications to improve their performance.

Nevertheless, weaknesses such as the severe operating conditions and the high associated cost will be difficult to overcome. Facing this scenario, it is important to explore strategies based on a different approach.

1.2 Objective

The objective of this work was to evaluate the oxidation of multinuclear aromatics using oxygen (in air) as oxidant to produce a ring-opened hydrocarbon product.

1.3 Scope

The oxidation of multinuclear aromatics to facilitate ring-opening using oxygen (in air) as oxidant was investigated. The use of other oxidants was not included in the scope of this work.

The oxidative ring-opening of multinuclear aromatics involves three main steps: (i) oxidation of multinuclear aromatics to produce quinonoids, (ii) further oxidation to form ring-opened carboxylic acids, and (iii) decarboxylation to remove the acid functionality as CO₂. A short description of the work conducted in regards with these three steps is presented in the following:

Chapter 2: *Autoxidation of Aromatics: An Interpretative Review*

The success of the oxidative ring-opening of multinuclear aromatics relies on the understanding of the fundamentals of aromatic oxidation. Therefore, this chapter reviews the available literature on the topic, placing emphasis on the reaction leading to selective cleavage of ring C–C bonds. The need to adopt a catalytic approach is discussed.

Chapter 3: *Low-Temperature Oxidative Asphaltenes Liquefaction for Petrochemicals: Fact or Fiction?*

The patent literature indicates that the upgrading of heavy aromatics materials for petrochemical production, including oxidative ring-opening, is possible by

oxidative liquefaction at low temperature, i.e., a non-catalytic approach. This chapter explores and validates the usefulness of the oxidative conversion strategies outlined and claimed in the patent literature.

Chapter 4: *Oxidative Ring-Opening over Metal Oxides*

Multinuclear aromatics are readily oxidized to quinonoids, but further oxidation and particularly ring-opening is difficult. This chapter focused on the evaluation of different metal oxide catalysts for the oxidative ring-opening of multinuclear aromatics. Reaction in liquid phase and transfer of lattice oxygen are explored.

Chapter 5: *Oxidative Ring-Opening of Aromatics: Decomposition of Biphenyl Carboxylic Acids and Zinc Biphenyl Carboxylates*

Effective removal of the carboxylic acid functionality, by rejecting the carbon as CO₂, is essential to produce ring-opened hydrocarbon products. This chapter investigates the decomposition of aromatic carboxylic acid species produced by the oxidative ring-opening of multinuclear aromatics in order to understand how to manipulate the reaction selectivity and favor the overall ring-opening process.

Chapter 6: *Oxidative Ring-Opening of Aromatics: Effect of Water on Reaction Selectivity*

Thermal decomposition of aromatic carboxylic acid species favors production of ring closed-products. Moreover, the reaction pathways leading to ring-closed products are accompanied by elimination of water, which suggests that water affects the reaction selectivity. This chapter studies the effect of water on the reaction selectivity for the thermal decomposition of aromatic carboxylic acids.

Chapter 7: *Oxidative Ring-Opening of Aromatics: Thermochemistry of Sodium, Potassium and Magnesium Biphenyl Carboxylates*

In thermal decomposition, ketonization and dehydration reactions compete with decarboxylation of aromatic carboxylic acids, decreasing the selectivity of the reaction towards the ring-opened products. In this chapter, a catalytic approach to

facilitate the decarboxylation step is considered. Metal carboxylates are used as catalytic surrogates. Alkaline and alkaline earth metals are investigated.

Chapter 8: *Oxidative Ring-Opening of Aromatics: Thermochemistry of Iron, Copper and Cobalt Biphenyl Carboxylates*

Following the same catalytic approach to modify the reaction selectivity to favor decarboxylation, and so the production of ring-opened products, this chapter studies the decomposition of bulk transition metal carboxylates.

Chapter 9: *Conclusions and Recommended Work*

In this chapter, the main conclusions of the oxidative ring-opening strategy and the insights that will contribute to the field of upgrading of heavy aromatic materials are highlighted.

Note. The work presented in Chapters 2–8 was either published or submitted for publication in different Scientific Journals. No major modifications were made when including the papers or short communications in the present thesis document. As a result, there might be some similarities in the introduction of each chapter.

1.4 References

- [1] Speight, J. G. In *Chapter 1 – Refining Heavy Oil and Extra-Heavy Oil*; Heavy and Extra-heavy Oil Upgrading Technologies; Gulf Professional Publishing: Boston, 2013.
- [2] Ancheyta, J.; Trejo, F.; Rana Singh, M. *Asphaltenes: Chemical Transformation during Hydroprocessing of Heavy Oils*; CRC Press: Boca Raton, FL, 2010.
- [3] Strausz, O. P.; Lown, E. M. *The Chemistry of Alberta Oils Sands, Bitumens and Heavy Oils*; Alberta Energy Research Institute: Calgary, Alberta, Canada, 2003.
- [4] Gray, M. *Upgrading of Oilsands Bitumen and Heavy Oils*; The University of Alberta Press: Edmonton, Canada, 2015.

- [5] Mullins, O. C. Review of the Molecular Structure and Aggregation of Asphaltenes and Petroleomics. *SPE J* **2008**, 13, 48-57.
- [6] Furimsky, E. In *Chapter 1 Introduction*; Studies in Surface Science and Catalysis; Elsevier: Amsterdam, 2007; Vol. 169, pp 1-4.
- [7] Gary, J. H.; Handwerk, G. E.; Kaiser, M. J. Petroleum Refining. Technology and Economics; CRC Press: Boca Raton, 2007; pp 1-463.

2. Autoxidation of Aromatics: A Review ¹

ABSTRACT

Autoxidation is a conversion pathway that has the potential to add value to multinuclear aromatic rich coal liquids, heavy oils and bitumens, which are typically considered low value liquids. In particular, autoxidation of these heavy materials could lead to products that may have petrochemical value, e.g. lubricity improvers and emulsifiers. Proper assessment of an oxidative transformation to ring-open the multinuclear aromatics present in heavy feeds relies on the understanding of the fundamentals of aromatic oxidation. This work reviews the selective oxidation chemistry of atoms that form part of an aromatic ring structure using oxygen (in air) as oxidant, i.e., the oxidation of aromatic carbons as well as heteroatoms contained in an aromatic ring. Examples of industrially relevant oxidations of aromatic and heterocyclic aromatic hydrocarbons are provided. The requirements to produce oxygenates involving the selective cleavage of the ring C–C bonds, as well as competing non-selective oxidation reactions are discussed. On the other hand, the Clar formalism, i.e., a rule that describes the stability of polycyclic systems, assists the interpretation of the reactivity of multinuclear aromatics towards oxidation. Two aspects are developed. First, since the interaction of oxygen with aromatic hydrocarbons depends on their structure, oxidation chemistries which are fundamentally different are possible, namely, transannular oxygen addition, oxygen addition to a carbon-carbon double bond, or free radical chemistry. Second, hydrogen abstraction is not necessary for the initiation of the oxidation of aromatics compared to that of aliphatics.

Keywords: Autoxidation, catalytic oxidation, multinuclear aromatics, PAHs, heterocyclic aromatics, Clar formalism.

¹ This work was accepted for publication in *Applied Petrochemical Research*.

2.1 Introduction

Processes for the oxidation of organic materials cover the entire selectivity spectrum ranging from total or near total combustion to give carbon oxides, to mild partial oxidation to functionalize organic molecules to produce chemical intermediates [1]. Selective oxidation is a direct and economic route to convert petroleum products into petrochemicals [2]. This type of chemistry is present in the large-scale production of commodities, as well as in the synthesis of small amounts of pharmaceuticals and fine chemicals [3]. Selective oxidation of alkanes (paraffins), alkenes (olefins) and aromatics feed materials produce oxygenated compounds, such as alcohols, aldehydes, ketones, carboxylic acids, anhydrides and epoxides, which are important commodities in the petrochemical industry. The breadth of the industrial application of oxidation can be seen from books that discuss industrially practiced oxidation processes, e.g. [4][5].

The scope of this review is much narrower. The review is concerned only with oxidation of atoms that form part of an aromatic ring structure. This topic received relatively little attention in literature since the report by *Tipson* [6]. Oxidation of aromatic carbons as well as heteroatoms contained in aromatic rings will be considered.

Heavy aromatic feed materials can in principle be converted into higher valued petrochemicals that are also mixtures, for example, lubricity improvers, emulsifiers and greases. Oxidized aromatic compounds may also be low cost intermediates that can be used as feed materials for the production of petrochemical products, or that are useful products in their own right. For example, autoxidation (oxidation using air) is commercially employed for asphalt hardening [7], which is an important process for producing asphalt for road construction. Autoxidation is also a conversion pathway by which value can potentially be added to other predominantly aromatic feed materials, such as coal liquids, petroleum vacuum residues, heavy aromatic oils and bitumens. Such complex mixtures are not normally considered for petrochemical production. Petrochemicals are usually produced from feed materials that are purified compounds, or well-defined mixtures of compounds. Yet, due to the low value associated with heavy aromatic feed materials, there is an incentive to add value and there is a cost benefit if it can be achieved.

Oxidative transformation of heavy aromatic oils is likely challenging and one of the objectives of this review is to assess the potential of oxidation as pathway for the conversion of aromatics and in particular multinuclear aromatics.

Table 2.1. Common oxidants for liquid phase oxidation (adapted from [8])

Oxidant	Active oxygen [wt %]	By-product	Comments
Air	23	N ₂ / Ar	Oxidation forms hydroperoxides; lowest cost for low pressure open loop processes
Purified O ₂	100 ^a	none ^a	Air separation needed, but purified O ₂ becomes more efficient for higher pressure and closed loop processes
H ₂ O ₂	47 ^b	H ₂ O	Usually available as aqueous solution
O ₃	33 ^c	O ₂ ^a	Generated from O ₂ by corona discharge
NaClO	22	NaCl	ClO ⁻ can produce chlorocarbon by-products
(CH ₃) ₃ CO ₂ H	18 ^d	(CH ₃) ₃ COH	Usually available in solution
CH ₃ COO ₂ H	21 ^d	CH ₃ COOH	Usually produced <i>in situ</i> by H ₂ O ₂ added to acetic acid
KHSO ₅	11	KHSO ₄	Water-compatible
C ₆ H ₅ IO	7	C ₆ H ₅ I	High cost; metal-catalyzed oxidations often selective

^a Depends on purity, but in practice purified O₂ from an air separation unit is ~99.5 wt%.

^b Depends on purity, but in practice the H₂O₂ in water is 35 wt% or less.

^c Depends on efficiency of corona discharge, typically ~2 wt% or less.

^d Depends on purity, typically available in solution.

When selecting an oxidant there are some points to consider: price, ease of handling, nature of the by-products and percentage of oxygen available. Depending on scale, production options change. Bulk industrial oxidation processes are largely limited to air, but fine chemistry can afford the luxury of using more expensive oxidants, as illustrated by Table 2.1 adapted from [8]. When converting low value heavy aromatic oils, air and possibly purified oxygen, are likely the only oxidants that make economic sense. Without proving the point, the review was restricted to

O₂ as oxidant. It also touches on the catalytic selective oxidation of multinuclear aromatic compounds.

2.2 Oxidation of Aromatic Hydrocarbons

The selective oxidation of aromatic hydrocarbons involves three general types of reactions [9], as illustrated by Figure 2.1:

- (a) Formation of oxygenates without the cleavage of the aromatic rings, e.g. formation of phenol or benzoquinone from benzene.
- (b) Formation of oxygenates accompanied by the cleavage of the aromatic rings, e.g. formation of maleic anhydride from benzene.
- (c) Formation of oxygenates by oxidation of the side chains attached to the aromatic rings, e.g. formation of benzaldehyde or benzoic acid from toluene.

Of these reactions, only (a) and (b) are considered in this review, since (c) does not involve the oxidation of an atom that is part of the aromatic ring structure.

Aromatic C–C bonds are strong and substitution reactions, reactions of type (a), are more readily achieved. For example, oxidation to produce quinonoids is well-described [10]. Reactions of type (a) may also lead to addition products that do not necessarily incorporate oxygen; these oxidative aromatic coupling reactions can be both intra- and intermolecular [11].

Even though aromatic oxidation involving splitting of the ring C–C bonds represented a milestone in the heterogeneous catalyzed oxidation technology [12], literature on the topic is somewhat limited. The literature on ring scission is mostly focused on the discussion of a few examples of industrially successful selective catalytic oxidations, e.g. the commercial production of phthalic anhydride from the vapor-phase oxidation of naphthalene. This type of chemistry is of particular interest for the present work, due to its potential application for the conversion of heavy aromatic materials. As a result, the oxidation of some key aromatic hydrocarbons such as

benzene, naphthalene, anthracene and phenanthrene will be discussed in the following sections. There are important differences in the way oxidation of these four compounds proceed.

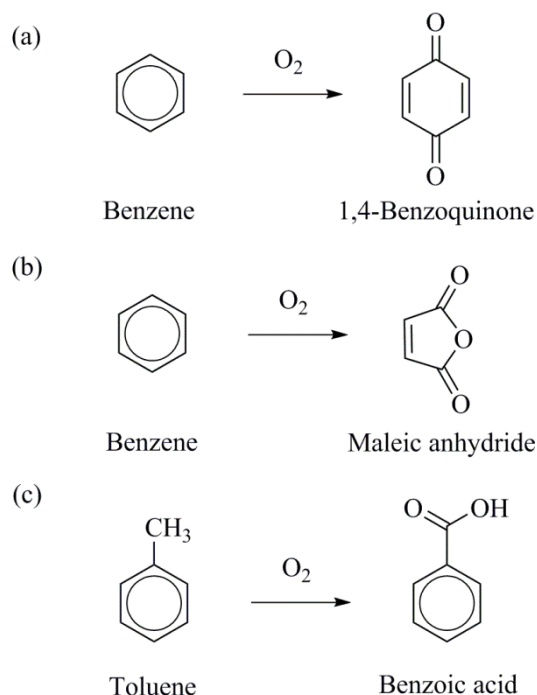


Figure 2.1. Examples of aromatic oxidation involving (a) non-cleavage of the aromatic ring, (b) cleavage of the aromatic ring, and (c) oxidation of the side chains attached to the aromatic ring

2.2.1 Benzene Oxidation

The vapor-phase oxidation of benzene to produce maleic anhydride, using air as oxidant, is one of the first successful catalytic oxidations of aromatic hydrocarbons. Commercial production of maleic anhydride from benzene started during around 1933. Currently, the industrial process for benzene to maleic anhydride autoxidation is only of historical and educational interest [12]. The selective vapor-phase oxidation of *n*-butane over vanadium phosphorous oxide (VPO) catalysts has been the dominant chemical route to produce maleic anhydride since the mid-1970s [13]. Because of its availability and lower cost, *n*-butane became an attractive raw material [14].

The industrial routes for phenol production from benzene all employ intermediate products and there are no processes to produce phenol by direct oxidation of benzene [15].

Even though benzene is the simplest aromatic hydrocarbon, its oxidation to maleic anhydride is a complicated chemical reaction, with many side-products. Production of phenol, quinone and hydroquinone from benzene autoxidation has been reported [16][17][18]. The presence of small amounts of other compounds such as formaldehyde, biphenyl, acrylic and formic acid has also been mentioned [17][18][19]. In this case, maleic anhydride is the only product obtained in yields high enough for commercial production. In industrial operation, benzene is oxidized with 67-72% of the theoretical yield of maleic anhydride [18].

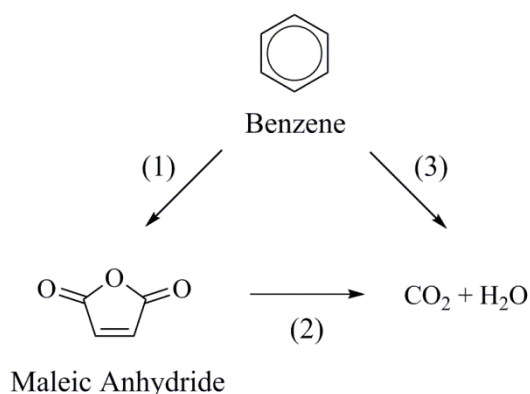


Figure 2.2. Benzene oxidation reaction scheme

The mechanism of benzene oxidation has been the subject of considerable research work. Yet, literature indicates some disagreements regarding the nature of the intermediates. The generally adopted reaction network for benzene oxidation is presented in Figure 2.2. This scheme is the basis of most kinetic studies. Benzene oxidizes in two independent ways to produce either maleic anhydride or total combustion products. Both reactions are the result of a number of short-lived intermediates [17]. Further oxidation of maleic anhydride also leads to the production of carbon oxides and water. In the absence of a catalyst, thermal decomposition of benzene is favored. Transition metal oxides have been successfully used to control the selectivity of the reaction and promote the production of maleic anhydride. Industrially, metal oxides are of

interest because the temperature window in which they catalyze the desired oxidation at appreciable rate is wider than the one offered by most metal catalysts [16].

For benzene oxidation, vanadium, molybdenum and tungsten oxides have proved to be very selective [16][18]. However, systems based on V_2O_5 have received special attention. According to the patent literature, the development of active and selective vanadium-based catalysts became an important research topic. A number of different catalyst compositions have been proposed and evaluated. Mixtures of vanadium and molybdenum oxides, in combination with one or more oxides of other elements, e.g P, W, Co, Fe, Ni or their mixtures, or in combination with salts, e.g. sodium borate, have been tested in the temperature range 340-450 °C [20][21][22].

Industrial catalysts for benzene oxidation are based on mixtures of V_2O_5 and MoO_3 . The latter can be found in concentrations up to 30% mol [18]. Typical promoters used are oxides or salts of elements such as W, Bi, Sn, P, Ag, Cu, Na, B, Ti and Ni [23]. The special catalytic behavior of vanadium-based catalysts is related to the valence changes of the metal during reaction [16]. Some interesting discussion on the structure, the redox behavior and the phases formed in the catalyst during reaction as well as the interactions of oxygen and benzene on the catalysts surface can be found in [23][24].

Mars and *Van Krevelen* studied the catalytic oxidation of some aromatic hydrocarbons, namely benzene, toluene, naphthalene and anthracene [25]. Their work suggested that the oxidation of these compounds occurred through a redox mechanism, (appropriately known as the Mars-Van Krevelen mechanism), which involves two independent steps. First, the reaction between the aromatic hydrocarbon and the metal oxide catalyst (MO_n) takes place (Eq. 1). Second, the partially reduced catalyst (MO_{n-1}) is reoxidized with gas-phase oxygen (Eq. 2).



Due to the generality of the kinetics following from this mechanism, it is worthwhile providing a brief description. Assuming that the first step is proportional to the partial pressure of

the aromatic hydrocarbon (p_{Ar}), i.e. first-order reaction, and to the fraction of catalyst surface covered with active oxygen (θ), the reaction rate can be expressed according to Eq. 3.

On the other hand, if the rate of reoxidation of the catalyst is assumed to be proportional to a certain power (m) of oxygen partial pressure and to the catalyst surface area not covered with active oxygen ($1 - \theta$), the reaction rate for the second step can be expressed according to Eq. 4.

$$r_{Ar} = k_1 p_{Ar} \theta \quad (\text{Eq. 3})$$

$$r_{O_2} = k_2 p_{O_2}^m (1 - \theta) \quad (\text{Eq. 4})$$

In steady state, the reaction rates of these two steps (reduction-oxidation cycle) are equal. Also, if for one aromatic molecule, β molecules of oxygen are required, it can be written:

$$\beta k_1 p_{Ar} \theta = k_2 p_{O_2}^m (1 - \theta) \quad (\text{Eq. 5})$$

$$\theta = \frac{k_2 p_{O_2}^m}{\beta k_1 p_{Ar} + k_2 p_{O_2}^m} \quad (\text{Eq. 6})$$

Combining Eq. 3 and 6, the overall reaction rate can be expressed as:

$$r_{Ar} = \frac{1}{\frac{1}{k_1 p_{Ar}} + \frac{\beta}{k_2 p_{O_2}^m}} \quad (\text{Eq. 7})$$

The validity of the kinetic expression (Eq. 7) with $m = 1$ for the oxidation of benzene was confirmed by Mars and Van Krevelen [25]. Furthermore, this type of equation was also valid for the oxidation of naphthalene and anthracene; the value of the rate constant k_2 of the reoxidation process on a $V_2O_5-Mo_3O/Al_2O_3$ catalyst was found to be the same for the catalytic oxidation of benzene, naphthalene and anthracene.

The reaction kinetics of benzene oxidation over a number of vanadium-based catalysts has been reported. A valuable compilation of kinetic studies for benzene oxidation can be found in [17][24]. Results from selected studies are presented in Table 2.2. At high concentrations of benzene, reactions (1) and (3) in Figure 2.2 appear to be of pseudo first-order on benzene [23].

The effect of the mass transfer rate on the pseudo-first order rate constants has been discussed [17]. The dependence of reaction (2) on the concentration of maleic anhydride is less clear [23]. It has been accepted that kinetic models derived from the reaction scheme presented in Figure 2.2 are a good approximation when the concentration of benzene is high and the formation of side-products, such as phenol and quinone, can be neglected. More comprehensive studies have taken into account the oxidation of benzene as well as the oxidation of maleic anhydride, quinone, and phenol [18].

Table 2.2. Catalytic oxidation of benzene: kinetics

Reaction Conditions		Catalyst	Kinetic expression	Kinetic Order ^a	Ref.
T [°C]	P [kPa]				
375-400	$p_B = 0.3-0.6$ $p_{O_2} = 20$	V ₂ O ₅ -MoO ₃ on Al ₂ O ₃	$r = kp_B$	1 st on B ~ 2 nd on M	[17]
450-530	$p_B \sim 1.3-2.6$ $p_{O_2} \sim 22$	Ag ₂ O, V ₂ O ₅ , MoO ₃ , Al ₂ O ₃ on SiC	-	1 st on B	[17]
325-450	$p_B = 1-2$ $p_{O_2} = 20$	V ₂ O ₅ on Al ₂ O ₃	-	1 st on B	[17]
377	$p_B = 0.1-4$ $p_{O_2} = 10-101$	V ₂ O ₅ -MoO ₃ on Al ₂ O ₃	$1/r = 1/k_1 p_B + \beta/k_2 p_{O_2}$	$p_B < 6$, 1 st on B $p_B > 6$, 0 th on B $p_{O_2} < 200$, 1 st on O ₂ $p_{O_2} > 300$, 0 th on O ₂	[25]
380-440	$C_B = (0.1-1.4) \times 10^{-3}$ mol/L $C_{O_2} = (1-3.2) \times 10^{-3}$ mol/L	V ₂ O ₅ -MoO ₃ on corundum	$C_{O_2} < 4 \times 10^{-3}$, $r = [O_2]^2/[M]^{0.74} (k_1[B]^{0.78} + k_3[B]^{0.71})$ $C_{O_2} > 4 \times 10^{-3}$, $r = 1/[M]^{0.74} (k_1[B]^{0.78} + k_3[B]^{0.71})$	$C_{O_2} < 4 \times 10^{-3}$, 2 nd on O ₂ $C_{O_2} < 4 \times 10^{-3}$, 0 th on O ₂	[18]

^a Kinetic order for the overall disappearance of benzene (B = benzene, M = maleic anhydride)

2.2.2 Naphthalene Oxidation

The oxidation of naphthalene to phthalic anhydride is commercially one of the most important vapor-phase catalytic oxidations of aromatic compounds. The first commercial process started operation in 1916.

Industrially, naphthalene oxidation is presently carried out in fixed-bed reactors operating in the temperature range 340-380 °C and using supported vanadium oxide catalysts [26][27]. Current processes are flexible and allow for using dual feedstocks, i.e. mixtures of naphthalene and *o*-xylene [26]. In recent years, the use of *o*-xylene as the main raw material has spread due to its lower cost, good availability and ease of transportation [28].

Compared to benzene, the presence of a second aromatic ring in the naphthalene molecule increases the complexity of the reaction network. Several parallel and consecutive reactions take place in this case. Even though naphthoquinone is a key intermediate in the reaction sequence, phthalic anhydride is not formed exclusively through this compound. Production of maleic anhydride and carbon oxides as secondary products has been reported [28].

Figure 2.3 presents the generally adopted reaction scheme. Naphthalene is oxidized by three independent routes. Production of phthalic anhydride and 1,4-naphthoquinone represents the most important primary reactions [17]. The distribution of these products may vary according to the initial point of attack in the naphthalene molecule [17]. It has been stated that for the sake of completeness, 1,2-naphthoquinone should be indicated as an intermediate in reaction (1); however, this compound is usually neglected because of its rapid oxidation to phthalic anhydride [27]. Naphthalene is also directly oxidized, to a much lesser extent, to maleic anhydride and carbon oxides [17][27]. Secondary reactions are also important in this network. Typically, a large fraction of the 1,4-naphthoquinone formed is further oxidized to give phthalic anhydride, while a small portion contributes to the production of maleic anhydride and carbon oxides. Similarly, part of the phthalic anhydride formed by reactions (1) and (3) is oxidized to give maleic anhydride and carbon oxides. Production of aromatic acids, i.e. phthalic and benzoic acids has

also been reported [16]. For reactor design purposes, the kinetic scheme of naphthalene oxidation may be simplified to reactions (1) to (4) [27], as discussed later on in this section.

It is believed that the stepwise oxidation of the naphthalene ring to form phthalic anhydride proceeds by a similar mechanism to that of benzene oxidation to form maleic anhydride. The formation of the 1,4-naphthoquinone (α -quinone), which is the equivalent of the quinone in benzene oxidation, supports this premise [16]. The formation of the 1,4-naphthoquinone also points out the difficulty of breaking the aromatic structure. The oxidation of the naphthalene molecule may be analyzed in three steps: addition of oxygen into the structure, breaking of one of the two rings in naphthalene and further destruction of the remaining benzene ring [16].

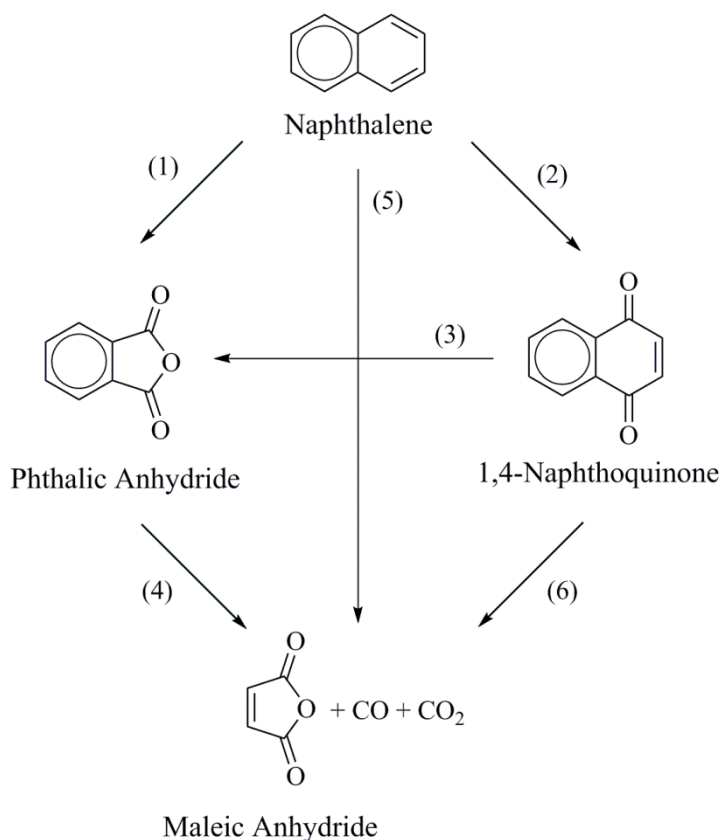


Figure 2.3. Naphthalene oxidation reaction scheme

At ambient conditions naphthalene is inert to air (oxygen) and cannot be partially oxidized. Therefore, the use of higher temperatures is required. In the absence of a catalyst, two scenarios

are possible [16]. First, oxidation at high temperature (i.e. at a temperature high enough for the reaction rate to be significant) favors total combustion over partial oxidation. Second, oxidation at moderate conditions promotes addition reactions (condensation reactions) and polymerization of the intermediates due to the longer reaction times needed to achieve significant conversion. The use of an appropriate catalyst is essential to control the reaction selectivity.

Transition metal oxides of the fifth and sixth groups of the periodic table have been the candidates of choice. Vanadium and molybdenum oxides as well as tin and bismuth vanadates have been tested as catalysts for this reaction [16][17]. Oxides of magnesium, aluminum, silicon, titanium, zirconium, copper and cobalt have shown rather poor performance in naphthalene oxidation [16]. Catalysts based on vanadium oxides are quite active and can cause over-oxidation to maleic anhydride or carbon oxides. Strict control of the reaction residence time or addition of less active oxides to the catalyst (e.g. manganese, copper or cobalt oxides) are common practices to avoid this problem [16]. For vanadium-based catalysts, yields to phthalic anhydride of more than 70% have been reported [17]. Similarly, selectivities towards phthalic anhydride of nearly 90% have been achieved using mixtures of V_2O_5 and K_2SO_4 supported on SiO_2 , i.e. commercial type of catalysts [29]. A great deal of information on the catalysts used for naphthalene oxidation is found in the patents while only some is found in the journal literature. There is no recent review dealing with commercially used catalysts for naphthalene oxidation. A valuable discussion on the parameters affecting the catalytic performance of vanadium-based catalysts (e.g. V_2O_5 concentration, active sites, role of alkali metal sulfates, among others) can be found in [28]. In addition, a compilation of the catalysts and conditions used in naphthalene oxidation can be found in [17].

The reaction mechanism and kinetics of naphthalene oxidation have been extensively studied. Yet, they are not completely elucidated. As mentioned in the previous section on benzene oxidation, it has been found that naphthalene oxidation also proceeds through a redox mechanism [25]. In other words, the aromatic hydrocarbon reacts with a metal oxide catalyst to give the oxidized products and a partially reduced catalyst; then, the catalyst is reoxidized by gas phase oxygen. Hence, the kinetic expression derived before, Eq. 7, can be used to describe this reaction too. At constant oxygen partial pressure, Eq. 7 can be rearranged to Eq. 8.

$$r_N = \frac{k_1 p_N}{1 + k_1 C p_N} \quad (\text{Eq. 8})$$

Where,

$$C = \frac{\beta}{k_2 p_{O_2}^m} \quad (\text{Eq. 9})$$

The latter expression shows that at low partial pressures of naphthalene (p_N), the oxidation rate should approach first-order in naphthalene concentration; whereas, at high partial pressures of naphthalene, it should approach zero-order in this reactant [17]. A number of kinetic studies using vanadium-based catalysts, namely V_2O_5 and $K_2S_2O_7$ or K_2SO_4 supported on SiO_2 , are in agreement with this behavior. Mars and Van Krevelen investigated the effect of naphthalene and oxygen pressure on the rate of naphthalene oxidation [25]. According to their work, the rate is approximately first-order with respect to naphthalene at $p_N < 0.5$ kPa, but it is almost independent of the naphthalene concentration at $p_N > 1$ kPa. A similar trend was observed by *Calderbank* [30], who studied the reaction over the range of naphthalene concentrations of 2-10 kPa, and by *Ioffe* and *Sherman* [31], who explored the pressure range 0.7-1.5 kPa. On the other hand, the dependence of reaction rate on the concentration of oxygen was found to vary almost linearly with the O_2 concentration in the region of oxygen partial pressures below 40 kPa [25].

Valuable compilations of kinetic studies for naphthalene oxidation were prepared by *Dixon* and *Longfield* [17] and *Wainwright* and *Foster* [28]. In general, reactions (1) to (4) in [Figure 2.3](#) appear to depend on the concentration of both oxygen and the organic reactant to an order between 0.5 and 1.0 [17]. The observed differences in individual studies are attributed to the variation in the reaction conditions rather than a real effect. There is little consistency in the reaction temperature, catalyst, reactor type and conversion achieved in the reported studies; therefore, comparisons are not easy [28].

2.2.3 Anthracene and Phenanthrene Oxidation

The catalytic vapor-phase autoxidation of anthracene to anthraquinone with yields of 85–90 % has been described in patents in the 1930's and has found some industrial application [1][17]. The vapor-phase oxidation of anthracene with air is the preferred synthesis method to produce

9,10-anthraquinone [32], and >90 % yield is possible. However, the most wide-spread use of oxidation in relation to anthracene, is the use of the autoxidation-and-reduction cycle of 9,10-dihydroxyanthracene and anthraquinone to produce hydrogen peroxide [1], as illustrated by Figure 2.4.

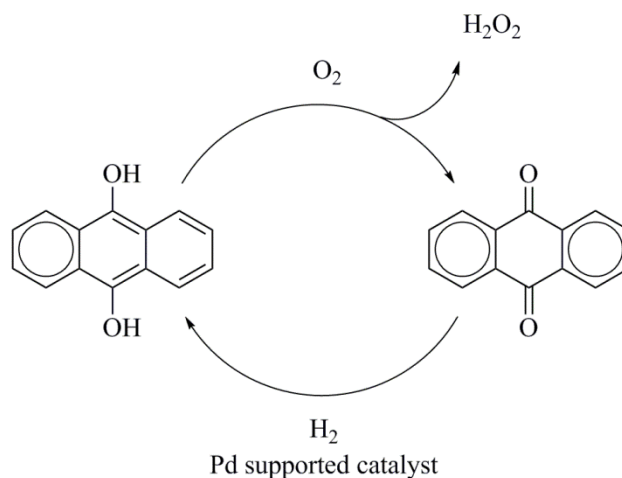


Figure 2.4. Catalytic hydrogen peroxide production through the anthraquinone process

Vapor-phase catalytic oxidations of anthracene and phenanthrene have been less extensively investigated compared to benzene and naphthalene oxidation. The additional aromatic ring further increases the complexity of the reaction network. Thus, depending on the position of attack and the extent of the reaction, oxidation products from the inner and outer rings are possible. As in other aromatic oxidations, achieving selectivity is a challenge and using an appropriate catalyst to promote the production of the desired products is necessary.

Almost complete conversion of anthracene with high selectivity to 9,10-anthraquinone is possible and 9,10-anthraquinone of 99% purity is industrially produced in this way [32]. Secondary and complete combustion products are also obtained in small amounts. Carbons in the 9- and 10-positions are the most reactive centers of attack in the anthracene molecule [6]. The attack of oxygen on these carbons results in the production of 9,10-anthraquinone. On the other hand, the unselective oxidation of the carbons in the 1- to 4-positions, i.e. carbons in the outer ring, gives ketone (1,4-antraquinone) and anhydride (2,3-naphthalic anhydride and piromellitic

anhydride) species as by-products [33]. Production of small quantities of phthalic anhydride, maleic anhydride, CO and CO₂ has also been reported [16][33][34]. The higher selectivity of the oxidation reaction can be explained in terms of the Clar-formalism [35], noting that in anthracene additional stabilization of the outermost rings can be achieved if the π -electrons on the 9,10-positions are more localized.

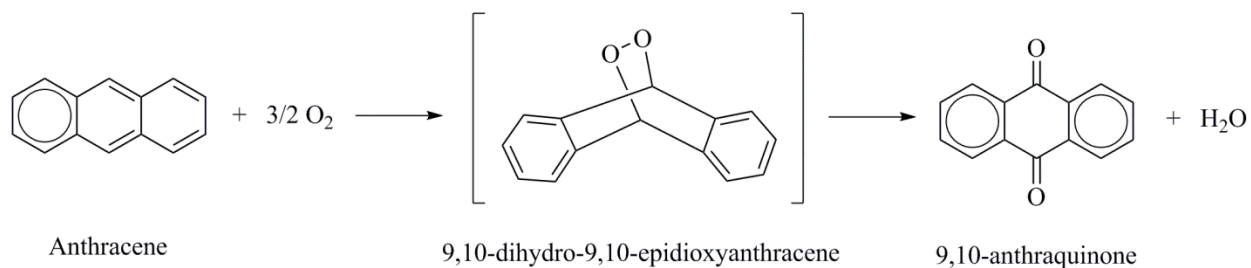


Figure 2.5. Vapor-phase oxidation of anthracene

The overall reaction for vapor-phase anthracene oxidation is shown in Figure 2.5. The oxidation process involves the interaction of one hydrocarbon molecule with three oxygen atoms. However, the actual reaction mechanism is more complex than that. With the localization of the π -electrons on the 9,10-positions, not only does the transannular addition of oxygen take place, but two aromatic sextets are also formed. Even more, the removal of hydrogen from an aromatic carbon is not required for oxidation to take place. The addition of oxygen causes the carbons at the 9,10-positions to change from sp^2 to sp^3 hybridized carbons. In other words, these carbons are now benzylic aliphatic carbons with a much weaker C–H bond, which facilitates hydrogen abstraction by further reaction with oxygen.

It has been suggested that the catalytic conversion takes place in two steps, which are in agreement with the Mars-Van Krevelen mechanism [17][25]. First, anthracene is oxidized by a metal oxide catalyst producing anthraquinone and water; during this step the oxide catalyst is reduced. Second, the catalyst is re-oxidized by gas phase oxygen to return to its original state.

Vanadium oxide, iron vanadate or vanadic acid doped with alkali or alkaline earth metal ions are suitable catalysts for anthracene oxidation [16][33][34]. Industrially, the reaction has

been carried out at temperatures in the range 320 to 390 °C and using catalysts consisting of V_2O_5 , K_2SO_4 and Fe_2O_3 on pumice; yields of 95-97 wt% of anthraquinone were reported [17]. A reaction scheme derived from the oxidation of anthracene using V_2O_5 - MoO_3 - P_2O_5 and V_2O_5 - Fe_2O_3 as catalysts can be found [33]. In this case, oxidation at the inner and outer rings of anthracene leads to 9,10-anthraquinone, 1,4-anthraquinone, and 2,3-naphthalic anhydride. At high conversion, the selectivities towards these compounds decreases and production of phthalic anhydride, piromellitic anhydride and CO_2 is favored.

The liquid-phase oxidation of anthracene and 9,10-anthraquinone has been investigated by thermal analysis [36]. In this study, a number of metal oxides (V_2O_5 , MoO_3 , Fe_2O_3 and NiO) were evaluated as catalysts. Among them, V_2O_5 showed the highest catalytic contribution during reaction; it measurably accelerated the autoxidation of both aromatic compounds. Experiments to determine whether this oxide just activated the O_2 from air, or whether oxidation took place by transfer of lattice oxygen were also performed. Interestingly, reaction under nitrogen atmosphere confirmed that V_2O_5 was capable of using the lattice oxygen for oxidation of anthracene and 9,10-anthraquinone in the liquid-phase. A Mars-Van Krevelen mechanism was likely.

Phenanthrene is used for industrial production of 9,10-phenanthrene quinone as well as diphenic acid by vapor-phase oxidation over vanadium-based catalysts [33]. Same as anthracene, the 9- and 10-carbons in the phenanthrene molecule are much more reactive than the other ones, and so the 9- and 10-positions are the preferred centers of attack [6]. As in the case of anthracene, this is explained by the Clar-formalism [35]. Selective oxidation on these carbons gives the 9,10-dione; whereas, further reaction produces anhydride (diphenic anhydride), lactone (2-hydroxy-diphenyl-2'-carboxylic acid lactone) and ketone (9-fluorenone) species as side-products [33]. When oxygen attacks the carbons on the outer rings (not preferred pathway), 1,2-naphthalic anhydride is produced [33]. On the other hand, a number of experimental studies taking place in the temperature range 370 to 440 °C and using vanadium pentoxide, mixtures of vanadium and molybdenum or iron oxides and tin vanadates as oxidation catalysts resulted in the production of phthalic anhydride and phthalic acid [17].

The reaction network for phenanthrene's oxidation is presented in Figure 2.6. The scheme was derived from the study of the reaction over V_2O_5 supported on SiO_2 with and without K_2SO_4 [37]. Phenanthrene is oxidized by two independent routes, which are governed by the position of attack, i.e. oxidation in the inner or outer rings.

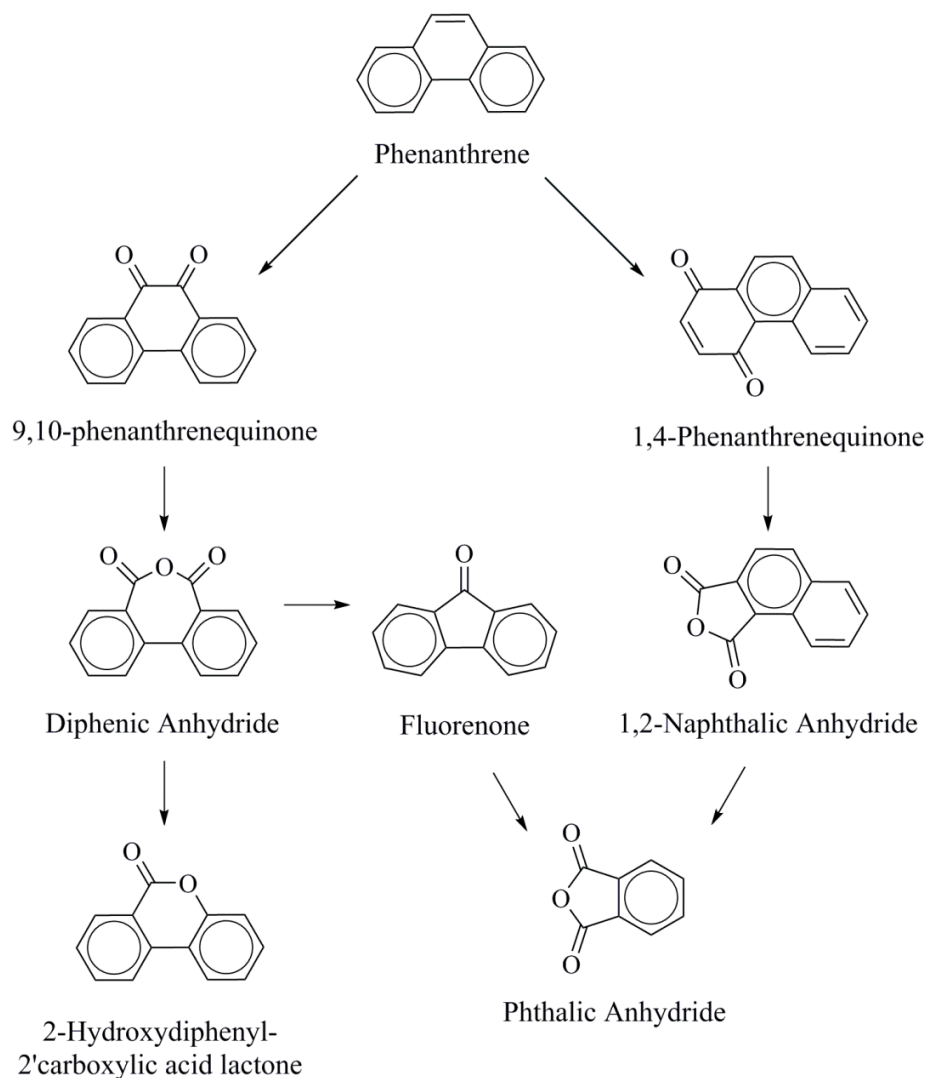


Figure 2.6. Phenanthrene oxidation reaction scheme

Compared to the benzene or naphthalene cases, there are a lot fewer publications dealing with the kinetics of the vapor-phase anthracene and phenanthrene oxidation. Mars and Van Krevelen found that at anthracene partial pressures > 0.1 kPa, the reaction rate was essentially

independent with respect to the concentration of the aromatic reactant [25]. In addition, the reaction rate showed some dependence on oxygen over the entire concentration range (oxygen partial pressures up to 100 kPa). Pyatnitskii derived a kinetic expression for aromatic oxidations [38] based on the work of Mars and Van Krevelen. In his work, the two independent steps of the redox mechanism (Eq. 1 and 2) were written as:

$$r_{Ar} = k_{Ar} p_{Ar} \theta^a \quad (\text{Eq. 10})$$

$$r_{o_2} = k_{o_2} p_{o_2}^m (1 - \theta)^b \quad (\text{Eq. 11})$$

Where, a and b are the orders with respect to adsorbed oxygen and to oxygen vacancies on the catalyst surface, respectively. These equations reduce to Eq. 3 and Eq. 4 when $a = 1$ and $b = 1$. In steady state:

$$r_{Ar} = r_{o_2} / \nu \quad (\text{Eq. 12})$$

Where, the number of oxygen molecules required to oxidize one aromatic molecule (Ar) to the products P_1, P_2, \dots, P_i , is represented by the stoichiometric coefficient (ν) as follows:

$$\nu = \nu_1 S_1 + \nu_2 S_2 + \nu_3 S_3 + \dots + \nu_i S_i \quad (\text{Eq. 13})$$

In which S_i is the selectivity for P_i and ν_i corresponds to the number of oxygen molecules necessary to oxidize one aromatic molecule to P_i . By replacing Eq. 10 and Eq. 11 in Eq. 5, it can be seen that the surface concentration of oxygen is a function of the ratio of the partial pressures of oxygen and the aromatic hydrocarbon (P_{O_2}/P_{Ar}):

$$\frac{\theta^a}{(1-\theta)^b} = \frac{k_{o_2}}{k_{Ar}} \frac{1}{\nu} \frac{p_{o_2}}{p_{Ar}} \quad (\text{Eq. 14})$$

For the simplest case $a = b = 1$, and combining Eq. 11 and Eq. 14, the total rate of oxidation can be expressed as:

$$r_{Ar} = \frac{k_{Ar}k_{O_2}p_{Ar}p_{O_2}}{(k_{O_2}p_{O_2} + v k_{Ar}p_{Ar})} \quad (\text{Eq. 15})$$

The kinetic expression (Eq. 15) derived in Pyatnitskii's work describes the oxidation of anthracene on V_2O_5 - K_2SO_4 with Fe_2O_3 and SiO_2 , and on $CoMoO_4/SiO_2$ [38]. On the other hand, the kinetics of the oxidation of phenanthrene is best described with empirical power law equations [38]. It is worth to mention that the rate of oxidation of phenanthrene is less than that of anthracene over the same V_2O_5 - K_2SO_4/SiO_2 catalyst.

2.2.4 Reactor Engineering

Vapor-phase catalytic aromatic oxidations are strongly exothermic reactions. Furthermore, the heat released is always greater than the calculated heat of reaction of the main reaction, due to side-reactions leading to the formation of CO_2 . For instance, while the heat of oxidation of naphthalene to phthalic anhydride corresponds to 1880 kJ/mol, in practice, due to over-oxidation the total heat liberated can reach 2900 kJ/mol [39].

Aromatic oxidation requires large amounts of heat to be removed from the reaction zone to maintain the temperature and keep the overall process under control. An uncontrolled reaction would cause a severe reduction of yields (complete combustion would be favored) as well as the loss of catalyst life [23]. Furthermore, it is a self-amplifying problem, i.e. an increase in temperature causes more combustion reactions that would further increase the temperature. Proper reactor design and heat management are therefore key aspects in industrial processes. Reaction at near-isothermal conditions is preferred in order to maintain optimal catalyst efficiency and product selectivity. Multitubular reactors and fluidized beds with heat exchange internals have been widely used for this purpose; after all, these configurations are suitable to minimize the temperature gradients across the catalyst bed.

Most of the processes for industrial production of maleic anhydride from benzene use multitubular reactors. A typical reactor contains a bundle of 10000 – 15000 vertical tubes, ~25 mm in diameter, enclosed by a jacket through which cooling medium circulates [23]. During operation, the reaction gas flows through the tubes and over the catalyst, while the process

pressure is kept between 0.15-0.25 MPa [19]. Circulating heat-transfer fluids or agitated eutectic salt mixtures are commonly used to deal with the large duty [23]. Steam, which can be used in other operations, is generated from the heat removed. Nearly 27 MJ of heat are dissipated per each tonne of reacted benzene, which translates to the production of almost 10 tonnes of saturated steam per tonne of reacted benzene [19]. Considering that the reaction is conducted at temperatures $>300\text{ }^{\circ}\text{C}$, production of high-pressure steam, typically 4-5 MPa steam, is possible.

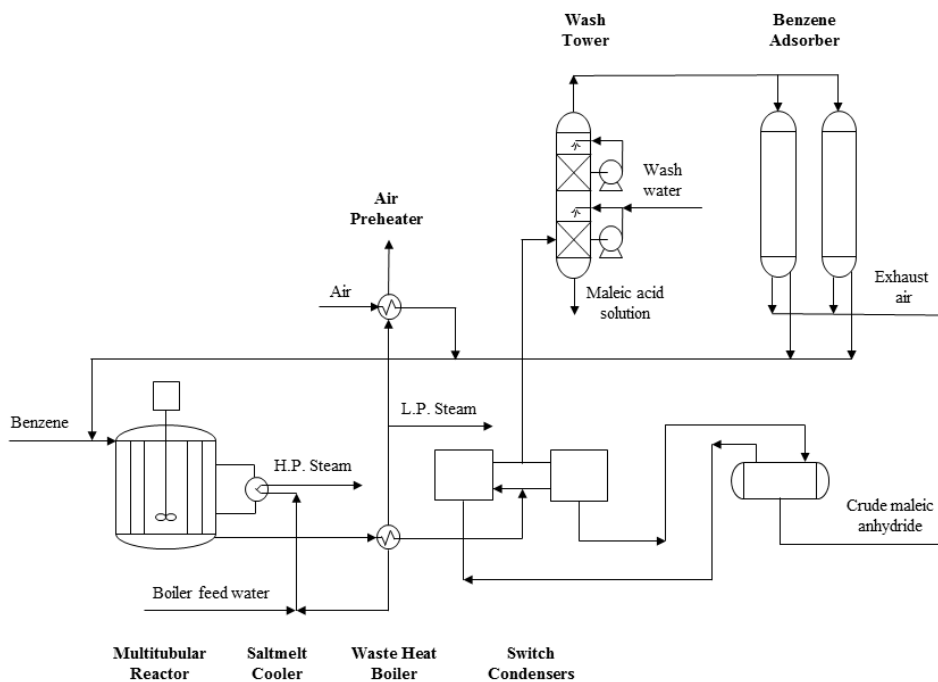


Figure 2.7. Ruhrol-Lurgi process for production of maleic anhydride by benzene oxidation

A typical flow diagram of a process using a multitubular reactor for benzene oxidation [23] is presented in Figure 2.7. In this configuration, a mixture of benzene and preheated air is reacted in the multitubular reactor. The conversion of benzene is not complete. The feed-product heat exchange decreases the duty of the feed preheating. On the other hand, switch condensers allow for recovering close to 90% of the maleic anhydride produced in the reaction. Refining of this product is completed later on by batch distillation. The remaining 10% of maleic anhydride is recovered in a two-stage scrubber unit using water and dilute alkali. Fumaric acid is also

obtained in this process. The unconverted benzene is separated from the exhaust air by adsorption with activated carbon, and it is returned as part of the reactor feed.

Control of the reaction temperature during catalytic aromatic oxidation can also be achieved using fluidized bed reactors [23]. Some commercial plants employ this technology to oxidize naphthalene to phthalic anhydride. Thus, during typical operation, liquid naphthalene is fed at the bottom of the catalyst bed; after instant evaporation, it distributes over the entire fluidized bed. Oxygen fed through a distributor plate is mixed with the vaporized naphthalene. The reaction temperature is kept in the range 345-385 °C through heat exchanger tubes in the fluidized bed. Moreover, a uniform temperature profile is obtained because of the intense agitation and mixing of the catalyst in the fluidized bed. High-pressure steam (> 4 MPa) is produced from the heat removed [40].

Table 2.3. Heat evolved during aromatic oxidation

Aromatic hydrocarbon	Overall oxidation reaction	$\frac{\Delta H^a}{[\text{kJ/mol}]}$	Ref.
Benzene	$C_6H_6 + 4\frac{1}{2}O_2 \rightarrow C_4H_2O_3 + 2CO_2 + 2H_2O$	-1917	
Naphthalene	$C_{10}H_8 + 4\frac{1}{2}O_2 \rightarrow C_8H_4O_3 + 2CO_2 + 2H_2O$	-1881	[16]
Anthracene	$C_{14}H_{10} + \frac{3}{2}O_2 \rightarrow C_{14}H_8O_2 + 2H_2O$	-559	

^a Theoretical heat of reaction (Heat released per mol of aromatic hydrocarbon reacted)

The increase in size for aromatic hydrocarbons, which is represented by the number of aromatic rings in a molecule, has an effect on the calculated (theoretical) heat of reaction. According to Table 2.3, the heat liberated during oxidation to the main oxidation product decreases in the order benzene > naphthalene > anthracene. As the molecules become heavier, fewer oxygen atoms react per mole of aromatic substrate to produce the main product, and so considerably, less heat is released. Irrespective of the aromatic feed, successful selective oxidation requires proper heat management.

2.3 Oxidation of Heterocyclic Aromatics

The selective oxidation of heterocyclic aromatics involves the same types of reaction as noted for the aromatic hydrocarbons [9], but added differentiation is required to distinguish between carbon oxidation and heteroatom oxidation. The general types of reactions are (Figure 2.8):

- (a) Formation of oxygenates by carbon oxidation without the cleavage of the aromatic rings, e.g. formation of coumaranone from benzofuran and the polymerization of pyrrole.
- (b) Formation of oxygenates by heteroatom oxidation without the cleavage of the aromatic rings, e.g. formation of benzothiophene-1,1-dioxide from benzothiophene.
- (c) Formation of oxygenates accompanied by the cleavage of carbon-carbon bonds of the aromatic rings, e.g. formation of N,2-(cyclopenta-1,5-dione)-aniline from 2,3-cyclopenteno-indole [41]. However, it should be noted that oxidative carbon-carbon scission in heterocyclic aromatic rings appears to be rare.
- (d) Formation of oxygenates accompanied by the cleavage of carbon-heteroatom bonds of the heterocyclic aromatic rings, e.g. *o*-nitrobenzopropenoic acid from quinoline.
- (e) Formation of oxygenates by oxidation of the side chains attached to the aromatic rings. e.g. oxidation of 4-methyl-pyridine to pyridine-4-carboxylic acid.

Of these reaction types, only (a)–(d) will be considered. It is also possible for oxidation of the multinuclear aromatics to take place on a carbocyclic ring that does not contain a heteroatom, as was discussed in the previous section. One variation on reaction types (a) and (b) is reactions leading to the formation of addition products. Oxidative addition does not necessarily lead to oxygen incorporation into the product.

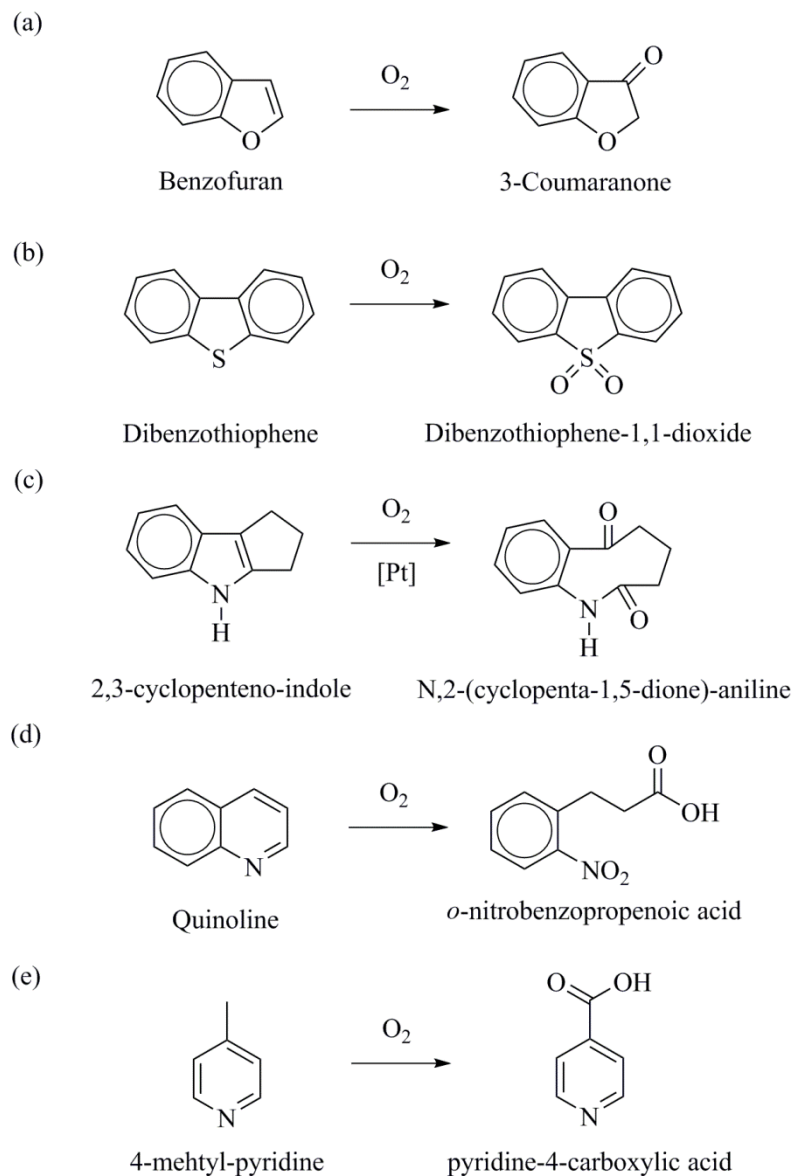


Figure 2.8. Examples of heteroaromatic oxidation involving **(a)** carbon oxidation without the cleavage of the aromatic rings, **(b)** heteroatom oxidation without the cleavage of the aromatic rings, **(c)** cleavage of carbon-carbon bonds of the aromatic rings, **(d)** cleavage of carbon-heteroatom bonds of the heterocyclic aromatic rings, **(e)** oxidation of the side chains attached to the aromatic rings

Even though selective oxidation is a direct and economic route to convert aromatic hydrocarbons into valuable chemicals, the scenario for heterocyclic aromatics is a little different.

Oxidation with air of these compounds as a synthesis route to obtain added value products is not reported in standard texts [42][43]. Their oxidation chemistry is rather discussed as part of the crude oil processing and fuel stability. For instance, sulfur- and nitrogen-containing compounds are typically undesired materials in crude oil. The oxidation of these compounds (i.e. oxidative desulfurization and oxidative denitrogenation) to give chemically modified products with properties that favor their separation or removal has been explored [44][45]. Furthermore, it is known that autoxidation of nitrogen heterocyclic aromatics plays a role in the formation of heavy addition products, e.g. nitrogen-containing compounds seem to be related with the formation of sludge in fuels [46], thereby affecting fuel storage stability.

The oxidation of the distinct aromatic heterocyclic compound classes is considered in the following sections. Emphasis is placed on the chemistry of five-membered heterocyclic compounds that contain sulfur, nitrogen, and oxygen, as well as on their benzologs. Some comments regarding the chemistry of pyridine, a nitrogen-containing six-membered heterocyclic compound, are also included as part of the discussion.

2.3.1 Oxidation of Aromatic S-heterocyclic Compounds

The first class of aromatic heterocyclic compounds considered in this work corresponds to the sulfur-containing compounds, which are represented by thiophene and its benzologs, e.g. benzothiophene and dibenzothiophene (Figure 2.9). These molecules are typically found in the heavier fractions of crude oil [47]. Refining of crude oil to final products, such as fuels and some petrochemicals, requires desulfurization of the oil. However, the sulfur contained in aromatic rings is more difficult to remove than aliphatic sulfur using traditional technologies, e.g. hydrodesulfurization (HDS) and thermal conversion [47].

Oxidation of thiophene and its benzologs as an alternative approach to HDS for sulfur removal has received a lot of attention. Oxidative desulfurization involves two steps. First, the reaction between an oxidant and sulfur alters the nature of the sulfur-containing compounds. Second, the properties of the oxidized products are exploited to facilitate their removal [44]. Oxidation with air has been extensively evaluated.

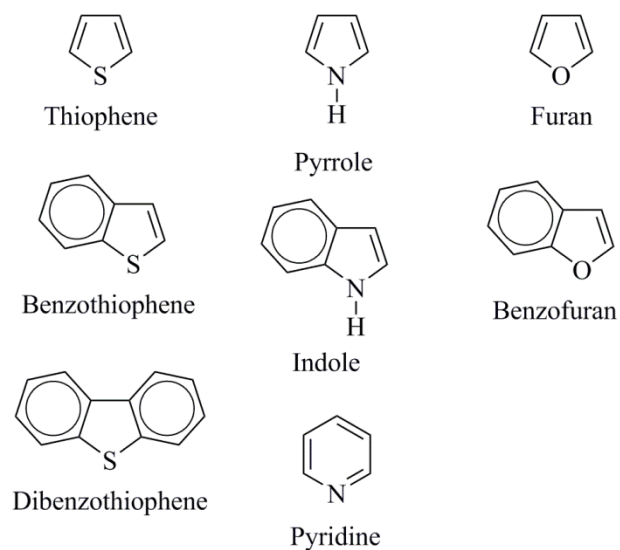


Figure 2.9. Examples of heterocyclic aromatic compounds

Autoxidation of S-heterocyclic aromatics involves the formation of hydroperoxides by oxidation of aliphatic compounds that are already present or are added to the reaction mixture. Hydroperoxides are key intermediates formed *in situ* by the oxygen. The thiophenic sulfur is subsequently oxidized by the hydroperoxides, rather than by oxygen directly (free radical chemistry). The chemistry taking place during the first step of this conversion illustrates the oxidative behavior of S-heterocyclic compounds in the presence of air. The thiophenic sulfur is oxidized to sulfoxides and sulfones (Figure 2.10).

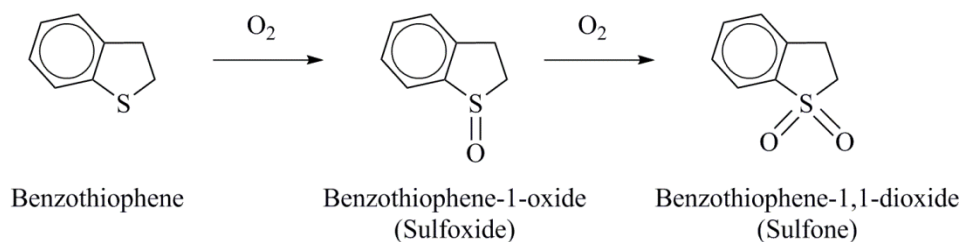


Figure 2.10. Oxidation of sulfur compounds by oxygen in air, as illustrated by the oxidation of thiophene

Table 2.4. Desulfurization of model mixtures and industrial feedstocks by liquid phase oxidation with air

Feed	Oxidant	Catalyst	Oxidation conditions	Comments	Ref.
Straight-run Kerosene	O ₂	Non-catalytic oxidation	120–200 °C 5–20 min High pressure Presence of water	Stirring rate and resident time affected the degree of oxidation of sulfur containing compounds.	[49]
Model Oil & Hydrodesulfurized Diesel Fuel	Air	Non-catalytic oxidation	140 °C Atm. Pressure	Lactones (e.g. γ -butyrolactone) used as solvents play a role on the oxygen-transfer.	[50]
Model Jet fuel & Real Jet fuel (JP-8)	O ₂	Fe (III) salts (nitrate and bromide)	25 °C 2–5 h	Oxidation reactivity sequence between ASBP, BP and DBP was evaluated ^a . Aldehydes were used as sacrificial materials to produce, with the oxygen fed, <i>in situ</i> peracids to oxidize the sulfur containing compounds.	[51]
Model Oil & Diesel fuel	O ₂	Co (II) salts (acetate and chloride)	40 °C Atm. pressure	Aldehydes were used as sacrificial materials to produce, with the oxygen fed, <i>in situ</i> peracids to oxidize the sulfur containing compounds.	[52]
Atmospheric residue	Air / O ₂	Pt, Pd, Ni, V (their salts or oxides)	130–180 °C 2–20 h	Metals catalyze decomposition of organic hydroperoxides.	[53]

^a ASBP: alkyl-substituted benzothiophene. BP: benzothiophene. DBP: dibenzothiophene

Moreover, thiophenes that could be considered refractive to HDS, are readily oxidized because of their increased electron density on the sulfur atom [48]. Temperatures below 200 °C

and pressures near atmospheric pressure are usual for oxidation of heterocyclic sulfur. Typical conditions for oxidative desulfurization processes are given in [Table 2.4](#).

Autoxidation of S-heterocyclic aromatics can also be performed using a catalyst or oxygen carrier, instead of employing free radical autoxidation. Catalysts facilitate the decomposition of hydroperoxides, and in doing so, accelerate the propagation step during autoxidation. Oxygen carriers, on the other hand, are more active oxidation agents than oxygen. Depending on their nature, they can be viewed as a type of catalyst which can be regenerated using molecular oxygen, i.e. oxidation by the Mars-Van Krevelen mechanism; this characteristic make their behavior similar to the one observed for metal oxides in the selective oxidation of aromatic compounds, as discussed in the previous section. Additional details on the topic can be found in [\[54\]](#).

The C-S bond strength is decreased when the sulfur is oxidized, which in principle allow the cleavage of the C-S bonds by catalytic [\[55\]](#), or by thermal decomposition. These assertions are based on the published homolytic bond dissociation energies for sulfones. In the case of a diaryl sulfone, which is representative of the sulfone group in dibenzothiophene-1,1-dioxide, the bond dissociation energy is reportedly 288 kJ/mol [\[56\]](#). However, this value was found to be inconsistent with the thermal stability of diaryl sulfones that suggested a much stronger bond [\[57\]](#).

Autoxidation of sulfur-containing compounds can also lead to the formation of addition products. For instance, a model oil consisting of *n*-heptane and dibenzothiophene reacted with air at 145-170 °C and atmospheric pressure resulted in the formation of some heavier products [\[58\]](#). In this case, besides the typical products involving the formation of both sulfoxides (dibenzothiophene-1-oxide) and sulfones (dibenzothiophene-1,1-dioxide), the formation of sediments was observed. This precipitation process involves a type of chemistry analogous to that explaining the gum formation, a common problem that undermines storage stability of transportation fuels. In the proposed reaction pathway, a sulfoxide reacts with a hydroperoxide to give an intermediate product that may be decomposed by reaction with another sulfoxide to yield an addition product [\[58\]](#).

The thiophene ring system, unless carrying electron-donating substituents, is relatively stable to atmospheric oxidation [59], and resist the action of moderate oxidizing agents [42][43]. Oxygen and peracids are known to preferentially attack the sulfur atom [43], while stronger oxidants are required to actually attack the aromatic carbons. Ozone, for example, attacks the double bond between the aromatic carbons which results in the cleavage of the ring; thus, oxidation of benzothiophene with ozone yields *o*-mercaptobenzaldehyde [59]. Similarly, strong oxidants, e.g. nitric acid, are able to break down the aromatic ring to give maleic and oxalic acids, while the ring sulfur is oxidized to sulfuric acid [59].

It is evident that oxidation chemistry of sulfur-containing compounds, using O₂ as oxidant, is simpler than the one observed for aromatic compounds, due to the high selectivity of autoxidation to oxidize the heterocyclic sulfur. In this case, there are no complex reaction networks. The formation of oxygenates by oxidation of the heteroatom is actually the main oxidative transformation. Even for addition reactions to take place, oxidation of the sulfur plays a role and autoxidation of the aromatic carbons is not observed except at extreme (combustion) conditions.

2.3.2 Oxidation of Aromatic N-heterocyclic Compounds

The second class of aromatic heterocyclic compounds examined in this work corresponds to the nitrogen-containing compounds. Examples of N-heterocyclic compounds are pyrrole, indole and pyridine (Figure 2.9). Aromatic nitrogen-containing compounds present in crude oil are normally classified in two categories: basic (derivatives of pyridine) and non-basic (derivatives of pyrrole). Irrespective of the category, these compounds are associated with a number of different problems during oil processing and their removal is desirable [45].

Oxidation of nitrogen-containing compounds has been explored as an alternative approach to traditional practices such as hydrodenitrogenation (HDN) by hydrotreating. Even though the fundamental idea behind this process, i.e. oxidative denitrogenation, is very similar to those of oxidative desulfurization (the aim is to produce chemically modified products that can be more

efficiently extracted from oils using polar solvents), very little has been reported on the topic [45].

Few studies dealing with the oxidation of industrial feedstocks have been reported, and in those cases the oxidation of the S- and N-containing compounds has been performed simultaneously [60][61]. The purpose of oxidative denitrogenation is mainly to remove basic nitrogen-containing compounds. Typical reaction conditions involve temperatures around 70 °C and atmospheric pressure. Peracetic acid or mixtures of hydrogen peroxide and acetic acid have been used as oxidizing agents to convert pyridines into N-oxides. While sulfones and sulfoxides are easily obtained during oxidative desulfurization, products of polymeric nature are obtained after the oxidation of N-heterocyclic aromatics [60]. It will be shown that this is due to the oxidation of pyrroles and not due to the oxidation of pyridines.

Because the oxidation chemistry of pyrroles and pyridines is quite different, some comments for each class of compound will be made in the following sub-sections in a separate manner.

2.3.2.1 Oxidation of Pyrroles

Simple pyrroles are easily oxidized. Compounds containing a pyrrole ring, such as indoles and carbazoles, have a negative effect on the oxidative stability of jet fuels [62]. The effect of pyrroles on color and sediment formation in fuels has been documented and explained through a number of oxidation and polymerization reactions [63]. These are all industrially important fouling reactions.

However, the nature of the products depends on the strength of the oxidizing agent. Strong oxidants, such as chromium trioxide in aqueous sulfuric acid, often lead to complex breakdown products. When the ring survives, maleimide derivatives are obtained [42]. Milder oxidants such as hydrogen peroxide convert pyrroles to pyrrolines [59]. In the case of oxygen, which is the oxidant of interest in this work, pyrrolic compounds autoxidize to form dark colored pigments known as “pyrrole black” [64][65]. In oil fractions exposed to air, pyrroles autoxidize to form so-called “red tars” [43][64]. Irrespective of the name, pyrrole black or red tar, these are all

mixtures of pyrrole addition products. Oxidative addition of pyrroles is due to aromatic carbon oxidation [64], a variation on the reaction type (a) shown in Figure 2.8.

The autoxidation of 2,5-dimethylpyrrole is presented in Figure 2.11 to illustrate how a typical reaction of a pyrrolic compound with air takes place. The first step corresponds to the formation of a molecular association complex (I) between the oxygen and the pyrrolic compound. Then, the electron transfer from the pyrrole nucleus of the complex to the oxygen produces a charge-transfer complex (II), which is suggested to be in equilibrium with an endoperoxide (III) [65]. Alkylated pyrroles and pyrroles having electron-donating substituents are more susceptible to oxidation than those having electron-withdrawing substituents [64]. Pyrroles that have a ketone or ester substituent are also more resistant to ring degradation and yield side-chain oxidation products [42].

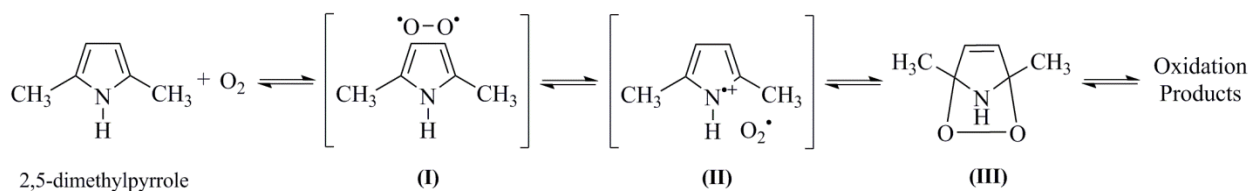


Figure 2.11. Oxidation of pyrrolic compounds by oxygen in air, as illustrated by the oxidation of 2,5-dimethylpyrrole

The oxidation chemistry of pyrrole and the corresponding benzopyrrole (indole) is quite similar. The presence of the benzene ring changes the preferred position of attack for oxidants from carbon in the 2- and 5-positions in the former to carbon in the 3-position in the latter [59]; however, it does not suppress the susceptibility of the pyrrole ring to give addition products [64]. The carbon adjacent to the nitrogen atom in a pyrrole ring is readily oxidized, which ultimately leads to oxidative coupling and formation of polymeric or addition products [64].

Depending on the conditions of the reaction, indole addition may or may not involve the incorporation of oxygen. In the presence of air and light, indole is autoxidized to give indoxyl which further reacts to produce indigo [43]. Indigo is a molecule containing two oxygen atoms

and it is the reaction product from two indole molecules. The nature of the reaction products found after the catalytic oxidation of indole using Mn(II)porphyrins as catalyst, suggested that the mechanism of indole addition involves both oxygen incorporation and hydrogen disproportionation [66]. On the other hand, a selectivity close to 90% towards oxidative addition product formation was found during the low temperature air oxidation of indole [67]. In this case, no evidence for oxygen incorporation in the products was found suggesting that the addition mechanism did not require oxygen incorporation even though oxygen was necessary for the reaction to proceed.

2.3.2.2 Oxidation of Pyridines

The lone pair of electrons on the nitrogen atom that is available for bonding, without disturbing the aromaticity of the ring, makes pyridine chemistry quite distinct from that of pyrrole [68][67]. Pyridines are therefore bases. Because the pyridine ring is π -electron deficient and oxidants act as electron acceptors, the oxidation of the ring is difficult [43]. In fact, strong oxidants, e.g. neutral aqueous potassium permanganate, and vigorous conditions are required for its breakdown. Side chains may be oxidized to the corresponding carboxylic acid group without breaking the ring [42]. The nitrogen atom, on the other hand, is a center of high electron density and as such can be easily oxidized to give pyridine N-oxide [43]. Alkaline hydrogen peroxide and various peracids have been used with this purpose [69].

It has been reported that quinoline is not autoxidized under mild reaction conditions (oxidation with air at 130 °C for 6 h) [67]. Oxygen, hydrogen peroxide and hydroperoxides in the absence of carboxylic acids are incapable of oxidizing the pyridinic nitrogen. The acid-base interaction between the peracid and the pyridine is consequently important for the reaction to proceed.

2.3.3 Oxidation of Aromatic O-heterocyclic Compounds

The last class of aromatic heterocyclic compounds considered in this work, corresponds to the oxygen-containing compounds, for example furan and benzofuran (Figure 2.9).

Of the mononuclear five-membered heterocyclic compounds, i.e. thiophene, pyrrole and furan, furan has the least aromatic character [68]. As a result, its chemistry is, to some extent, different from that described for thiophene and pyrrole. Furan is particularly sensitive to oxidation. In the presence of oxygen or air, it is unstable [43]. The autoxidation of furan involves the 1,4-addition of oxygen to the diene system to give the transannular peroxide. Further reaction opens the aromatic ring by producing succinaldehyde (Figure 2.12) [43].

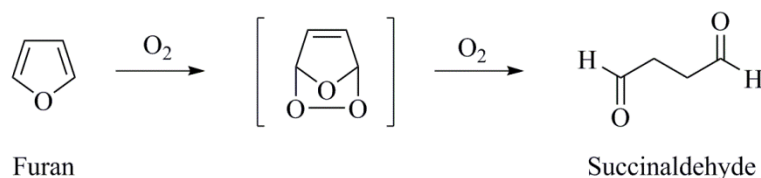


Figure 2.12. Oxidation of furan with air as oxidant

On the other hand, the vapor-phase catalytic oxidation of furan and its derivatives, using air as oxidant, produces maleic acid as the main reaction product [70]. Formation of small amounts of acetic and oxalic acids have also been reported [71]. Typical oxidation conditions involve the use of vanadium-based catalysts for reaction in the temperature range 290-410 °C [70][72]. During catalytic oxidation, furan derivatives have to undergo oxidative elimination of the side chain [72]. Substituents are oxidized to furan carboxylic acids, which are then decarboxylated to furan (Figure 2.13). As of this point, the reaction involves the formation of an endoperoxide, followed by the formation of malealdehyde and finally maleic acid [71]. Substituents on the aromatic ring influence the reaction rate and decrease the yield to maleic acid [72].

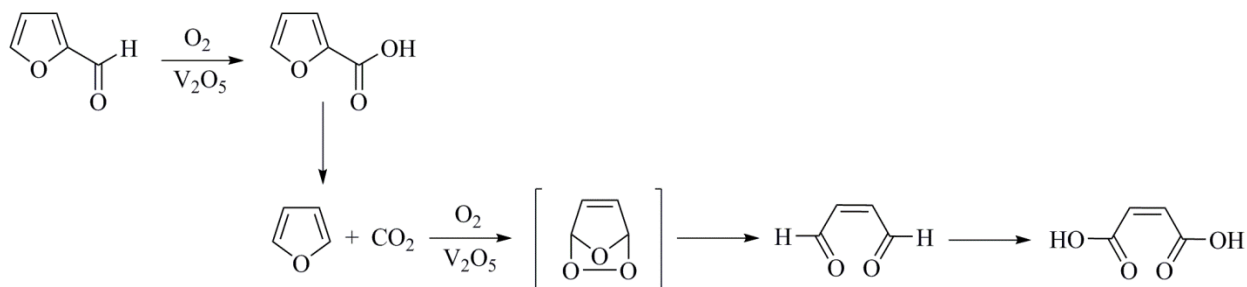


Figure 2.13. Oxidation of furan and furan derivatives using V_2O_5 as catalyst and air as oxidant

Details on the oxidation of furan using singlet oxygen (photochemical oxidation) as well as other oxidants common to the organic chemists can be found in [42][71][73].

The reactivity of benzofuran is different from that of furan. The oxidation of benzofuran with air is not reported on in standard texts [42][62][43], or in specialized texts [74]. In fact, it seems that oxidation of this oxygen-containing compound requires the use of a catalyst to enable oxidative addition (coupling) reactions [75][76][77]. On the other hand, low temperature autoxidation of benzofuran resulted in the formation of addition products [67]. In this case, the experimental evidence indicated that coumaranone, the ketone obtained by oxidation of benzofuran, was a key intermediate in the oxidative dimerization process. Carbon-carbon coupling through the 2- and 3- positions of the furan ring in this ketone compound led to the addition product.

2.4 Discussion

2.4.1 Reactivity of Aromatic Hydrocarbons towards Oxidation

2.4.1.1 The Aromatic Sextet

Even though aromatic compounds have been the center of countless studies, it is valuable to refer to two specific contributions in relation to the relative stability of aromatic compounds compared to cyclic aliphatic compounds and conjugated polyenes. Hückel's rule, given by the formula $4n + 2$, where n is zero or an integer, successfully explained the stability of benzene, compared to other monocyclic conjugated polyenes [78]. On the other hand, the Clar's π -sextet rule has enabled a description of the stability of polycyclic systems [79].

According to Clar's rule, the aromatic sextet or π -sextet is denoted by a circle. The appropriate way to draw Clar structures is explained in [80]. Due to the importance of the Clar description of multinuclear aromatics as way to explain the oxidation of aromatics, a brief

description is included here. Three simple rules are followed to build aromatic structures [80][81]:

- (1) Circles denoting π -sextets cannot be drawn in adjacent benzenoid rings. This representation would erroneously indicate the presence of 12 π -electrons, when in reality only 10 π -electrons are present.
- (2) On ignoring the rings with π -sextets, all other benzenoid rings must have a Kekulé structure. Hence, rings might have one or two double bonds, or might be empty but there must not be unpaired electrons.
- (3) Conditioned to the above constraints, a Clar structure must contain the maximum number possible of π -sextets. When dealing with a linear string of benzenoid rings (e.g. anthracene), the π -sextet can occupy any of the rings, which is designated by using an arrow.

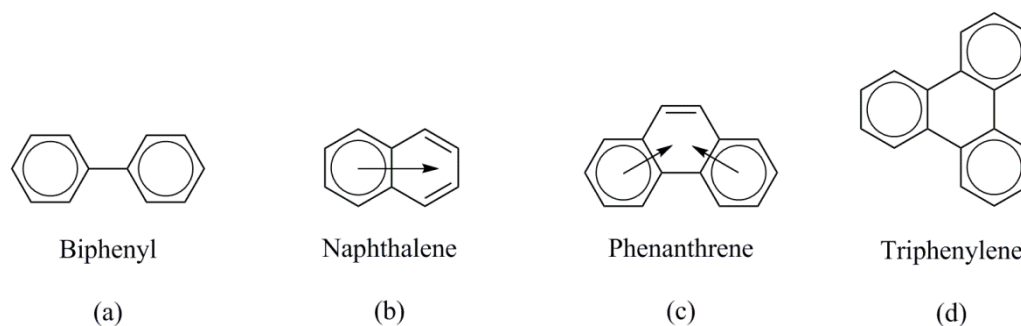


Figure 2.14. Types of aromatic rings according to Clar's π -sextet

Clar's rule classifies aromatic rings into four categories [35], as illustrated by Figure 2.14:

- (a) **Rings having localized π -sextets.** Aromatic rings having a localized π -sextet, also known as benzenoid rings, display benzenoid-like stability [82]. Benzenoid rings are considered to be the most aromatic centers in the polyaromatic hydrocarbons; other rings are less aromatic in comparison, and so, are chemically more reactive than the benzenoid rings [79].

- (b) **Rings sharing a migrating π -sextet.** Some multinuclear aromatics can be represented by more than one Clar structure. The aromatic sextet in naphthalene can exist in any of the two rings. However, resonance makes the rings in this molecule equal in terms of electron density, and so, it is not possible to assign the π -sextet to any one ring alone. Instead, the π -sextet migrates between the rings as denoted by the arrow in [Figure 2.14b](#). In linear acenes, the benzenoid character of the π -sextet is diluted when increasing the length of the hydrocarbon [\[82\]](#); higher acenes are much more reactive due to migration of the π -sextet and loss of the aromatic nature.
- (c) **Rings with localized double bonds.** In some cases, the presence of rings with localized π -sextets leads to the formation of true double bonds. For instance, the outer rings in phenanthrene exhibit a local aromaticity and have more aromatic character than the central ring [\[79\]](#); as a result, two external π -sextets and a central double bond are formed ([Figure 2.14c](#)). This double bond is as reactive as any olefinic double bond [\[35\]](#).
- (d) **Empty rings.** The so-called empty rings refer to those rings without π -electrons. They are found in “fully benzenoids” structures ([Figure 2.14d](#)).

For multinuclear aromatics in which different Clar structures are possible, the one with the greatest number of aromatic sextet carbons is preferred [\[83\]](#). Aromatic compounds with a higher fraction of aromatic sextet carbons are more stable, compared to those with a higher fraction of isolated double bonds [\[83\]](#).

2.4.1.2 Influence of Structure on Oxidation Reactivity

The Clar formalism is a valuable tool to rationalize the reactivity of multinuclear aromatics towards oxidation. Formulas with π -sextets not only indicate the stability of a molecule but also point out to the reactive positions on the ground state [\[82\]](#). Thus, the structure of an aromatic compound can be related with the type of oxidation chemistry observed; it also explains the differences in reactivity among aromatic hydrocarbons.

Figure 2.15 presents the structures of multinuclear aromatics consisting of three fused rings arranged in different geometric configurations. The oxidation chemistry of these compounds, using oxygen as oxidant, will be discussed to illustrate the use of the Clar formalism in explaining oxidation reactivity of multinuclear aromatics.

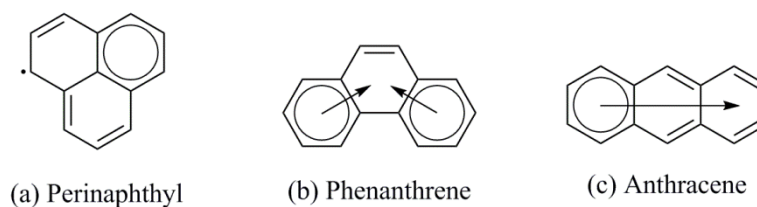


Figure 2.15. Clar formalism applied to aromatic compounds having three fused rings

The triangular building principle results in aromatic hydrocarbons that form radicals [82]. The first member of this series corresponds to perinaphthyl (Figure 2.15a). Four resonance structures of this compound have been reported [84]. An aromatic sextet and double bonds are possible, but more importantly, a permanent free radical is present. Due to the diradical nature of oxygen, it can directly perform addition without prior hydrogen abstraction or any other electronic rearrangement (Figure 2.16a). This radical-radical coupling should have the lowest activation energy when comparing the oxidation chemistry of (a), (b) and (c) in Figure 2.15. Once the oxygen is added, the resonance in perinaphthyl is restricted. Only two of the rings can share a π -sextet, while, a double bond is formed on third one. Oxygen attack is likely to occur in the latter (reactive position).

The angular configuration of phenanthrene leads to the formation of two aromatic sextets in the outer rings (Figure 2.15b). The carbon atoms in these rings are quite stable, and so, difficult to oxidize. On the contrary, the double bond in the middle ring is very reactive. Oxygen can perform direct addition without previous hydrogen abstraction to give a diradical species: a free radical located on one of the carbons involved in the double bond, and another radical situated on the second oxygen of the O_2 molecule that was added (Figure 2.16b). Further oxidation involves some electronic rearrangement and bond breaking. The hydrogen bonded to the carbon initially

attacked can migrate to stabilize the free charge on the second carbon. Similarly, additional hydrogen can stabilize the radical on the second oxygen atom (from the O₂ molecule added) forming a hydroperoxide. The now weaker O-O bond in the hydroxide species can be broken to give a ketone. On the other hand, oxidation of the second carbon of the double bond might involve hydrogen abstraction. It is expected that oxidation of phenanthrene requires more energy than oxidation of perinaphthyl.

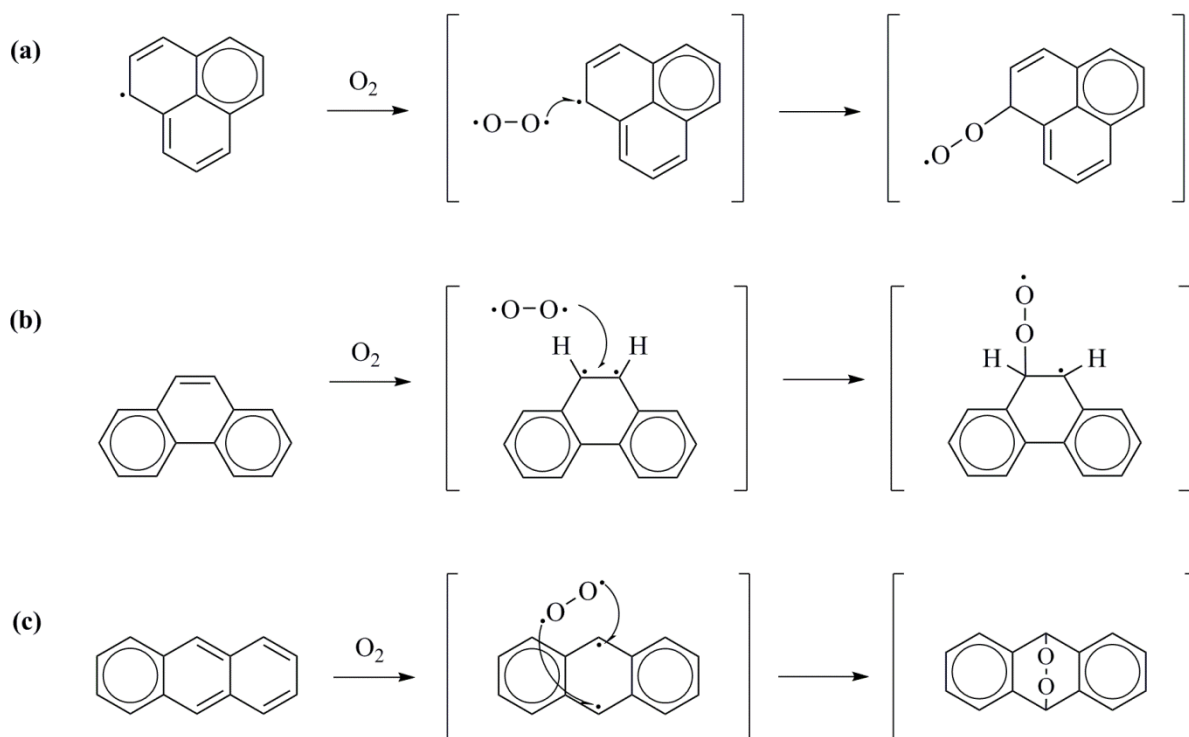


Figure 2.16. Pre-oxidative behavior of (a) perinaphthyl, (b) phenanthrene and (c) anthracene

Because anthracene is a linear aromatic hydrocarbon, one migrating π -sextet is shared between the three rings (Figure 2.15c). Although all carbons should have a similar reactivity, oxygen preferentially attacks the middle ring, namely the 9,10-positions. This corresponds to the resonance structure with two aromatic sextets in the outer rings and a diradical on the 9,10-positions. During autoxidation, the resonance electronic structure of the molecule is disturbed and the two π -electrons at the 9- and 10-position become localized, allowing the oxygen to be added to these two non-adjacent carbons through a *para*-attack (Figure 2.16c). Moreover, the

transannular addition of oxygen is favored by the formation of two aromatic sextets in the outer rings of the oxidized product, i.e. 9,10-anthraquinone. The reactivity of the *para*-position, which is caused by the localization of two π -electrons, is important in the addition reactions of acenes [82]. The transannular addition of oxygen to the 9,10-positions in anthracene takes place more readily than oxygen addition to the 9,10-position in phenanthracene [6].

By comparing the oxidation chemistry of aromatic compounds consisting of three fused rings, it becomes evident that the structure influences the way in which oxygen can interact with a given substrate. The reactivity towards oxidation for linear, angular and condensed aromatic hydrocarbons is different.

2.4.1.3 Pre-oxidative Behavior of the Non-Catalytic Oxidation of Multinuclear Aromatics

Based on the work that appeared around the time that *Tipson* [6] was writing his review, advances were made in the understanding of how oxygen interacts with aromatics. The first “pre-oxidation” step, which also explained why fluorescence of aromatics was quenched in the presence of dissolved oxygen, was that the oxygen acted as an electron acceptor, with the aromatic molecule being the electron donor [6]. The initiation of oxidation of aromatic hydrocarbons appears to be different in its sequence to that found in aliphatic hydrocarbon oxidation. The latter involves hydrogen abstraction from the hydrocarbon being oxidized in order to form the free radicals required to start the chain process [85][86]. Hydrogen abstraction is not necessary for the pre-oxidative step in aromatic oxidation.

In anthracene the oxygen first adds in a transannular fashion to two carbons, which causes the carbons to change from sp^2 to sp^3 hybridized carbons. Only after this step is the hydrogen on the sp^3 hybridized carbon (non-aromatic hydrogen) abstracted, or transferred. Intermediate products, such as anthrone and oxanthrone were identified and reported in reaction products from the oxidation of anthracene [87]. In phenanthrene the oxygen first adds to one of the carbons in the double bond. This reaction can be described as radical addition to an olefin, which causes C–O bond formation with one of the carbons of the C=C group and the formation of a carbon centered radical on the other carbon. These carbons are no longer aromatic, but aliphatic, which

facilitates hydrogen migration, transfer and/or abstraction. In perinaphthyl the oxygen can directly perform addition; radical-radical coupling is energetically favorable. It can be seen that, regardless of the type of oxidation chemistry taking place, i.e. transannular oxygen addition, oxygen addition to a double bond or free radical chemistry, the first “pre-oxidation” step in aromatic oxidation does not involve hydrogen abstraction as is the case in aliphatic autoxidation. In fact, it facilitates subsequent hydrogen abstraction.

2.4.2 Reactivity of Oxygen towards Heterocyclic Aromatics

It has been shown that oxygen can directly interact with multinuclear aromatics (carbocyclic rings) to oxidize the aromatic carbons. The way in which O₂ interacts is influenced by the peculiarities of the structure of the aromatic substrate, which dictates the most reactive positions. The reactivity towards oxidation in heterocyclic aromatic hydrocarbons is in turn influenced by the presence of a heteroatom in an aromatic ring.

In the case of S-heterocyclic aromatic compounds, autoxidation in the liquid phase involves the formation of hydroperoxides species by oxidation of molecules other than the S-heterocyclic aromatic. Oxidation of thiophenes is achieved by the hydroperoxides, rather than by oxygen itself. Furthermore, the process is highly selective and the oxidation of the heterocyclic sulfur, to give sulfoxides and sulfones, is the main oxidative transformation. Vapor-phase oxidation of S-heterocyclic aromatic compounds requires different conditions and takes place by a catalytic process. In this case, the oxidation of the S-containing compounds yields sulfur dioxide and sulfur trioxide and smaller aromatic compounds compared to the initial molecules. Metal oxides or salts of metals having several oxidation states are used as catalysts [88].

Autoxidation of N-heterocyclic aromatic compounds follows different chemical routes depending on the basic or non-basic character of the nitrogen atom. Oxidation of the pyridinic nitrogen with air is difficult. Other oxidants, e.g. peracids, have been used to convert pyridines into N-oxides. On the other hand, oxidation of pyrroles is readily achieved by oxygen. In this case, the main oxidative transformation involves the oxidation of the aromatic carbons to form products of polymeric nature (addition products), in which oxygen might or might not be present.

In the case of O-heterocyclic aromatic compounds, the reactivity towards autoxidation of furan and its derivatives is quite different of that of benzofuran and its benzologs. Oxygen can readily attack the aromatic carbons of furan to ring-open the structure. On the other hand, autoxidation of the aromatic carbons of the 5-membered ring in benzofuran leads to addition products.

2.4.3 Catalysis in Aromatic Oxidation

Transition metal oxides, in particular vanadium oxides, are the most important catalysts in industrially successful processes for the selective oxidation of aromatics with air (see [Section 2](#)). A detailed discussion on the catalytic chemistry of vanadium oxides dealing with topics such as redox behavior, geometry of the catalyst surface, role of the carrier, among others, can be found in [\[89\]](#).

The vapor phase oxidation of aromatic hydrocarbons occurs mainly by the two-step Mars-Van Krevelen mechanism [\[25\]](#). In the first step, the aromatic hydrocarbon is oxidized by oxygen from the oxide lattice. Desorption of the oxygenated product forms an oxygen vacancy and leaves an active site in a reduced state at the surface of the catalyst [\[1\]](#). In the second step, reoxidation of the catalyst active site takes place. This process is achieved either by incorporation of gas phase oxygen or by diffusion of bulk lattice oxygen [\[1\]\[90\]](#).

Gaseous oxygen is adsorbed on metal oxides surfaces in the form of activated electrophilic species, i.e., O^- (oxide) or O_2^- (superoxide) species, before being incorporated into the lattice in the form of nucleophilic oxygen, i.e., O^{2-} (oxide ion) species [\[8\]](#). The contribution of non-lattice oxygen to oxidation has not been completely ruled out [\[89\]](#). The role of the different oxygen species in catalytic oxidation processes has been extensively discussed and a rigorous discussion on the topic can be found in [\[91\]](#). For metal oxides with a significant mobility of lattice oxygen, regeneration of the catalyst by diffusion of bulk oxide ions is very efficient; in these cases, the dead time of the active sites is short and the turn-over frequency is high [\[1\]](#).

It has been suggested that the activity and selectivity of metal oxides towards hydrocarbon oxidation depends on the metal-oxygen (M-O) bond strength within the catalyst [92]. Oxides with strong M-O bonds are likely to retain their oxygen making them inactive for oxidation. On the contrary, oxides with weak M-O bonds are likely to give their oxygen away, which might lead to rapid but unselective oxidation. To achieve high selectivity, oxides with M-O bonds of intermediate strength should be present in the catalyst.

M-O bond strengths have been measured using different approaches. *Andersen and Kung* [93] correlated the differential heat of reoxidation, measured by calorimetry, with the reaction selectivity for the oxidative dehydrogenation of butane on V_2O_5/Al_2O_3 . In this case, the selectivity was low when the heat of reoxidation was small but it increased with the increase in the heat of reoxidation. Results suggested that the heat of reoxidation measures the M-O bond strength and indicates the ease of removal of lattice oxygen. *Simons et al.* [94] studied the interaction between 1-butene and butadiene with a series of metal oxides (MnO_2 , V_2O_5 , CuO , Co_3O_4 , Fe_2O_3 , NiO , TiO_2 , SnO_2 , ZnO and Cr_2O_3) over the temperature range 300-600 °C. They related the M-O bond strength with Q_o , a single parameter that represented the heat necessary to dissociate $\frac{1}{2} O_2$ from the oxide catalysts. Their work indicated that catalytic activity decreased with increasing the M-O bond strength, i.e., high values of Q_o , and that a maximum of selectivity could be obtained for intermediate M-O bond strength, i.e., values of Q_o of 210-250 kJ/mol (50-60 kcal·mol⁻¹).

Regardless of the complexity of the chemistry of metal oxide catalysts in aromatic oxidation, there are a few comments that are worth making. First, the action of oxygen as oxidant of multinuclear aromatics includes the addition to a double bond, addition to *p*-centers (transannular addition) and formation of *o*-, pseudo-*p*- or *p*-diones (Figure 2.17) [6]. These primary pathways do not rely on the presence of a metal oxide catalyst, e.g. V_2O_5 . However, the selective formation of oxygenates accompanied by the cleavage of the aromatic rings has only been successful at industrial level when catalyzed by metal oxides, e.g. V_2O_5 . Second, catalytic aromatic oxidation has a significant effect on minimizing undesired side reactions, i.e. network of free radical reactions and total combustion. Metal oxide catalysts may enable transition states that would not require the aromatic carbons to assume a free radical nature. Also, catalysts

enable conversion processes requiring lower oxidation temperatures, which inherently reduces losses due to combustion reactions. Third, metal oxides accelerate selective oxidation of aromatics. By accelerating selective oxidation compared to other oxidation reactions, catalysts facilitate the production of intermediate oxidation products, namely the desired products, to be isolated in commercial yields under controlled reaction conditions.

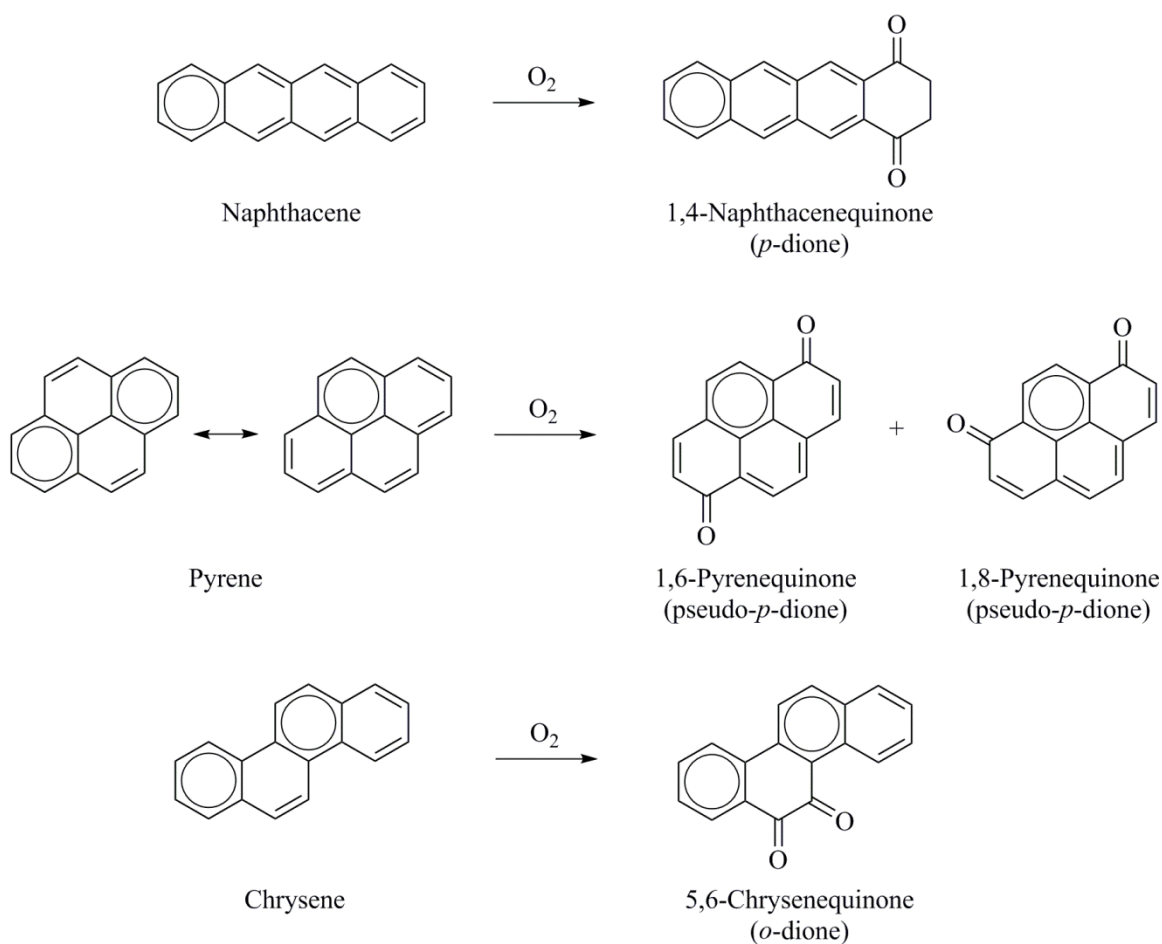


Figure 2.17. Types of diones obtained by oxidation of multinuclear aromatics

2.4.4 Implications for Industrial Use

Production of oxygenated chemicals by the oxidation of aromatic hydrocarbons with oxygen can be considered an industrially proven technology (Section 2.2). These processes make use of

purified hydrocarbons as starting materials. The same principle applies to oxidation with oxygen for the manufacturing of smaller volume chemical products, which were not reviewed.

As explained in the introduction, the review was motivated by the potential use of autoxidation to add value to materials that contain a high concentration of multinuclear aromatics in a mixture, such as heavy oil, bitumen, and coal liquids. The application that appears to have the most scope for value addition is the use of O₂ instead of H₂ as reagent for ring-opening of multinuclear aromatics. The purpose of ring-opening is to ultimately convert the multinuclear aromatics into smaller and/or less refractory molecules for refining to transport fuels and chemicals.

Oxidative degradation is a recurring theme in the literature on coal conversion and in particular, the wet oxidative conversion of coal to lower molecular mass coal acids [95][96][97][98]. Although it was found that oxidation using O₂ was slower compared to chemical oxidation [99], the outcome was similar.

The oxidative ring-opening of some multinuclear aromatic compounds appear to be quite facile, for example, oxidation pathway of benzo[a]pyrene with O₂ leads primarily to the ring-opened product [100]. Low temperature wet oxidative dissolution of coal with O₂ was reported to achieve dissolution yields of around 70 % [97][98].

Analogous claims were made for petroleum derived asphaltenes, but these could not be substantiated [101]. Oxidative hardening appears to dominate the autoxidation of heavy petroleum fractions [7]. Conversion leading to oxidative addition reactions is related to the presence of specific compound classes [67].

The implication for the potential industrial application of autoxidation for ring-opening of multinuclear aromatics is far reaching. It implies that when addition-prone compound classes are present, a non-radical pathway for oxidative ring-opening must be employed. This is possible by catalytic oxidation, for example, by making use of metal oxide catalysts. It remains to be seen

whether catalysts can be employed with heavy oil and bitumen in a way that would enable acceptable catalyst cycle times and catalyst life time for practical industrial application.

2.5 Conclusions

Heavy aromatic feed materials, e.g. coals liquids, bitumen and heavy oils could potentially benefit from conversion by oxidation with air. Oxygen may act as a reagent to ring-open multinuclear aromatics and give smaller and/or less refractory compounds for refining to transportation fuels and petrochemicals. Based on these premises, this work reviewed the autoxidation chemistry of the atoms that are part of an aromatic ring structure, i.e., aromatic carbons and heteroatoms contained in an aromatic ring.

The following observations were made from the available literature on selective catalytic oxidation of aromatic hydrocarbons:

- (a) Production of oxygenates accompanied by cleavage of the aromatic rings has only been successful at industrial scale when catalyzed by transition metal oxides, in particular vanadium oxides. Catalyzed processes operate in the temperature range 320–450°C.
- (b) The catalytic action of metal oxides involves (i) minimizing the undesired reactions, i.e. free radical chemistry and total combustion, by preventing the formation of transition states that are of free radical nature, (ii) lowering the oxidation temperatures, which helps controlling the selectivity losses due to total combustion, and (iii) accelerating selective oxidation compared to other oxidation reactions, which facilitates the isolation of intermediate oxidation products at commercial yields.
- (c) The chemistry of metal oxide catalysts in aromatic oxidation is complex. Even though processes have been described by the two-step Mars-Van Krevelen mechanism, a redox mechanism which states that oxidation takes place by transfer of lattice oxygen, the contribution of non-lattice oxygen to oxidation has not been completely ruled out.

- (d)** The absence of a metal oxide catalyst is detrimental for the reaction selectivity. Depending on the temperature of reaction, non-catalyzed oxidation favors total combustion over partial oxidation or promotes addition reactions (condensation and polymerization reactions).

There are significant differences in the autoxidation chemistry of heterocyclic aromatics compared to that of multinuclear hydrocarbon aromatics (carbocyclic rings that do not contain heteroatoms). Some points to consider are:

- (e)** The way in which oxygen interacts with heterocyclic aromatic compounds during oxidation is influenced by the nature of the heteroatom present in an aromatic ring.
- (f)** Liquid-phase oxidation of S-heterocyclic aromatics is achieved by hydroperoxides species, rather than by oxygen itself. The oxidation of the aromatic sulfur to form sulfoxides and sulfones species is the main oxidative transformation.
- (g)** Oxidation of N-heterocyclic aromatics depends on the basic or non-basic character of the nitrogen atom. Pyridines do not interact directly with oxygen and so, oxidation to give N-oxides requires the use of other oxidants, e.g. peracids. Pyrroles readily interact with oxygen; oxidation of the aromatic carbons leads to products that may or may not contain oxygen.
- (h)** The reactivity of oxygen towards O-heterocyclic aromatic compounds is quite different for furan and its derivatives compared to that of benzofuran and its benzologs. Oxidation of furan readily ring-opens the structure, whereas oxidation of benzofuran leads to addition products. The most common outcome is formation of heavier products by oxygen mediated addition reactions.
- (i)** With exception of furan and its derivatives, the oxidation with air of heterocyclic aromatics does not lead to ring-opening except at severe non-selective oxidation conditions (total combustion conditions).

The Clar formalism is a valuable tool in the understanding of the fundamentals of aromatic oxidation and its implications for industrial use. Some relevant comments are:

- (j) The interaction of oxygen with multinuclear aromatics is particular to their structure. As a result, fundamentally different oxidation chemistries are possible, namely, transannular oxygen addition, oxygen addition to a carbon-carbon double bond, or free radical chemistry.
- (k) The sequence during the initiation of the oxidation of aromatic hydrocarbons seems to be different compared to that found in aliphatic hydrocarbons. Regardless of the type of chemistry taking place, the first “pre-oxidation” step does not involve hydrogen abstraction.
- (l) Free radical oxidation can likely not be used for conversion of petroleum due to the loss in selectivity, e.g. addition reactions. The only realistic strategy for oxidative ring-opening of heavy aromatic feed materials is catalytic oxidation.

2.6 References

- [1] Heterogeneous hydrocarbon oxidation (ACS Symp. Ser. 638); Warren, B. K., Oyama, S. T. Eds.; American Chemical Society: Washington DC, 1996.
- [2] Sittig, M. Combine oxygen and hydrocarbons for profit; Gulf Publishing Company: Houston, TX, 1962.
- [3] Denisov, E. T.; Mitskevich, N. I.; Agabekov, V. E. Liquid-phase oxidation of oxygen-containing compounds; Consultants Bureau: New York, 1977.
- [4] Liquid phase oxidation via heterogeneous catalysis. Organic synthesis and industrial applications; Clerici, M. G., Kholdeeva, O. A. Eds.; Wiley: Hoboken, NJ, 2013.
- [5] Handbook of advanced methods and processes in oxidation catalysis. From laboratory to industry; Duprez, D., Cavani, F. Eds.; Imperial College Press: London, 2014.

- [6] Tipson, R. S. Oxidation of polycyclic aromatic hydrocarbons. A review of the literature (National Bureau of Standards Monograph 87); US Government Printing Office: Washington DC, 1965.
- [7] Petersen, J. C. Asphalt oxidation - an overview including a new model for oxidation proposing that physicochemical factors dominate the oxidation kinetics. *Fuel Sci. Technol. Int.* 1993, 11, 57-87.
- [8] Centi, G.; Cavani, F.; Trifiro, F. *Selective Oxidation by Heterogeneous Catalysis*; Kluwer Academic/Plenum Publishers: New York, 2001.
- [9] Lücke, B.; Martin, A. The Future Role of Aromatics in Refining and Petrochemistry, Proc. Of the DGMK-Conference on Petrochemistry, Erlangen, Germany, 1999, p 139.
- [10] The chemistry of the quinonoid compounds (2 Parts); Patai, S. Ed.; John Wiley & Sons: London, 1974.
- [11] Grzybowski, M.; Skonieczny, K.; Butenschön, H.; Gryko, D.T. Comparison of oxidative aromatic coupling and the Scholl reaction. *Angew. Chem. Int. Ed.* 2013, 52, 9900-9930.
- [12] Lücke, B.; Narayana, K.V.; Martin, A.; Jähnisch, K. Oxidation and Ammoxidation of Aromatics. *Adv. Synth. Catal.* 2004, 346, 4107-1424.
- [13] Song, N.; Zhang, D.; Huang, H.; Zhao, H.; Tian, F. Behavior of vanadium–phosphorus-oxides catalyst for butane oxidation to maleic anhydride in a single-tube packed bed reactor. *Catalysis Today* 1999, 51, 85-91.
- [14] Cavani, F.; Trifirò, F. Some innovative aspects in the production of monomers via catalyzed oxidation processes. *Applied Catalysis A: General* 1992, 88, 115-135.
- [15] Benzene and its industrial derivatives; Hancock, E. G. Ed.; Ernest Benn: London, 1975.
- [16] Marek, L. F.; Hahn, D. A. The catalytic oxidation of organic compounds in the vapor phase; Chemical Catalogue Company: New York, 1932.
- [17] Dixon, J. K.; Longfield, J. E. Hydrocarbon oxidation. In *Catalysis. Vol. VII. Oxidation, hydration, dehydration and cracking catalysts*; Emmett, P.H. Ed.; Reinhold: New York, 1960, p. 183-280.
- [18] Bielański, A; Haber, J. *Oxygen in Catalysis*; Marcel Dekker, Inc: New York, 1991.

- [19] Lohbeck, K.; Haferkorn, H.; Fuhrmann, W.; Fedtke, N. Maleic and Fumaric acids. In Ullman's Encyclopedia of Industrial Chemistry; Wiley-VCH Verlag GmbH & Co, Weinheim, 2012.
- [20] Bayne, J.; King, I. R.; Richard, M.; Laporte Industries Limited. Vapor Phase oxidation of benzene to maleic anhydride using an aluminum phosphate supported catalyst. Pat. Appl. US 3697550, 1972.
- [21] Di Cio, A.; Vitali, A.; Prolizenz AG. Oxidation of benzene to maleic anhydride using a new catalyst. Pat. Appl. US 3917655, 1975.
- [22] Barker, R. S.; Halcon International, Inc. Method of oxidizing benzene to maleic anhydride using a vanadium, molybdenum, boron, containing catalyst. Pat. Appl. US 3867412, 1975.
- [23] Trivedi, B. C.; Culbertson, B. M. Maleic Anhydride; Plenum Press: New York, 1982.
- [24] Bielański, A.; Najbar, M. V₂O₅-MoO₃ catalysts for benzene oxidation. Applied Catalysis A: General 1997, 157, 223-261.
- [25] Mars, P.; Van Krevelen, D. W. Oxidations carried out by means of vanadium oxide catalysts. Chem. Eng. Sci. Special Suppl., 1954, 3, 41-59.
- [26] Mason, R.T. Naphthalene. In Kirk-Othmer Encyclopedia of Chemical Technology; John Wiley & Sons, Inc. 2002.
- [27] De Maria, F.; Longfield, J. E.; Butler, G. Catalytic Reactor Design. Ind. Eng. Chem. 1961, 53, 259-266.
- [28] Wainwright, M. S.; Foster, N. Catalysts, Kinetics and Reactor Design in Phthalic Anhydride Synthesis. Catal. Rev. – Sci. Eng. 1979, 19, 211-292.
- [29] Dálessandro, A.F.; Farkas, J. The kinetics of the catalytic oxidation of naphthalene. Coll. Sci. 1956, 11, 653-670.
- [30] Calderbank, P. H. Ind. Chemist 1952, 28, 291.
- [31] Ioffe, I. I.; Sherman, Y. G. J. Phys. Chem. (U.S.S.R.) 1954, 28, 2095.
- [32] Cofrancesco, A. J. Anthraquinone. In Kirk-Othmer Encyclopedia of Chemical Technology; John Wiley & Sons, Inc. 2000.
- [33] Brückner, A.; Baerns, M. Selective gas-phase oxidation of polycyclic aromatic hydrocarbons on vanadium oxide-based catalysts. Applied Catalysis A: General. 1997, 157, 311-334.

- [34] Vogel, A. Anthraquinone. In Ullman's Encyclopedia of Industrial Chemistry. Wiley-VCH Verlag GmbH & Co, Weinheim, 2012.
- [35] Clar, E. The aromatic sextet; John Wiley & Sons: London, 1972.
- [36] Montoya Sánchez, N.; De Klerk, A. Oxidative ring-opening over metal oxides. Prepr. Pap.-Am. Chem. Soc., Div. Energy Fuels 2014, 59(2), 558-561.
- [37] Brooks, J. D. The catalytic oxidation of phenanthrene. J. Appl. Chem. 1955, 5, 250-260.
- [38] Pyatnitskii, Y. I. Heterogeneous catalytic oxidation of aromatic hydrocarbons in the gas phase. Russian Chemical Reviews 1976, 45 (8), 762-776.
- [39] Vrbaski, T. Oxidation of aromatic compounds. U.S. Patent 3,306,915, 1963.
- [40] Lorz, P. M.; Towae, F. K.; Enke, W.; Jäckh, R.; Bhargava, N.; Hillesheim, W. Phthalic Acid and Derivatives. In Ullmann's Encyclopedia of Industrial Chemistry. Wiley-VCH Verlag GmbH & Co, Weinheim, 2007.
- [41] Witkop, B.; Patrick, J.B.; Rosenblum, M. Ring effects in autoxidation. A new type of Camps reaction. J. Am. Chem. Soc. 1951, 73, 2641-2647.
- [42] Joule, J.A.; Mills, K. Heterocyclic Chemistry, 5th ed. Wiley: Chichester, U.K., 2010.
- [43] Bansal, R. K. Heterocyclic chemistry 4th ed. Anshan Ltd: Tunbridge Wells, 2008.
- [44] Javadli, R.; De Klerk, A. Desulfurization of heavy oil. Appl. Petrochem. Res. 2012, 1, 3-19.
- [45] Prado, G. H. C.; Rao, Y.; De Klerk, A. Nitrogen removal from oil: a review. Energy Fuels 2017, 31, 14-36.
- [46] Hardy, D. R.; Wechter, M. A. Characterization of soluble macromolecular oxidatively reactive species (SMORS) from middle distillate diesel fuels: Their origin and role in instability. Energy Fuels 1994, 8, 782-787.
- [47] Gray, M.R.; Ayasse, A.R.; Chan, E.W.; Veljkovic, M. Kinetics of hydrodesulfurization of thiophenic and sulfide sulfur in Athabasca bitumen. Energy Fuels 1995, 9, 500-506.
- [48] Ma, X.; Sakanishi, K.; Mochida, I. Hydrodesulfurization Reactivities of Various Sulfur Compounds in Vacuum Gas Oil. Ind. Eng. Chem. Res., 1996, 35, 2487-2494.

- [49] Paniv, P.M.; Pysh'ev, S.V.; Gaivanovich, V.I.; Lazorko, O.I. Current Problems, Nontraditional Technologies, Noncatalytic oxidation desulfurization of the kerosene cut, *Chem. Tech. Fuels. Oils*, 2006, 42, 159-166.
- [50] Xu, X.; Moulijn, J. A.; Ito, E.; Wagemans, R.; Makke, M. Deep desulfurization of fossil fuels by air in the absence of a catalyst. *Chem. Sustain.* 2008, 1, 817-819.
- [51] Ma, X.; Zhou, A.; Song, C. A novel method for oxidative desulfurization of liquid hydrocarbon fuels based on catalytic oxidation using molecular oxygen coupled with selective adsorption. *Catal. Today.* 2007, 123, 276-284.
- [52] Murata, S.; Murata, K.; Kidena, K.; Nomura, M. A novel oxidative desulfurization system for diesel fuels with molecular oxygen in the presence of cobalt catalysts and aldehydes. *Energ. Fuel.* 2004, 18, 116-121.
- [53] Ford, J.F.; Rayne, T.A.; Adlington, D.G. Desulfurization of hydrocarbons using oxidative and hydro-treatments. U.S. Patent 3,341,448, 1967.
- [54] Attar, A.; Corcoran, W.H. Desulfurization of organic sulfur compounds by selective oxidation. 1. Regenerable and nonregenerable oxygen carriers, *Ind. Eng. Chem. Prod. Res. Dev.*, 1978, 17, 102.
- [55] You, N.; Kim, M. J.; Jeong, K.; Jeong, S.; Park, Y.; Jeon, J. Catalytic Removal of Sulfur Dioxide from Dibenzothiophene Sulfone Over Mg-Al Mixed Oxides Supported on Mesoporous Silica. *Journal of Nanoscience and Nanotechnology* 2010, 5, 3663-3666.
- [56] Herron, J. T. Thermochemistry of sulfoxides and sulfones. In *The chemistry of sulphones and sulfoxides*; Pata, S., Rappoport, Z., Stirling, C. Eds.; John Wiley & Sons: Chichester, 1988, p 95-106.
- [57] Weh, R.; De Klerk, A. Thermochemistry of sulfones relevant to oxidative desulfurization. *Energy Fuels*, 2017, 31, 6607-6614
- [58] Javadli, R.; De Klerk, A. Desulfurization of Heavy Oils. Oxidative Desulfurization (ODS) As Potential Upgrading Pathway for Oil Sands Derived Bitumen. *Energy Fuels* 2012, 26, 594-602.
- [59] Katritzky, A. R. *Handbook of Heterocyclic Chemistry*, 1th ed. Pergamon Press: Oxford, 1985.

- [60] Ishihara, A.; Wang, D.; Dumeignil, F.; Amano, H.; Qian, E. W.; Kabe, T. Oxidative desulfurization and denitrogenation of a light gas oil using an oxidation/adsorption continuous flow process. *Appl. Catal., A* 2005, 279, 279–287.
- [61] Shiraishi, Y.; Tachibana, K.; Hirai, T.; Komasa, I. Desulfurization and denitrogenation process for light oils based on chemical oxidation followed by liquid-liquid extraction. *Ind. Eng. Chem. Res.* 2002, 41, 4362–4375.
- [62] Balster, L. M.; Zabarnick, S.; Striebitch, R. C.; Shafer, L. M.; West, Z. J. Analysis of polar species in jet fuel and determination of their role in autoxidative deposit formation. *Energy Fuels* 2006, 20, 2564-2571.
- [63] Oswald, A. A.; Noel, F. Role of pyrroles in fuel instability. *J. Chem. Eng. Data*, 1961, 6, 294-301.
- [64] Jones, R.A.; Bean, G.P. *The chemistry of Pyrroles*; Academic Press: London, 1977.
- [65] Jones, R.A. *Pyrroles*. Wiley: New York, 1990.
- [66] Linhares, M.; Rebelo, S. L.; Simões, M. M. Q.; Silva, A. M. S.; Graça, M.; Neves, P. M. S.; Cavaleiron, J. A. S.; Freire, C. Biomimetic oxidation of indole by Mn(III)porphyrins. *App. Catal. A*, 2014, 470, 427-433.
- [67] Siddiquee, M. N.; De Klerk, A. Heterocyclic addition reactions during low temperature autoxidation. *Energy Fuels* 2015, 29, 4236-4244.
- [68] Davies, D. T. *Aromatic heterocyclic chemistry*. Oxford University Press: Oxford, 1992.
- [69] Katritzky, A. R.; Lagowski, J. M. *Chemistry of the heterocyclic N-Oxides*; Academic Press: London, 1971.
- [70] Milas, N. A.; Walsh, W.L. Catalytic oxidations I. Oxidations in the furan series. *J. Am. Chem. Soc.*, 1935, 57, 1389-1393.
- [71] Badovskaya, L.A.; Povarova, L.V. Oxidation of furans (Review). *Chemistry of Heterocyclic Compounds* 2009, 45, 1023-1034.
- [72] Kreile, D. R.; Slavinskaya, V.A.; Shimanskaya, M. V.; Lukevits, E. Y. The reactivity of furan compounds in vapor-phase catalytic oxidation. *Chemistry of Heterocyclic Compounds* 1969, 5, 579-581.

- [73] Mensah, T. A.; Ho, C.; Chang, S. S. Products identified from photosensitized oxidation of selected furanoid flavor compounds. *J. Agric. Food Chem.*, 1936, 34, 336-338.
- [74] Mustafa, A. *Benzofurans (The chemistry of heterocyclic compounds Vol. 29)*; Wiley: New York, 1974.
- [75] Dao-Huy, T.; Haider, M.; Glatz, F.; Schnürch, M.; Milhovilovic, M. D. Direct arylation of benzo[b]furan and other benzo-fused heterocycles. *Eur. J. Org. Chem.* 2014, 8119–8125.
- [76] Dwight, T. A.; Rue, N. R.; Charyk, D.; Josselyn, R.; DeBoef, B. C-C bond formation via double C-H functionalization: Aerobic oxidative coupling as a method for synthesizing heterocoupled biaryls. *Org. Lett.* 2007, 9, 3137–3139.
- [77] Do, H.-Q.; Daugulis, O. An aromatic Glaser-Hay reaction. *J. Am. Chem. Soc.* 2009, 131, 17052–17053.
- [78] Waack, R. The Stability of the “Aromatic Sextet”. *Journal of Chemical Education* 1962, 39, 469-472.
- [79] Solà, M. Forty years of Clar’s aromatic π -sextet rule. *Frontiers in Chemistry* 2013, 1 (22), 1-8.
- [80] Balaban, A. T. Clar Formulas: How to draw and how not to draw formulas of polycyclic aromatic hydrocarbons. *Polycyclic Aromatic Compounds* 2004, 24, 83-89.
- [81] *Graphene Chemistry: Theoretical Perspectives*, First Edition; Jiang, D.; Chen, Z. Ed.; John Wiley & Sons: United Kingdom, 2013.
- [82] Clar, E. *Polycyclic Hydrocarbons (Vol 1)*. Academic Press: London, 1964.
- [83] Ruiz-Morales, Y.; Mullins, O. Polycyclic Aromatic Hydrocarbons of Asphaltenes Analyzed by Molecular Orbital Calculations with Optical Spectroscopy. *Energy Fuels* 2007, 21, 256-265.
- [84] Klein, D.J.; Rosenfeld, V. Forcing, Freedom, & Uniqueness in Graph Theory & Chemistry. *Croatica Chemica Acta* 2014, 87, 49-59.
- [85] Emanuel, N.M.; Denisov, E. T.; Maizus, Z. K. *Liquid-Phase Oxidation of Hydrocarbons*; Plenum Press: New York, 1967; translated by B.J. Hazzard.
- [86] Sheldon. R. A.; Kochi, J. K. *Metal-Catalyzed Oxidations of Organic Compounds*; Academic Press: New York, 1981.

- [87] David, B.; Boule, P. Phototransformation of PAHs adsorbed on SiO₂ in aqueous suspension. In *Polycyclic aromatic compounds. Synthesis, properties, analytical measurements, occurrence and biological effects*; Garrigues, P., Lamotte, M. Eds.; Gordon and Breach Science Publishers: Amsterdam, 1993, p. 127-133.
- [88] Ismagilov, Z.; Yashnik, M. Kerzhentsev, M.; Parmon, V.; Bourane, A.; Al-Shahrani, F. M.; Hajji, A. A, Koseoglo, O.R. Oxidative Desulfurization of Hydrocarbon Fuels. *Catalysis Reviews* 2011, 53, 199-255.
- [89] Vanadia catalysts for processes of oxidation of aromatic hydrocarbons. Grzybowska-Świerkosz, B. Ed.; Polish Scientific Publishers: Warsaw, 1984.
- [90] Kung, H. H. In *Transition Metal Oxides: Surface Chemistry and Catalysis; Studies in Surface Science and Catalysis*; Elsevier: Amsterdam, 1989; Vol. 45, pp 169-199.
- [91] Bielański, A; Haber, J. Oxygen in Catalysis on Transition Metal Oxides. *Catal. Rev. Sci. Eng.* **1979**, 19(1), 1-41.
- [92] Sachtler, W. M. H.; De Boer, N. H. In *Proc. Intern. Congr. Catalysis, Amsterdam 1964*, 3, 252.
- [93] Andersen, P. J.; Kung, H. H. Differential Heat of Reoxidation of Reduced V₂O₅/γ-Al₂O₃. *J. Phys. Chem.* **1992**, 96, 3114-3123.
- [94] Simons, TH. G. J.; Verheijen, E. M. J.; Batist, PH. A.; Schuit, G. C. A. Oxidation on Metal Oxides Surfaces. In *Oxidation of Organic Compounds. Advances in Chemistry Series, Vol. 76*; American Chemical Society: 1968.
- [95] Wender, I.; Heredy, L.A.; Neuworth, M.B.; Dryden, I.G.C. Chemical reactions and the constitution of coal. In *Chemistry of coal utilization. Second supplementary volume*; Elliott, M.A. Ed.; Wiley: New York, 1981, p. 425-521.
- [96] Hayatsu, R.; Scott, R. G.; Winans, R. E. Oxidation of coal. In *Oxidation in organic chemistry. Part D*; Trahanovsky, W. S. Ed.; Academic Press: New York, 1982, p. 279-354.
- [97] Hayashi, J.; Matsuo, Y.; Kusakabe, K.; Morooka, S. Depolymerization of lower rank coals by low-temperature O₂ oxidation. *Energy Fuels* **1997**, 11, 227-235.
- [98] Anderson, K. B.; Crelling, J. C.; Huggett, W. W.; Perry, D.; Fullinghim, T.; McGill, P.; Kaelin, P. Oxidative hydrothermal dissolution (OHD) of coal and biomass. *Prepr. Pap.-Am. Chem. Soc., Div. Fuel Chem.* **2011**, 56 (2), 310-311.

- [99] Stock, L. M.; Obeng, M. Oxidation and decarboxylation. A reaction sequence for the study of aromatic structural elements in Pocahontas No. 3 coal. *Energy Fuels* **1997**, *11*, 987-997.
- [100] Lee-Ruff, E.; Wang, C. Photooxydation of 6-methylbenzo[a]pyrene and related compounds. In *Polycyclic aromatic compounds. Synthesis, properties, analytical measurements, occurrence and biological effects*; Garrigues, P., Lamotte, M. Eds.; Gordon and Breach Science Publishers: Amsterdam, 1993, p. 93-101.
- [101] Montoya Sánchez, N.; De Klerk, A. Low-temperature oxidative asphaltenes liquefaction for petrochemicals: fact or fiction? *Appl. Petrochem. Res.* **2016**, *6*, 97-106.

3. Low Temperature Oxidative Asphaltenes Liquefaction for Petrochemicals: Fact or Fiction? ¹

ABSTRACT

Asphaltene is the heavy and heteroatom-rich fraction of petroleum that is rejected during a solvent deasphalting process. In patent literature there are claims that state that this material can be converted into an aromatic petrochemical feedstock by oxidative liquefaction at low temperature. To evaluate the validity of these claims, asphaltenes from an industrial solvent deasphalting process were oxidized with dry and water-saturated air at temperatures in the range 45–100 °C. Infrared spectroscopy of the oxidized product confirmed that oxygen was incorporated as C=O and C–O. Under all experimental conditions studied little oxidative degradation was observed that would lead to the production of a petrochemical feedstock. Nevertheless, some observations of scientific value were made about the low-temperature conversion of asphaltenes. During autoxidation with dry air, the n-pentane-insoluble fraction increased. On the contrary, when oxidation was conducted with water-saturated air, the formation of additional n-pentane-insoluble material was suppressed. Mild heating of asphaltenes under nitrogen atmosphere also caused the n-pentane-insoluble content to increase. Spectroscopic evidence showed that esters are formed during oxidation at ~100 °C. The temperature dependence of this reaction was explained and a possible reaction pathway for cycloalkane to ester conversion was presented. Ester selectivity was determined by the competition between hydrogen abstraction and β -scission of the alkoxy radical.

Keywords: Asphaltenes autoxidation, wet oxidation, heating of asphaltenes.

¹ This work was published as Montoya Sánchez, N.; De Klerk, A. Low-temperature oxidative asphaltenes liquefaction for petrochemicals: fact or fiction? *Appl. Petrochem. Res.* **2016**, 6, 97-106.

3.1 Introduction

Asphaltenes are a solubility class. Industrially it is produced as the rejection product from a solvent deasphalting process to produce deasphalted oil, which is the upgraded product. The asphaltene fraction contains the heaviest and most polar compounds in crude oil, as well as a significant fraction of heteroatoms and metals. Compared to bitumen, asphaltenes are more aromatic in nature, and have an even lower H:C ratio (1.1 approximately) [1]. Even though, asphaltenes are considered the least favorable fraction for upgrading, they have the potential to be converted to higher value liquid products, including petrochemicals. Industrially, there are pathways for doing so, but more efficient alternative conversion chemistries are required to make it economically attractive.

Traditionally the conversion of asphaltenes to petrochemical products is not considered. There are limited markets for asphalt and heavy oil. Upgrading to lighter oil by standard refining technologies, such as delayed coking, can achieve liquid yields of the order of 40–50 wt% [2]. In heavy oils that contain a significant fraction of asphaltenes, rejecting most or all of the asphaltenes as waste material could be an expensive strategy. For example, in Canadian oilsand-derived bitumen the asphaltene fraction represents more than 10 wt% of the total bitumen [3], often close to 15 wt%.

According to the patent literature, low-temperature oxidation of asphaltenes might be an alternative strategy to add value to this material [4][5]. Lighter oil-soluble oxygenates, or water-soluble oxygenates, which would be rich in phenolic compounds when derived from asphaltene oxidation, could have value as petrochemical feedstocks. To produce petrochemicals, further separation would be required, but such separation technology is known from the recovery of phenolic compounds from coal liquids and ammoniacal water [6].

The patent literature [4][5] claims that contacting asphaltenes with an oxygen-containing gas, e.g. air, at temperatures below 100 °C produces liquid products. It was reported that the liquid yield of pentane extractable materials increased after oxidation, with liquid yields of the order of 15 wt% being achieved [4]. Particularly, it has been pointed out that oxidation at

temperatures close to 50 °C produced liquid products suitable to be used as drying oils and refinery feedstocks for production of organic chemicals [4][5]. In addition, it has been suggested that air saturated with water vapor is a significantly better oxidizing agent able to increase the liquid yield [4]. The oxidation can be performed using a force draft oven or a packed-bed reactor. Under these premises, it seems that low-temperature oxidation of asphaltenes might be possible and that at least part of the asphaltenes can be transformed from a low-value solid to a higher value petrochemical feedstock, before the asphaltenes is further upgraded using conventional technologies.

Unfortunately the literature also contains reports that state that oxidation, even at temperatures as low as 60 °C and oxidation times as long as 229 h at 130 °C, leads to substantial hardening with little lighter liquid products being produced [7][8][9][10]. These studies all dealt with heavy oils, rather than just the asphaltenes fraction. Yet, it cast doubt on the validity of the claims in the patent literature. The purpose of this concise experimental study was exploring and validating the possibility of using low temperature oxidative asphaltenes liquefaction as upgrading strategy. The conversion strategies outlined in the patent literature were repeated and the usefulness of this strategy for petrochemical production from asphaltenes was evaluated.

3.2 Experimental Section

3.2.1 Materials

The asphaltenes were obtained from an industrial C₅ solvent deasphalting process at the Long Lake Upgrader in Alberta, Canada and were supplied by Nexen Energy ULC. Selected properties of these asphaltenes are provided in Table 3.1 n-Pentane (98 wt%) was used as solvent and it was purchased from Sigma-Aldrich. High-purity nitrogen (99.998 %) and extra-dry air were obtained from Praxair. All chemicals were used without further purification. Distilled water was prepared using a Millipore water purification system.

It should be noted that the industrial nature of the raw material has some implications for its properties, particularly on the asphaltene content. Traditionally, in solvent deasphalting

processes the feed and the solvent are mixed together, in ratios varying from 3:1 up to 10:1 [11], leading to the precipitation and separation of the asphaltene fraction. Neither the solvent to feed ratio, nor the settling time allowed for phase separation is near that of the laboratory precipitation procedure. Although, the efficiency of deasphalting in such cases may differ, it has been reported to being up to 80 % efficient compared to rigorous laboratory precipitation [11]. As a consequence, the material present in the separated asphaltene fraction is not only asphaltenes. In fact, the term asphaltenes being a solubility class has a relative meaning and it should not be taken on an absolute basis, as one can do with a compound class. The industrially obtained raw material has an actual asphaltene content of ~70 wt %. This content was measured according to standard laboratory techniques in which the solvent to feed ratio (40:1) exceeds by far the industrial conditions. Details are provided in the analysis section.

Table 3.1. Properties of asphaltenes from industrial C₅ solvent deasphalting process

Property	Industrially obtained asphaltenes
Asphaltene content [wt%] ^a	66.9 ± 0.6
Density [kg/L] ^b	1.1 ± 0.1
¹ H NMR aliphatic:aromatic	7.2 ± 0.2
Elemental Composition	
H	8.1 ± 0.1
C	82.1 ± 0.1
N	1.2 ± 0.0
O	0.9 ± 0.3
S	7.8 ± 0.1

^a Asphaltenes precipitated with *n*-pentane

^b Density by liquid displacement

3.2.2 Procedure and Equipment

Oxidation of asphaltenes was performed based on the reaction conditions and the experimental setup reported in the patent literature [4]. Two types of experiments were carried out, so that dry air and moist air were used as the oxidizing agents.

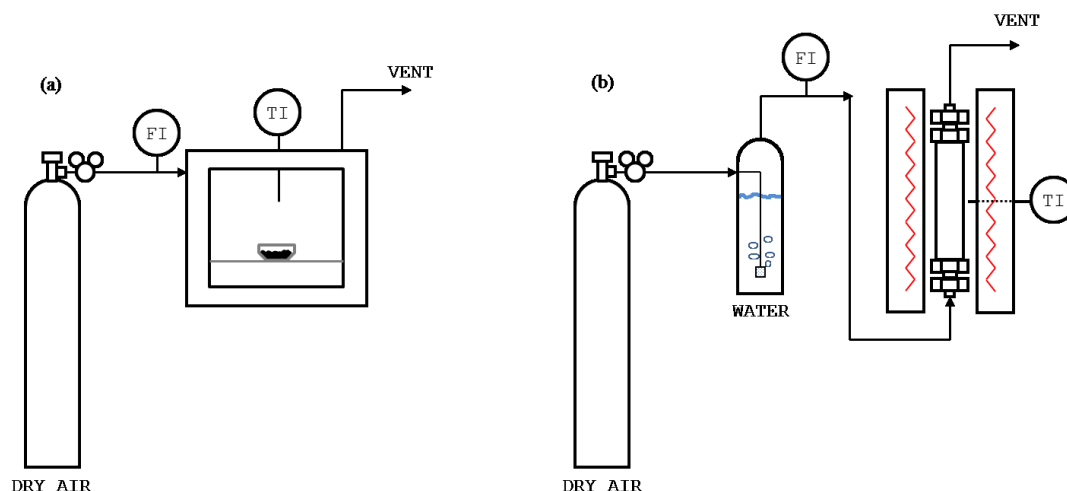


Figure 3.1. Experimental setup for asphaltene oxidation with (a) dry air and (b) moist air

The equipment employed for the first part of the study, namely oxidation of asphaltene using dry air, consisted of a Yamato DP43 oven, which was connected to a dry air supply line. The air flow was controlled by a glass Supelco rotameter and adjusted to 250 mL min^{-1} . The oven temperature was monitored with a thermometer. For each oxidation experiment, three samples of asphaltene weighing approximately 1.2 g were used. The samples were placed inside the oven after it reached a constant temperature, and they were heated during 16 h. Experiments were performed at four different temperatures: 45, 56, 86, and 100 °C. The products were weighed and analyzed. Blank experiments using an inert nitrogen atmosphere were also carried out. A scheme of the experimental setup is presented in [Figure 3.1](#).

The apparatus used for the second type of experiments performed in this study, namely oxidation of asphaltene using moist air, consisted of a stainless steel column of 2.56 cm (1 inch) internal diameter, and 25.66 cm length (10 inches), which was connected to a moist air line

supply. The moist air was fed from the bottom to the top of the column and it was produced by bubbling air through water in a 250 mL Erlenmeyer flask. In addition, the air flow was regulated with a glass Supelco rotameter and it was adjusted to a flow rate of 3 standard cubic feet per hour per 100 g of asphaltenes. A Lindberg Blue M tube furnace, coupled with a Thermo Fisher temperature controller was used as heating mantle. A scheme of the experimental setup is presented in [Figure 3.1](#).

For each oxidation experiment, the column was packed as a fixed-bed reactor. Thus, layers of glass beads, of approximately 5 cm (2 in) length, were symmetrically placed at the top and bottom of the column. Round pieces of a fine stainless steel mesh were situated at the ends of these glass beads. A bed of asphaltenes of about 15 cm (6 in) was situated in the middle of the column. The packed column was heated up to the reaction temperature. A typical heat-up time was 8 min. Oxidation reactions were conducted at 52 and 100 °C, for 2 h. Additional experiments at 52 °C for different reaction times (2, 4 and 8 h) were also performed. Note that some experiments used dry air for comparison purposes. Products were collected for further analysis.

3.2.3 Analysis

The following analyses were performed to characterize the reaction products:

- (a) The asphaltenes content of the products was determined by precipitation with n-pentane. The procedure is as follows: 1 g of sample was weighted and mixed with 40 mL of n-pentane in a 50-mL flask. Then, the mixture was continuously stirred with a magnetic bar, at room temperature for 1 h. After that the mixture was left without stirring for a period of 24 h. The mixture was filtered with a 0.22 μm Millipore nitrocellulose membrane filter under vacuum conditions and it was rinsed with fresh n-pentane until the eluent became colorless. The filter with the precipitated asphaltenes was transferred to an aluminum cup and was left in a fume hood for 48 h to ensure complete evaporation of the solvent. Finally, the dried asphaltenes were weighed and the asphaltenes content was calculated.

It is worth mentioning that the method used in the present study to determine the asphaltenes content of the samples does not allow for differentiating between asphaltenes and coke. Nonetheless, it is very unlikely that a significant amount of coke would have been produced at the reaction conditions, i.e. low temperature and atmospheric pressure. Thermal conversion of asphaltenes resulting in the formation of coke has been reported for reaction under more severe conditions. For instance, Cold lake-derived asphaltenes has been reported to form coke by conversion at 400 °C [12]. In addition, it has been stated that the presence of heptane-soluble material inhibits formation of coke by asphaltenes. As described in the materials section, although the raw material or industrial asphaltenes used in this study are mostly asphaltenes, it contains about ~30 wt% of other components (maltenes) from oil.

- (b)** Infrared spectroscopy was used to provide information about the chemical changes in the asphaltenes related to the oxidation reactions. An ABB MB3000 Fourier Transform infrared spectrometer with Horizon MB FTIR software was used to collect the infrared spectra. The spectrometer was equipped with a Pike MIRacle Reflection attenuated total reflectance (ATR) diamond crystal plate. The infrared analysis was performed at a resolution of 4 cm⁻¹ and an average of 120 scans over the spectral region of 4000–600 cm⁻¹. To perform comparisons at specific wave numbers, all spectra were scaled based on the symmetric deformation mode of the methyl (–CH₃) groups at ~1375 cm⁻¹. The underlying assumption was that oxidation of methyl groups is more difficult and under the mild oxidation conditions investigated, little oxidation of methyl groups was anticipated. This is based on the two orders of magnitude lower oxidation rate of methyl groups compared to secondary aliphatic carbons [13].
- (c)** The micro carbon residue (MCR) of the products was calculated from thermogravimetric analysis. A Mettler Toledo TGA/DSC1 with LF furnace, sample robot and, MX5 internal microbalance was used. The resolution of the balance was 0.1/1 µg. Analyses were carried out under nitrogen atmosphere. All micro carbon residue measurements were determined in accordance with the standard test method ASTM D4530.

3.3 Results

3.3.1 Low-Temperature Dry Autoxidation of Asphaltenes

The first part of the work dealt with the autoxidation (oxidation with air) of asphaltenes in the absence of added water. In this case, oxygen from dry air was responsible for producing the oxidized products. Reactions were carried out for 16 h at 45, 56, 86, and 100 °C. In addition, blank experiments using an inert atmosphere (air substituted with N₂) were performed to determine whether heating during product workup has an effect on its own.

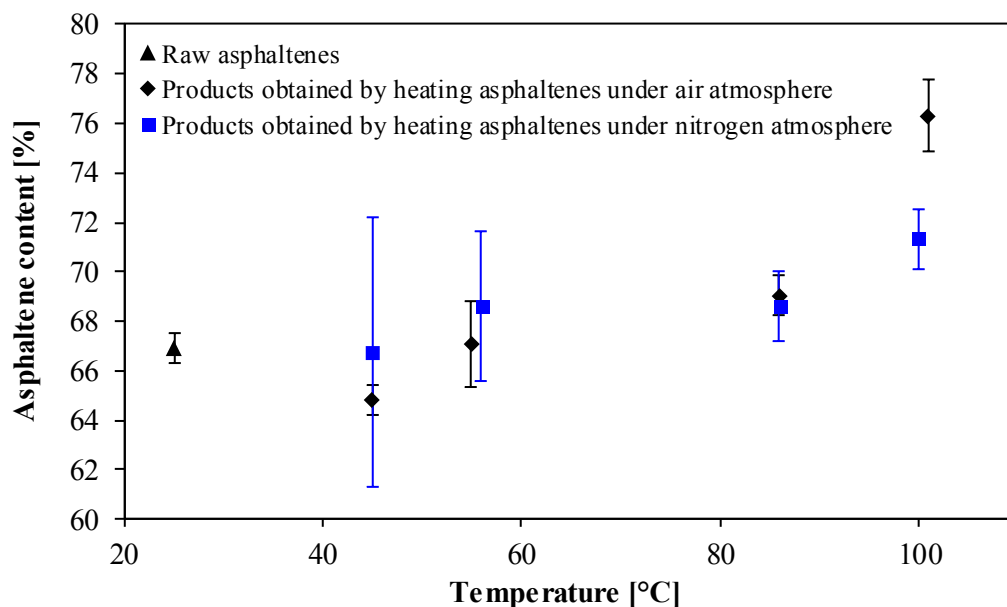


Figure 3.2. Asphaltenes content of the products obtained by heating asphaltenes feed in air and nitrogen atmospheres for 16 h at 45, 55, 86, and 100 °C

After reaction, the asphaltenes content of the products was measured, and then compared with the asphaltenes content of the raw material (Figure 3.2). There was little difference between the asphaltenes content of the asphaltenes feed and that of the samples that were oxidized at 45, 56 and 86 °C, respectively. In this temperature range, there was not a meaningful difference in the asphaltene content between the samples that were oxidized and the ones that were just heated

under nitrogen atmosphere. It should further be noted that the increase in mass due to oxygen incorporation and the decrease in mass due to production of volatile oxidation products were minor; in fact, the mass of the oxidized products decreased in approximately 0.01–0.03 wt% compared to the mass of the initial asphaltenes feed.

The impact of oxidation on the product properties was more apparent when the reaction temperature was increased to 100 °C. In this case both autoxidation and heating under inert atmosphere affected the asphaltenes content of the products. For the oxidized sample an increase in the asphaltenes content from 66.9 ± 0.6 to 76.3 ± 1.9 wt% was observed. On heating, the asphaltenes content of the product increased to 71.3 ± 1.2 wt%. It is evident that the increase in the asphaltenes content of the oxidized product is not only a consequence of the chemistry of autoxidation, but there is also a contribution because of thermal effect. Directionally the effect of oxidation was the opposite of what was claimed in the patent literature [4][5].

A comparison of the infrared spectra of the raw asphaltenes feed and the total oxidized products from oxidation at different conditions are presented (Figure 3.3). The presence of C=O and C–O stretching vibrations in the oxidized products confirmed the incorporation of oxygen in the asphaltenes structure due to autoxidation. Infrared spectroscopy is particularly sensitive for detecting carbon-oxygen vibrations, which have high absorptivity in the infrared spectrum.

The spectra showed some diversity in the chemical environment of the carbonyl groups and the C–O functionality [14]. Prominent absorption bands in the $1713\text{--}1742\text{ cm}^{-1}$ region as well as in the $1202\text{--}1234\text{ cm}^{-1}$ region were found. A considerable increase of the C=O and C–O stretching vibrations was observed in the samples that reacted at 86 and 101 °C, whereas, less intense absorption bands were noted in the sample oxidized at 55 °C. These interactions were not observed in the products obtained at 45 °C. Absorption bands indicating the presence of other oxygen-containing functional groups, such as sulfoxides, were minor. Even though no quantification was made, a relative comparison is possible. The infrared analysis suggested a higher extent of oxidation when increasing the temperature.

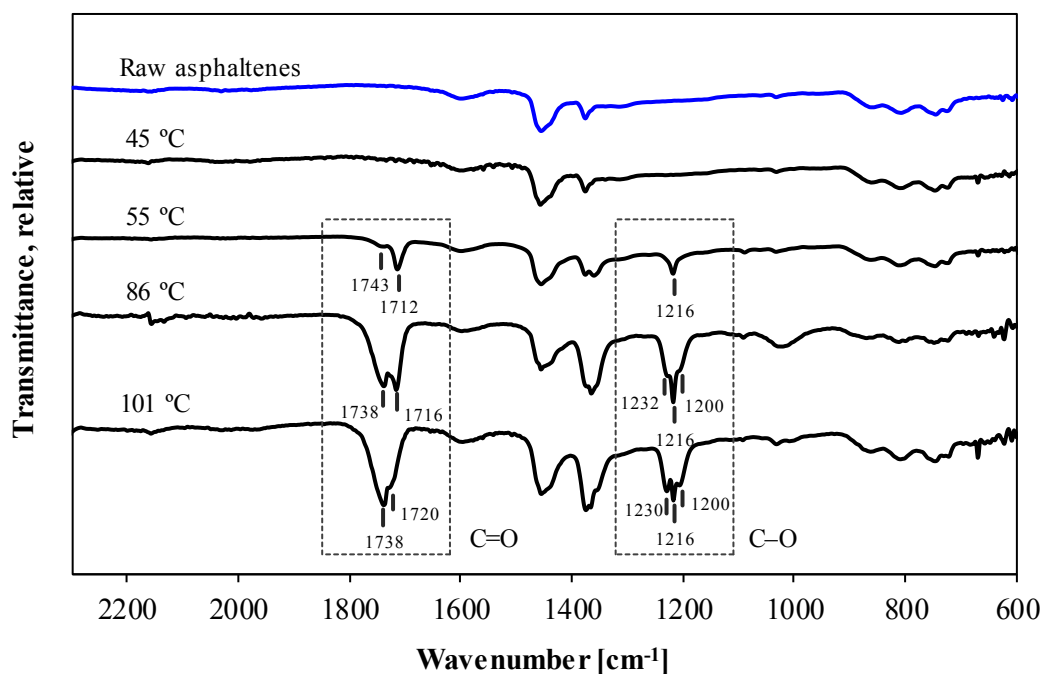


Figure 3.3. Infrared spectra of the raw asphaltene and the total oxidized product after 16 h oxidation at 45, 56, 86, and 100 °C

Table 3.2. Relative peak intensities of absorptions at different regions of the IR spectra for oxidized asphaltene

Stretching vibrations [cm ⁻¹]	Functional group	Total oxidized product			Oxidized maltene fraction			
		56 °C	86 °C	100 °C	45 °C	56 °C	86 °C	100 °C
1734-1442	C=O	0.2	1.1	1.0	-	0.6	0.2	1.0
1713-1722	C=O	1.4	1.7	1.0	0.8	1	0.2	1.0
1454	C-H	1.6	0.9	1.0	2.6	1.8	2.3	1.0
1230-1259	C-O	-	1	1.0	0.7	0.8	0.5	1.0
1217-1219	C-O	1.1	1.4	1.0	1.4	1.8	-	1.0
1200-1203	C-O	-	1.1	1.0	-	0.8	0.5	1.0

Some semi-quantitative information was extracted from the IR analyses (Table 3.2). The relative peak intensity of the C=O and C-O vibrations in each sample is an indication of the

relative increase or decrease for each group. The absorptivities for the different vibration bands are different and observed changes should not be over-interpreted.

After reaction, the asphaltenes fraction of the oxidized samples was precipitated using n-pentane (using the same procedure to measure asphaltenes content and separate maltenes). The products soluble in the pentane were recovered, and a brown, oily extract was obtained. The infrared spectra of the different extracted liquid products were compared (Figure 3.4). In all the samples both C=O and C–O absorption bands were observed indicating the presence of oxygenated compounds. The intensity of these absorption bands changed with the change in temperature, which is indicative of changes in the oxidation selectivity.

The infrared spectra of the products obtained in the blank experiments were also compared. Neither the products obtained after heating nor the ones extracted with n-pentane showed any signs of change in their infrared spectra. This is not surprising because infrared analysis is not a sensitive technique to detect small changes in hydrocarbon composition.

The micro carbon residue of the raw asphaltenes, the oxidized asphaltenes and the ones that were heated under inert atmosphere was measured and compared (Table 3.3). There was little difference between the MCR value of the feed asphaltenes and that of the reaction products. Only a minor increase in MCR value of the oxidized products obtained at 86 and 100 °C was observed. At these temperatures, autoxidation might have affected the asphaltenes structure in such a way that products are slightly more prone to form coke.

The kinetics of the reactions taking place during the autoxidation and blank experiments might be slow and most likely not favored by low temperature. As a result, for the selected reaction conditions no significant changes were initially observed. Probably, when experiments were performed at 100 °C, the temperature was high enough to accelerate the reaction process. After reaction at 100 °C small changes in the product properties were found, notably, higher asphaltenes content.

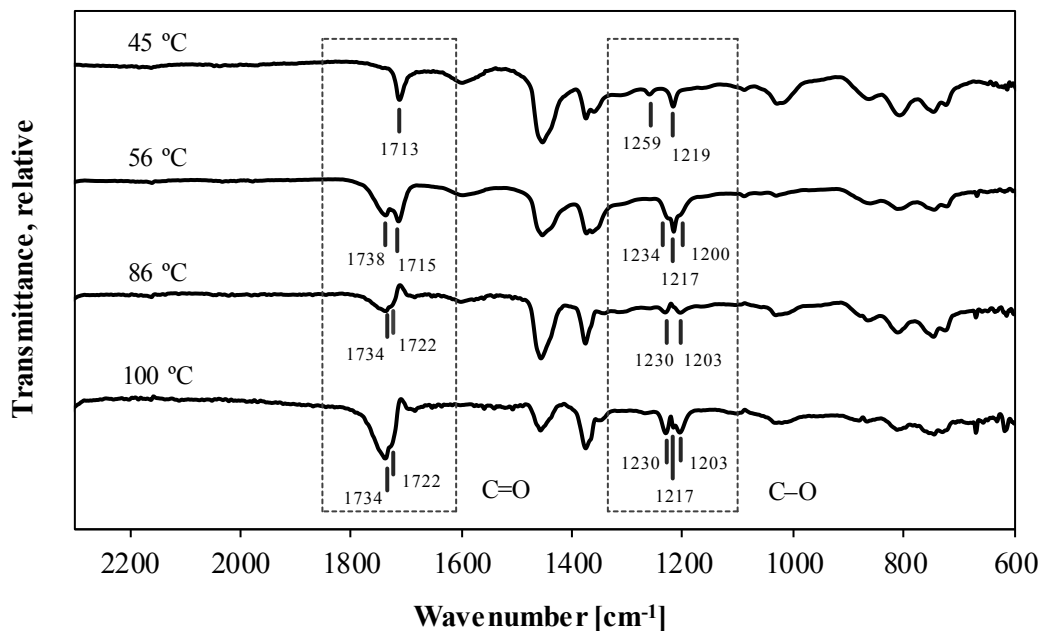


Figure 3.4. Infrared spectra of the maltenes fraction separated from of the oxidized products obtained after 16 h oxidation at 45, 56, 86, and 100 °C

Table 3.3. Micro carbon residue data for raw asphaltenes, oxidized asphaltenes, and asphaltenes heated in nitrogen atmosphere for 16 h

Sample	Temperature [°C]	MCR [wt %]
Raw asphaltenes	-	40.7 ± 0.7
Products from heating asphaltenes in air atmosphere	45	-
	55	40.6 ± 0.3
	86	41.5 ± 0.6
	100	41.6 ± 0.3
Products from heating asphaltenes in nitrogen atmosphere	45	40.3 ± 0.1
	55	40.4 ± 0.2
	86	40.6 ± 0.3
	100	40.9 ± 0.2

3.3.2 Low-Temperature Water-Assisted Oxidation of Asphaltenes

Literature indicates that the presence of water has a positive effect in the low-temperature oxidation of heavy oil and asphaltenes [4][15]. The second part of the work was, therefore, focused on the oxidation of asphaltenes using air saturated with water vapor, or moist air. Some control experiments were also performed in which dry air was used at the same conditions.

As before, the asphaltene content of the oxidized products was measured after oxidation and compared with the raw material Table 3.4. The asphaltene content of the products increased from 66.9 ± 0.6 wt% to a maximum of 70.5 ± 1.1 wt% after 8 h of reaction at 52 °C. Although reactions at 52 °C were conducted at different reaction times, there were not meaningful differences in the asphaltene contents and MCR values of the respective oxidized products. No trend for changes in the asphaltene content with oxidation time was observed for oxidation at 52 °C.

Table 3.4. Asphaltene and micro carbon residue data for unreacted asphaltenes and asphaltenes heated at low temperature in air and moist air atmospheres for different reaction times

Sample	Temperature [°C]	Time [h]	Asphaltene content [wt%]	MCR [wt %]
Raw asphaltenes	-	-	66.9 ± 0.6	40.7 ± 0.7
Products from heating asphaltenes in moist air atmosphere	52	2	70.0 ± 2.1	40.4 ± 0.2
	52	4	70.0 ± 0.1	40.7 ± 0.2
	52	8	70.5 ± 1.1	40.2 ± 0.4
Products from heating asphaltenes in air atmosphere	100	2	65.9 ± 2.2	^a
	52	2	61.5 ± 4.7	40.2 ± 0.6
	100	2	79.8 ± 1.6	40.3 ± 0.3

^a The MCR value for this sample was not measured

The formation of C=O and C–O functional groups were nevertheless confirmed by infrared spectroscopy (Figure 3.5). The relative changes in absorption at different wave numbers were recorded for relative comparison Table 3.5.

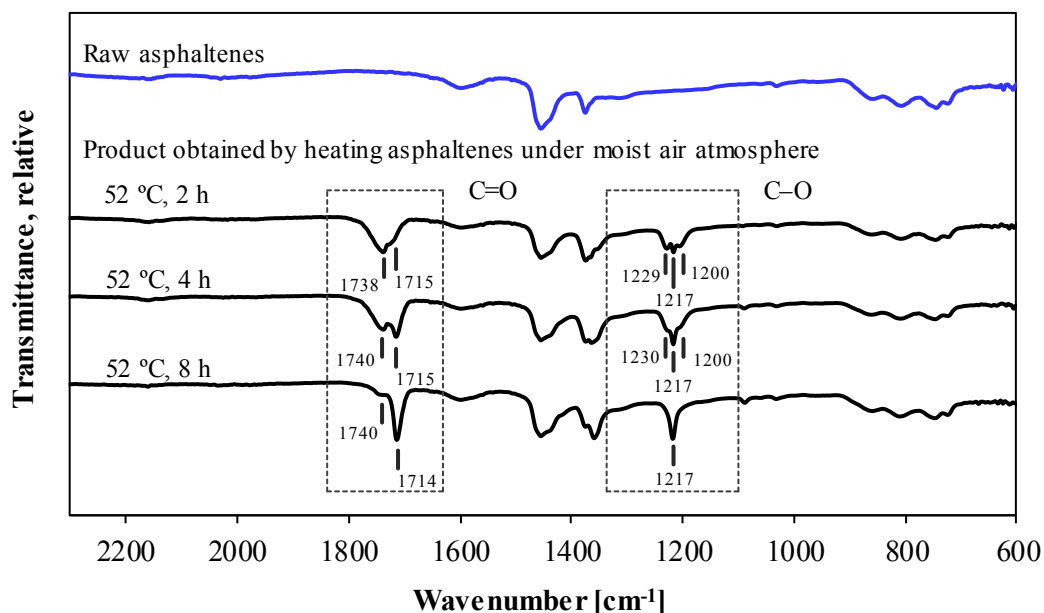


Figure 3.5. Infrared spectra of raw asphaltene feed and total oxidized product after wet air oxidation at 52 °C for 2, 4 and 8 h respectively

Table 3.5. Relative peak intensities of absorptions at different regions of the IR spectra for the total oxidized products after oxidation using moist air at 52 °C

Stretching vibrations [cm ⁻¹]	Functional group	Oxidized asphaltenes		
		2h	4h	8h
1738-1740	C=O	3.9	3.5	1.0
1714-1715	C=O	0.3	0.7	1.0
1454	C-O	0.8	0.8	1.0
1229-1230	C-O	0.5 ^a	0.5 ^a	-
1217	C-O	0.6	0.8	1.0
1200	C-O	0.4 ^a	0.4 ^a	-

^a Relative to the absorption at 1217 cm⁻¹ after 8 h oxidation

In the second set of experiments that were performed at 100 °C, the asphaltene feed was oxidized with water saturated air and dry air [Table 3.4](#). The infrared spectra of these oxidized products were measured; absorption bands indicating the presence of C=O and C-O groups

confirmed the incorporation of oxygen into the reaction products. Some diversity in the chemical environment of these interactions was observed.

The difference between asphaltenes formation due to oxidation using moist air and dry air can be clearly seen from Figure 3.6. There is little difference in the asphaltene content of the raw material and the samples oxidized at 52 °C. However, it seems that at this particular temperature the presence of water during reaction slightly increases the asphaltene content of the products, going from 66.9 ± 0.6 to 70.0 ± 2.1 wt %. On the contrary, the asphaltene content of the products obtained by autoxidation at 100 °C is significantly higher than the one observed for the products obtained when water was added to the feed at the same temperature (79.8 ± 1.6 and 65.9 ± 2.2 wt%, respectively). Moreover, when water assisted the oxidation of asphaltenes at 100 °C no increase in the asphaltene content of the product compared to the raw material was observed.

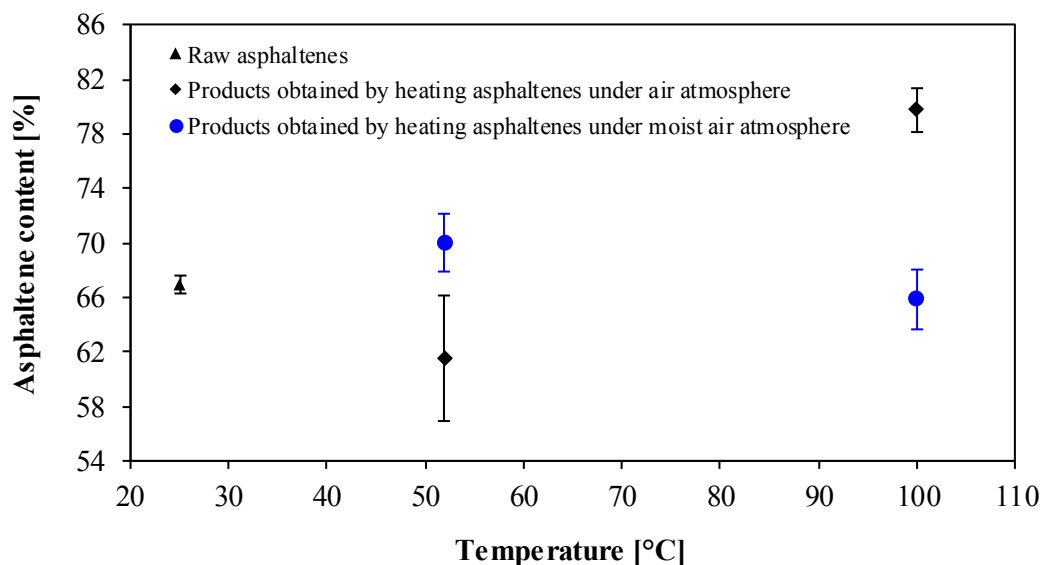


Figure 3.6. Asphaltene content of the products obtained by heating asphaltenes for 2 h at 52 and 100 °C, under air and moist air atmosphere

3.4 Discussion

3.4.1 Benefits from Oxidation

The premise that was investigated by this work is that the yield of maltenes (n-pentane soluble material) can be increased by mild oxidation of asphaltenes, and that these materials may have potential application as petrochemicals [4][5]. This claim could not be substantiated by the present experimental investigation, although the beneficial effect of using moist air, rather than dry air was demonstrated.

Under all oxidation conditions there was either no significant change in asphaltenes content, or there was a meaningful increase in asphaltenes content in the oxidized product (Figure 3.2; Table 3.4). Little oxidative degradation took place and oxygen was incorporated in C=O and C–O functional groups (Figure 3.3, Figure 3.4 and Figure 3.5). Oxidation may also give rise to addition reactions [16], particularly in materials that are rich in naphtheno-aromatics, such as the asphaltenes feed. Thus, the polarity, solubility parameter and molecular mass of the molecules were likely increased by oxidation. Collectively these changes should result in an increase in asphaltenes content [17], as was indeed observed.

When oxidation was conducted with moist air, the formation of asphaltenes was affected (Table 3.4); this was particularly evident for oxidation conducted at 100 °C. Oxidation was not prevented, but it was affected by the presence of water. It is not clear in what way the water was able to moderate the oxidation, beyond its obvious dilution effect. Water was present only as a saturated vapor so that dilution was limited. The extent of oxidation moderation by water suggests either some phase equilibrium effect (e.g. gas solubility), or chemical equilibrium effect (e.g. hydrolysis-dehydration reaction equilibrium). It was reported that during oxidation of heavy oil at 200 °C water enhanced CO₂ production and that water mitigated some of the other deleterious effects of low-temperature oxidation, such as increased viscosity and acidity [15].

Interestingly, the increase in asphaltenes content was not accompanied by an increase in MCR (Table 3.3 and Table 3.4). The average numeric values suggested a minor increase, but this

was not meaningful. It is usual to correlate these two properties when describing the chemical changes involved in the thermal conversion of oil and oil-derived materials. However, one should understand they measure different characteristics. The asphaltenes content indicates the amount of components soluble in aromatic solvents and insoluble in paraffinic solvents; whereas, the MCR indicates the coke forming tendency of a material. Even molecules with limited solubility and low H:C ratio, such as asphaltenes, may go through chemical changes without completely becoming a different solubility class, such as coke. The solvent-resid phase diagram presented by Wiehe [18] shows that one possible path during conversion of asphaltenes involves changes in their hydrogen content or molecular weight without affecting their nature as asphaltenes. Configuration of the molecules changes but they still belong to the same solubility class. On the other hand, it is worth to mention that thermal conversion of asphaltenes may produce more volatile products. Under more severe or prolonged oxidation an increase in MCR is anticipated due to loss of hydrogen as water.

The present work indicated that oxidation of asphaltenes on its own is not enough as upgrading strategy. Oxidation can be considered as a first step in an asphaltene liquefaction scheme, but not the only step. Under the right conditions, when oxygen is inserted into the asphaltenes structure, C–C bonds can be broken [19]. However, this type of chemistry was not prevalent under the conditions investigated based on the patent literature [4][5].

3.4.2 Oxidation Selectivity

The manipulation of oxidation selectivity in complex hydrocarbon mixtures has broader relevance that extends beyond the use of oxidation for asphaltenes upgrading. Oxidation is extensively employed in the petrochemical industry, e.g. [20]. Evaluating the experimental results from this perspective was, therefore, of potential interest.

The selective autoxidation of alkanes is a highly desirable petrochemical conversion, because air oxidation is one of the least costly methods of alkane C–H bond activation. The selectivity of free radical hydrocarbon oxidation is mainly influenced by temperature and oxygen availability [21]. Oxygen availability was not changed, except by secondary effects related to

changes in the temperature. The nature of the oxygenates formed during asphaltenes oxidation at different temperatures (Figure 3.3, Figure 3.4 and Figure 3.5) changed. Although conversion was also affected, conversion was low in all instances and these changes in the nature of the oxygen-containing functional groups must have been caused mainly by changes in the temperature.

At the lowest temperatures a strong C=O band appears near 1715 cm^{-1} (Table 3.2). In tandem a C–O band appears near 1217 cm^{-1} . If these two absorption bands were related, it would suggest the formation of esters, which would be peculiar, because alcohols and ketones were anticipated to be the primary oxidation products. The strong C–O absorption near 1217 cm^{-1} is more likely that of aromatic ethers, because there is a concomitant increase in absorption in the $1050\text{--}1010\text{ cm}^{-1}$ region [14], which is particularly apparent as the broad band in the spectra of the oxidized maltenes fraction (Figure 3.4). The wave number of the C=O absorption is also indicative of an aliphatic ketone, rather than an ester. At the lowest temperatures studied, $\sim 50\text{ }^{\circ}\text{C}$, the main oxygenate functional groups identified by infrared spectroscopy are ketones and aromatic ethers.

As the temperature was increased from ~ 50 to $\sim 100\text{ }^{\circ}\text{C}$, a C=O band appeared near 1735 cm^{-1} and it grew in size relative to the C=O band near 1715 cm^{-1} . Simultaneously two C–O bands appeared near 1230 and near 1200 cm^{-1} , respectively. If these two absorption bands were related, as they appeared to be (Table 3.2), then it might be due to the formation of an ester functionality. The wave numbers of the C=O and C–O absorptions correspond to that reported for esters and cyclic esters [14]. With prolonged wet oxidation these absorption bands decrease over time (Figure 3.5; Table 3.5), which suggested ester hydrolysis and possible carboxylic acid decomposition to eliminate CO_2 . If this is indeed a correct interpretation, then one should be able to suggest a pathway that would lead to ester formation, despite the mild oxidation conditions and that would explain the temperature sensitivity of this reaction.

A plausible pathway for ester formation that would explain the temperature sensitivity of this reaction can be suggested for the oxidation of cycloalkanes. Since oil sand-derived material is rich in multicyclic molecules where cycloalkane and aromatic rings are adjoining [22], indan is a realistic representation of a substructure that will be found in more complex molecules found

in asphaltenes. The suggested pathway of ester formation is, therefore, illustrated by the oxidation of indan hydroperoxide as model molecule (Figure 3.7). The initial steps leading to the formation of the hydroperoxide are not shown.

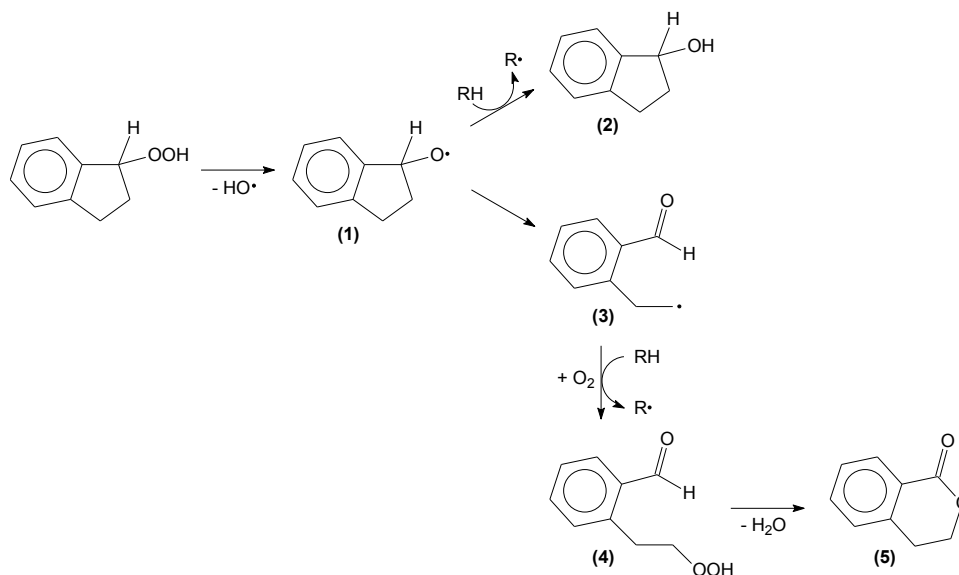


Figure 3.7. Reaction pathway explaining ester formation during low temperature autoxidation of cycloalkane containing feed materials, as illustrated by the oxidation of indan

Decomposition of the hydroperoxide leads to the formation of the oxygen-centered alkoxy radical of indan (1). The alkoxy radical (1) can abstract hydrogen from another hydrocarbon to produce an alcohol (2). At low temperature this is the dominant pathway. The alkoxy radical (1) can also undergo β-scission, which leads to ring-opening to produce (3). The β-scission of (1) requires higher activation energy, but it is nevertheless a well-known and deleterious side reaction during the low-temperature autoxidation of cyclohexane [23]. The carbon-centered radical in (3) is a typical free radical propagation intermediate and will readily be oxidized to form a hydroperoxide intermediate (4). The sequence of steps leading from (3) to (4) is the same as the one involved in the formation of the indan hydroperoxide by the autoxidation of indan. Decomposition of the hydroperoxide (4) takes place in an analogous way to the decomposition of the indan hydroperoxide. However, the fragments of the ring-opened cycloalkane are attached to a structurally ridged unit, the aromatic ring, thereby increasing the probability of an “in cage”

reaction. The “in cage” elimination of water and ring closure to form an ester (5) is, therefore, a likely reaction. The ester formation pathway is favored by temperature, because β -scission leading from (1) to (3) is in competition with hydrogen abstraction (2) and it requires higher activation energy.

3.4.3 Heating Effects on Asphaltenes Content

An interesting observation, which was not related to the primary purpose of the investigation, was that the raw asphaltenes feed was detrimentally affected by heating to 100 °C. The asphaltenes content of the feed that was maintained at 100 °C for 16 h (Figure 3.2) increased compared to the raw material feed, but this was not reflected by a change in MCR value (Table 3.3). The observed increase in the asphaltenes content on heating under inert atmosphere adds evidence that indicates that oilsands bitumen-derived materials are heat sensitive [24]. Although the exact temperature range for this heat sensitivity has not been determined, prolonged exposure to temperatures in the range 100–150 °C and possibly somewhat higher temperature, should be avoided.

Oilsand-derived asphaltenes have a high free radical content, of the order 10^{18} spins/g, as measured by electron spin resonance spectroscopy [25]. These free radicals might participate in reactions occurring during heating. It is speculated that due to the restricted mobility of molecules in the asphaltenes, which is a solid at ambient conditions, free radical addition reactions are slow and limited in extent over prolonged periods. However, the molecules and free radicals have the potential to become mobile. It is anticipated that prolonged heating can affect the mobility of these molecules and enable the movement that otherwise would not be possible or would be very slow at lower temperatures. On heating, the increase in the asphaltenes content might reflect molecular rearrangements, self-reactions among the molecules and even inter-molecular free radical addition reactions that took place.

3.5 Conclusions

The possibility of using low-temperature oxidative asphaltenes liquefaction as upgrading strategy to increase the yield of the maltenes fraction was investigated. Dry air and water-saturated air were used as the oxidizing agents. The main conclusions derived from the experimental investigation were:

- (a) Little oxidative degradation was observed under all experimental conditions. The presence of C=O and C–O functional groups confirmed the incorporation of oxygen in the asphaltenes structure.
- (b) The impact of the low-temperature autoxidation (oxidation with dry air) on the product properties was evident when the reaction was carried out at relatively high temperatures, particularly 100 °C. A significant increase in the asphaltenes content of the oxidized product was observed.
- (c) Although statistically it could not be proven, the experimental data suggests that water was capable of moderating the oxidation by preventing formation of additional asphaltenes. However, beyond the limited dilution effect of water, the influence of water during oxidation is not clear; it might be related either to some phase equilibrium effect (e.g. gas solubility), or chemical equilibrium effect (e.g. hydrolysis-dehydration reaction).
- (d) Despite the mild oxidation conditions, changes in the nature of the oxygen-containing functional groups indicated changes in the oxidation selectivity with temperature and due to the increased presence of water in the water-saturated air.
- (e) Spectroscopic evidence was presented that esters were formed during oxidation at ~100 °C with dry air. The esters formed during oxidation with water saturated air were not persistent and the esters were converted over time, presumably with hydrolysis as an intermediate reaction step and possible carboxylic acid decomposition to eliminate CO₂.

- (f) A reaction pathway to explain temperature-dependent ester formation in cycloalkanes was presented. Ester selectivity was determined by the competition between β -scission and hydrogen abstraction reactions of the alkoxy radical.
- (g) Heating of the raw asphaltenes feed under inert (nitrogen) atmosphere has a detrimental effect on its own. The observed increase in the asphaltenes content highlighted the heat sensitivity of the oilsands bitumen-derived materials.
- (h) Based on the experimental evidence from the present study, the premise of using low-temperature oxidative asphaltenes liquefaction as upgrading strategy for petrochemical production does not hold. An increase in the yield of the maltene fraction due to mild oxidation of asphaltenes was not observed.

3.6 References

- [1] Ancheyta, J.; Trejo, F.; Singh Rana, M. In *Asphaltenes: chemical transformation during hydroprocessing of heavy oils*; CRC Press: Boca Raton, FL, 2009.
- [2] Petroleum Refining Vol. 3 Conversion Processes; Leprince, P. Ed; Editions Technip: Paris, 2001, p. 381-407.
- [3] De Klerk, A.; Gray, M.; Zerpa, N. Unconventional Oil and Gas: Oilsands. In *Future Energy*, 2ed; Letcher, T. Ed; Elsevier: Amsterdam, 2014, pp 95-115.
- [4] Pitchford, Armin C. Asphaltene oxidation. US Patent 3,484,365, December 16, 1969.
- [5] Duyvesteyn, Willem P. C.; Morley, Raymond L. Oxidation of asphaltenes. US Patent 7,811,444 B2, October 12, 2010.
- [6] Chemical feedstocks from coal; Falbe, J. Ed; John Wiley & Sons: New York, 1982.
- [7] Babu, D. R.; Cormack, D. E. Effect of oxidation on the viscosity of Athabasca bitumen. *Can. J. Chem. Eng.* **1984**, 62, 562-564.
- [8] Herrington, P. R. Oxidation of bitumen in the presence of a constant concentration of oxygen. *Petrol. Sci. Technol.* **1998**, 16, 1061-1084.

- [9] Siddiquee, M. N.; De Klerk, A. Continuous and prolonged oxidation of bitumen for upgrading by microbial digestion. *Prepr. Pap.-Am. Chem. Soc., Div. Energy Fuels* **2013**, 58 (2), 649-651.
- [10] García Zapata, J. L.; De Klerk, A. Viscosity changes during mild oxidation of oilsands derived bitumen: Solvent effects and selectivity. *Energy Fuels* **2014**, 28, 6242-6248.
- [11] Grey, M. R. *Upgrading Oilsands Bitumen and Heavy Oil*. University of Alberta Press: Edmonton, AB, 2015.
- [12] Wiehe, I. A.; A Phase-separation kinetic model for coke formation. *Ind. Eng. Chem. Res.* **1993**, 32, 2447-2454.
- [13] Hudlický, M. *Oxidations in organic chemistry* (ACS Monograph Ser. 186); American Chemical Society: Washington DC, 1990.
- [14] Silverstein, R. M.; Webster, F. X.; Kiemle, D. J. *Spectroscopic Identification of Organic compounds, 7th Edition*; John Wiley: New York, 2005.
- [15] Lee, D. G.; Noureldin, N. A.; Effect of water on the low-temperature oxidation of heavy oil. *Energy Fuels* **1989**, 3, 713-715.
- [16] Siddiquee, M. N.; De Klerk, A. Hydrocarbon Addition Reactions during Low-Temperature Autoxidation of Oilsands Bitumen. *Energy Fuels* **2014**, 28, 6848-6859.
- [17] Wiehe, I. A. *Process chemistry of petroleum macromolecules*; CRC Press: Boca Raton, FL, 2008.
- [18] Wiehe, I. A.; A Solvent-resid phase diagram for tracking resid conversion. *Ind. Eng. Chem. Res.* **1992**, 31, 530-536.
- [19] Montoya Sánchez, N.; De Klerk, A. Oxidative ring-opening over metal oxides. *Prepr. Pap.-Am. Chem. Soc. Div. Energy Fuels* **2014**, 59(2), 558.
- [20] *Liquid phase oxidation via heterogeneous catalysis. Organic synthesis and industrial applications*; Clerici, M. G., Kholdeeva, O. A. Eds; Wiley: Hoboken, NJ, 2013.
- [21] De Klerk, A. Continuous-mode thermal oxidation of Fischer-Tropsch waxes. *Ind. Eng. Chem. Res.* **2003**, 42, 6545-6548.
- [22] Strausz, O. P.; Lown, E. M. *The chemistry of Alberta oil sands, bitumens and heavy oils*; Alberta Energy Research Institute: Calgary, AB, 2003.

- [23] Tolman, C. A.; Druliner, J. D.; Nappa, M. J.; Herron, N. Alkane oxidation studies in Du Pont's central research department. *In Activation and functionalization of alkanes*; Hill, C. L. Ed.; John Wiley & Sons.: New York, 1989, p. 303-360.
- [24] Gonzalez, V.; De Klerk, A. Influence of acid chemistry on bitumen viscosity. *Prepr. Pap.-Am. Chem. Soc. Div. Energy Fuels* **2015**, 60(1), 9-12.
- [25] Niizuma, S.; Steele, C. T.; Gunning, H. E.; Strausz, O.P. Electron spin resonance study of the free radicals in Athabasca asphaltene. *Fuel* **1977**, 56, 249-256.

4. Oxidative Ring-Opening over Metal Oxide Catalysts ¹

ABSTRACT

Production and upgrading of heavy crude oils is required to meet the future market demand for transportation fuels and petrochemicals. Therefore, upgrading of heavy materials such as asphaltenes has to be addressed. Conversion of multinuclear aromatic compounds is rather challenging. Traditionally, hydroprocessing is considered as an option; however, it is a hydrogen intensive technology with significant thermodynamic constrains. Oxidative ring-opening over metal oxide catalysts might be an alternative approach. In principle, performing ring-opening of aromatic structures could be achieved using oxygen as an oxidant. However, free radical chemistry poses a challenge in terms of selectivity. Using an appropriate catalyst might enable a selective reaction pathway. The aim of this work was to study the possibility of using metal oxide catalysts to perform oxidative ring-opening of multinuclear aromatics in the liquid phase. Autoxidation (air atmosphere) and catalytic oxidation (nitrogen atmosphere) of anthracene and anthraquinone in combination with V₂O₅, MoO₃, Fe₂O₃ and NiO were investigated. The presence of V₂O₅ measurably accelerated air oxidation of the model compounds; whereas, MoO₃, Fe₂O₃ and NiO had a noticeable effect only at very high temperatures. On the other hand, it was confirmed that catalytic oxidation of both anthracene and anthraquinone took place by transfer of lattice oxygen from V₂O₅. Moreover, a more detailed analysis of the reaction products indicated that catalytic oxidation was leading to ring-opening.

Keywords: Ring-opening, multinuclear aromatics, catalytic oxidation, metal oxides.

¹ This work was published as Montoya Sánchez, N.; De Klerk, A. Oxidative ring-opening over metal oxides. *Prepr. Pap.-Am. Chem. Soc., Div. Energy Fuels* 2014, 59(2), 558-561.

4.1 Introduction

One of the challenges in upgrading of asphaltenes and aromatic oils, such as coal liquids, is the conversion of multinuclear aromatic compounds. Hydroprocessing is possible, but it is not only subject to demanding thermodynamic constraints [1], but it is also H₂ intensive.

An alternative approach is to make use of an oxidative pathway, instead of the reductive pathway that consumes H₂. In principle it should be possible to make use of air as oxidant, perform the ring-opening of multinuclear aromatic structures and increase the H:C ratio of the product (Figure 4.1).

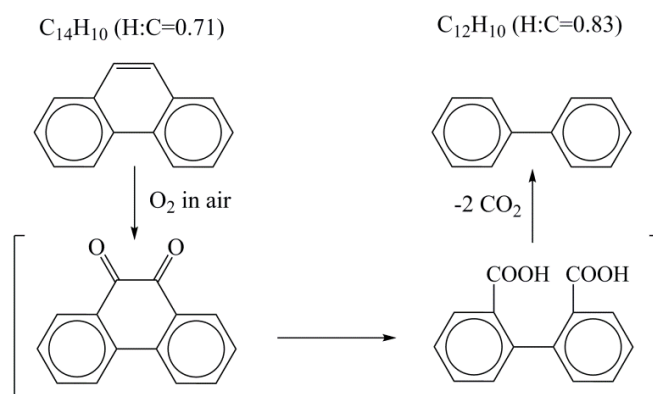


Figure 4.1. Autoxidation of phenanthracene to illustrate the concept of oxidative ring-opening

The initial oxidation of multinuclear aromatics to produce quinonoids would be comparatively easy [2]. It was anticipated that ring-opening would be the challenging step, particularly when a single carbon linked two aromatic rings. In such a case ring-opening of the quinonoid would require the scission of an aliphatic-aromatic C–C bond. Although oxidative ring-opening by a free radical mechanism is possible, selectivity was a concern. It was postulated that catalytic oxidation, using an appropriate catalyst, may enable a transition state that would not require the aromatic carbon to assume a free radical nature. In this way it might be possible to perform ring-opening more easily and selectively.

The objective of this work was to determine whether selective oxidative ring-opening of multinuclear aromatics was technically feasible using metal oxide catalysts. It was possible to envision a process concept where the metal oxide catalyst is the oxidant and it can be regenerated by air oxidation, rather than using air directly as the oxidant for the oxidative ring-opening.

4.2 Experimental Section

4.2.1 Materials

Anthracene (99%), anthraquinone (97%), vanadium oxide (V_2O_5 , 98%), molybdenum oxide (MoO_3 , 99.5%), iron oxide (Fe_2O_3 , 99%) and nickel oxide (NiO , 99%) were obtained from Sigma-Aldrich. Chloroform (99.9%) was purchased from Fisher Scientific. All chemical were used without any further purification. Nitrogen (99.998%) and extra dry air were obtained from Praxair.

4.2.2 Equipment and Procedure

Oxidation of the aromatic model compounds (anthracene and anthraquinone) and their mixtures with metal oxide catalysts (molar ratio 1:1) was studied through high pressure differential scanning calorimetry (HP-DSC). A Mettler Toledo HP-DSC 1 was used. Standard aluminum 40 μ L crucibles with perforated lids were used as reactors. Autoxidation reactions were carried out in air atmosphere while catalytic oxidations took place under nitrogen atmosphere. In all cases, the initial pressure was set at 4 MPa; then, the samples were heated from 150 to 550 $^{\circ}C$ at a rate of 10 $^{\circ}C \cdot min^{-1}$. At these conditions, oxidation of the aromatic model compounds took place in the liquid phase. Prior to the experiments, metal oxide catalysts were calcined at 500 $^{\circ}C$ for 1 h under air and then stored in a desiccator.

Catalytic oxidation of anthraquinone employing V_2O_5 as catalyst was also studied using Swagelok batch reactors. In this case, one gram of sample was placed in a stainless steel, 15 mL batch reactor. The system was purged several times and then pressurized to 4 MPa using nitrogen. The reactor was heated to 430 $^{\circ}C$ for one hour in a fluidized sand bath (Tecne SBS-4).

Typical heat-up time was 6 min. At these conditions, anthraquinone was kept in liquid phase. After reaction, gaseous products were collected in gas sampling bags and the remaining reaction products were recovered by washing with chloroform.

4.2.3 Analysis

The reaction products dissolved in chloroform were analyzed by gas chromatography with mass spectrometry (GC–MS). The gaseous products were analyzed by gas chromatography with flame ionization detector and thermal conductivity detector (GC–FID/TCD). The GC–MS analyses were carried out using an Agilent 7820A GC connected to a 5977E MS detector. The system was equipped with a 30 m × 0.25 mm × 0.25 μm HP-5MS J&W capillary column. Helium was used as the carrier gas at a constant flow rate of 1 mL·min⁻¹ and 1 μL of sample was introduced via split injection mode (split ratio 10:1). The oven temperature program was started at 90 °C and held for 2 min; then, the temperature was raised up to 320 °C at a rate of 5 °C·min⁻¹ and held for 1 min. The transfer line was kept at 325 °C. Mass detection was operated at full scan mode (mass to charge ratio range 50-550 m/z) at a rate of 2.5 scans per second. The ion temperature source was set at 230 °C. Compounds were identified by comparing the mass spectra of the products with those from the National Institute of Standards and Technology (NIST) through the NIST MS Search 2.0 – Mass Spectra Library. In addition, the retention time and the mass spectrum for some of the main products were confirmed by comparison with commercially available standards.

Gaseous reaction products were analyzed in a 7890A GC connected to both FID and TCD detectors. Separation was performed on a Hay Sep R column, 2.44 m × 3 mm, using helium as carrier gas at a constant flow of 25 mL·min⁻¹. The injector temperature was set at 200 °C. The temperature program started at 70 °C held isothermally for 7 min, followed by 10 °C·min⁻¹ increase to 250 °C where it was held for 2 min. This temperature was then increased at 30 °C·min⁻¹ to 300 °C and held for 8 min.

4.3 Results and Discussion

4.3.1 Autoxidation of Anthracene

The first step was to confirm that the air oxidation of anthracene is possible and that it is accelerated in the presence of metal oxide catalysts. The metal oxides selected were V_2O_5 , MoO_3 , Fe_2O_3 and NiO . Literature indicates that V_2O_5 and MoO_3 have been successfully used in vapor phase aromatic oxidations [3][4]; as a result, they might work as catalysts in liquid phase oxidation. On the other hand, it has been reported that iron and nickel oxides are active catalysts for the liquid phase oxidation of aromatics in the presence of oxygen and significant amounts of water [3]. Also, they are in the middle range of metal-oxygen bond strength [5], which suggests they might be appropriate candidates for selective oxidation (see Section 2.4.3 in Chapter 2). Furthermore, vanadium and nickel are the two most abundant metals in the oil sands derived asphaltenes, forming a connection between the selected catalysts and the possible feed to be upgraded in the future.

The autoxidation was performed in a HP-DSC in the liquid phase and the main thermal events that were observed are listed (Table 4.1). Melting and oxidation onset temperatures for a blank (no catalyst) experiment and for metal oxide conversions were determined. Similarly, enthalpy of fusion was found in all cases. On the other hand, enthalpy of oxidation was not determined due to the complexity of the calorigrams. The presence of several convoluted peaks made the analysis difficult.

The onset temperature and enthalpy of melting were found to be very similar between pure anthracene and anthracene that was mixed with MoO_3 , Fe_2O_3 and NiO . From prior instrument calibration it was known that repeatability of onset temperature using the DSC was better than 1 °C and the repeatability of enthalpy measurements were better than 5 % relative change. Until this point no major catalytic effect leading to oxidation was perceived for MoO_3 , Fe_2O_3 and NiO .

On the contrary, significant differences were observed when V_2O_5 was used as catalyst. In this case, the onset of oxidation occurred at a much lower temperature, 183 °C. The anthracene

was partly oxidized before melting, which was reflected in a decrease of about 5 °C in the onset temperature of melting and a decrease in melting enthalpy of around 30 J·g⁻¹ (calculated on original anthracene mass). Since the melting enthalpy of anthracene is a constant, the observed decrease in enthalpy is a measure of the oxidation conversion. The oxidation conversion was already around 20 % by the time the anthracene started melting. Since the onset temperature of melting was affected, it also suggested that the product formed by the oxidation was not volatile at the melting conditions; the oxidation product was likely to be anthraquinone.

Then, it is clear that from the catalysts tested, vanadium oxide seems to be the one with the highest catalytic contribution at lower temperatures.

Table 4.1. Main Thermal Events found in HP-DSC Analyses for the Autoxidation of Anthracene

Model Compound	Catalyst	Type of Transition ^a	Onset Temperature [°C]	Enthalpy change [J/g _{Anthracene}]
Anthracene	-	S-L	215.6	150
		Oxid	257	^b
Anthracene	V ₂ O ₅	S-L	209.9	119
		Oxid	183	^b
Anthracene	MoO ₃	S-L	216.5	159
		Oxid	260	^b
Anthracene	Fe ₂ O ₃	S-L	215.6	154
		Oxid	274	^b
Anthracene	NiO	S-L	216.0	160
		Oxid	251	^b

^a Phase transition from solid to liquid noted as S-L. Energy changes which are not heat capacity related, oxidation, noted as Oxid.

^b The baseline of the calorigrams revealed several exothermic transitions in the form of convoluted peaks; hence, enthalpy of oxidation was not determined.

4.3.2 Catalytic Oxidation of Anthracene

The results from the autoxidation study indicated that the metal oxides accelerated anthracene oxidation. It was of interest to know whether the catalysts just activated the O₂ from the air, or whether oxidation took place by transfer of lattice oxygen from the metal oxides, following a Mars-Van Krevelen mechanism. It was after all a liquid phase oxidation and generally the Mars-Van Krevelen mechanism is associated with gas phase oxidation reactions.

Table 4.2. Main Thermal Events found in HP–DSC Analysis for the Catalytic Oxidation of Anthracene

Model Compound	Catalyst	Type of Transition ^a	Onset Temperature [°C]	Enthalpy change [J/g _{Anthracene}]
Anthracene	-	S-L	216.3 ± 0.1	150 ± 19
		TDec	521 ± 8	^b
		S-L	215.2 ± 0.2	162 ± 2
Anthracene	V ₂ O ₅	Oxid-1	248 ± 4	67 ± 18
		Oxid-2	370 ± 1	150 ± 9
		Oxid-3	467 ± 1	^b
Anthracene	MoO ₃	S-L	216.6 ± 0.1	167 ± 6
		Oxid-3	467 ± 4	189 ± 53
Anthracene	Fe ₂ O ₃	S-L	215.9 ± 0.2	155 ± 7
		Oxid-3	483 ± 4	^b
Anthracene	NiO	S-L	216.5 ± 0.1	158 ± 4
		Oxid-3	503 ± 10	^b

^a Phase transition from solid to liquid noted as S-L. Thermal decomposition noted as TDec. In all of the DSC measurements a high temperature oxidation was found (noted Oxid-3). Oxidations at lower temperature have been noted as Oxid-1 and Oxid-2.

^b The peak to be integrated was incomplete at the end of the temperature program; hence, no enthalpy was not estimated.

The same experimental procedure used for autoxidation was repeated, but with nitrogen instead of air (Table 4.2) and all experiments were performed in triplicate. Care was taken to

properly purge the HP–DSC so that there was no residual O₂. It should be noted that oxidation of anthracene with the selected metal oxides was carried out using a molar ratio of 1:1. At this ratio, the oxygen balance for the reaction ([APPENDIX A](#)) showed that incomplete conversion of the anthracene was expected.

Results from HP–DSC analyses indicate that anthracene is thermally stable under the conditions selected for this study. Besides melting and thermal decomposition processes (onset temperature 216.3 ± 0.1 °C and 521 ± 8 °C, respectively), no evidence for any other transition was found in the blank experiments. On the other hand, it is clear that this behavior is modified when anthracene is in the presence of metal oxide catalysts. Thus, an exothermic event (Oxid-3) taking place at high temperature but below the thermal decomposition temperature of anthracene was observed in all cases. Furthermore, when using V₂O₅ as catalyst two additional exothermic events (Oxid-1 and Oxid-2) were found. Considering that anthracene is thermally stable at the experimental conditions and that experiments were carried out in an inert atmosphere, it is likely that these exothermic events are related to catalytic oxidation of the anthracene.

It is worth mentioning that unlike the results from the autoxidation experiments, no significant changes in the onset temperature or enthalpy of melting of anthracene were observed when using any of the metal oxides under inert atmosphere. Thus, there is no evidence of anthracene oxidation before melting.

In order to confirm that the exothermic Oxid-1 event observed by DSC was indeed oxidation, a separate experiment was conducted whereby the anthracene was heated under inert conditions with V₂O₅ as catalyst to 310 °C only. Reaction products from this experiment were analyzed by GC-MS and the presence of anthraquinone was confirmed. More importantly, it confirmed that oxidation took place by transfer of lattice oxygen from the V₂O₅, which was the only source of oxygen in the reaction medium.

4.3.3 Autoxidation of Anthraquinone

Since it is comparatively easy to oxidize anthracene to anthraquinone [2], it was decided to repeat the autoxidation experiments, but with anthraquinone as starting material. The onset temperature of oxidation increased (Table 4.3) compared to that of anthracene (Table 4.1). Once again V_2O_5 seemed to accelerate oxidation much more than any of the other catalysts. In fact, the other metals oxides seemed to have an inhibitory effect, delaying the onset of oxidation.

Table 4.3. Main Thermal Events found in HP–DSC Analyses for the Autoxidation of Anthraquinone

Model Compound	Catalyst	Type of Transition ^a	Onset Temperature [°C]	Enthalpy [J/gAnthracene]
Anthraquinone	-	S-L	284.8	166
		Oxid	393	^b
Anthraquinone	V_2O_5	S-L	283.9	132
		Oxid	313	^b
Anthraquinone	MoO_3	S-L	283.2	164
		Oxid	444	^b
Anthraquinone	Fe_2O_3	S-L	284.9	168
		Oxid	387	^b
Anthraquinone	NiO	S-L	283.2	167
		Oxid	449	^b

^a Phase transition from solid to liquid noted as S-L. Energy changes which are not heat capacity related, oxidation, noted as Oxid.

^b The baseline of the calorigrams revealed several exothermic transitions in the form of convoluted peaks; hence, enthalpy of oxidation was not determined. In general the complexity of the baseline was less than found for anthracene (Table 4.1). There were less overlapping events and the change in the slope of the baseline suggested that the oxidation products were volatile at 4 MPa and the temperature of conversion.

It is worth mentioning that the temperature and enthalpy of melting for the anthraquinone was not affected by the presence of the catalysts except in the case of V_2O_5 . Oxidation of the anthraquinone took place before melting only in the presence of V_2O_5 . The onset temperature of

melting was not affected, but there was a decrease in the enthalpy of melting of about $35 \text{ J}\cdot\text{g}^{-1}$ (calculated on original anthraquinone mass). Using a similar argument as before, this indicated that about 20 % of the anthraquinone was converted before melting was completed. However, no clear onset of oxidation was observed in the calorigram before melting. Furthermore, the shape of the peak associated with melting indicated that two events were taking place in parallel, which could have affected the enthalpy value.

4.3.4 Catalytic Oxidation of Anthraquinone

Table 4.4. Main Thermal Events According to HP-DSC Analysis for the Catalytic Oxidation of Anthraquinone

Model Compound	Catalyst	Type of transition ^a	Onset Temperature [°C]	Enthalpy [J/gAnthracene]
Anthraquinone	-	S-L	283.9 ± 0.3	170 ± 2
		TDec	531 ± 3	^b
		S-L	283.7 ± 0.1	160 ± 3
Anthraquinone	V_2O_5	Oxid-1	386 ± 1	295 ± 5 ^c
		Oxid-2	431 ± 1	
		Oxid-3	496 ± 7	^b
Anthraquinone	MoO_3	S-L	284.2 ± 0.2	168 ± 4
		Oxid-3	513 ± 1	173 ± 10
Anthraquinone	Fe_2O_3	S-L	285.2 ± 0.3	169 ± 1
		Oxid-3	512 ± 2	^b
Anthraquinone	NiO	S-L	283.6 ± 0.1	170 ± 1
		Oxid-3	523 ± 1	^b

^a Phase transition from solid to liquid noted as S-L. Thermal decomposition noted as TDec. In all of the DSC measurements a high temperature oxidation was found (noted Oxid-3). Oxidations at lower temperature have been noted as Oxid-1 and Oxid-2.

^b The peak to be integrated was incomplete at the end of the temperature program; hence, no enthalpy was not estimated.

^c The peaks representing Oxid-1 and Oxid-2 events were not separated.

It was necessary to demonstrate that the metal oxides could also transfer lattice oxygen to anthraquinone. The oxidation of anthraquinone was performed under N₂ atmosphere with the different metal oxides (Table 4.4).

Results from HP–DSC analyses were similar to the ones obtained for anthracene. Melting and thermal decomposition were the only two events observed in the temperature range studied. The onset temperature of melting of anthraquinone was 283.9 ± 0.3 °C and the onset of thermal decomposition was at 531 ± 3 °C. Thus, anthraquinone was thermally stable at the chosen experimental conditions over the duration of the thermal analysis until it reached its decomposition temperature.

A different behavior was observed when the anthraquinone was in the presence of the catalysts. An exothermic event (Oxid-3) occurred at a lower temperature than the thermal decomposition temperature for anthraquinone and it was observed in all cases. Also, two exothermic events occurred when using V₂O₅ as catalyst (Oxid-1 and Oxid-2). Analogous events were observed when converting anthracene under inert atmosphere over V₂O₅. It indicated that V₂O₅ was capable of oxidizing anthraquinone, which might include some oxidative ring-opening reactions. The nature of the products from this conversion was therefore of interest.

4.3.5 Product Characterization

The most promising metal oxide for the oxidation of anthraquinone was V₂O₅. In order to produce a larger volume of product for characterization, the V₂O₅ catalyzed oxidation of anthraquinone was repeated in a batch-reactor under N₂ atmosphere. A blank experiment (no V₂O₅) with anthraquinone and an experiment with anthraquinone and V₂O₅ were performed. A temperature of 430 °C was selected, because it is higher than Oxid-1 in Table 4.4, but lower than the onset of the other oxidation events. The products that were not volatile at ambient conditions were collected for analysis by GC–MS (Figure 4.2 and Figure 4.3). The main products were identified using the electron impact mass spectra, as well as commercially obtained model compounds (Table 4.5).

Although the DSC experiments indicated that the onset of thermal decomposition of anthraquinone was about 100 °C higher than the operating temperature selected, it is worthwhile to point out that decomposition, unlike melting, is a kinetic event. At the heating rate employed during DSC analysis the decomposition rate became noticeable at 531 ± 3 °C, but that did not imply that no thermal reactions would take place at lower temperatures. With 1 h of reaction time, thermal reactions that are slow at 430 °C could still contribute to thermal conversion. It was important to distinguish the products from thermal degradation of anthraquinone from that of the catalytic oxidation of anthraquinone.

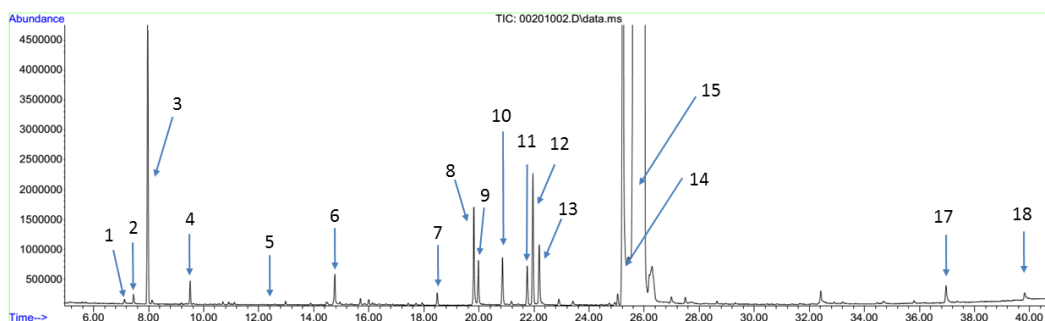


Figure 4.2. GC-MS analysis of products obtained by conversion of anthraquinone (no V_2O_5) at 430 °C, 4 MPa N_2 for 1 h

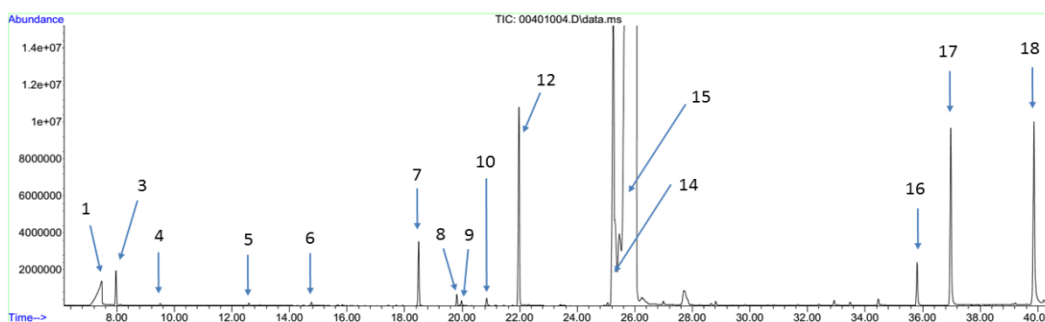


Figure 4.3. GC-MS analysis of products obtained by conversion of anthraquinone with V_2O_5 at 430 °C, 4 MPa N_2 for 1 h

It was not surprising to find very similar reaction products in the blank experiment with no V₂O₅ and the V₂O₅ catalyzed experiment (Table 4.5). The production of lighter compounds seems to be more significant in the blank experiment, in which only thermal decomposition took place. Over the V₂O₅ catalyst, some heavier molecules were also produced. The difference in relative abundance of compounds highlights differences in the reaction selectivity; the catalyst enables different reaction pathways.

Table 4.5. Compounds Identified through GC–MS for Catalytic Oxidation of Anthraquinone

Peak Number	Compound	Figure 4.2	Figure 4.3
1	Benzoic acid ^a	x	x
2	Tetralin ^a	x	
3	Naphthalene ^a	x	x
4	Benzene, 1,3-bis(1,1-dimethylethyl)- ^b	x	x
5	Biphenyl ^a	x	x
6	1-hexadecanol ^b	x	x
7	Benzophenone ^a	x	x
8	Dodecil acrylate ^b	x	x
9	Propanoic acid, decyl ester ^b	x	x
10	Fluorenone ^a	x	x
11	9H-Fluorenone, 9methylene ^b	x	
12	Anthracene ^a	x	x
13	Ethanone, 1-(9,10-dihydro-9-anthracenyl)- ^b	x	
14	Anthrone ^a	x	x
15	Anthraquinone ^a	x	x
16	12-Ethylbenz[a]anthracene-7-carbaldehyde ^b		x
17	9,10-Anthracenedione, 1-phenyl- ^b	x	x
18	Indan-1,3-dione, 2-(1-naphthylmethylene)- ^b	x	x

^a Mass spectrum and retention time for these compounds was confirmed through the analysis of standards.

^b Although specific compounds and in some instances specific isomers are indicated, these should be seen only as indicative of the true nature of the products. The true identities of these compounds have not been confirmed.

The presence of compounds such as benzoic acid, naphthalene, biphenyl and benzophenone, among others, shows that ring-opening of multinuclear aromatics took place. In particular, the relative abundance of benzophenone (peak 7) and addition products formed due to ring-opening (peaks 16-18) were higher for the reaction over V_2O_5 . The results provided sufficient evidence that catalytic oxidation leading to ring-opening was taking place, but the reaction sequence was obscured by the contribution of thermal cracking. This was a consequence of the extended reaction time.

The DSC results indicated that the Oxid-1 event (Table 3.4) was initiated and completed while heating from 386 to 431 °C at a heating rate of 10 °C·min⁻¹, i.e. within 4½ min. In future work shorter contact times will be employed to learn more about the reaction network of V_2O_5 catalyzed ring-opening of anthraquinone.

4.4 Conclusions

The possibility of using metal oxide catalysts to catalyze the oxidative ring-opening of multinuclear aromatics was investigated. The metal oxides investigated were V_2O_5 , MoO_3 , Fe_2O_3 and NiO in combination with anthracene and anthraquinone. The main conclusions from the experimental investigation were:

- (a) Anthracene was measurably oxidized by air after melting in the absence of any metal oxide.
- (b) In the presence of V_2O_5 , air oxidation of anthracene took place at measurable rate before melting.
- (c) The catalytic effect of MoO_3 , Fe_2O_3 and NiO during the air oxidation of anthracene was noticeable only a very high temperature.

- (d) The onset of oxidation of anthracene by V_2O_5 under N_2 atmosphere was observed at 248 ± 4 °C. Anthraquinone was found in the reaction product (confirmed by GC-MS).
- (e) V_2O_5 was capable of using lattice oxygen for the oxidation of anthracene in the liquid phase. A Mars-Van Krevelen mechanism was likely.
- (f) Air oxidation of anthraquinone exhibited analogous behavior to that of anthracene. Only V_2O_5 measurably accelerated oxidation.
- (g) Under N_2 atmosphere, the oxidation of anthraquinone was catalyzed by V_2O_5 , with an onset at 386 ± 1 °C.
- (h) V_2O_5 was capable of using lattice oxygen for the oxidation of anthraquinone in the liquid phase.
- (i) A more detailed analysis of the products from thermal decomposition and V_2O_5 decomposition of anthraquinone provided evidence that catalytic oxidation was leading to ring-opening.
- (j) The work showed that oxidative ring-opening of multinuclear aromatics by transfer of lattice oxygen from V_2O_5 was technically viable.

4.5 References

- [1] Le Page, J. F. *Applied heterogeneous catalysis*; Technip: Paris, 1987, pp 366-401.
- [2] Tipson, R. S. *Oxidation of polycyclic, aromatic hydrocarbons. A review of the literature* (National Bureau of Standards monograph 87); National Bureau of Standards: Washington DC, 1965.
- [3] Marek, L. F.; Hahn, D. A. *The catalytic oxidation of organic compounds in the vapor phase* (ACS Monograph Ser. 61); Chemical Catalogue Company: New York, 1932.

- [4] Dixon, J. K.; Longfield, J. E. Hydrocarbon oxidation. In *Catalysis Vol. VII*; Emmett, P. H. Ed.; Reinhold: New York, 1960; p 183-280.
- [5] Hucknall, D. J. *Selective oxidation of hydrocarbons*; Academic Press: London, 1974, pp 147-150.

5. Oxidative Ring-Opening of Aromatics: Decomposition of Biphenyl Carboxylic Acids and Zinc Biphenyl Carboxylates ¹

ABSTRACT

Ring-opening conversion of multinuclear aromatics can be used to upgrade heavy aromatic oils to lighter products, and it is usually performed reductively with H₂. Oxidative ring-opening is an alternative strategy that involves three steps: (i) oxidation of multinuclear aromatics to quinonoids, (ii) further oxidation and ring-opening to produce aromatic carboxylic acids, and (iii) decarboxylation of aromatic carboxylic acids. In the last step, decomposition by ketonization is an undesirable side reaction that leads to a ring-closed product. Selectivity control during aromatic carboxylic acid decomposition was investigated using biphenyl-2-carboxylic acid, biphenyl-2,2'-dicarboxylic acid, zinc(II) biphenyl-2-carboxylate, and zinc(II) biphenyl-2,2'-dicarboxylate. The reaction networks of thermal decomposition of the aromatic carboxylic acids were determined. Decomposition of biphenyl-2-carboxylic acid took place mainly by decarboxylation to produce biphenyl, dehydration and ring closure to produce fluorenone, and the formation of diphenic anhydride as intermediate product leading to fluorenone. Decomposition of biphenyl-2,2'-dicarboxylic acid proceeded through decarboxylation to biphenyl-2-carboxylic acid as intermediate, as well as two seemingly related pathways, leading to the formation of a hydroxy-fluorenone and a cyclic trione. Over the temperature range from 340 °C to 400 °C, thermal decomposition invariably resulted in a higher ketonization than decarboxylation selectivity. Decomposition of the analogous zinc carboxylates demonstrated that ketonization could be suppressed and the most abundant products were biphenyl > fluorenone > fluorene. It was possible to achieve a biphenyl (decarboxylation) to fluorenone (ketonization) selectivity ratio of 17:1 during batch reactor decomposition of zinc(II) biphenyl-2,2'-dicarboxylate at 380 °C. Reaction stoichiometry indicated that water should affect selectivity, which is consistent with observations in the literature, but this aspect was not investigated further.

Keywords: Aromatic carboxylic acids, thermal decomposition, catalytic decomposition.

¹ Reprinted with permission from Montoya Sánchez, N.; De Klerk, A. Oxidative ring-opening of aromatics: Decomposition of biphenyl carboxylic acids and zinc biphenyl carboxylates. *Energy Fuels* 2015, 29, 7910-7922. Copyright 2015 American Chemical Society. <http://pubs.acs.org/doi/abs/10.1021/acs.energyfuels.5b02066>.

5.1 Introduction

The efficient conversion of multinuclear aromatics is one of the major challenges faced in the upgrading of asphaltene and aromatic oils. Heavy aromatic materials can and are upgraded by hydroprocessing [1][2][3], but such upgrading is severe and hydrogen-intensive. In fuel oil or oil transport applications, where upgrading is necessary only to improve fluidity, it is preferable to employ less costly processes. Although coking or visbreaking may be employed [3], low liquid yield is obtained from very aromatic oils and asphaltene. It is necessary to ring-open multinuclear aromatics to improve fluidity. Vapor-phase oxidative ring opening of aromatics is practiced for the production of chemicals [4]. This chemistry can, in principle, also be applied to heavier materials, but it has been found that liquid-phase oxidation of heavy oils leads to a decrease in fluidity [5][6]. It is suspected that the decrease in fluidity is caused by free radical addition reactions [7]. Oxidation must be catalytic and not free-radical-based to limit the extent of additional reactions.

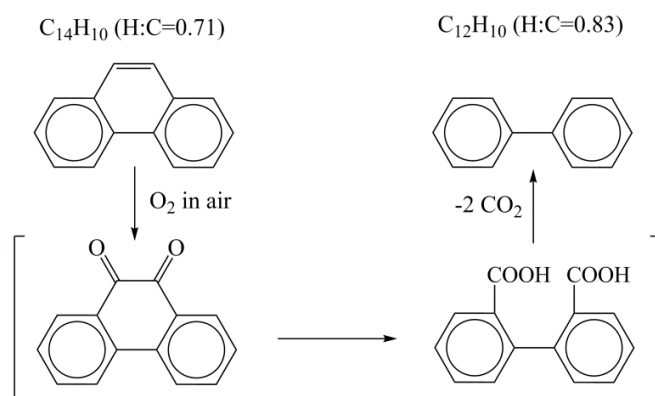


Figure 5.1. Autoxidation of phenanthrene to illustrate the concept of oxidative ring-opening

Catalytic oxidative ring opening might be an alternative approach to traditional practices, such as hydroprocessing, for the upgrading of aromatic oils and asphaltene. The insertion of oxygen into the aromatic structure leads to C–C bond scission and ring-opening of the multinuclear aromatics, with ultimately an increase in the H:C ratio of the products (Figure 5.1).

Experimental evidence was presented that the oxidative ring opening of multinuclear aromatics by transfer of lattice oxygen from an appropriate metal oxide catalyst, such as V_2O_5 , was technically feasible [8]. As expected, the oxidative cleavage of the C–C bonds resulted in the formation of carboxylic acid groups and some ring-opened products were formed. Nonetheless, the production of these ring-opened compounds was obscured by the contribution of thermal cracking, which is a free-radical process. Furthermore, the results suggested that the reaction might be limited by the chemical equilibrium between ring-opening and ring-closure reactions.

For oxidative ring-opening to be a viable process for asphaltenes conversion, additional work has to be done to shift this equilibrium towards the production of more ring-opened products and limit the contribution of free radical chemistry by decreasing the temperature. Removal of the carboxylic acid functionality by rejecting the carbon as CO_2 would help to disturb the chemical equilibrium and improve the overall performance of the reaction. Therefore, a study of the decomposition of carboxylic acid species produced by the oxidative ring opening of multinuclear aromatics is pertinent to the development of catalytic oxidative ring opening as a process.

In this study, the decomposition of biphenyl dicarboxylic acid and biphenyl monocarboxylic acid were investigated. The biphenyl carboxylic acids are key intermediates in the oxidative ring opening of phenanthrene. These model compounds were studied to elucidate the reaction network of biphenyl carboxylic acid decomposition. Thermal decomposition and catalytic decomposition, using zinc carboxylates as intermediates, were studied with the objective of understanding how to manipulate the reaction selectivity during decomposition. Determining the reaction parameters that would increase the selectivity to the ring-opened product (biphenyl), and limit the side reactions that lead to ring-closure, was of particular interest.

5.2 Experimental Section

5.2.1 Materials

Two aromatic carboxylic acids were selected as model compounds to conduct the thermal decomposition studies. Biphenyl-2,2'-dicarboxylic acid (97%) and biphenyl-2-carboxylic acid (98%) were obtained from Sigma-Aldrich. The zinc carboxylates used to perform the catalytic decomposition work were synthesized using the same carboxylic acids and some commercially available materials. Zinc carbonate basic ($\geq 58\%$, on a Zn basis) was purchased from Sigma-Aldrich, and tetrahydrofuran (99.9%) and acetone (99.5%) were obtained from Fisher Scientific. Deionized water was prepared using a Millipore water purification system. All chemical were used without further purification.

High-purity reference materials used for the temperature and enthalpy calibration of the differential scanning calorimeters employed in this study were commercially available and used as received. Indium (99.999%) and zinc (99.999%) were supplied by Impag AG. Nitrogen of ultrahigh purity (99.999%) obtained from Praxair was used to maintain an inert atmosphere during calorimetric and thermogravimetric analyses.

Phthalic anhydride (99%), biphenyl (99%), fluorenone (98%), 9-methyl-9H-fluorene ($\geq 99\%$), fluorene (98%), fluorenone (98%), and diphenic anhydride (98%) were obtained from Sigma-Aldrich and were used to facilitate the identification of the decomposition products via gas chromatography coupled with mass spectrometry (GC-MS) analyses. Chloroform (98%, HPLC grade, Fisher Scientific) was used as the general solvent for these analyses.

5.2.2 Synthesis of Zinc Carboxylates

Zinc carboxylates were synthesized by means of a neutralization reaction. Basic zinc carbonate and a slight excess (2% molar excess) of the corresponding aromatic carboxylic acid were mixed, using an aqueous solution of tetrahydrofuran (THF) as solvent. The reaction mixture was heated at 90 °C with uniform stirring for several hours to complete the reaction.

Solid zinc carboxylates, of a light beige color, were recovered by evaporation of the solvent under reduced absolute pressure (80 kPa, absolute), using a rotary evaporator (Heidolph, Model Hei-VAP Precision with Glassware Set G3).

The zinc carboxylates were further purified by washing them thoroughly with acetone, and then they were dried at ~100 °C until they reached constant mass. Final products were finely ground and stored in a desiccator before analysis.

5.2.3 Equipment and Procedure

All decomposition experiments for the aromatic carboxylic acids and their corresponding zinc carboxylates were performed using Swagelok batch reactors. Samples of these compounds were placed in 15 mL stainless steel batch reactors. Before reaction, care was taken to properly purge the system with nitrogen so that there was no residual oxygen. Decomposition of the aromatic carboxylic acids was carried out at 4 MPa (initial pressure), whereas for the zinc carboxylates, the pressure was kept at atmospheric conditions. Pressure was used to keep the acids in the liquid phase under reaction conditions and was not necessary for the zinc carboxylate salts. The reactors were heated between 20 min and 2 h using a fluidized sand bath (Tecne SBS-4). Typical heat-up time was 6 min. After reaction, gaseous products were collected in gas sampling bags and the remaining products were recovered by washing with chloroform.

5.2.4 Analyses

Calorimetric and analytical techniques were used to support the experimental investigation.

(a) Decomposition and Thermal Behavior. The decomposition and thermal behavior of the aromatic carboxylic acids and their respective zinc carboxylates were studied by differential scanning calorimetry (DSC). Note that the results from DSC analysis allowed one to determine the reaction temperature used in the decomposition experiments (i.e., experiments using batch reactors).

The analysis of the aromatic carboxylic acids was carried out in a high-pressure differential scanning calorimeter (Mettler–Toledo HPDSC 1). Decomposition reactions were carried out under a nitrogen atmosphere, and the pressure was set at 4 MPa. Care was taken to properly purge the HP-DSC system so that there was no residual oxygen in the sample chamber. High-pressure conditions were required to avoid sample loss by evaporation. On the other hand, thermal analysis of the zinc carboxylates was conducted in a normal pressure differential scanning calorimeter (Mettler–Toledo DSC 1). Experiments were conducted under a nitrogen atmosphere. For this particular study, the sample chamber nitrogen flow rate and the sheathing nitrogen flow rate were kept at 100 mL min⁻¹ during all of the experiments. Both calorimeters were of the heat flux (disk) type and were equipped with FRS-5 sensors.

For all of the thermal analyses, standard 40 µL aluminum crucibles with pins and perforated lids were employed. The typical procedure involved piercing the lids of the crucibles on a clean rubber surface, using a needle with a diameter of ~1 mm. After weighing the samples, crucibles were sealed using a crucible sealing press. Sample sizes were maintained in the range of 5–12 mg. Samples were weighed on an analytical balance (Mettler–Toledo, Model XS105 Dual Range Analytical Balance) with 10 µg readability in the range of 0–105 g. Similarly, all thermal analyses were performed at a heating rate of 10 °C min⁻¹ and samples were heated from 25 °C to 550 °C. Reversibility of thermal events was studied by heating just past the observed thermal event and then cooling below the transition and heating up again. Temperature and enthalpy were checked against indium and zinc standards. All analyses were performed in triplicate.

(b) Mass Loss Profile for the Zinc Carboxylates. The mass loss profile for the zinc carboxylates was determined by thermogravimetric analysis. A Mettler-Toledo TGA/DSC1 system with an LF furnace, a sample robot, and a MX5 internal microbalance was used. Experiments were carried out under a nitrogen atmosphere. A sheathing nitrogen flow rate of minimum 20 mL min⁻¹ was maintained during experiments. Also, standard 70 µL alumina crucibles without lids were employed. Samples were heated from 25 °C to 600 °C, at a heating rate of 10 °C min⁻¹. Similar

experiments using a simultaneous thermogravimetric analysis/Fourier transform infrared spectroscopy (TGA-FTIR) system allowed the nature of the gases evolved during thermogravimetric analysis to be studied. The equipment used consisted of a thermogravimetric analyzer (TA Instruments, Model Q-500) coupled to an Agilent Model Cary-670 FTIR spectrometer. In this case, the evolved gases were transported to a gas cell installed in the FTIR spectrometer. The transfer line was kept at 200 °C. The sample was scanned 32 times by the FTIR spectrometer, with a sampling interval of 6 s.

(c) Chemical Identity of the Synthesized Metal Carboxylates. Infrared spectroscopy was used to confirm the chemical identity of the synthesized metal carboxylates. An FTIR spectrometer (ABB, Model MB3000) with Horizon MB FTIR software was used to collect the infrared spectra. The spectrometer was equipped with a Pike MIRacle Reflection attenuated total reflectance (ATR) diamond crystal plate. The infrared analysis was performed at a resolution of 4 cm^{-1} , using an average of 120 scans over the spectral region of 4000–500 cm^{-1} .

(d) Analysis of Reaction Products. Gas chromatography with mass spectrometry (GC-MS) was used to analyze the reaction products. The reaction products were dissolved in chloroform after the batch decomposition experiments. Analyses were carried out using an Agilent Model 7820A GC system that was connected to a Model 5977E MS detector. Separation was performed on a 30 m \times 0.25 mm \times 0.25 μm HP-5MS J&W capillary column, using helium as the carrier gas at a constant flow rate of 1 mL min^{-1} . The oven temperature program was started at 90 °C and held for 2 min; then, the temperature was increased to 320 °C at a rate of 5 °C min^{-1} and held for 1 min. The transfer line was kept at 325 °C. The ion temperature source was set at 230 °C. Compounds were identified by comparing the mass spectra of the products with those from the National Institute of Standards and Technology (NIST) through the NIST MS Search 2.0–Mass Spectra Library. In addition, the retention time and the mass spectrum for the main products were confirmed by comparison with commercially available standards.

5.2.5 Calculations

Quantification of the energy change associated with a decomposition event observed during thermal analysis is complicated by the mass loss. Mass loss affects the baseline heat flow of the DSC and changes the sample mass used to calculate the enthalpy change. The enthalpy values corresponding to the energy released or consumed during a thermal event were calculated by dividing the energy associated with the event by the average mass of the sample during the event (Eq. 1). The arithmetic average sample mass corresponded to the average mass at the onset and endset temperatures of the event.

$$\text{Enthalpy of transition} \left[\frac{\text{kJ}}{\text{kg}} \right] = \frac{\text{Energy released due to thermal event} [\text{kJ}]}{\text{Average sample mass involved in thermal event} [\text{kg}]} \quad (1)$$

5.3 Results and Discussion

5.3.1 Thermal Decomposition of Aromatic Carboxylic Acids

5.3.1.1 Product Characterization

Decomposition of biphenyl-2-carboxylic and biphenyl-2,2'-dicarboxylic acid was investigated. Aromatic acid compounds were specifically selected, so that the findings of this work may assist the previously mentioned oxidative ring-opening strategy. Experiments were conducted in batch reactors, and the reaction temperature was selected according to the results from DSC analysis. The products that were not volatile under ambient conditions were collected for analysis by GC-MS. The main reaction products were identified using the electron impact mass spectra, as well as commercially available standards (Table 5.1 and Table 5.2). To facilitate comparison, the identification of products from the zinc carboxylates are shown in the same tables, but these compounds will be discussed only in Section 5.3.2.

The product distribution for the different thermal decomposition reactions was semiquantitatively determined in order to elucidate the reaction pathways (Table 5.3).

Thermal decomposition of biphenyl-2-carboxylic acid, the aromatic monocarboxylic acid, was conducted at 350 and 385 °C. A relatively simple and very similar product distribution was observed in both cases (Figure 5.2). In terms of the lighter products, essentially the same compounds were obtained at both temperatures. Biphenyl, fluorene, fluorenone, and diphenic anhydride (peaks 3, 5, 15, and 19, respectively) comprise the lighter reaction products. In particular, fluorenone and biphenyl are the most abundant ones (Table 5.3). The difference in the relative abundance of the different compounds indicates a change in the reaction selectivity due to temperature. Also, the production of heavier molecules, formed due to the most likely addition reactions, seems to be more significant when decomposition was carried out at a higher temperature. The implication is that the addition products are thermally stable, since cracking is usually favored by higher temperature, and higher temperature does not favor free radical addition. The addition products that were identified (Table 5.1 and Table 5.2) indicated some aromatic C–C bond formation subsequent to elimination of the carboxylic acid group, but mainly addition through the carbon on the 9-position of fluorene. This would explain the increase in addition product formation at higher temperature, because these C–C bonds formed by addition are strong and were thermally stable under the test conditions.

An increase in temperature favored both biphenyl selectivity and selectivity to addition products. These two outcomes seem to be linked through the way in which hydrogen is redistributed at high temperature and how intermediates are stabilized, i.e., by hydrogen or by carbon addition. In a mixture where hydrogen transfer is facilitated, it is anticipated that addition product selectivity would be suppressed. For example, <5% addition selectivity was typically found when benzoic acid and derivatives were pyrolyzed at 400 °C diluted in different aromatic solvents [9]. Addition product formation was explained in terms of free radical addition. Despite the thermal nature of the conversion, there is evidence that decarboxylation of aromatic carboxylic acids proceeds mainly through an ionic pathway instead [10]. Evidence for an ionic pathway was also presented for the decarboxylation of aromatic acids at lower temperatures [11].

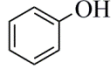
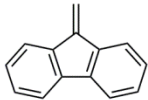
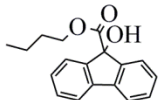
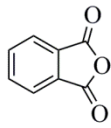
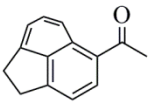
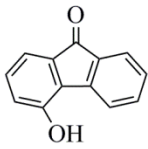
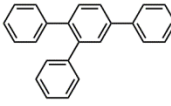
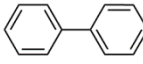
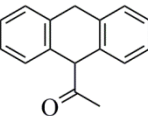
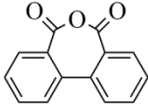
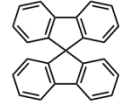
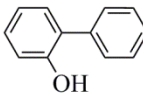
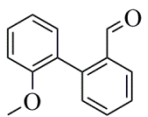
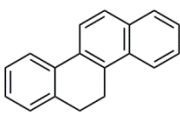
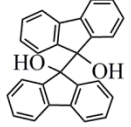
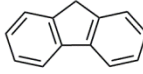
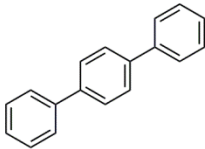
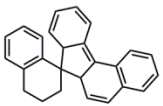
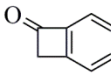
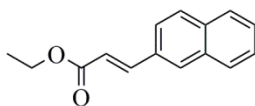
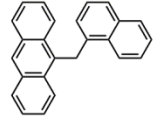
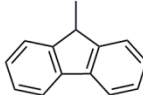
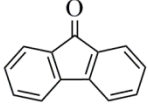
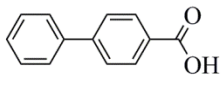
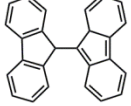
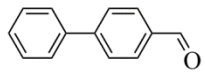
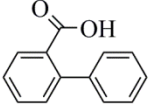
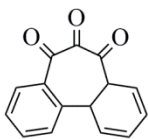
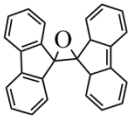
Table 5.1. Products from decomposition reactions identified by GC-MS analysis

Peak	Products	Biphenyl-2-carboxylic acid		Biphenyl-2,2'-dicarboxylic acid		Zinc(II) biphenyl-2,2'-dicarboxylate			Zinc(II) biphenyl-2-carboxylate	
		Temperature [°C]		340	400	263	380	35	250	390
		Time [min]		20	20	20	20	60	60	60
1	Phenol ^b			x	x	x	x			
2	Phthalic Anhydride ^a			x						
3	Biphenyl ^a	x	x	x	x	x	x	x	x	x
4	o-Hydroxybiphenyl ^b		x		x				x	x
5	Fluorene ^a	x	x		x		x	x		x
6	Benzocyclobuten-1(2H)-one ^b			x						
7	9H-Fluorene, 9-methyl ^b						x	x		x
8	[1,1'-Biphenyl]-4-carboxaldehyde ^b								x	x
9	Unidentified						x	x		
10	Acenaphthene, 5-acetyl ^b						x	x		x
11	Ethanone, 1-(9,10-dihydro-9-anthracenyl)- ^b						x			x
12	2'-Methoxy-[1,1'-biphenyl]-2-carboxaldehyde ^b								x	x
13	Unidentified (C ₁₄ H ₁₀) ^b							x		
14	Unidentified ^b						x			
15	Fluorenone ^a	x	x	x	x		x	x	x	x
16	Biphenyl-2-carboxylic acid ^a	x	x	x	x					
17	9H-Fluorene, 9-methylene- ^b							x		
18	4-hydroxy-9-fluorenone ^b			x	x				x	x
19	Diphenic anhydride ^a	x	x	x	x					
20	5,6-Dihydrochrysene ^b						x	x		
21	p-Terphenyl ^b						x	x		
22	2-Propenoic acid, 3-(2-naphthalenyl)- ^b			x						
23	Biphenyl-4-carboxylic acid ^b			x						
24	Dibenzo[<i>a,c</i>]cycloheptene-5,6,7-trione ^b			x	x					
25	Flurenol butyl ester ^b				x					
26	1,1':2',1''-Terphenyl, 4'-phenyl- ^b		x							x
27	9,9'-Spirobifluorene ^b	x	x							
28	9,9'-bis-(9H-fluorene), 9,9'-hydroxy- ^b		x							
29	Spiro[7H-benzo[<i>c</i>]fluorene-7,1'(2'H)-naphthalene], 3',4'-dihydro- ^b		x	x	x					
30	(1-Naphthyl)(9-phenanthryl)methane ^b							x		
31	9,9'-Bi-9H-fluorene ^b				x					
32	9,9'-Bifluorene, 9,9'-epoxy- ^b	x	x							

^a Mass spectrum and retention time of these compounds were verified by analysis of commercial standards.

^b These compounds should be seen only as indicative of the nature of the products. The true identities of these compounds have not been confirmed.

Table 5.2. Chemical Structure of the Products from Decomposition Reactions Identified by Gas Chromatography-Mass Spectroscopy (GC-MS)

Peak	Compound	Peak	Compound	Peak	Compound	Peak	Compound
1 ^b		9 ^b	Unidentified	17 ^b		25 ^b	
2 ^a		10 ^b		18 ^b		26 ^b	
3 ^a		11 ^b		19 ^a		27 ^b	
4 ^b		12 ^b		20 ^b		28 ^b	
5 ^a		13 ^b	Unidentified	21 ^b		29 ^b	
6 ^b		14 ^b	Unidentified	22 ^b		30 ^b	
7 ^b		15 ^a		23 ^b		31 ^b	
8 ^b		16 ^a		24 ^b		32 ^b	

^a Mass spectrum and retention time of these compounds were verified by analysis of commercially obtained compounds.

^b These compounds should be seen only as indicative of the nature of the products. The true identities of these compounds have not been confirmed.

Table 5.3. Relative abundance of the reaction products from thermal decomposition of aromatic carboxylic acids

Peak	Reaction Product	Biphenyl-2-carboxylic acid		Biphenyl-2,2'-dicarboxylic acid	
		350 °C	385 °C	340 °C	400 °C
3	Biphenyl	2.5×10^8	8.9×10^8	1.1×10^7	6.3×10^8
5	Fluorene	4.7×10^6	2.8×10^7	-	7.8×10^7
15	Fluorenone	5.7×10^8	1.3×10^9	1.4×10^9	2.2×10^9
16	Biphenyl-2-carboxylic acid	2.4×10^9	2.9×10^9	6.4×10^7	2.2×10^7
18	4-Hydroxy-9-fluorenone	-	-	1.5×10^7	3.4×10^7
19	Diphenic anhydride	2.7×10^7	7.3×10^6	3.3×10^8	8.9×10^6
24	Dibenzo[a,c]cycloheptene-5,6,7-trione	-	-	1.6×10^7	5.7×10^7
29	Spiro[7H-benzo[c]fluorene-7,1'(2'H)-naphthalene], 3',4'-dihydro-	-	-	-	4.5×10^7

Decomposition reactions for biphenyl-2,2'-dicarboxylic acid, the aromatic dicarboxylic acid, were carried out at 340 and 400 °C. As expected, the more-complex product distribution found in these experiments is an indication of the additional difficulty in the decomposition chemistry, because of the presence of a second carboxylic acid group in the parent molecule (Figure B.1 in the APPENDIX B). Regarding the lighter products, similar compounds were produced at 340 and 400 °C. Biphenyl, fluorenone, biphenyl-2-carboxylic acid, 4-hydroxy-9-fluorenone, diphenic anhydride, and dibenzo[a,c]cycloheptene-5,6,7-trione (peaks 3, 15, 16, 18, 19, and 24, respectively) are present as part of the product slate in both cases; although their relative abundance changed with temperature, fluorenone seems to remain as the major reaction product.

On the other hand, production of heavier compounds is quite significant when the temperature reached 400 °C. Compounds containing naphthenic and aromatic rings, and some oxygenated functionality denote the nature of these heavy products (e.g., peaks 25, 29, and 31). Moreover, the occurrence of addition reactions, as well as secondary reactions that involve C–C bond formation and oxygen elimination, would explain how they formed.

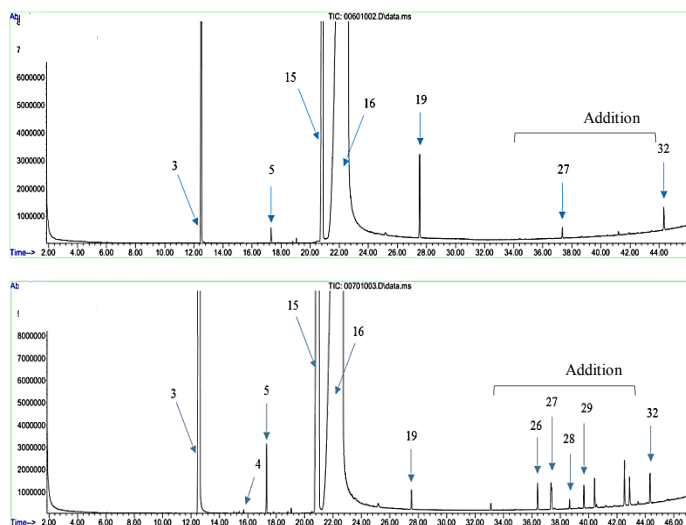


Figure 5.2. Chromatogram of biphenyl-2-carboxylic acid decomposition products after 20 min reaction under 4 MPa N₂ pressure at **(a)** 350 °C, and **(b)** 385 °C

5.3.1.2 Reaction Network

Understanding the chemistry that was taking place during the thermal decomposition of aromatic carboxylic acids is of particular interest for this work. Therefore, once the reaction products were identified, determining the reaction network for the decomposition process became the next step.

Experimental evidence suggested that decomposition of biphenyl-2-carboxylic acid involved multiple reactions (Figure 5.3). Furthermore, the nature of the reaction products shows that decomposition takes place via two major pathways, namely, decarboxylation and ketonization. Such chemical routes can be explained in terms of the primary products. On one side, biphenyl is a clear product of decarboxylation; it formed because the acid functionality was rejected as carbon dioxide. On the other hand, fluorenone is the result of unimolecular dehydration of the aromatic carboxylic acid. When water is removed from the acid molecule, a new C–C bond is formed; as a consequence, the product contains a ketone group within the now ring-closed structure. It was not surprising to find this type of compound among the reaction products. According to the literature, ring closure by intramolecular ketonization was known to be a

possibility and it is one of the older synthetic pathways for the preparation of cyclic ketones [12]. Note that fluorenone is also obtained via acid anhydride decomposition. Upon heating, the bimolecular reaction of the biphenyl-2-carboxylic acid produces diphenic anhydride as a disproportionation product, together with biphenyl. The diphenic anhydride is then converted to fluorenone via the removal of carbon dioxide. Formation of the anhydride by the bimolecular reaction of two acids is severely equilibrium limited and proceeds to an appreciable extent only when little water is present, or water is effectively removed [13].

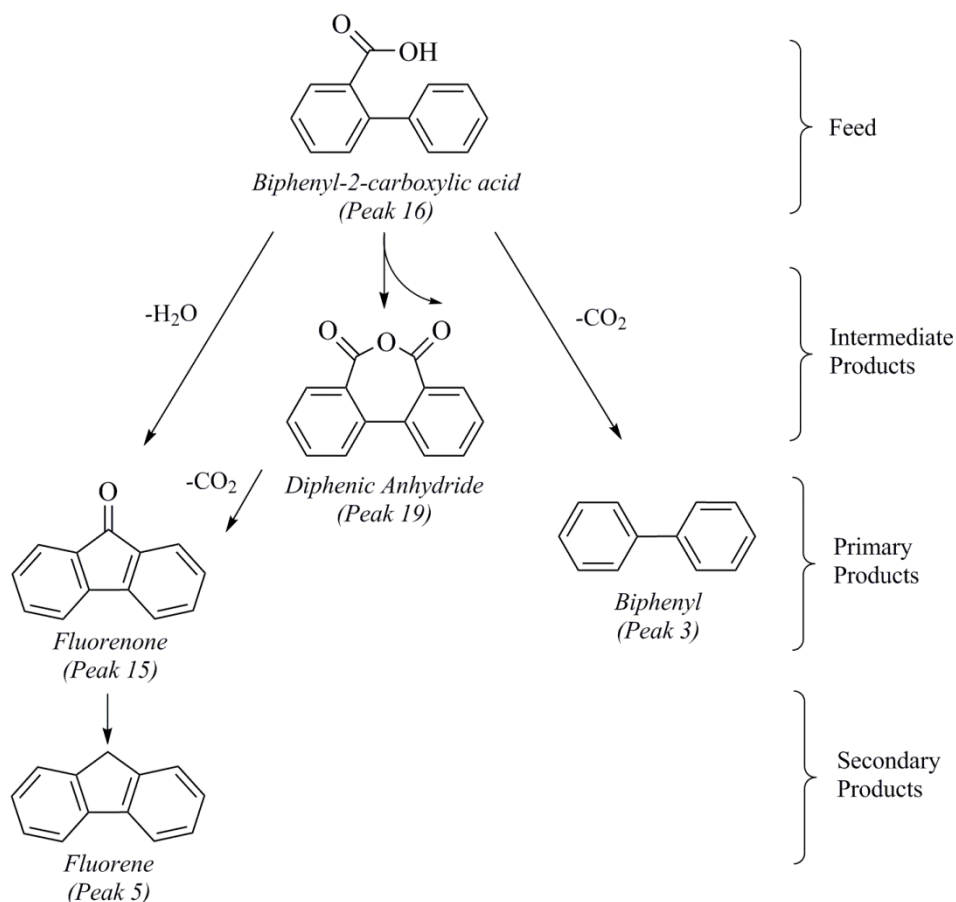


Figure 5.3. Reaction network for thermal decomposition of biphenyl-2-carboxylic acid under inert atmosphere

On a more quantitative basis, results from Table 5.3 indicated that the relative ratio of biphenyl to fluorenone increases as the decomposition temperature increases. The relative ratio

of biphenyl to fluorenone increased from 0.43:1 to 0.70:1 when the temperature increased from 350 °C to 385 °C. According to these values, although the production of biphenyl increased slightly when decomposition took place at 385 °C, the production of fluorenone was favored and ketonization was the preferred reaction pathway. Bimolecular disproportionation to produce diphenic anhydride and biphenyl became a less important pathway as the temperature increased. However, it was previously reported that cross-linking reactions of aromatic carboxylic acids could be attributed to a reaction pathway leading through the anhydride and free-radical decomposition to produce the cross-linked products [14]. The decrease in diphenic anhydride at higher temperature may be due to faster decomposition kinetics leading to heavier products, which were observed to increase with the increase in temperature. It was also reported that CO is a meaningful product from anhydride decomposition [15].

The suggested reaction network for the decomposition of biphenyl-2,2'-dicarboxylic acid is illustrated in Table 5.4. Although a more-complex reaction system is observed in this case, the relative abundance of the primary products once more supports that thermal decomposition proceeds via two main pathways: decarboxylation of one of the carboxylic acid groups to produce the monocarboxylic acid and intramolecular reactions of the dicarboxylic acid.

It is easy to see that biphenyl-2-carboxylic acid, the monocarboxylic acid, and biphenyl are products of a stepwise decarboxylation process, following the same pathway as that described in Figure 5.3. Moreover, it is clear that consecutive removal of the acid functionality as carbon dioxide is a favorable type of chemistry, because it avoids ring-closure problems by intramolecular ketonization and it produces compounds with increasingly higher H:C ratio. However, it does not prevent dehydration of biphenyl-2-carboxylic acid to produce fluorenone, following the same pathway as in Figure 5.3. The contribution of biphenyl-2-carboxylic acid disproportionation to produce diphenic anhydride is likely minor on account of the low abundance of biphenyl-2-carboxylic acid in the reaction mixture.

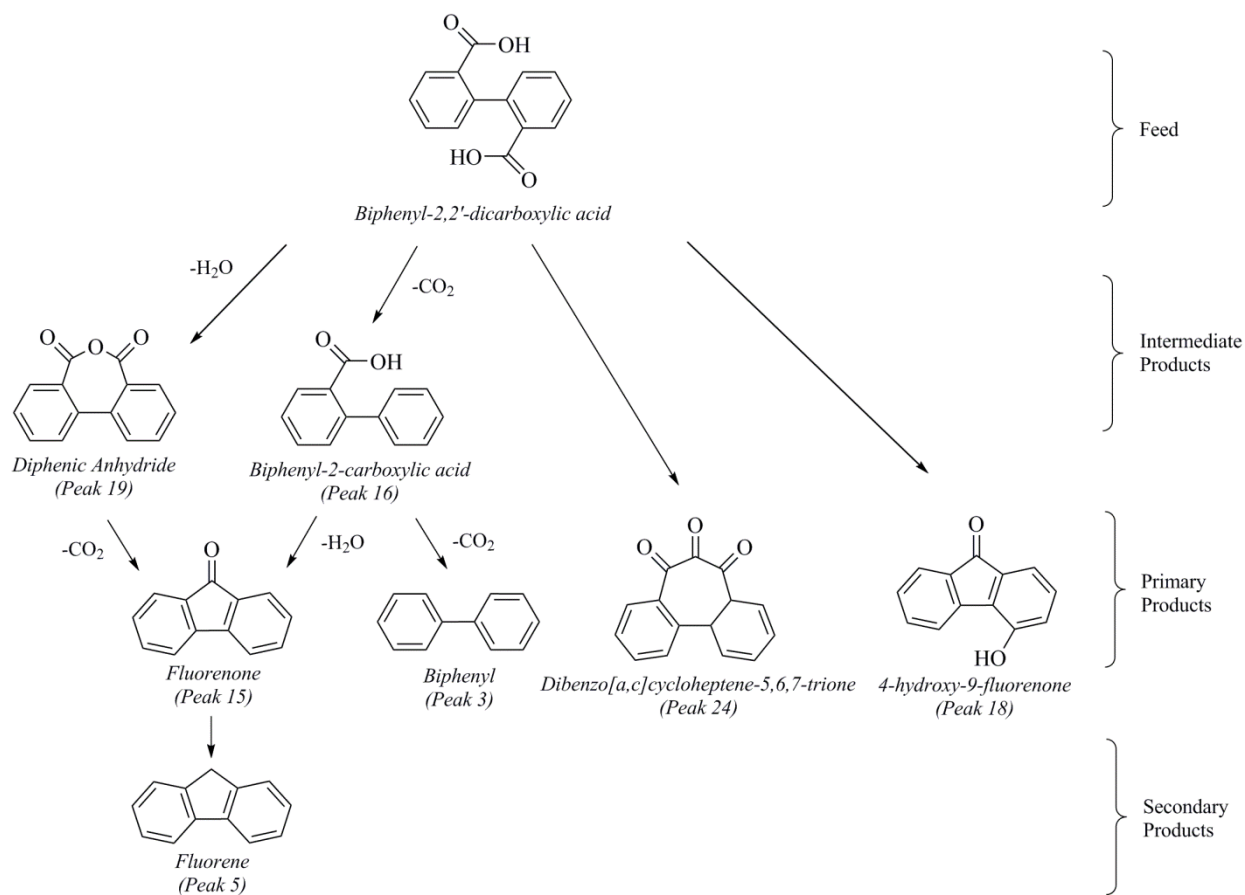


Figure 5.4. Reaction network for thermal decomposition of biphenyl-2,2'-dicarboxylic acid under inert atmosphere

Intramolecular reactions of biphenyl-2,2'-dicarboxylic acid, the dicarboxylic acid, produced some products that were not observed during the decomposition of biphenyl-2-carboxylic acid. The formation of 4-hydroxy-9-fluorenone required the elimination of H₂O and CO from biphenyl-2,2'-dicarboxylic acid. It is speculated that the CO may have been transferred as a carbonyl group to another compound, rather than being eliminated as carbon monoxide. This may help to explain the formation of a product that was tentatively identified as dibenzo[a,c]cycloheptene-5,6,7-trione. The mass spectrum obtained for this compound is presented in Figure 5.5 for the sake of reference. The molecular ion is at 236 m/z. The mass fraction at 76 m/z (instead of 77 m/z) is due to the substituted benzene in the biphenyl backbone.

The loss of 3×28 m/z fragments, without the intermediate 14 m/z loss typical of CH_2 groups, was ascribed to the loss of fragments containing CO.

The formation of cyclic tricarbonyl compounds with adjacent carbonyl groups have been reported for oxidation reactions, but it involves the oxidation of aliphatic carbon already present in the compounds [16], and does not explain the insertion of a carbonyl group. It is speculated that the product could be formed by the addition of one of the carboxylic acid groups of biphenyl-2,2'-dicarboxylic acid to a carbonyl group that is followed by decomposition and ring closure, analogous to the reaction described by Diels and Kassebart [17]. In their work, acetic acid was added to each carbonyl of a quinonoid (a quinonoid similar to that shown in Table 5.1). Hence, the formation of the cyclic trione and the hydroxy-fluorenone may not occur via independent pathways.

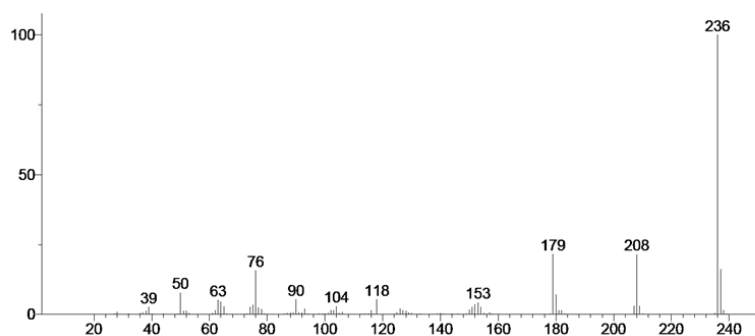


Figure 5.5. Electron impact mass spectrum of compound tentatively identified as dibenzo[*a,c*]cycloheptene-5,6,7-trione

Fluorenone was the most abundant reaction product from biphenyl-2,2'-dicarboxylic acid decomposition (Table 5.3). Fluorenone is the product of intramolecular ketonization of the biphenyl-2,2'-dicarboxylic acid; diphenic anhydride is formed as an intermediate product. As previously mentioned, fluorenone is also produced via the dehydration of biphenyl-2-carboxylic acid. Avoiding or controlling the production of ketones, which are nothing more than products of intramolecular ring closure, is precisely one of the challenges that must be addressed during the decomposition of carboxylic acids.

The relative ratio of biphenyl to fluorenone was calculated for the decomposition of biphenyl-2,2'-dicarboxylic acid. The ratio of biphenyl to fluorenone increased from 0.01:1 to 0.28:1 as the decomposition temperature increased from 340 to 400 °C. Directionally, an increase in temperature improved the selectivity to biphenyl, which is similar to what was observed for the decomposition of biphenyl-2-carboxylic acid. For this particular case, this relative ratio changed by an order of magnitude. Numerically, the calculated ratio of biphenyl to fluorenone was smaller for the decomposition of the dicarboxylic acid than the monocarboxylic acid. It suggests that the presence of an additional carboxylic acid group make the system more prone to produce ketones.

5.3.1.3 Thermal Decomposition Selectivity

The analysis of the reaction network for the decomposition of the two selected aromatic carboxylic acids showed that decarboxylation and ketonization are the most relevant decomposition reaction pathways, and biphenyl and fluorenone are typical reaction products resulting from these chemical routes. Moreover, the relative ratio between these products demonstrated that ketonization is the preferred reaction pathway; therefore, the possibility of favoring ring-opened products after thermal decomposition of the carboxylic acid is low. Selectivity to the ring-opened products increased with increasing temperature, but within the temperature range investigated (340–400 °C), the selectivity to ring-opened products never exceeded that of ketonization at low conversion. The chemistry observed in the decomposition of the monocarboxylic acid is simpler than that observed in the decomposition of its dicarboxylic acid counterpart. More importantly, it is clear that removing water from the feed or intermediate products leads to ring closure.

The reaction networks for thermal decomposition of biphenyl-2-carboxylic acid (Figure 5.3) and biphenyl-2,2'-dicarboxylic acid (Figure 5.4) showed that water definitively plays a role. The reaction pathways leading to ketonization were accompanied by the elimination of water. The pathways leading to ring opening required the elimination of oxygen as CO₂. The importance of water is also stressed by proposed mechanisms for the decarboxylation of aromatic carboxylic acids [11][18][19]. It was also reported that the decarboxylation rate was accelerated in the

presence of water [20]. The effect of water on aromatic carboxylic acid decomposition was found to be autocatalytic [21], which also points to an ionic decarboxylation pathway. It would also explain why no ketonization or addition products were reported after low-temperature aqueous phase decomposition of aromatic carboxylic acids [22]. The importance of an ionic decarboxylation pathway involving water is best expressed by the observations of Kluger et al. [23]: “...any observed acid or base catalysis in a decarboxylation reaction is inconsistent with a unimolecular mechanism and implicates a role for water.”

Although the contribution of free-radical decomposition cannot be ruled out, it seems that, at temperatures where free radical decomposition occurs, it is the unimolecular ketonization with elimination of water that is the main product of free radical decomposition. Even at high temperature, decarboxylation seems to be bimolecular (associative) in nature and follows an ionic decomposition pathway. This interpretation is consistent with the observations, but no direct proof of this interpretation is provided by the present study.

The experimental evidence indicates that, in order to improve the oxidative ring-opening concept, a strategy that favors decarboxylation and avoids water elimination from the carboxylic acids is needed. Two strategies can be considered:

- (1) Decomposition in the presence of water to suppress reactions involving dehydration and even promoting the reverse reaction of products formed by dehydration; and
- (2) Manipulating the decomposition chemistry by catalysis to favor decarboxylation to produce CO₂.

5.3.2 Catalytic Decomposition of Aromatic Carboxylic Acids

5.3.2.1 Metal Carboxylates as Catalytic Surrogates

Catalytic carboxylic acid decomposition has been the subject of considerable research work. Metal and metal oxide catalysts have been used to aid decarboxylation by changing the reaction selectivity, and enabling different and desired reaction pathways [24][25][26][27]. A great volume of literature is focused on the catalytic decomposition of aliphatic carboxylic acids.

Formic, acetic, and propionic acids are among the most frequently used acids, because of their relatively simple structure [24][25]. Catalytic decomposition of aromatic carboxylic acids has been investigated less frequently, but the reports that have been published indicate that there is a benefit in using catalysts to facilitate decarboxylation of aromatic carboxylic acids [28][29].

Catalysis of carboxylic acid decomposition proceeds via metal carboxylate intermediates, which can be approximated as the metal carboxylate in isolation. There is a strong correlation between the catalytic properties exhibited by the metals or metal oxides in the decomposition of a carboxylic acid, and the chemical properties of the corresponding bulk metal carboxylate [24]. In other words, studying the decomposition of the bulk metal carboxylate can approximate the catalytic behavior of an actual metal or metal oxide catalyst for the decomposition of the carboxylic acid. The advantage of using metal carboxylates as surrogates for catalysts is that it simplifies the investigation of the reaction network. Furthermore, it limits the interference of other parameters important in catalysis, such as mass transfer, surface area, and catalyst accessibility. Consequently, using metal carboxylates is a very convenient way to approach the catalytic decomposition of aromatic carboxylic acids.

5.3.2.2 Catalyst Selection for Carboxylic Acid Decomposition

It has been reported that Cu, Ag, Ni, Fe, Pd, Pt, and Rh are active metals for decarboxylation of carboxylic acids [26]. Similarly, metal oxides such as ZnO, NiO, MgO, CaO, BaO, SrO, Fe₂O₃, TiO₂, Cr₂O₃, SiO₂, and Al₂O₃ have been used to catalyze this type of reaction [24], [26], [30][31][32]. Even alkali metals, such as Na and K, have an effect on the nature of the decarboxylation [20]. The metal affects the selectivity and the reaction pathway that is followed [33][34]. It was anticipated that the role of the metal in determining product selectivity would be more important for multivalent metals, where metal bridging of the carboxylate groups could potentially favor ketonization.

The objective of the present work was to demonstrate the proof of concept, namely, that catalysts have the potential to improve product selectivity to the ring-opened product during the decomposition of aromatic carboxylic acids, and to decrease the decomposition temperature. For

this purpose, zinc was selected as the metal, mainly because of the simplicity of synthesis, cost, and limited number of oxidation states of the metal and prior use with heavy oils [32].

Thus, zinc salts for biphenyl-2,2'-dicarboxylic acid and biphenyl-2-carboxylic acid were synthesized and their thermal behavior and decomposition were investigated.

5.3.2.3 Infrared Spectroscopy of Zinc Carboxylates

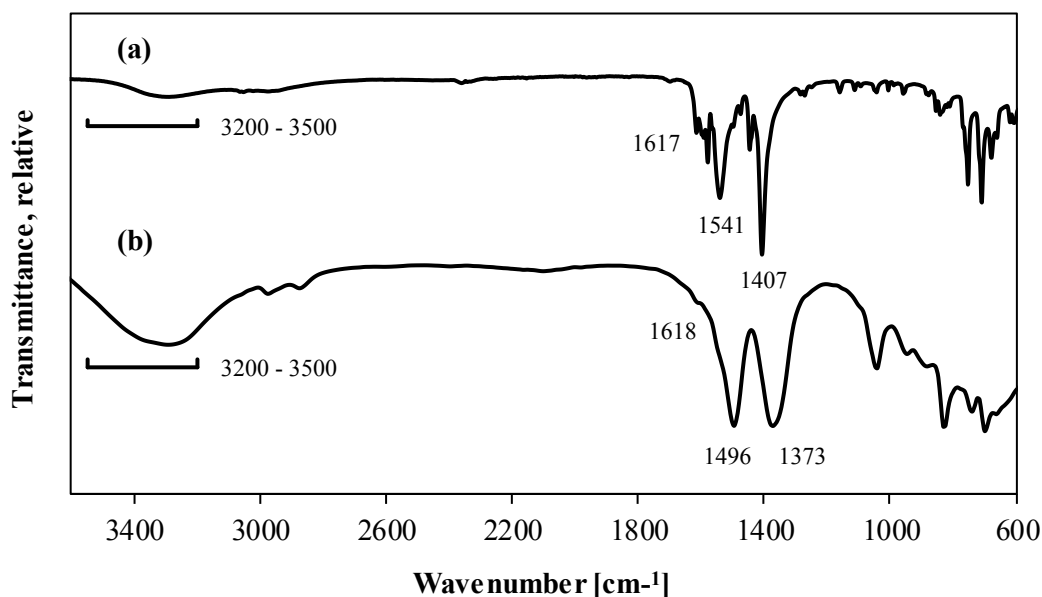


Figure 5.6. Infrared spectrum of (a) zinc(II) biphenyl-2,2'-dicarboxylate, and (b) zinc(II) biphenyl-2-carboxylate

Infrared spectroscopy was used to confirm the chemical identity of the synthesized zinc carboxylates. Two particular vibrations are characteristic of the infrared spectra of metal carboxylates. Typically, a strong asymmetrical stretching, $\nu_{as}(\text{CO}_2^-)$, at $\sim 1610\text{--}1550\text{ cm}^{-1}$ and a relatively weaker symmetrical stretching, $\nu_s(\text{CO}_2^-)$, near the 1400 cm^{-1} region, indicate the presence of the carboxylate group [35]. These characteristic absorption bands for metal carboxylates were observed in the infrared spectra of both synthesized compounds (Figure 5.6). In the case of the zinc(II) biphenyl-2,2'-dicarboxylate, the $\nu_{as}(\text{CO}_2^-)$ and the $\nu_s(\text{CO}_2^-)$ were

observed at 1541 cm^{-1} and at 1407 cm^{-1} , respectively. For the zinc(II) biphenyl-2-carboxylate, the same stretching bands were observed at 1496 cm^{-1} and at 1373 cm^{-1} , respectively.

The zinc carboxylates contained lattice water. Lattice water refers to water molecules trapped in the crystalline structure and is characterized by the antisymmetric and symmetric OH stretching at $\sim 3550\text{--}3200\text{ cm}^{-1}$ and the HOH bending at $\sim 1630\text{--}1600\text{ cm}^{-1}$ [36]. It is important to mention that no carboxylic acid absorption bands were observed in the IR spectra of the synthesized metal carboxylates, indicating that acceptable purity for these compounds was achieved.

5.3.2.4 Thermal Analysis of Zinc Carboxylates

Thermal analysis has been extensively used to study the thermal stability of metal carboxylates [24]. Thus, decomposition of the synthesized zinc carboxylates was investigated by differential scanning calorimetry (DSC) and thermogravimetric (TGA) analyses, in the temperature range from $25\text{ }^{\circ}\text{C}$ to $550\text{ }^{\circ}\text{C}$ under inert atmosphere. The main thermal events are listed (Table 5.4). The onset temperatures, the enthalpy associated with each transition, and the observed mass loss were determined. Furthermore, the use of infrared spectroscopy, in combination with TGA, assisted with the identification of H_2O and CO_x in particular. Ultimately, results from these analyses guided the experiments performed in batch reactors, which enabled the less-volatile reaction products to be identified via GC-MS analysis.

Table 5.4. Thermal decomposition of zinc carboxylates studied by DSC and TGA analyses

Metal carboxylate	Transition	DSC Analysis ^a		TGA Analysis	
		Onset temperature	Enthalpy of transition ^b	Onset temperature	TGA mass loss
		[°C]	[kJ/kg]	[°C]	[wt%]
Zinc(II) biphenyl-2,2'-dicarboxylate	1	162.8 ± 1.9	123.8 ± 4.8	155.4 ± 0.3	5.1 ± 0.1
	2	256.0 ± 1.5	81.8 ± 2.4	250.1 ± 0.6	4.2 ± 0.1
	3	371.2 ± 6.4 ^c	^d	368.6 ± 0.5 ^f	5.6 ± 0.5
	4	436.42 ± 2.3 ^c	^d	434.0 ± 0.4 ^f	45.9 ± 1.4
Zinc(II) biphenyl-2-carboxylate	1	235.5 ± 0.2	595.8 ± 9.8	236.6 ± 1.3	22.4 ± 0.2
	2	385.6 ± 3.0	^e	363.9 ± 3.5	3.7 ± 1.0

^a All transitions observed by DSC analysis were irreversible (opposite transition was not observed on dynamic cooling).

^b Positive values indicate endothermic energy changes and were calculated using Equation 1.

^c Onset temperature was ill-defined because the transition consisted of multiple convoluted peaks and the behavior of the baseline was greatly affected by the mass loss.

^d The baseline of the calorigram revealed several transitions in the form of convoluted peaks; thus, enthalpy of transition was not determined.

^e The baseline of the calorigram revealed energy changes, but a well-defined peak was not observed. Enthalpy was not estimated.

^f TGA signal displayed a complex behavior; temperature was ill-defined because these events partially overlapped each other.

5.3.2.4.1 Zinc(II) Biphenyl-2,2'-dicarboxylate

The DSC analysis of the zinc(II) biphenyl-2,2'-dicarboxylate revealed four main transitions that resulted in energy changes and must be interpreted (Figure 5.7). All these thermal events are associated with some mass loss. Thus, some general observations can be made:

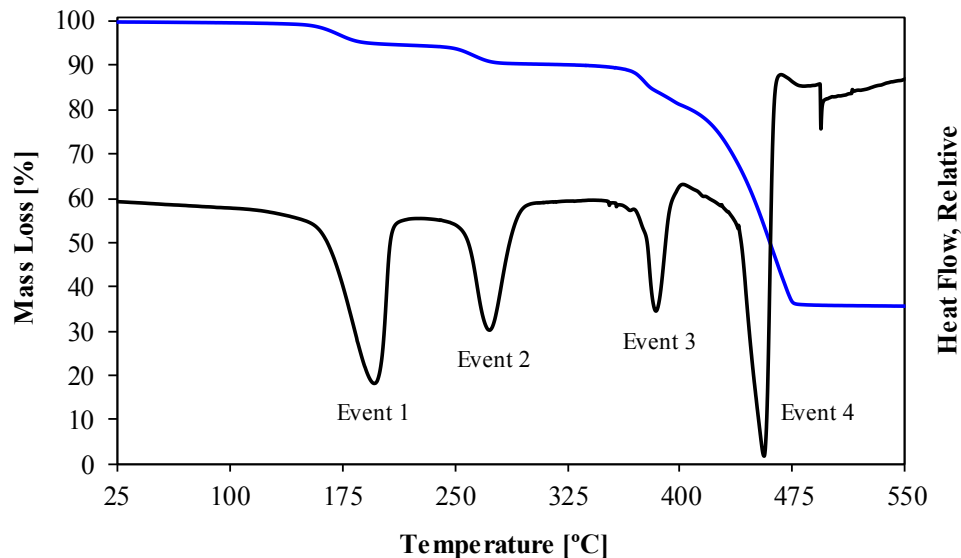


Figure 5.7. DSC heat flow signal and TGA mass loss data for decomposition of zinc(II) biphenyl-2,2'-dicarboxylate under inert atmosphere

- (a) The first event is represented by a well-defined and relatively sharp peak. It has an onset temperature of 162.8 ± 1.9 °C with $\Delta H = 124 \pm 5$ kJ kg⁻¹. This value is just slightly higher, compared to the onset temperature of the first event observed by TGA analysis at 155 ± 1 °C. (Temperature measurements performed by DSC are considered more accurate than the same with TGA.) The mass loss associated with this event indicates that it is not a phase transition. Irreversibility of this thermal event was confirmed by DSC analysis. Furthermore, water was found in the volatile products according to the infrared analysis of the gas product from the TGA (Figure 5.8). The IR spectrum of the gases produced at 162 °C contains the O–H stretching vibrations ($3400\text{--}4000$ cm⁻¹) and O–H bending vibrations (~ 1500 and ~ 1700 cm⁻¹) typical from water molecules. The presence of lattice water and the subsequent loss of this water were confirmed by infrared spectroscopy. The enthalpy change associated with the event (Table 5.4) was more than the enthalpy of vaporization of water at that temperature. Both the temperature and additional energy required to liberate the lattice water indicated that the lattice water was strongly bound.

- (b) The second event, with an onset temperature of 256.0 ± 1.5 °C, is again a relatively sharp and well-defined peak. It is accompanied by a mass loss that was observed at a slightly lower temperature (250 ± 1 °C) by TGA. It was an irreversible thermal event associated with mass loss. According to the FTIR results (Figure 5.8), both water and CO₂ were released. In addition to the infrared absorption for water, absorption bands for carbon dioxide at $2250\text{--}2400$ cm⁻¹ and ~ 667 cm⁻¹ were present in the gaseous product. The relatively high onset temperature and the fact that CO₂ production was confirmed by TGA-FTIR analysis suggest that this thermal event is the first step in the decomposition of the metal carboxylate.
- (c) The onset temperatures for the third and fourth events corresponded to 371.2 ± 6.4 °C and 436.4 ± 2.3 °C, respectively. The onset temperatures for these two thermal events coincide with the mass loss observed during TGA analysis, at 369 ± 1 °C and 434 ± 1 °C, respectively. The behavior was more complex. Between these events, mass loss continued to occur, this can be seen from the endothermic slope of the DSC calorigram between the third and fourth events, as well as from the continuous mass loss observed by TGA. The events partially overlapped, indicating that more than one change occurred in parallel. Also, $\sim 55\%$ of the original mass of the metal carboxylate was lost during these transitions. Moreover, the production of CO₂ was again detected by FTIR, pointing to decomposition of the bulk zinc carboxylate. There was no absorption at 2143 cm⁻¹ (Figure 5.8), which is characteristic of gaseous CO [37].

Carbon dioxide is a logical and expected decarboxylation product for this process. The fact that it was produced in different steps suggests that a stepwise decarboxylation mechanism might be occurring. It was speculated that removal of the first carboxylate group as CO₂ might have lower activation energy. Rajadurai [26] discussed the decarboxylation mechanisms proposed in the literature, and the concerted interaction of two carboxylate groups is a common theme. This also follows from the evidence supporting an associative ionic pathway of decarboxylation [23]. After elimination of the first carboxylate group, bond rearrangements could have taken place, and removal of the second carboxylate group might become more challenging. However, the mass loss was

unequally divided between the decomposition events, which does not support the speculation. Additional investigation is required to make any firm conclusions about the mechanistic steps involved.

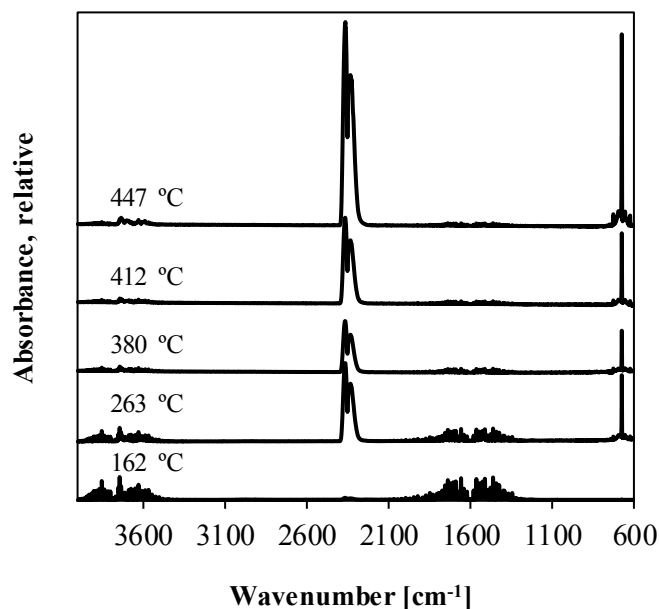


Figure 5.8. Infrared spectra of the gases evolved from the zinc(II) biphenyl-2,2'-dicarboxylate TGA-FTIR analysis

5.3.2.4.2 Zinc(II) Biphenyl-2-carboxylate

Thermal analysis of the zinc(II) biphenyl-2-carboxylate revealed a less-complicated decomposition behavior. Only two thermal events were observed in this case, both of which were accompanied by mass loss (Figure 5.9):

- (a) The first thermal event has an onset temperature of 235.5 ± 0.2 °C, with $\Delta H = 62 \pm 5$ kJ kg⁻¹ and it consists of a sharp and well-defined peak. According to TGA, most of the mass loss occurred in this single irreversible event, and ~22% of the original mass was lost to vapor-phase products. Lattice water and CO₂ were concomitantly eliminated. The

onset of decomposition occurred at lower temperature than for zinc(II) biphenyl-2,2'-dicarboxylate.

- (b) The second event involved a shift in the baseline of the calorigram, accompanied by a slight mass loss (~3.7% of the original mass). This was a gradual change. The onset temperature was 385.6 ± 3.0 °C, and mass loss was observed in the TGA starting at 364 ± 4 °C.

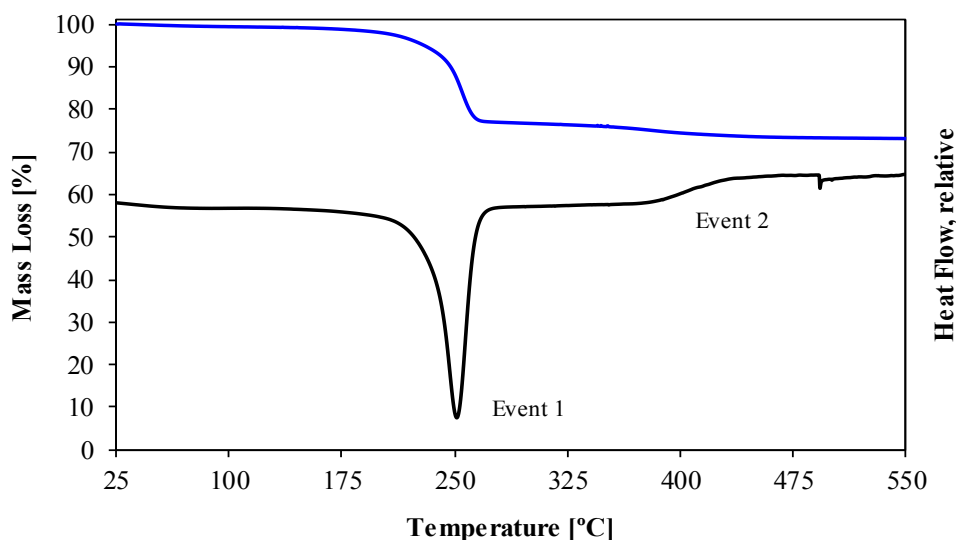


Figure 5.9. DSC heat flow signal and TGA mass loss data for decomposition of zinc(II) biphenyl-2-carboxylate under inert atmosphere

5.3.3 Decarboxylation Selectivity during the Decomposition of Zinc Carboxylates

In order to produce a larger volume of product for characterization, decomposition of the zinc(II) biphenyl-2-carboxylate and the zinc(II) biphenyl-2,2'-dicarboxylate was carried out in batch reactors under a nitrogen atmosphere. The temperature for these experiments was selected based on the results from thermal analysis. After reaction, the nonvolatile reaction products were recovered by washing with chloroform, and were analyzed by gas chromatography with mass spectrometry (GC–MS). The main reaction products were identified and listed in [Table 5.1](#).

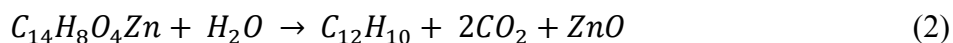
Biphenyl and fluorenone were used as the key markers to determine the preferred reaction pathway when zinc facilitated the decomposition.

Addition product selectivity was much less than observed during thermal decomposition of the corresponding carboxylic acids. This was anticipated, since the decomposition chemistry does not rely on free-radical chemistry, but involves charged intermediates. Nevertheless, because of the temperature range explored, some free-radical processes may still have occurred.

Table 5.5. Relative Abundance of the Reaction Products from Thermal Decomposition of Zinc Carboxylates

Peak	Compound	Zinc(II) biphenyl-2,2'-dicarboxylate		Zinc(II) biphenyl-2-carboxylate
		380 °C	435 °C	390 °C
3	Biphenyl	5.1×10^8	1.1×10^9	1.9×10^8
5	Fluorene	2.0×10^6	7.0×10^7	1.2×10^7
14	Xanthene-9-carboxylic acid	2.7×10^6	-	-
15	Fluorenone	3.0×10^7	2.2×10^8	6.7×10^7
21	<i>p</i> -Terphenyl	5.9×10^6	-	-

Decomposition of the zinc(II) biphenyl-2,2'-dicarboxylate was studied at temperatures of 263, 380, and 435 °C. The chromatograms obtained for the decomposition products are provided in the [APPENDIX B \(Figure B.2\)](#). A much less diverse product distribution was found in this case, when compared with the results obtained in the decomposition of the parent dicarboxylic acid. At 263 °C, the decomposition product was dominated by biphenyl. It is evident that the presence of zinc as catalytic metal favored the formation of lighter products; more importantly, biphenyl was, by far, the main reaction product also at higher temperatures ([Table 5.5](#)). The calculated relative ratio of biphenyl to fluorenone is 17:1 for reactions at 380 °C and 5:1 for reactions at 435 °C. Water was not deliberately added. It is speculated that the biphenyl selectivity is partially influenced by the lack of water, which is required to satisfy the stoichiometric requirements to yield biphenyl (see [Eq. 2](#)).



Decomposition of the zinc(II) biphenyl-2-carboxylate was investigated at 250 and 390 °C. According to the chromatographic analysis (Figure B.3 in the APPENDIX B), the rate of reaction was low at 250 °C, even though thermal analysis showed that the onset of decomposition was below this temperature. The main differences, with respect to thermal analysis, were that (i) batch reactor operation was isothermal and (ii) the atmosphere was stagnant and subject to autogenous increase in pressure. Since decomposition was already significant at 250 °C (Figure 5.9), it is unlikely that the isothermal conditions were to blame for the slow rate of decomposition. However, the stagnant atmosphere under autogenous pressure could inhibit decomposition if the transition state during decomposition is sensitive to CO₂ partial pressure. At higher temperature, this rate limitation was overcome. The abundance of the main products found after reaction at 390 °C is reported (see Table 5.5). Biphenyl is the main reaction product; the relative ratio of biphenyl to fluorenone is 3:1 for reaction at 390 °C.

Compared to thermal decomposition of the acids, a clear change in the reaction selectivity was achieved, because of the zinc. The onset of decarboxylation was at lower temperature and the ring-opened product, biphenyl, was the dominant product. These are empirical observations and the mechanism, by which the decomposition is facilitated, as well as the role of water in the mechanism, has not been elucidated by the current investigation.

5.4 Conclusions

The reaction network and product selectivity during the elimination of carboxylic acid groups attached to aromatics was experimentally investigated using the model compounds biphenyl-2-carboxylic acid and biphenyl-2,2'-dicarboxylic acid. Thermal decomposition of these acids was studied in the temperature range of 340–400 °C. The main conclusions and observations were as follows:

- (a) Thermal decomposition of the aromatic acids produced a variety of products. In all instances, the three most abundant products were biphenyl, fluorenone, and diphenic anhydride.
- (b) At higher temperatures (380–400 °C), more free-radical addition products were observed, because of the formation of thermally stable aromatic C–C bonds subsequent to the elimination of carboxylic acid groups.
- (c) Over the temperature range investigated for thermal decomposition, the selectivity to biphenyl (ring-opened product) never exceeded the selectivity to fluorenone (ring-closed product). The selectivity to biphenyl improved with increasing temperature.
- (d) There were three main reaction pathways in the thermal decomposition of biphenyl-2-carboxylic acid, the aromatic monocarboxylic acid. The pathways were (i) the elimination of CO₂ to produce biphenyl, (ii) the elimination of H₂O to produce fluorenone, and (iii) the formation of diphenic anhydride, presumably via bimolecular reaction with another carboxylic acid. The diphenic anhydride is an intermediate product and it formed fluorenone upon the elimination of CO₂.
- (e) Thermal decomposition of biphenyl-2,2'-dicarboxylic acid, the aromatic dicarboxylic acid, also proceeded along three dominant pathways. The main pathway was decarboxylation to produce biphenyl-2-carboxylic acid and subsequent decomposition as described in point (d). The other two pathways leading to the formation of the hydroxy-fluorenone and a cyclic trione may not be independent pathways, but may be part of the same bimolecular decomposition.
- (f) The observation in point (e) suggested that decarboxylation is bimolecular (associative) in nature and follows an ionic decomposition pathway, whereas unimolecular ketonization involves the elimination of water that is the main product of free-radical decomposition. No direct proof of this interpretation was provided.

The use of catalytic acid decomposition to improve selectivity to the ring-opened product was also explored in this work. Zinc was the only metal tested. Zinc(II) biphenyl-2-carboxylate and zinc(II) biphenyl-2,2'-dicarboxylate were synthesized as surrogates for the anticipated surface species during catalytic decomposition of the corresponding acids. Decomposition of these zinc carboxylates was studied, and the main conclusions and observations were as follows:

- (g) The decomposition of the zinc carboxylates produced H₂O and CO₂, but no CO was detected. The formation of addition products was low and product selectivity was different from that observed during the thermal decomposition of the carboxylic acids. In order of abundance, the three most abundant products from zinc carboxylate decomposition were biphenyl > fluorenone > fluorene. The same order was observed for both monocarboxylate and dicarboxylate decomposition.
- (h) Zinc(II) biphenyl-2-carboxylate decomposition occurred predominantly as a single event with an onset temperature of 235 °C. Lattice water and CO₂ were simultaneously eliminated. Under stagnant atmosphere and autogenous pressure, the rate of decomposition was significantly suppressed. Decomposition at 390 °C resulted in a biphenyl to fluorenone selectivity ratio of 3:1.
- (i) Zinc(II) biphenyl-2,2'-dicarboxylate decomposition involved multiple thermal events. Most of the mass loss due to decomposition occurred in the temperature range of 370–475 °C. Decomposition at lower temperature favored biphenyl formation, which is the opposite of what was observed during thermal decomposition of the corresponding acid. The biphenyl to fluorenone selectivity ratio was 17:1 for reaction at 380 °C and 5:1 for reaction at 435 °C.
- (j) Reaction stoichiometry indicated that water played a role in determining product selectivity, but this aspect was not investigated in the present work.

(k) Proof of concept was provided, in that the use of catalytic decomposition, as opposed to thermal decomposition, is able to increase the selectivity to ring-opened products during the decomposition of multinuclear aromatic carboxylic acids.

5.5 References

- [1] Ancheyta, J.; Speight, J. G. *Hydroprocessing of Heavy Oils and Residua*; CRC Press: Boca Raton, FL, 2007.
- [2] Ancheyta, J.; Trejo, F.; Rana, M. S. *Asphaltenes. Chemical Transformation during Hydroprocessing of Heavy Oils*; CRC Press: Boca Raton, FL, 2009.
- [3] Gray, M. R. *Upgrading Oilsands Bitumen and Heavy Oil*; University of Alberta Press: Edmonton, AB, Canada, 2015.
- [4] Marek, L. F.; Hahn, D. A. *The Catalytic Oxidation of Organic Compounds in the Vapor Phase*; ACS Monograph Series 61; Chemical Catalogue Company: New York, 1932.
- [5] Babu, D. R.; Cormack, D. E. Effect of oxidation on the viscosity of Athabasca bitumen. *Can. J. Chem. Eng.* **1984**, 62, 562–564.
- [6] García Zapata, J. L.; De Klerk, A. Viscosity changes during mild oxidation of oilsands-derived bitumen: Solvent effects and selectivity. *Energy Fuels* **2014**, 28, 6242–6248.
- [7] Siddiquee, M. N.; De Klerk, A. Hydrocarbon addition reactions during low-temperature autoxidation of oilsands bitumen. *Energy Fuels* **2014**, 28, 6848–6859.
- [8] Montoya Sánchez, N.; De Klerk, A. Oxidative ring-opening over metal oxides. *Prepr. Pap.–Am. Chem. Soc., Div. Energy Fuels* **2014**, 59 (2), 558–561.
- [9] Manion, J. A.; McMillen, D. F.; Malhotra, R. Decarboxylation and coupling reactions of aromatic acids under coal-liquefaction conditions. *Energy Fuels* **1996**, 10, 776–788.
- [10] Eskay, T. P.; Britt, P. F.; Buchanan, A. C., III. Does decarboxylation lead to cross-linking in low-rank coals? *Energy Fuels* **1996**, 10, 1257–1261.

- [11] Mundle, S. O. C.; Lacrampe-Couloume, G.; Sherwood Lollar, B.; Kluger, R. Hydrolytic decarboxylation of carboxylic acids and the formation of protonated carbonic acid. *J. Am. Chem. Soc.* **2010**, 132, 2430–2436.
- [12] Smith, B. H. *Bridged Aromatic Compounds*; Academic Press: New York, 1964; pp 100–104.
- [13] Satchell, D. P. N.; Satchell, R. S. Substitution in the groups COOH and COOR. In *The Chemistry of Carboxylic Acids and Esters*; Patai, S., Ed.; Interscience: London, 1969; pp 375–452.
- [14] Eskay, T. P.; Britt, P. F.; Buchanan, A. C., III. Pyrolysis of aromatic carboxylic acids: Potential involvement of anhydrides in retrograde reactions in low-rank coal. *Energy Fuels* **1997**, 11, 1278–1287.
- [15] Ashida, R.; Painter, P.; Larsen, J. W. Kerogen chemistry. 4. Thermal decarboxylation of kerogen. *Energy Fuels* **2005**, 19, 1954–1961.
- [16] Cullis, C. F.; Fish, A. Carbonyl-forming oxidations. In *The Chemistry of the Carbonyl Group*; Patai, S., Ed.; Interscience: London, 1966; pp 79–176.
- [17] Diels, O.; Kassebart, R. Polymerization processes produced by pyridine. II. The formation of a blue-colored 1,2,3-triketone from phenanthraquinone (in Ger.). *Justus Liebigs Ann. Chem.* **1938**, 536, 78–88.
- [18] Mundle, S. O. C.; Kluger, R. Decarboxylation via addition of water to a carboxyl group: Acid catalysis of pyrrole-2-carboxylic acid. *J. Am. Chem. Soc.* **2009**, 131, 11674–11675.
- [19] Vandersteen, A. A.; Mundle, S. O. C.; Kluger, R. Protonated carbonic acid and reactive intermediates in the acidic decarboxylation of indolecarboxylic acids. *J. Org. Chem.* **2012**, 77, 6505–6509.
- [20] Dabestani, R.; Britt, P. F.; Buchanan, A. C., III. Pyrolysis of aromatic carboxylic acid salts: Does decarboxylation play a role in cross-linking reactions? *Energy Fuels* **2005**, 19, 365–373.
- [21] Dunn, J. B.; Burns, M. L.; Hunter, S. E.; Savage, P. E. Hydrothermal stability of aromatic carboxylic acids. *J. Supercrit. Fluids* **2003**, 27, 263–274.
- [22] Fu, J.; Savage, P. E.; Lu, X. Hydrothermal decarboxylation of pentafluorobenzoic acid and quinolinic acid. *Ind. Eng. Chem. Res.* **2009**, 48, 10467–10471.

- [23] Kluger, R.; Howe, G. W.; Mundle, S. O. C. Avoiding CO₂ in catalysis of decarboxylation. *Adv. Phys. Org. Chem.* **2013**, 47, 85–128.
- [24] Mars, P.; Scholten, J. J. F.; Zwietering, P. The catalytic decomposition of formic acid. *Adv. Catal.* **1963**, 14, 35–113.
- [25] Kim, K. S.; Barteau, M. A. Pathways for carboxylic acid decomposition on TiO₂. *Langmuir* **1988**, 4, 945–953.
- [26] Rajadurai, S. Pathways for carboxylic acid decomposition on transition metal oxides. *Catal. Rev.: Sci. Eng.* **1994**, 36, 385–403.
- [27] Mehrotra, R. C.; Bohra, R. *Metal Carboxylates*; Academic Press: New York, 1983.
- [28] Takemura, Y.; Nakamura, A.; Taguchi, H.; Ouchi, K. Catalytic decarboxylation of benzoic acid. *Ind. Eng. Chem. Prod. Res. Dev.* **1985**, 24, 213–215.
- [29] Fu, X.; Dai, Z.; Tian, S.; Long, J.; Hou, S.; Wang, X. Catalytic decarboxylation of petroleum acids from high acid crude oils over solid acid catalysts. *Energy Fuels* **2008**, 22, 1923–1929.
- [30] Dias, H. P.; Gonçalves, G. R.; Freitas, J. C. C.; Gomes, A. O.; Eustáquio, V. R.; De Castro, E. V. R.; Vaz, B. G.; Aquije, G. M. F. V.; Romão, W. Catalytic decarboxylation of naphthenic acids in crude oils. *Fuel* **2015**, 158, 113–121.
- [31] Oh, H.-Y.; Park, J.-H.; Rhee, Y.-W.; Kim, J.-N. Decarboxylation of naphthenic acid using alkaline earth metal oxide. *J. Ind. Eng. Chem.* **2011**, 17, 788–793.
- [32] Ding, L.; Rahimi, P.; Hawkins, R.; Bhatt, S.; Shi, Y. Naphthenic acid removal from heavy oils on alkaline earth-metal oxides and ZnO catalysts. *Appl. Catal., A* **2009**, 371, 121–130.
- [33] Dzik, W. I.; Lange, P. P.; Gooßen, L. J. Carboxylates as sources of carbon nucleophiles and electrophiles: comparison of decarboxylative and decarbonylative pathways. *Chem. Sci.* **2012**, 3, 2671–2678.
- [34] Lugo-José, Y. K.; Monnier, J. R.; Williams, C. T. Gas-phase, catalytic hydrodeoxygenation of propanoic acid, oversupported group VIII noble metals: Metal and support effects. *Appl. Catal., A* **2014**, 469, 410–418.
- [35] Silverstein, R. M.; Bassler, G. C.; Morrill, T. C. *Spectrometric Identification of Organic Compounds*, 4Edition; John Wiley: New York, 1981; p 121.

- [36] Nakamoto, K. *Infrared and Raman Spectra of Inorganic Coordination Compounds Part B*, 6th Edition; Wiley: Hoboken, NJ, 2009; pp 57–58.
- [37] Colthup, N. B.; Daly, L. H.; Wiberley, S. E. *Introduction to Infrared and Raman Spectroscopy*, 3rd Edition; Academic Press: Boston, 1990.

6. Oxidative Ring-opening of Aromatics: Effect of Water on Reaction Selectivity¹

ABSTRACT

Conversion of heavy aromatic oils to lighter products is challenging. Oxidative ring-opening of multinuclear aromatics is an alternative approach to hydrotreating. Oxidative ring-opening involves three steps. First, oxidation of the multinuclear aromatics to produce quinonoids. Second, oxidation to cleavage the C-C bond adjacent to the quinonoid to form a terminal carboxylic acid. Third, decarboxylation of the carboxylic acid to produce the oxygenate-free ring-opened product. In the last step, decarboxylation of the carboxylic acid competes with dehydration and ketonization, which determines the reaction selectivity towards ring-opened or ring-closed products. It was suggested that water affected selectivity and that selectivity to ring-opened products could be improved by excess water. The aim of this work was to investigate the effect of water on the reaction selectivity for the thermal decomposition of a model aromatic carboxylic acid, *biphenyl-2-carboxylic acid*. It was confirmed that the presence of water during thermal decomposition increased selectivity to the ring-opened product, *biphenyl*, over that to the ring-closed product, *fluorenone*. When thermal decomposition was performed at 350 °C in the presence of 30 % or more excess water, the selectivity ratio of biphenyl to fluorenone was 2, compared to 0.5 when thermal decomposition was conducted without water. It appeared that water participated as an intermediary to facilitate the proton or hydrogen transfer during decarboxylation, but no proof of this was presented. It was also found that reaction selectivity was sensitive to mass transport of water.

Keywords: Aromatic carboxylic acids, thermal decomposition, mass transport of water.

¹ This work was published as Montoya Sánchez, N.; De Klerk, A. Oxidative ring-opening of aromatics: Effect of Water on Reaction Selectivity. *Prepr. Pap.-Am. Chem. Soc., Div. Energy Fuels* 2016, 61 (1) 489-492.

6.1 Introduction

Traditionally, the upgrading of heavy aromatic oils to lighter products is performed using hydrogen intensive technologies, such as hydroprocessing. Hydroprocessing is not only subject to demanding thermodynamic constraints [1], but it is also a very costly option.

Oxidative ring-opening is an alternative approach, which makes use of an oxidative pathway. In this strategy, initial oxidation of the multinuclear aromatics leads to the formation of quinonoids. Further oxidation leads to the cleavage of C–C bonds, opening the ring by forming terminal carboxylic acid groups. Decarboxylation of the now ring-opened product, rejecting the carbon as CO₂, increases the H:C ratio of the final product [2]. In the last step, undesirable side-reactions produce ring-closed products.

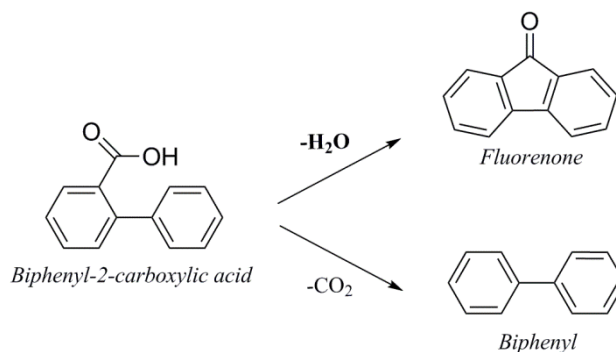


Figure 6.1. Main and competing reaction pathways for decomposition of biphenyl-2-carboxylic acid

The thermal decomposition of biphenyl carboxylic acids was studied [3]. It was demonstrated that decarboxylation, dehydration and ketonization are the main decomposition pathways. Biphenyl and fluorenone are the typical reaction products resulting from these competing chemical routes. Unfortunately, the selectivity towards the ring-opened product, *biphenyl*, never exceeded the selectivity towards the ring-closed product, *fluorenone*. The reaction pathways leading to ring-closed products were accompanied by elimination of water (Figure 6.1), whereas that to the desired product required elimination of CO₂. Hence, the

experimental evidence suggested that water plays a role and it might be the key to improve the selectivity to the ring-opened product.

It was postulated that conducting the thermal decomposition of biphenyl carboxylic acids in the presence of water would help to suppress the reactions involving dehydration and even promoting the reverse reaction of the products formed by dehydration. This in turn would help to change the selectivity favoring the production of more ring-opened products advancing the concept of oxidative ring-opening.

The objective of this work was to determine the effect of water on the reaction selectivity for the thermal decomposition of biphenyl-2-carboxylic acid.

6.2 Experimental Section

6.2.1 Materials

Biphenyl-2-carboxylic acid (98%), biphenyl (99%), fluorenone (98%), and hexachlorobenzene (99%) were purchased from Sigma Aldrich. Chloroform (99.9%) was obtained from Fisher Scientific. All chemical were used without any further purification. Deionized water was prepared using a Millipore water purification system. Nitrogen (99.998%) obtained from Praxair was used to maintain an inert atmosphere during all experiments.

6.2.2 Equipment and Procedure

The thermal decomposition of biphenyl-2-carboxylic acid in the presence of water was studied using batch reactors. Decomposition reactions were carried out using 10, 30, 50, and 70% excess water. For every mole of acid that decomposes via dehydration, one mole of water is produced. Thus, for the purpose of this document, x -% of excess water means the moles of water added is equal to the moles of acid plus an additional x -% on a molar basis. Also, blank experiments involving the decomposition of the acid without the presence of water were performed for comparison purposes.

In all cases, an amount of sample was placed in a stainless steel, 15 mL batch reactor manufactured from Swagelok tubing and fittings. The system was purged several times and then pressurized to 4 MPa using nitrogen. The reactor was heated to 350 °C for 20 minutes using a fluidized sand bath (Tecne SBS-4). Typical heat-up time was 6 minutes. Pressure was used to keep the biphenyl-2-carboxylic acid in liquid phase during reaction. At these conditions, water was present as a vapor. After reaction, the gaseous products were collected in sampling bags for analysis. The remaining products that were not volatile at ambient conditions were washed with chloroform and recovered for analysis. All experiments were performed multiple times.

According to the experimental results (see Results), the way in which the decomposition reactions were performed was slightly altered and numbered I, II and III to distinguish between the procedures. Thus, Procedures II and III are modifications of the initial procedure, Procedure I.

6.2.2.1 Procedure I

One gram of acid and a specific excess of water, added on top of the acid, were placed in a batch reactor. The batch reactor was sealed and placed in the fluidized sand bath heater. In each set of experiments four reactors were prepared and placed in the fluidized sand bath heater one at a time. Each set of experiments was performed on a separate day and consisted of 4 reactions conducted in sequence. In each reactor a different excess water value was tested, i.e. one reaction for 10%, 30%, 50% and 70% excess water every day. These reactions will be referred to as group I reactions and it took reactions on four different days to complete reactions in quadruplicate for any given amount of excess water.

6.2.2.2 Procedure II

The same steps described in Procedure I were followed, but with one modification. The set of reactions performed each day consisted of reactions using the same percent excess of water. A total of four sets of reactions were performed. These reactions will be referred to as group II

reactions and in a single day quadruplicate reactions were performed for a single amount of excess water.

6.2.2.3 Procedure III

The same steps described in Procedure II were followed, but with two modifications. The amount of acid used was decreased from 1.0 to 0.5 grams and the acid was added on top of the water.

6.2.3 Analyses

All analyses were performed using different detectors in combination with gas chromatography.

Identification and semi-quantitative determination of the reaction products dissolved in chloroform was performed by gas chromatography coupled with mass spectrometry (GC-MS). The analyses were carried out using an Agilent 7820A GC connected to a 5977E MS detector. The system was equipped with a 30 m × 0.25 mm × 0.25 μm HP-5MS J&W capillary column. Helium was used as the carrier gas at a constant flow rate of 1 mL min⁻¹ and 1 μL of sample was introduced with a 10:1 split ratio. The oven temperature program was started at 90 °C for 2 min and then increased at 5 °C min⁻¹ to 320 °C and held for 1 min.

The biphenyl to fluorenone selectivity ratio was calculated using the GC-MS abundance data. Quantification of the biphenyl-2-carboxylic acid conversion in the liquid product was performed by gas chromatography with flame ionization detector (GC-FID), using an Agilent 7890A GC-FID equipped with a DB-5 MS column (30 m × 0.25 mm × 0.25 μm). The same temperature program as that for GC-MS analyses was used. Hexachlorobenzene was added as an internal standard. For quantification of conversion, a calibration curve was prepared.

The gaseous products were analyzed by gas chromatography coupled with both flame ionization detector and thermal conductivity detector (GC-FID/TCD). Separation was performed

on a Hay Sep R column, 2.44 m × 3 mm, using helium as carrier gas at a constant flow of 25 mL min⁻¹. The injector temperature was set at 200 °C. The temperature program was started at 70 °C for 7 min and then increased at 10 °C min⁻¹ to 250 °C and held for 2 min, before being increased at 30 °C min⁻¹ to 300 °C and held for 8 min.

6.3 Results

6.3.1 Product Characterization

The identity of the reaction products was confirmed by GC-MS analysis. Decomposition of biphenyl-2-carboxylic acid with no water present yielded biphenyl, fluorene, fluorenone, diphenic anhydride as the main reaction products. Also, some heavy addition reaction products were observed after reaction. Decomposition of the carboxylic acid in the presence of water yielded the same products as without water, but without the heavy addition products. Biphenyl and fluorenone were the main reaction products.

6.3.2 Selectivity of Reaction

After reaction, the relative ratio of biphenyl to fluorenone was calculated, and then compared with the value obtained for the blank experiment, i.e. thermal decomposition in the absence of water. This ratio is a measure of the reaction selectivity towards ring-opened or ring-closed products. To facilitate comparison, the calculated average relative ratios of biphenyl to fluorenone for the different groups of reactions are presented in [Table 6.1](#). The results for the blank and every reaction procedure, i.e. Procedure I, II and III, are presented separately.

From the sample standard deviation of the results it can be noted that the blank experiment, which contained no water, had less variation than most of the other experiments. It can further be noted that the sample standard deviation for the experiments using Procedure I was larger than that for Procedure II, which was in turn larger than that for Procedure III. In fact, the change in procedure was a deliberate attempt to decrease the sample standard deviation.

Table 6.1. Average Relative Ratio of Biphenyl to Fluorenone from Thermal Decomposition of Biphenyl-2-carboxylic Acid

Water excess [%]	Average relative ratio of biphenyl to fluorenone ^a			
	Blank ^b	I	II	III
10		0.76 ± 0.55	0.39 ± 0.01	0.99 ± 0.57
30	0.40 ± 0.07	1.60 ± 1.38	1.66 ± 0.12	1.93 ± 0.20
50		1.20 ± 1.39	1.66 ± 0.69	1.48 ± 0.11
70		0.38 ± 0.36	1.32 ± 1.29	1.83 ± 0.29

^a Average (x) and sample standard deviation (s) reported as $x \pm s$.

^b Conversion of biphenyl-2-carboxylic acid was 17 ± 7 %.

6.3.2.1 Procedure I Reactions

Four sets of experiments were conducted according to Procedure I. Each set was performed on a separate day and consisted of 4 reactions, each of which used a different excess of water. The relative ratio of biphenyl to fluorenone calculated for the individual experiments is presented in [Figure 6.2](#). In this case, a ratio greater than one implicates that production of ring-opened products is favored; on the contrary, a ratio smaller than one indicates that production of ring-closed products is preferred. Results show a great scatter of data. Individual experiments for a given excess of water point out to an opposite behavior. In some experiments, selectivity towards ring-opened products is increased, while in others is not.

Due to the large sample standard deviation ([Table 6.1](#)) in the set of experiments conducted using Procedure I, no statistically meaningful difference was found between the average ratio of biphenyl to fluorenone of the blank experiment and that of the reactions changing the amount of water. The large standard deviation highlighted the poor repeatability of the results. This issue had to be addressed.

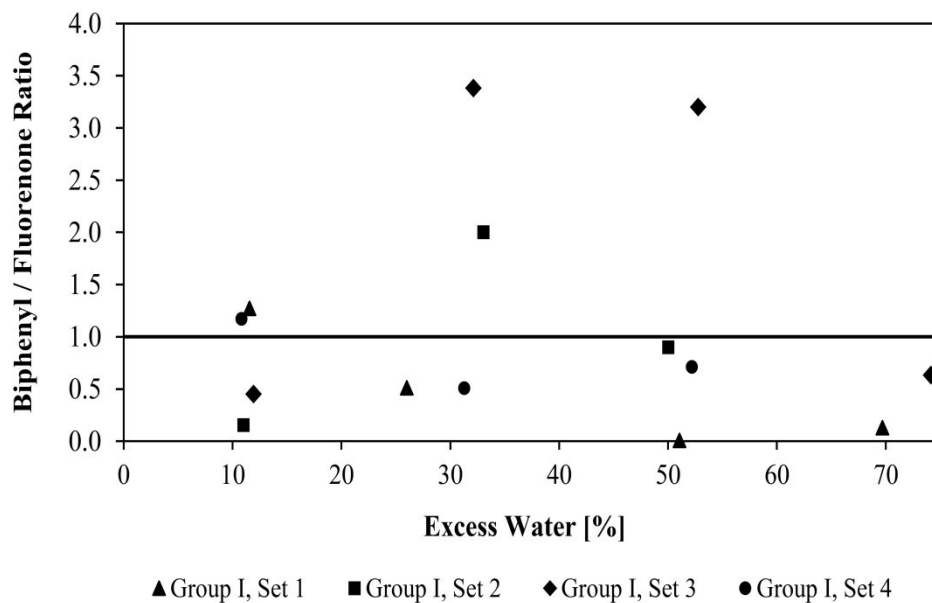


Figure 6.2. Effect of water on reaction selectivity for reactions performed using Procedure I

6.3.2.2 Procedure II Reactions

It was speculated that the lack of reproducibility of the data following Procedure I might have been related to the way in which repeat reactions were performed. Therefore, a modification of the experimental procedure was introduced, and four new sets of reactions were performed according to Procedure II. Each set of quadruplicate reactions at a single concentration of excess water was performed on a separate day. By doing so, small variations in parameters such as ambient temperature, humidity and time for sample processing were more controlled.

The ratio of biphenyl to fluorenone obtained for reactions following Procedure II is presented in [Figure 6.3](#). To facilitate comparison, results from Procedure II (hollow markers) and the results from Procedure I (solid markers) are shown.

Using Procedure II there was little variability on the data collected for reactions using 10% and 30% excess of water. As a result, the standard deviation for these data is significantly lower than the one calculated for their counterparts using Procedure I ([Table 6.1](#)). For instance, the

ratio of biphenyl to fluorenone for reaction using 30% excess of water was 0.39 ± 0.01 for Procedure II, while it was 0.76 ± 0.55 for Procedure I.

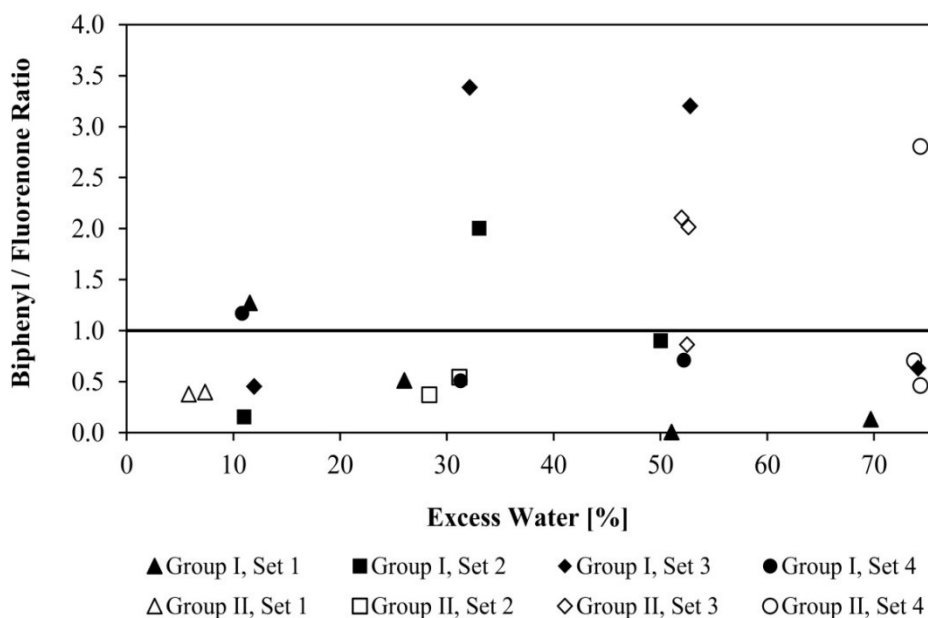


Figure 6.3. Effect of water on reaction selectivity for reactions performed using Procedure II (hollow markers) and Procedure I (solid markers)

On the other hand, for Procedure II more scatter in the data was observed when the amount of water was increased. For reactions performed using 50% excess of water, two of experiments yielded a similar ratio giving a value close to 2, while one of the experiments gave a ratio of only 0.86. Similarly, for reactions performed using 70% excess of water, two of the reactions gave a relative ratio below 1, while a third reaction yielded a ratio of 2.8.

The experimental results suggested that the poor reproducibility was not due to the procedure, but that variation was introduced by something intrinsic to the reaction. Furthermore, the average value of the biphenyl to fluorenone ratio found for the blank experiment shows a very small standard deviation compared to any of the values for all the water present experiments. It was clear that variability was introduced only when water was present. It was postulated that selectivity during reactions with water was affected due to mass transport.

6.3.2.3 Procedure III Reactions

For a severely transport limited reaction, the reaction rate is equal to the mass transfer rate. It is possible that the decomposition of biphenyl-2-carboxylic acid in the presence of water is not kinetically controlled, but diffusion limited. Thus, if the decomposition reaction is to be assisted by water, in order to modify the selectivity and favor the production of ring-opened products, the local concentration of water matters. Water must diffuse through the acid bulk phase and in the absence of mechanical agitation (a limitation of the reactor setup used) the liquid phase might not have the same concentration of water everywhere. Procedure III reduced the diffusion path by decreasing the amount of reactants.

Results for the individual experiments conducted using Procedure III are presented in [Figure 6.4](#). Improved reproducibility of the data was obtained for reactions carried out using 30, 50 and 70% excess of water. In all cases the ratio of biphenyl to fluorenone was greater than one; the selectivity of the reaction changed. The preferred decomposition pathway was decarboxylation and therefore, production of the ring-opened product.

There was little difference on the average ratio of biphenyl to fluorenone of the experiments using 30, 50 and 70% excess of water during reaction. However, when comparing the same ratio of those reactions using 50% and 70% excess of water (1.48 ± 0.11 and 1.83 ± 0.29 , respectively) with the one of the blank experiment (0.40 ± 0.07), it is clear that the ratios are different and the difference is statistically meaningful. Results for the reactions carried out using 10% excess water showed higher variability.

Conversion in the presence of excess water was on average higher than in the blank experiment without water. For example, the conversion with 70 % excess water was $29 \pm 2\%$ and conversion without water was $17 \pm 7\%$.

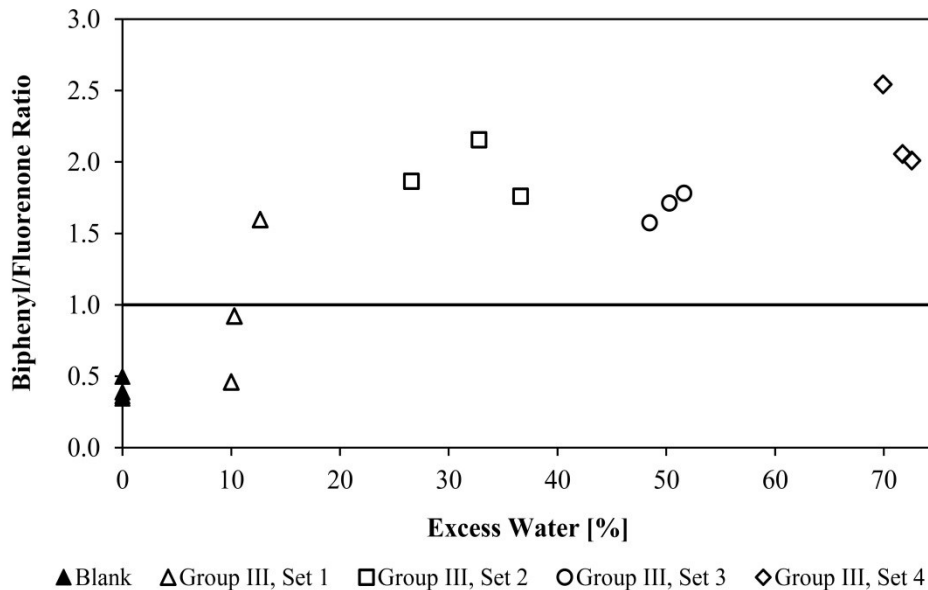


Figure 6.4. Effect of water on reaction selectivity for reactions performed using Procedure III (hollow markers). The results of the blank experiments without water (solid markers) are also shown

6.4 Discussion

6.4.1 Effect of Water on Reaction Selectivity

Despite of the variability of the experimental results, it is clear that water plays a role and has a positive impact on the reaction selectivity. When water assisted the thermal decomposition of the biphenyl-2-carboxylic acid, production of the ring-opened product was favored and decarboxylation became the preferred reaction pathway. Yet, the exact role of water during reaction is not well understood.

According to the literature, unimolecular decomposition of formic acid occurs through decarboxylation and dehydration in the aqueous and gas phase, respectively [4]. The presence of water changes the dominant reaction pathway from dehydration to decarboxylation [4][5]. Moreover, theoretical calculations showed that water decreases the activation energy of both reactions; though, the energy barrier for decarboxylation is lowered to a greater extent making

this the governing pathway [4]. Most likely, these observations can be extended to the present study and might explain the observed change in the reaction selectivity.

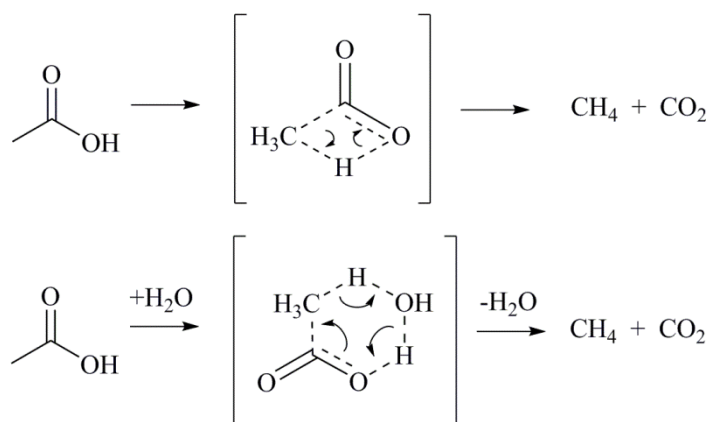


Figure 6.5. Mechanism and transition states for the thermal decomposition of acetic acid with and without water present [5]

From a mechanistic point of view, the presence of water during decomposition of carboxylic acids alters the size and geometry of the transition states [5]. For instance, thermal decarboxylation of acetic acid can be described as occurring from a strained 4-center transition state (Figure 6.5). On the other hand, when water is introduced during acetic acid decomposition, the size of the transition state increases to a 6-center configuration, a much less strained geometry, which facilitates the proton transfer.

During the decomposition of biphenyl-2-carboxylic acid, the removal of the acid functionality as CO_2 requires one hydrogen atom to be transferred from the acid-OH group to the acid-phenyl group. However, this hydrogen atom is not located close to the phenyl moiety. If water acts as an intermediary, the proton transfer during the transition becomes much easier. Under this premise, water might potentially influence the intermediate steps of the reaction preventing the dehydration of the acid to form fluorenone and promoting decarboxylation to form biphenyl. On a side note, it should be noted that water would also promote the hydrolysis of

the diphenic anhydride (an observed intermediate reaction product) [3] preventing formation of fluorenone by bimolecular ketonization.

Results from the present study highlight the beneficial effect of water on the reaction selectivity for the decomposition of aromatic carboxylic acids. Therefore, incorporation of water as a co-feed for oxidative ring-opening would be considered in future work.

6.4.2 Variability in Selectivity due to Water

Reaction selectivity was measured by calculating the average ratio of biphenyl to fluorenone. Results indicate that the decomposition of biphenyl-2-carboxylic acid was not equilibrium constrained under the conditions tested; there was too much variability. It was reasoned that the variability in selectivity ratio was due to mass transport of water.

At the experimental conditions, 350 °C and 4 MPa initial pressure, the aromatic carboxylic acid reacted as a liquid and water as a vapor. It was likely (Figure 6.5) that water participated in the transition state during decomposition, promoting decarboxylation of the acid and formation of the ring-opened product, biphenyl. In this way, diffusion of water through the acid bulk phase is a fundamental component of the reaction, which would affect both reaction rate and product selectivity. Adequate mass transport is necessary to ensure a constant local concentration of water molecules, readily available to participate in the reaction.

The heterogeneous nature of the system and the absence of mechanical agitation affected mass transport. Likely, the high temperature of reaction increased the solubility of the reagents easing the diffusion of water molecules through the interface. Aromatic compounds are known to increase their solubility in water with the increase in temperature [6][7]. Nonetheless, in these experiments the aromatic acid was the continuous liquid phase and batch reactor operation with stagnant atmosphere was not designed to increase the mass transfer coefficients and promote effective diffusion among the phases.

The high sensitivity of the reaction to the way in which decomposition is conducted calls for a different approach in terms of reaction engineering. In future work the mass transport would have to be controlled. The extent to which the selectivity to the ring-opened product can be increased can only be determined if mass transport is not limiting.

6.5 Conclusions

The effect of water on the thermal decomposition of biphenyl-2-carboxylic acid was explored. The main conclusions from the experimental investigation were:

- (a) A change in the reaction selectivity for the acid decomposition was found by comparing the average relative ratio of ring-opened to ring-closed products when reaction was conducted with and without the presence of water.
- (b) The relative ratio of biphenyl (ring-opened product) to fluorenone (ring-closed product) was of the order 2 when decomposition was carried out in presence of 30 % or more excess water, compared to 0.5 for thermal decomposition in the absence of water.
- (c) The exact role of water during thermal decomposition was not elucidated by this work. Based on literature the water might be participating as an intermediary to facilitate the proton or hydrogen transfer that stabilizes the ring-opened product, i.e., biphenyl in the present investigation.
- (d) Under the reaction conditions studied chemical equilibrium was not reached.
- (e) Mass transport was important and inadequate control over mass transport resulted in variability in the selectivity ratio of biphenyl to fluorenone. Controlling mass transport is important for controlling the product selectivity.

6.6 References

- [1] Le Page, J. F. *Applied heterogeneous catalysis*; Technip: Paris, 1987, p 366-401.
- [2] Montoya Sánchez, N.; De Klerk, A. Oxidative ring-opening over metal oxides. *Prepr. Pap.-Am. Chem. Soc., Div. Energy Fuels* **2014**, 59(2), 558-561.
- [3] Montoya Sánchez, N.; De Klerk, A. Oxidative ring-opening of aromatics: Decomposition of biphenyl carboxylic acids and zinc biphenyl carboxylates. *Energy Fuels* **2015**, 29, 7910-7922.
- [4] Akiya, N.; Savage, P. Role of Water in Formic Acid Decomposition. *AIChE J.* **1998**, 44, 406-415.
- [5] Clark, J.; Nimlos, M.; Robichaud, D. Bimolecular decomposition pathways for carboxylic acids of relevance to biofuels. *J. Phys. Chem. A* **2015**, 119, 501-516.
- [6] Gizir, A.; Clifford, A. Solubility of polycyclic aromatic hydrocarbons in subcritical water from 298 K to 498 K. *J. Chem. Eng. Data* **1998**, 43, 1043-1047.
- [7] Andersson, T.; Hartonen, K.; Riekkola, M. Solubility of Acenaphthene, Anthracene, and Pyrene in Water at 50 °C to 300 °C. *J. Chem. Eng. Data* **2005**, 50, 1177-1183.

7. Oxidative Ring-Opening of Aromatics: Thermochemistry of Sodium, Potassium and Magnesium Biphenyl Carboxylates ¹

ABSTRACT

Oxidative ring-opening is a potential alternative to hydrodearomatization and cracking for the conversion of multinuclear aromatic compounds to lighter products. Oxidation of multinuclear aromatics produces quinonoids that can be ring-opened by forming carboxylic acids, which can be decarboxylated to produce lighter oxygen-free hydrocarbons. The efficiency of this reaction depends on the thermochemistry of the metal carboxylate intermediate. Undesirable side-reactions compete with decarboxylation. Using metal carboxylates as catalytic surrogates is a convenient strategy to investigate the catalytic decomposition of carboxylic acids. The thermal behavior of sodium, potassium and magnesium biphenyl-2,2'-dicarboxylates was investigated, over the temperature range 25 to 600 °C, to evaluate the suitability of these metals as catalytic materials for decarboxylation, as well as to gain an understanding of the steps involved in the decomposition. In all cases, thermal analysis revealed quite complex behavior. Thermal events including the loss of lattice water, phase transitions and decomposition were observed. The strong basic properties of alkali and alkaline earth metals resulted in the formation of thermally stable carboxylates with decomposition temperatures above 400 °C. Infrared spectroscopy indicated that the Na, K and Mg carboxylates all existed in ionic (or bridging) configuration, but a bidentate type of interaction was additionally observed for the magnesium carboxylate. Formic acid was also identified during the initial stages of sodium biphenyl-2,2'-dicarboxylate decomposition suggesting the formation of an ester intermediate (not confirmed). The thermal stability of the biphenyl-2,2'-dicarboxylates increased in the order Na < K < Mg, which differed from thermal stability sequence of the alkanooates.

Keywords: Alkali metals, alkaline earth metal, metal carboxylates, thermal analysis, thermal decomposition, decarboxylation.

¹ Reprinted with permission from Montoya Sánchez, N.; De Klerk, A. Oxidative ring-opening of aromatics: Thermochemistry of sodium, potassium and magnesium biphenyl carboxylates. *Thermochim. Acta* 2016, 645, 31-42. Copyright 2016 Elsevier. <https://doi.org/10.1016/j.tca.2016.11.002>.

7.1 Introduction

Multinuclear aromatic compounds are common in the high-boiling distillation fractions of oils and coal liquids. Conventional refining technologies used for the conversion of these materials include visbreaking, coking, catalytic cracking, and residue hydro-conversion [1]. Oxidative ring-opening is a potential alternative reaction pathway for the conversion of multinuclear aromatics to lighter and less refractory products. The aim of this conversion chemistry is to partially oxidize multinuclear aromatic compounds to its quinonoid form, and then, with further oxidation to convert the quinonoid to a carboxylic acid, leading to the opening of the aromatic ring [2][3]. In the last step, decarboxylation of the aromatic carboxylic acid, eliminating the added oxygen as CO₂, takes place.

Unfortunately, undesirable side-reactions, such as ketonization and dehydration, compete with decarboxylation, decreasing the selectivity of the reaction towards the ring-opened products. Using a catalyst to facilitate the decarboxylation step is therefore necessary [3].

Catalysis of carboxylic acid decomposition proceeds via metal carboxylate intermediates and the activity and selectivity of decomposition depend on the metal. Interestingly, the reaction on a heterogeneous catalyst can be approximated by decomposition of the metal carboxylate in isolation. The catalytic activity of a metal or metal oxide for carboxylic acid decomposition relates to the thermal stability of the corresponding bulk metal carboxylate [4]. Thermal analysis is therefore a useful and powerful tool to study the catalytic decomposition of carboxylic acids.

Biphenyl-2,2'-carboxylic acid is the product from oxidative ring-opening of phenanthrene, which is used as model compound to represent multinuclear aromatics. In this work, selected alkali and alkaline earth metals are investigated as potential decarboxylation catalysts for biphenyl-2,2'-carboxylic acid. It is known that Na and K supported on Al₂O₃, as well as MgO as a bulk metal oxide, are all basic catalysts [5][6]. Basic catalysis would readily form surface carboxylates that could lead to decarboxylation. Furthermore, these are not scarce or expensive materials and can readily be manufactured as bulk heterogeneous catalysts. Alkali metal and

alkaline earth metal catalysts are therefore attractive from both an economic and an application point of view.

The aim of this work was to investigate the thermochemistry of selected alkali and alkaline earth metal biphenyl metal carboxylates to determine the potential suitability of sodium, potassium and magnesium as materials for decarboxylation catalysts. Unfortunately, there appeared to be no data on the thermal behavior or the thermal stability of these organic salts, such data was available only for some of the metal alkanoates [7].

A secondary objective was to compare the thermochemistry of these metal carboxylates, where the carboxylate group is attached to an aromatic, to the thermochemistry of alkanoates, where the group is attached to an aliphatic chain. Any generalizations would be helpful in future work, since it would enable inferences to be drawn from data for the metal alkanoates, which is more readily available.

7.2 Experimental Section

7.2.1 Materials

Sodium, potassium and magnesium biphenyl-2,2'-carboxylates, the compounds of study, were not commercially available and had to be synthesized. These metal carboxylates were prepared from commercially obtained materials. The chemicals, calibration materials and cylinder gases used are listed in [Table 7.1](#).

Table 7.1. Commercially available chemicals employed in this study

Compound	Formula	CASRN ^a	Mass fraction purity ^b	Supplier
Biphenyl-2,2'-dicarboxylic acid	C ₁₄ H ₁₀ O ₄	482-05-3	0.97	Sigma-Aldrich
Sodium carbonate	Na ₂ CO ₃	497-19-8	0.995	Sigma-Aldrich
Potassium carbonate	K ₂ CO ₃	584-08-7	0.990	Sigma-Aldrich
Magnesium hydroxide	Mg(OH) ₂	1309-42-8	0.95	Sigma-Aldrich
Ethanol	C ₂ H ₆ O	64-17-5	0.998	Fisher Scientific
Methanol	CH ₄ O	67-56-1	0.999	Fisher Scientific
2-Propanol	C ₃ H ₈ O	67-63-0	0.999	Fisher Scientific
Acetone	C ₃ H ₆ O	67-64-1	0.997	Fisher Scientific
Nitrogen	N ₂	7727-37-9	0.99999 ^c	Praxair
Indium	In	7440-74-6	0.99999	Impag AG
Formic acid	CH ₂ O ₂	64-18-6	0.98	EMD
Magnesium oxide	MgO	1309-48-4	0.99	Sigma-Aldrich
Dimethyl sulfoxide-d ₆	(CD ₃) ₂ SO	2206-27-1	0.999 ^d	Sigma-Aldrich

^a CASRN: Chemical Abstracts Services Registry Number.

^b Purity of the material guaranteed by the supplier.

^c Mole fraction purity.

^d Isotopic purity (atom % D).

7.2.2 Synthesis of Metal Carboxylates

Metal carboxylates were synthesized by mixing an appropriate metal-containing compound, such as a metal hydroxide or metal carbonate, with a slight excess (2% molar excess) of the biphenyl-2,2'-dicarboxylic acid. The solvent and temperature selected for the synthesis varied depending on the metal used for reaction as is indicated.

Sodium biphenyl-2,2'-dicarboxylate and potassium biphenyl-2,2'-dicarboxylate were prepared according to the work of Franzosini, et al [8][9]. Biphenyl-2,2'-dicarboxylic acid was mixed either with sodium or potassium carbonate, using methanol as a solvent. The reaction

mixture was stirred for several hours without heating. The metal carboxylates were recovered by evaporation of the solvent under reduced absolute pressure (80 kPa, absolute), using a rotary evaporator (Heidolph, Model Hei-VAP Precision with Glassware Set G3). Purification of the alkali metal carboxylates was conducted by recrystallization. A mixture of ethanol and methanol (1:1 by volume) was used to obtain the sodium carboxylate, whereas a mixture of 2-propanol, ethanol and methanol (4:2:1 by volume) was employed in the case of the potassium carboxylate.

Magnesium biphenyl-2,2'-dicarboxylate was synthesized based on the general synthesis procedure for reactions in non-aqueous media described by Mehrotra and Bohra [10]. Ethanol was used as solvent and magnesium hydroxide as the starting metal-containing material. The reaction mixture was heated to and kept at 60 °C (total reflux) and stirred for several hours until completion of the reaction. Once the metallic salt precipitated, it was recovered by evaporation of the solvent at reduced pressure conditions as outlined before.

After recovery and purification, all synthesized metal carboxylates were thoroughly washed with acetone, and then dried at approximately 100 °C until they reached constant mass. The final solid products were finely ground and were stored in a desiccator. The purity of the synthesized metal carboxylates was evaluated and it is reported in Table 7.2.

Table 7.2. Chemicals synthesized in this study

Compound	Formula	Mass fraction purity
Sodium biphenyl-2,2'-dicarboxylate	$C_{14}H_8O_4Na_2 \cdot xH_2O$	0.97 ^a
Potassium biphenyl-2,2'-dicarboxylate	$C_{14}H_8O_4K_2 \cdot xH_2O$	> 0.99 ^a
Magnesium biphenyl-2,2'-dicarboxylate	$C_{14}H_8O_4Mg \cdot xH_2O$	> 0.96 ^b

^a Calibrated by FTIR analysis.

^b Not calibrated by FTIR analysis due to overlapping. Estimated by thermogravimetric analysis under nitrogen atmosphere and heating to 600°C.

7.2.3 Equipment and Procedure

Fourier transform infrared (FTIR) spectroscopy and ^1H Nuclear Magnetic Resonance (NMR) were used to confirm the chemical identity of the synthesized metal carboxylates. The former was also used in the analysis of the products obtained after thermal analysis. Infrared spectra were collected using an ABB MB3000 Fourier Transform Infrared spectrometer with Horizon MBTM FTIR software. The spectrometer was equipped with a Pike MIRacle Reflection attenuated total reflectance (ATR) diamond crystal plate. Spectra were collected at a resolution of 4 cm^{-1} , using an average of 120 scans over the spectral region of $4000\text{--}500\text{ cm}^{-1}$. On the other hand, ^1H Nuclear Magnetic Resonance (NMR) spectra were obtained in a Nanalysis 60 MHz NMReady – 60 spectrometer with Mnova NMR software. The equipment was pre-calibrated with deuterated dimethyl sulfoxide (DMSO- d_6). Close to 8.5 mg of sample were dissolved in 0.7 mL of deuterated dimethyl sulfoxide, placed in NMR tubes and analyzed using the following parameters: spectral width 14 ppm; scans per sample: 128; average scan time: 25.5 s

The thermal behavior of the synthesized compounds was studied through differential scanning calorimetry (DSC). A normal pressure differential scanning calorimeter (Mettler–Toledo DSC 1) was used. This equipment is a heat flux (disk) type calorimeter and is equipped with FRS-5 sensor. The sample chamber nitrogen flow rate and the sheathing nitrogen flow rate were kept at 100 mL min^{-1} during all of the experiments. Standard $40\text{ }\mu\text{L}$ aluminum (Al) crucibles with perforated lids were employed for all thermal analyses. Samples were weighed on an analytical balance (Mettler–Toledo, Model XS105 Dual Range Analytical Balance) with $10\text{ }\mu\text{g}$ readability in the range of $0\text{--}105\text{ g}$. The typical sample sizes employed for DSC varied between 6 and 10 mg. All metal carboxylates were analyzed in the $25\text{ to }550\text{ }^\circ\text{C}$ temperature range at a heating rate of $10\text{ }^\circ\text{C min}^{-1}$. The experimental work was conducted in nitrogen atmosphere and analyses were performed in triplicate. Reversibility of the thermal events was confirmed by heating the sample just past the observed transition, and then the cooling down below the event and heating up again. All heating segments employed a heating rate of $10\text{ }^\circ\text{C min}^{-1}$ and all cooling segments employed a cooling rate of $-10\text{ }^\circ\text{C min}^{-1}$. The temperature and heat flow calibration of the DSC was regularly checked by determining the onset of melting and enthalpy of melting of indium. The temperature measurements were accurate to within $0.4\text{ }^\circ\text{C}$ and the

enthalpy measurements were accurate to within 3.5% relative over multiple calibration checks expressed as sample standard deviations from literature values for indium (156.6 °C and 28.6 J g⁻¹ [11]).

Visual observation of the thermal events was carried out using an Olympus BX51 microscope and Mettler FP84HT TA Microscopy Cell (DTA/DSC sensor) with FP90 central processor. Samples were placed in transparent glass crucibles of 7 mm in diameter. Glass cover disks of also 7 mm in diameter were used as lids. Samples were subjected to a temperature program in the range 25 to 375 °C.

Decomposition and mass loss profiles of the metal carboxylates were investigated by thermogravimetric analysis (TGA). A Mettler Toledo TGA/DSC1 system, equipped with a LF 1100 furnace, a sample robot and a MX5 internal microbalance (5 g range and 1 µg readability) was used to collect the experimental data. Samples of around 10 mg in size were placed in standard 70 µL alumina (Al₂O₃) crucibles, and were heated from 25 to 600 °C at a heating rate of 10 °C min⁻¹. All experiments were conducted in nitrogen atmosphere and the flow was adjusted to 100 mL min⁻¹. Also, a sheathing nitrogen flow rate of minimum 20 mL min⁻¹ was maintained during the experiments. All experiments were performed in triplicate.

In order to determine the nature of the evolved gases during thermogravimetric analysis, selected experiments were repeated using thermogravimetric analysis (TA Instruments, Model Q-500) coupled with Fourier transform infrared spectrometer (Agilent Model Cary-670). The thermogravimetric analyzer was equipped with a vertical dual range microbalance (0–200 mg and 0–1 g) with 0.1 µg sensitivity. Samples of about 10 mg were placed in standard 50 µL platinum crucibles and were heated according to the same temperature program and nitrogen flow previously described. The evolved gases were transferred to the FTIR spectrometer gas cell using a line kept at 200 °C. The gaseous sample was scanned 32 times by the FTIR spectrometer, with a sampling interval of 6 s and the spectra were collected at a resolution of 2 cm⁻¹. The non-instantaneous nature of this analysis has some implications in the way in which the experimental data are interpreted. In practice, the collected infrared spectra cover the gases evolved in a temperature range; after all, a certain amount of time is spent on the scanning process. According

to the experimental procedure, each infrared spectrum is reported for a temperature value that corresponds to the average temperature over a temperature range of 10 °C.

The solid residue obtained after thermogravimetric analysis of the magnesium carboxylate was analyzed by X-ray diffraction. A Rigaku Ultima IV diffractometer equipped with a cobalt tube (38 kV38 mA), D/Tex detector with Fe filter, and silicon sampler holder was used. Samples ran from 5 to 90° on continuous scan, at a speed of 2.0° 2-theta per minute, with a step size of 0.02°. Interpretation of the data was done using JADE 9.5 software.

7.2.4 Calculations

TGA and DSC analyses of the synthesized metal carboxylates allowed for determining the onset and endset temperatures, mass loss and enthalpy associated to different thermal events. Results from thermal analysis are summarized in Table 7.4 and Table 7.5 and are reported according to the format described by Eq. (1), where \bar{q} corresponds to the average value (Eq. (2)) of n independent observations of the quantity q , and $s(q_k)$ correspond to the experimental standard deviation (Eq. (3)), which is used in this document as a measure of the uncertainty of the experimental data.

$$q = \bar{q} \pm s(q_k) \quad (1)$$

$$\bar{q} = \frac{1}{n} \sum_{k=1}^n q_k \quad (2)$$

$$s^2(q_k) = \frac{1}{n-1} \sum_{j=1}^n (q_j - \bar{q})^2 \quad (3)$$

7.3 Results and Discussion

7.3.1 Infrared Spectroscopy

Synthesis of the metal carboxylates was confirmed by infrared spectroscopy. The infrared spectrum for metal carboxylates exhibits two particular vibrations. Typically, a strong asymmetric stretching, $\nu_{as}(\text{CO}_2^-)$, is found in the region of 1610–1550 cm^{-1} , and a somewhat weaker symmetrical stretching, $\nu_s(\text{CO}_2^-)$, is present around 1400 cm^{-1} [12]. Usually, the

asymmetric stretching of a carboxylate group is in a more crowded region of the infrared spectrum than the symmetric one. The characteristic absorption bands were observed for all of the metal carboxylates synthesized and the corresponding wavenumbers are listed in [Table 7.3](#).

Table 7.3. Characteristic stretching vibrations in the infrared spectra for the synthesized metal biphenyl-2,2'-dicarboxylates.

Biphenyl-2,2'- carboxylate	Carboxylate stretching vibrations, ν [cm^{-1}]				$\Delta\nu$ [cm^{-1}] ^a	
	Asymmetric, $\nu_{\text{as}}(\text{CO}_2^-)$		Symmetric, $\nu_{\text{s}}(\text{CO}_2^-)$		Standard	Alternate
Sodium	1550	-	1388	-	162	-
Potassium	1558	-	1380	-	178	-
Magnesium	1589 ^b	1535	1448	1411 ^b	178	87

^a $\Delta\nu = \nu_{\text{as}}(\text{CO}_2^-) - \nu_{\text{s}}(\text{CO}_2^-)$

^b Stretch displaying the highest intensity, used to calculate the standard $\Delta\nu$.

The characteristic asymmetric stretching, $\nu_{\text{as}}(\text{C}=\text{O})$, of the biphenyl-2,2'-dicarboxylic acid at 1674 cm^{-1} was no longer present in the metal carboxylates; instead, it was replaced for two new absorption bands. The infrared spectra of biphenyl-2,2'-dicarboxylic acid, sodium biphenyl-2,2'-dicarboxylate, potassium biphenyl-2,2'-dicarboxylate, and magnesium biphenyl-2,2'-dicarboxylate are presented in [Figure 7.1](#).

It is not uncommon for metal carboxylates to have water molecules trapped in the crystalline structure of the organic salts. These molecules, referred to as lattice water, are characterized by the antisymmetric and symmetric OH stretching in the region of around $3550\text{--}3200 \text{ cm}^{-1}$ and the HOH bending around $1630\text{--}1600 \text{ cm}^{-1}$ [13]. Broad bands, of moderate intensity, in these regions of the infrared spectra were observed in all cases suggesting that all three synthesized metal carboxylates contained some lattice water.

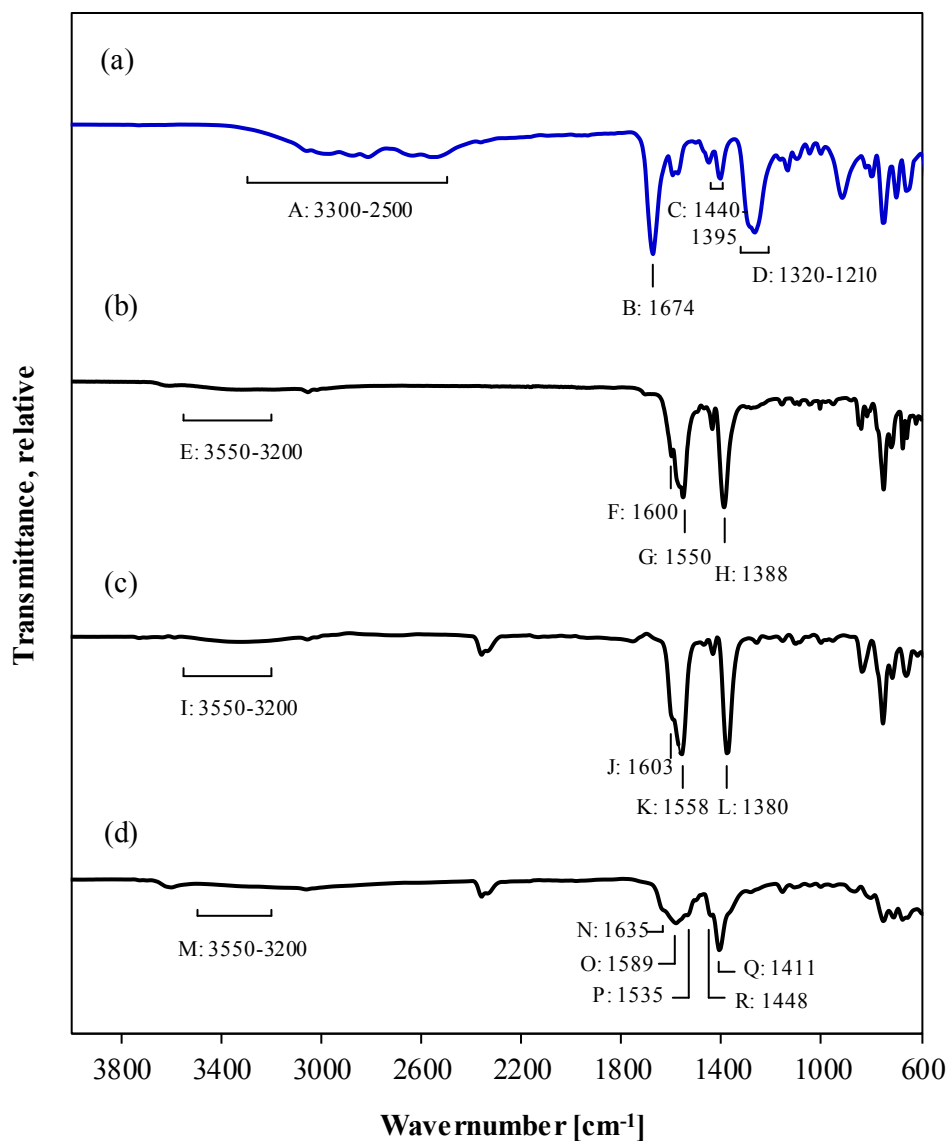


Figure 7.1. Infrared spectra of (a) biphenyl-2,2'-dicarboxylic acid, and (b) sodium, (c) potassium and (d) magnesium biphenyl-2,2'-dicarboxylates. A: O–H stretching; B: $\nu_{as}(\text{C}=\text{O})$ stretching; C: O–H bending; D: C–O stretching; E, I, M: OH stretching for lattice water; F, J, N: HOH bending for lattice water; G, K, O, P: $\nu_{as}(\text{CO}_2^-)$ stretching; H, L, Q, R: $\nu_s(\text{CO}_2^-)$ stretching

The infrared spectra of the sodium and potassium biphenyl-2,2'-dicarboxylates revealed very sharp and well-defined asymmetric and symmetric stretching vibrations. Great symmetry, typical of the carboxylates of highly electropositive elements [10], was found in both cases. The shape and intensity of the two characteristic bands were quite similar. Furthermore, a small change in

the frequency of the stretching bands was observed when increasing the size of the alkali metal atom. The separation of the characteristic bands ($\Delta\nu$) increased from 162 cm^{-1} to 178 cm^{-1} when sodium was replaced by potassium as the cation. No splitting of the carboxylate bands was observed.

The spectrum of magnesium biphenyl-2,2'-dicarboxylate showed more complex behavior compared to that observed for the carboxylates of the alkali metals. In this case, the relative intensity between the characteristic absorption bands was quite different. A wide, slightly round and not very intense absorption band described the asymmetric stretch; whereas, a more intense and quite sharp band described the symmetric one. This difference in the relative intensity of the characteristic vibrations suggested a less symmetrical type of structure [10]. The partial splitting of both characteristic stretching bands indicated that more than one type of bonding mode is very likely [10][13].

The two absorption bands that appeared around 2350 cm^{-1} in the infrared spectra of the potassium and magnesium carboxylates (Figure 7.1) are not characteristic absorptions of these compounds. On the contrary, they represent changes in the background CO_2 concentration. In order to ensure the quality of the experimental data, before collecting the infrared spectrum of the samples, the measurement of a reference spectrum under the same conditions of analysis of the samples (average of scans, resolution, and detector gain, among others) is required. Although, the reference spectrum was collected regularly, some background CO_2 was still observed in some of the samples.

The calculated $\Delta\nu$ for the sodium and potassium carboxylates (162 and 178 cm^{-1} , respectively) points out to either ionic or bridging configurations. Although these two types of structures cannot be differentiated using the $\Delta\nu$ value alone, it is known that ionic configurations are very common for alkali metal carboxylates [10]. On the other hand, the splitting of the carboxylate bands observed for the magnesium carboxylate resulted in two different values of $\Delta\nu$. The standard value, 178 cm^{-1} , indicated an ionic or bridging type of interaction; whereas, the alternate value, 87 cm^{-1} , pointed out that some of the material had a bidentate type of bonding [13]. In this case, the nature of the metal cation may explain the observed behavior. It has been

reported that calcium acetate has two types of acetate groups. One of those groups displays a more covalent character, with $\Delta\nu$ of 86 cm^{-1} , while the other is purely ionic, with $\Delta\nu$ of 148 cm^{-1} [10]. Calcium, like magnesium, is an alkaline earth metal, which might explain the similarity in the bonding configuration found in this study (Table 7.3) and that reported for calcium acetate. Also, magnesium carboxylates are known to exhibit covalent bonding [10]

7.3.2 ^1H NMR Analysis

Synthesis of the metal carboxylates was also verified by nuclear magnetic resonance spectroscopy. The ^1H NMR spectra of the biphenyl-2,2'-carboxylic acid as well as the sodium, potassium and magnesium biphenyl-2,2'-dicarboxylates were measured and compared. The ^1H NMR spectrum of the biphenyl-2,2'-carboxylic acid in DMSO- d_6 showed signals at 12.37 (broad peak) and 7.41 ppm, which are typical of the carboxylic acid and aromatic hydrogen. Carboxylic acids have chemical shift values greater than 10 ppm while aromatics have chemical shift values within the range of 6.5–8.0 [23]. In the ^1H NMR spectra of the synthesized metal carboxylates, there was no indication of hydrogen from a carboxylic acid group. Only peaks corresponding to aromatic hydrogen were observed. Chemical shift values of 7.04, 7.08, and 7.25 ppm were observed in the spectra of the sodium, potassium and magnesium carboxylates, respectively.

7.3.3 Sodium Biphenyl-2,2'-dicarboxylate

Thermogravimetric analysis of the sodium biphenyl-2,2'-dicarboxylate over the temperature range 25 to 600 °C resulted in mass loss that could be classified into seven regions labeled I to VII (Figure 7.2). The calorigram that was obtained by differential scanning calorimetry of sodium biphenyl-2,2'-dicarboxylate is also shown on Figure 7.2 and thermal events are labeled *i* to *iv*. For the TGA mass loss curve the temperature range over which each mass loss occurred, the amount of mass loss and the nature of the gaseous compounds that were released are listed in Table 7.4. Similarly, for the calorigram the onset, endset and peak temperatures of the thermal events, as well as the energy change associated with each of them are listed in Table 7.5.

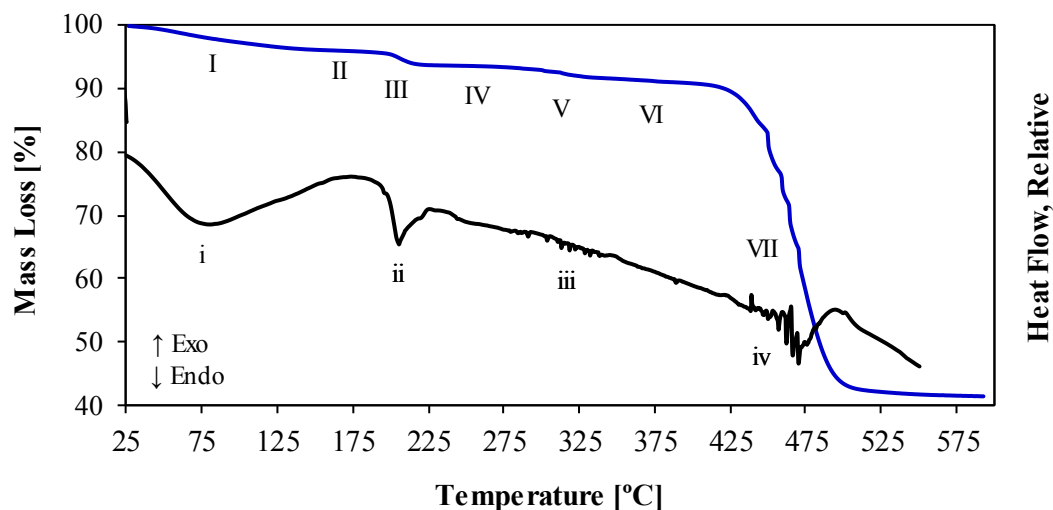


Figure 7.2. TGA mass loss profile (collected with Mettler Toledo TGA/DSC1 system) and DSC heat flow signal for decomposition of sodium biphenyl-2,2'-dicarboxylate

Initially, the loss of water was confirmed by FTIR analysis. This event was observed in the calorigram as two very wide, round and overlapped endothermic peaks (transition *i*). The main event has a peak temperature close to 76 °C, whereas the second one, which can be described as a shoulder, has a peak temperature of around 126 °C. The onset temperature for the loss of water was 28.2 ± 1.8 °C. The estimated energy required to release the water from the sodium carboxylate structure is 166 ± 14 kJ kg⁻¹. It is worth mentioning that the negative slope in the baseline of the mass loss profile and calorigram indicated that mass was being lost since the beginning of the thermal analysis (Figure 7.2). Visual inspection of the samples suggested that the sodium carboxylate was hygroscopic. Also, for samples left outside of the desiccator, FTIR analysis showed an increase in the intensity of the OH stretching in the region of around 3550–3200 cm⁻¹. It is suggested that the loss of water corresponds to the loss of lattice water as well as the loss of water that could be absorbed from the environment (Figure 7.3).

Table 7.4. Thermal decomposition and mass loss profile of the synthesized biphenyl-2,2'-carboxylic acid salts studied by TGA and TGA-FTIR analyses

Metal	Region _{a,b}	Temperature (T _{onset} - T _{endset})		Mass loss [%]	$\Delta m / \Delta T$ [g/°C]	Gaseous Products
		[°C]	[°C]			
Na	I	^d	116.1 ± 6.8	4.0 ± 0.9 ^e	0.06	Water
	II ^c	135.0 ± 0.1	196.0 ± 0.1	0.9 ± 0.2	0.01	Water, formic acid
	III	197.1 ± 1.1	214.1 ± 1.7	2.1 ± 0.3	0.12	Water ^f , formic acid
	IV ^c	222.1 ± 0.1	290.1 ± 0.1	0.7 ± 0.1	0.01	Water, formic acid, CO ₂
	V	297.8 ± 2.3	236.2 ± 8.3	1.5 ± 0.3	0.05	Water ^f , CO ₂
	VI ^c	337.1 ± 0.0	406.1 ± 0.0	1.5 ± 0.6	0.02	Water ^f , CO ₂
	VII	443.3 ± 2.9	489.5 ± 3.3	47.5 ± 0.7	1.03	CO ₂
K	I	61.4 ± 1.4	108.7 ± 3.3	7.1 ± 0.5	0.15	Water
	II ^c	130.0 ± 0.1	398.1 ± 0.1	2.1 ± 0.1	0.01	Water, CO ₂ ^g
	III	440.4 ± 0.5	490.5 ± 1.6	32.6 ± 0.2	0.65	CO ₂
Mg	I	65.1 ± 5.6	151.1 ± 1.4	6.7 ± 0.7	0.08	Water
	II ^c	185.1 ± 0.0	420.0 ± 0.1	2.5 ± 0.7	0.01	Water ^f , CO ₂
	III	470.2 ± 0.9	512.5 ± 1.4	73.2 ± 0.3	1.73	CO ₂

^a All experiments were conducted in nitrogen atmosphere and the flow was adjusted to 100 mL·min⁻¹. The experimental pressure corresponds to the atmospheric pressure, which for typical laboratory conditions is 102.2 kPa.

^b Mass loss profiles of the synthesized alkali and alkaline earth metal carboxylates were conveniently described in terms of temperature regions containing the main thermal events. These regions do not necessarily cover the whole temperature range of analysis.

^c A plateau on the mass loss profile was observed. The onset and endset temperatures were conveniently selected to help describing the events observed by DCS analysis of the metal carboxylate in the same temperature range.

^d The onset temperature was not estimated. The baseline of the mass loss profile displayed a negative slope at the start of the measurement suggesting that some mass loss was already taking place. DSC analysis of the metal carboxylate using a temperature program starting at -20 °C also showed a negative slope when the heating of the carboxylate started. It is speculated that the sodium carboxylate is hygroscopic.

^e The mass loss was calculated as the difference between the mass of metal carboxylate present at the beginning of the experiment and the mass of metal carboxylate remaining at the endset temperature of the thermal event.

^f The intensity of the vibrations indicating the presence of water in the IR spectra of the gases was really low compared to the other products.

^g The intensity of the vibrations indicating the presence of water and CO₂ in the IR spectra of the gases was really low.

Table 7.5. Thermal decomposition of the synthesized biphenyl-2,2'-carboxylic acid salts studied by DSC analysis

Metal	Transition a, b	Onset Temperature [°C] ^c	Endset Temperature [°C] ^c	Peak Temperature [°C] ^e	Enthalpy of transition [kJ·kg ⁻¹] ^f
Na	<i>i</i>	28.2 ± 1.8	163.5 ± 5.7	76.6 ± 1.2	-166 ± 14
	<i>ii</i>	197.4 ± 0.2	220.8 ± 2.8	205.1 ± 0.3	-20 ± 1
	<i>iii</i>	287.6 ± 1.8	347.0 ± 5.9	-	-1 ± 0 ^f
	<i>iv</i>	Above 420 ^d	-	-	-
K	<i>i</i>	65.2 ± 5.2	124.8 ± 5.0	96.0 ± 3.0	-285 ± 25
	<i>ii</i>	174.8 ± 7.1	179.1 ± 7.0	176.6 ± 7.5	-1 ± 0
	<i>iii</i>	292.1 ± 1.5	303.7 ± 0.2	299.7 ± 0.4	-53 ± 2
	<i>iv</i>	Above 430 ^d	-	-	-
Mg	<i>i</i>	45 ± 1.7	224.7 ± 5.4	114.6 ± 5.6	-472 ± 76
	<i>ii</i>	328.1 ± 11.8	358.5 ± 1.1	351.3 ± 0.8	-17 ± 1
	<i>iii</i>	359.9 ± 1.1	372.1 ± 0.8	366.5 ± 0.9	28 ± 2
	<i>iv</i>	Above 465			

^a All experiments were conducted in nitrogen atmosphere and the flow was adjusted to 100 mL·min⁻¹. The experimental pressure corresponds to the atmospheric pressure, which for typical laboratory conditions is 102.2 kPa.

^b All transitions observed by DSC analysis were irreversible (the opposite transition was not observed upon dynamic cooling).

^c Onset and endset temperatures were estimated but were ill-defined. Transitions consisted of multiple convoluted peaks and the behavior of the baseline was greatly affected by the mass loss.

^d The behavior of the baseline was very complex due to the mass loss associated to decomposition of the metal carboxylate. Multiple small convoluted transitions were observed. Just an estimation of the onset temperature is given.

^e The peak temperature reported here corresponds to the main thermal event when convoluted peaks are observed.

^f Energy changes: endothermic values are negative, exothermic values are positive.

^g The baseline of the calorigram revealed several small convoluted peaks of both endothermic and exothermic nature; thus, the enthalpy reported is the total energy associated to all these events.

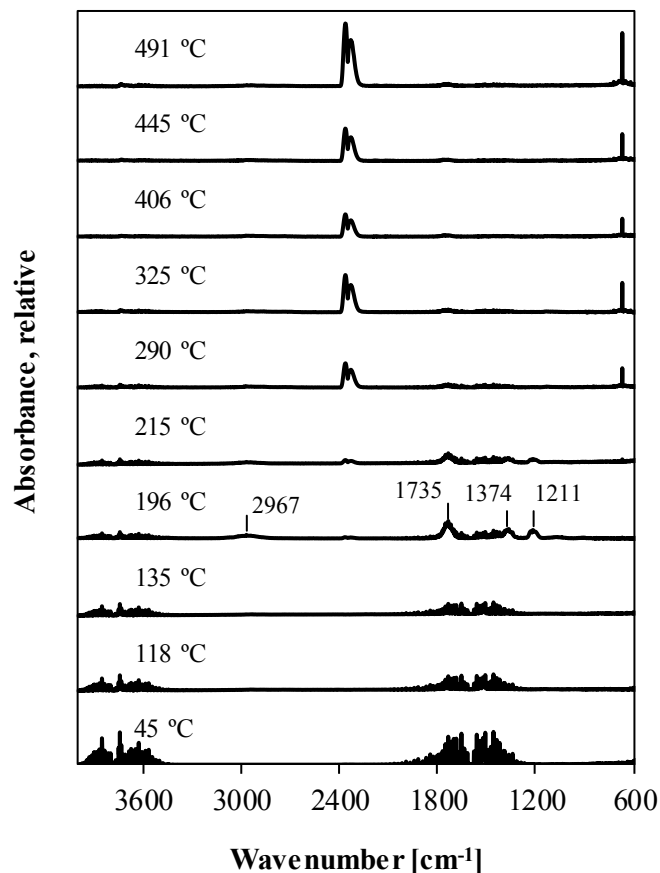


Figure 7.3. Infrared spectra of the gaseous products evolved during thermal analysis of the sodium biphenyl-2,2'-dicarboxylate

Further heating of the sodium carboxylate to around 200 °C led to a minor mass loss, ~2% of the original mass of the metal carboxylate. This event was detected as a wide, endothermic and irreversible peak according to DSC (transition *ii* in Figure 7.2). It has an onset temperature of 197.4 ± 0.2 °C with $\Delta H = -20 \pm 1$ kJ kg⁻¹. This value correlates well with the onset temperature of the third event observed by TGA analysis (197.1 ± 1.1 °C). According to DSC-microscopy, no phase changes were observed during transition *ii*.

Besides water, the evolution of some other volatile, organic compounds, which was identified as formic acid, was observed by FTIR (Figure 7.4). The infrared spectrum of formic acid was recorded and shown for comparison. The similitude between the experimental data and the commercially available standard is evident. On one hand, the strong band at 1735 cm⁻¹

corresponds to the C=O stretching vibration typical of the carboxylic acid functionality. The two bands located at 1374 and 1211 cm^{-1} represent the C–O and O–H bending, respectively, and the broad absorption in the region of 3100–2800 cm^{-1} indicates the O–H stretching [12]. On the other hand, there are some differences in the 1000–600 cm^{-1} region of the infrared spectra which may be explained due to the conditions used for collecting the experimental data. The spectrum of the products obtained during thermal analysis was measured in the gas phase at 200 °C. Whereas, the spectrum of the formic acid used for comparison was recorded for liquid phase acid at room temperature. The infrared spectra of formic acid have been studied, and variations regarding the presence and the intensity of the different absorption bands due to changes in temperature and phase of analysis have been discussed [14][15]. The presence of weak absorption bands at 875 and 669 cm^{-1} in the infrared spectra of liquid formic acid has been reported [15]. The former absorption, a broad band, is due to hydrogen bonds, which is an interaction that would not be present in the gas phase [16]. Similarly, the infrared spectrum of deuterated formic acid showed a sharp absorption at 670 cm^{-1} which indicates an oligomeric form in the liquid phase [17].

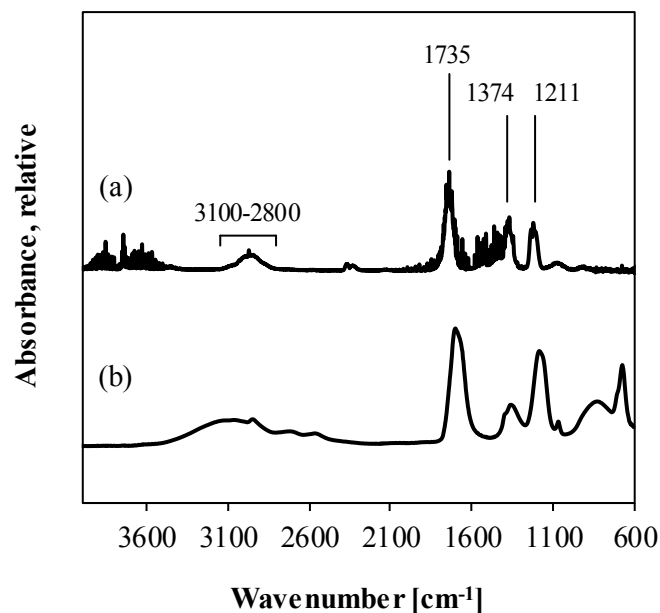


Figure 7.4. Infrared spectra of the (a) gas product evolved during heating of the sodium biphenyl-2,2'-dicarboxylate at 200 °C, and (b) liquid formic acid at room temperature

The fact that formic acid is released as gaseous product suggests that ring-closure through the formation of an ester is likely. A potential reaction pathway is suggested that would lead to the elimination of formic as a product (Figure 7.5). Water is required and the reaction results in the elimination of one carboxylate group, with the remaining carboxylate group forming a cyclic ester by intramolecular ring-closure.

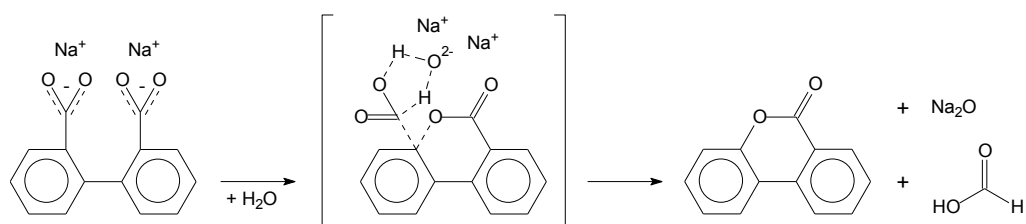


Figure 7.5. Possible reaction pathway leading to formic acid formation during decomposition of sodium biphenyl-2,2'-dicarboxylate.

The infrared spectrum of the solid residue obtained after heating the sodium carboxylate to a temperature a little higher than the endset temperature of transition *ii* was recorded (Figure 7.6). It was anticipated that the development of C=O and C–O absorptions would confirm the formation of an ester. However, there was no evidence of the presence of a carbonyl group in the region of 1730–1715 cm^{-1} , typical of esters. It is likely that the infrared analysis was not able to detect the small change; after all, only ~2% of the original mass of the metal carboxylate was lost due to production of formic acid.

Continuous but little mass loss, ~3.5% of the original carboxylate, involving production of water and CO_2 occurred while heating the sodium carboxylate over the temperature range ~200–400 °C (regions IV, V and VI). The presence of these gaseous products suggests that decomposition of the bulk carboxylate might have been taking place at a really slow rate. Interestingly, DSC-microscopy confirmed that heating of the sodium carboxylate over the temperature ~230–250 °C resulted in the formation of a liquid phase. However, no indication of melting was observed by DSC analysis.

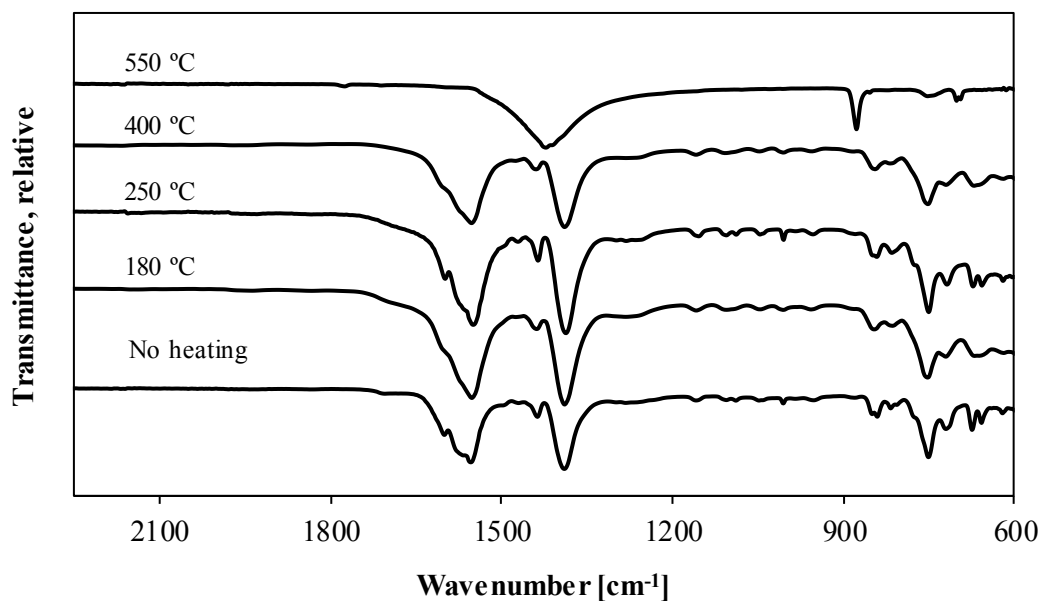


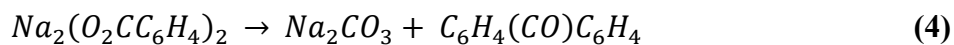
Figure 7.6. Infrared spectra of the solid residue obtained after DSC analysis of the sodium biphenyl-2,2'-dicarboxylate

According to DSC, a series of very small and overlapped peaks were found over the temperature range $287.6 \pm 1.8 \text{ }^\circ\text{C}$ to $347.0 \pm 5.9 \text{ }^\circ\text{C}$. The complexity of the calorigram and the presence of multiple convoluted peaks made the analysis difficult. As a result, the reported onset and endset temperatures should be understood more as an indication of where these transitions are taking place. From an enthalpy point of view, small endothermic and exothermic events were observed. The calculated total energy, namely the energy adsorbed and the energy released due to these transitions, corresponds to $1 \pm 0 \text{ kJ kg}^{-1}$. Initially, it was speculated that some of these transitions may be related to rearrangements in the carboxylate structure. It is known that carboxylates of alkali metals exist in a number of polymorphic forms; as a result, they tend to undergo several transitions prior melting [10]. No peak indicating the melting of the carboxylate has been noted up to this point, although the formation of a liquid phase, just before these small transitions took place, was observed. On the other hand, production of some CO_2 and water was also observed. Even though, the low enthalpy value of these transitions does necessarily not point out to chemical changes, it might be possible that some decomposition took place at a very slow rate.

Decomposition of the sodium biphenyl-2,2'-dicarboxylate occurred at a very high temperature, 443.3 ± 2.9 °C (Region VII). In this case, close to 37% of the original mass of the metal carboxylate was lost and production of CO₂ was confirmed by FTIR. Decomposition seemed to be a complex process. Multiple thermal events in the form of convoluted peaks were observed by DSC. Even more, the presence of a sharp peak among these transitions suggested that melting of the carboxylate could have taken place during decomposition. Reversibility of the peak could not be verified by DSC. On the other hand, the onset temperature and the enthalpy of decomposition were not determined due to the complex behavior of the calorigram. The baseline was greatly affected by the mass loss and reconstruction was not possible.

It has been reported that sodium carboxylates, e.g. RCO₂Na (R = C₂H₅, C₃H₇, C₁₀H₂₁, C₁₂H₂₅), are very stable compounds which decompose at high temperature, 350–560 °C, to yield carbonates and ketones as the main inorganic and organic products, respectively [10]. It has also been reported that zinc biphenyl metal carboxylates decompose to form of a number of organic ring-opened and ring-closed compounds [3]. The decomposition of this type of metal carboxylates, which is simpler than the one observed for their corresponding parent aromatic carboxylic acids, resulted in significant production of fluorenone. Production of this ketone increased as the temperature of reaction increased.

It is expected that decomposition of the sodium biphenyl-2,2'-dicarboxylate would yield a similar product distribution to the one observed in the case of the zinc biphenyl carboxylates. Nevertheless, the typical behavior found in other sodium carboxylates and the high temperature of reaction (decomposition occurred between $443.3 \pm 2.9 - 489.5 \pm 3.3$ °C) suggests that in practice the decomposition of the sodium biphenyl-2,2'-dicarboxylate may be approximated by Eq. (4). Production of fluorenone and sodium carbonate is very likely [3][10]. Formation of sodium carbonate as the solid product of decomposition was confirmed by FTIR analysis (Figure 7.7). Furthermore, the mass loss for the decomposition of the sodium biphenyl-2,2'-dicarboxylate to yield Na₂CO₃ was calculated and corresponded well with the experimentally observed mass loss from thermogravimetric analysis (Table 7.6). A difference of about 11% between these two values was observed.



Heating of the sodium biphenyl-2,2'-dicarboxylate to 900°C revealed an additional event taking place. According to TGA, the onset temperature of this event was 820 ± 7.9 °C. A small change in the slope of the mass profile was observed. It is suspected that decomposition of the sodium carbonate to yield the sodium oxide and CO₂ started to occur. However, the infrared spectrum of the solid residue collected after heating to 900 °C still displayed the absorptions bands of the sodium carbonate

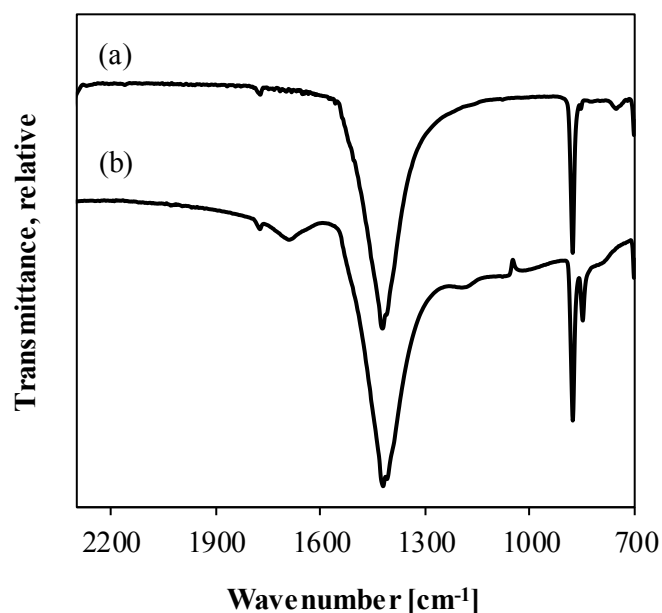


Figure 7.7. Infrared spectrum of the (a) solid residue obtained after thermal decomposition of the sodium biphenyl-2,2'-dicarboxylate when heated to 600 °C, (b) sodium carbonate

Table 7.6. Mass loss of the synthesized biphenyl-2,2'-carboxylic acid salts after decomposition determined by TGA and calculated according to the expected inorganic residue

Metal	Expected decomposition inorganic residue	TGA mass loss mass fraction ^a	Calculated mass loss mass fraction
Na	Na ₂ CO ₃	0.42	0.37
K	K ₂ CO ₃	0.60	0.48
Mg	MgO	0.17	0.16

^a Mass fraction = mass of the residue obtained by heating the metal carboxylate up to 600 °C / mass of metal carboxylate obtained after the release of lattice water

7.3.4 Potassium Biphenyl-2,2'-dicarboxylate

A typical mass loss profile and calorigram obtained after thermal analysis of the potassium biphenyl-2,2'-dicarboxylate are presented in [Figure 7.8](#). The events observed during thermogravimetric analysis are labeled I to III, and information in terms of the onset and endset temperatures, and the nature of the gaseous products associated to each event is presented in [Table 7.4](#). Similarly, transitions observed by DSC are labeled *i* to *iv*, and the onset, endset and peak temperatures as well as the enthalpy associated to them are listed in [Table 7.5](#).

Sodium and potassium carboxylates exhibited a similar thermal behavior. In this case, the first temperature region is again associated with the loss of lattice water. According to TGA, the loss of water started at 61.4 ± 1.4 °C. DSC analysis showed that it happened as a multistage process, represented by three endothermic, wide and overlapped peaks in the calorigram. These peaks have a peak temperature of approximately 96, 112 and 127 °C, respectively. The overall transition has an onset temperature of 65.2 ± 5.2 °C, which correlates well with the value obtained by TGA, and a $\Delta H = -285 \pm 25$ kJ kg⁻¹. For potassium carboxylate to release the lattice water, the energy required is a little less than the double of the energy required in the case of sodium carboxylate. This increase in the energy requirement is not surprising; after all, the additional convoluted peak observed in this case (3 peaks instead of 2) suggests that additional water is coordinated to the structure.

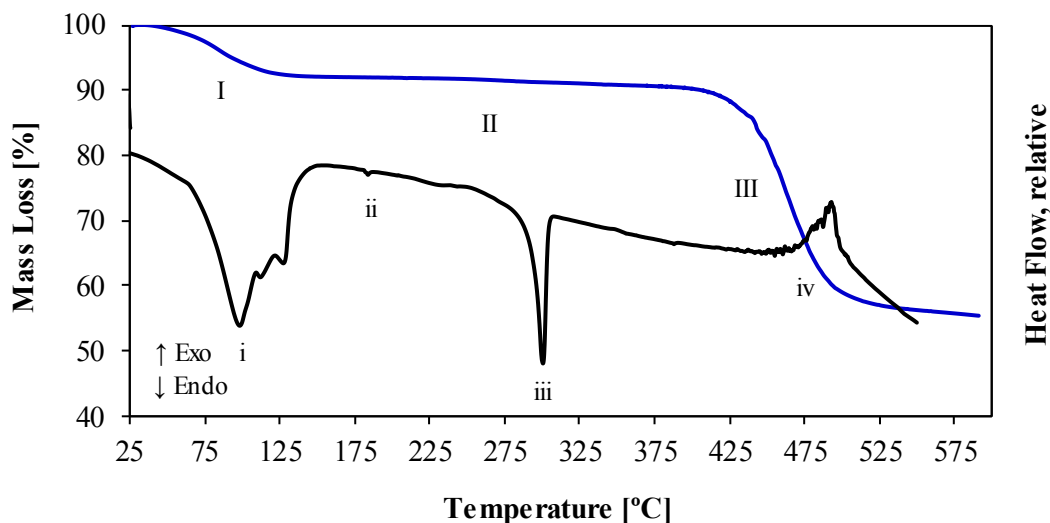


Figure 7.8. TGA mass loss profile (collected with Mettler Toledo TGA/DSC1 system) and DSC heat flow signal for decomposition of potassium biphenyl-2,2'-dicarboxylate

Potassium carboxylate proved to be thermally stable up to very high temperatures. Only ~2% of the original compound was lost by heating over the temperature range ~130–398 °C (region II). The calculated rate of mass loss with temperature ($\Delta m/\Delta T$) during this temperature segment was only $0.01 \text{ g } ^\circ\text{C}^{-1}$, which in comparison is an order of magnitude lower than the one calculated during the loss of lattice water ($0.15 \text{ g } ^\circ\text{C}^{-1}$). FTIR analysis confirmed production of little CO_2 and water; weak absorption bands for these products were observed. According to DSC, two transitions which did not involve mass loss were observed in region II. First, transition *ii* corresponds to an irreversible event with an onset temperature of $174.8 \pm 7.1 \text{ } ^\circ\text{C}$ and it is accompanied by an energy change of $0.5 \pm 0.14 \text{ kJ kg}^{-1}$. The behavior of this event was not repeatable between DSC runs which correlates with the high value of the standard deviation calculated for all temperature determinations, i.e. onset, endset and peak temperatures. Second, transition *iii* has an onset temperature of $292.1 \pm 1.5 \text{ } ^\circ\text{C}$ and consists of a very sharp and well-defined peak. The fact that no mass is lost during this event suggests that it is a phase transition. On one hand, formation of a liquid phase was confirmed by employing DSC-microscopy (Figure 7.9). On the other hand, reversibility of this thermal event was investigated by DSC analysis. Samples of the potassium carboxylate were heated just past the observed transition, then cooled down to $-40 \text{ } ^\circ\text{C}$ for 600 s, and finally heated up again. Under dynamic cooling the reverse phase

transition was not observed. Similarly, during the second heating period the initial event was not observed. It is speculated that the formation of the liquid phase involves not only a physical but a chemical change.

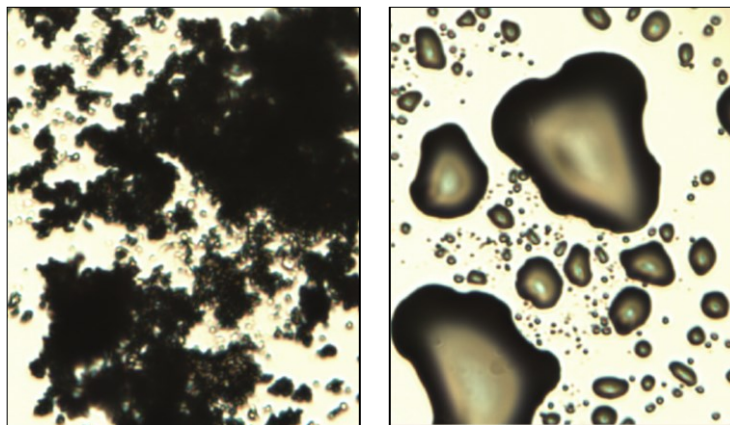


Figure 7.9. DSC-microscopy images of the potassium biphenyl-2,2'-dicarboxylate: solid (left) and liquid phase formed during transition *iii* (right)

Figure 7.10 presents the infrared spectra of the solid residue obtained after heating the potassium carboxylate past the transitions observed by DSC analysis. After the loss of lattice water, partial splitting of the antisymmetric carboxylate stretch was observed. This change in the $\nu_{\text{as}}(\text{CO}_2^-)$ became more noticeable when heating the carboxylate to the point where transition *ii* takes place. The additional vibration at 1580 cm^{-1} resulted in an alternate value of $\Delta\nu$ of 200 cm^{-1} , which suggests a change in the mode of bonding of part of the material to a possibly a monodentate type of structure [10]. The splitting of the antisymmetric stretch remains, although is a little bit softer, after transition *iii* takes place.

Thermal decomposition of the potassium carboxylate occurred at $440.4 \pm 0.5\text{ }^\circ\text{C}$ and involved the loss of approximately 33% of the original mass of compound. This process was perceived by DSC analysis as an exothermic peak consisting of a series of small and convoluted transitions (transition *iv* in Figure 7.8). It is speculated that more than one phenomenon took place during decomposition. Rearrangements of the carboxylate structure are possible. The complexity of the calorigram prevented the determination of a characteristic temperature or an

enthalpy of transition. It is worth to mention that the exothermic nature of the decomposition process for the potassium carboxylate constitutes an interesting difference when compared to the decomposition of its sodium counterpart. A similar thermal behavior was expected for these two compounds given that they are both alkali metal carboxylates. However, no additional work was performed at this point to elucidate this difference.

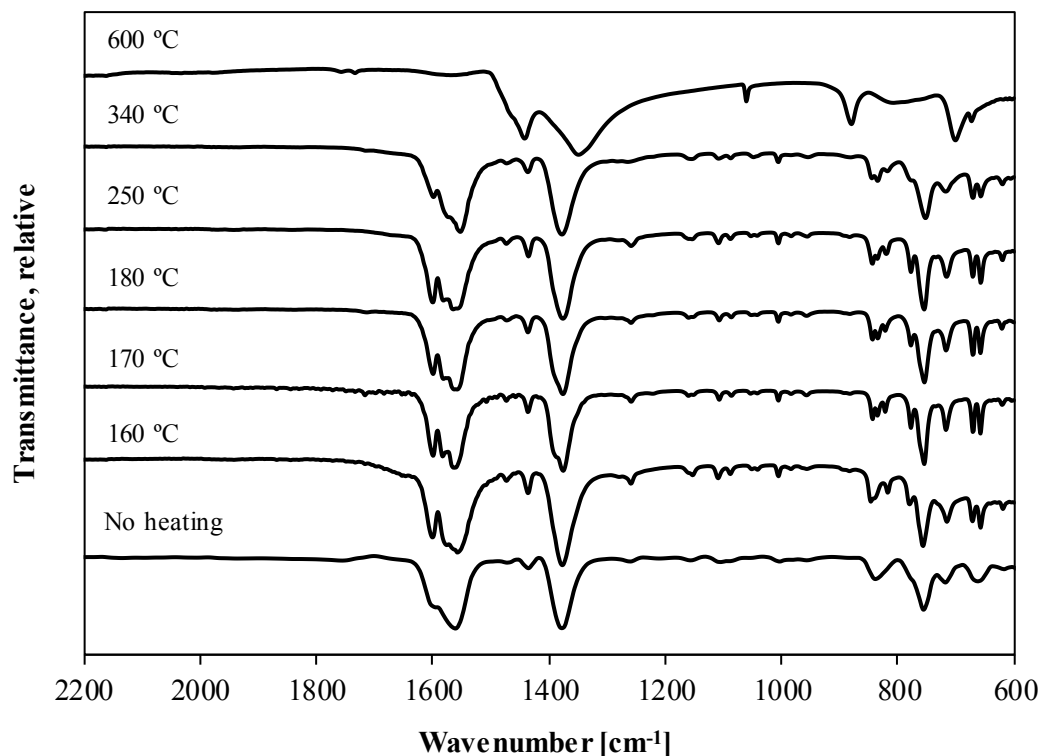


Figure 7.10. Infrared spectra of the solid residue obtained after DSC analysis of the potassium biphenyl-2,2'-dicarboxylate

It has been reported that decomposition of alkali metals (Li, Na, K, Rb and Cs) formates yields carbonates and oxalates as the main inorganic reaction products [10]. Spectroscopic evidence suggested that decomposition of the potassium biphenyl-2,2'-dicarboxylate produced a mixture of potassium carbonate and bicarbonate as the inorganic product. Figure 7.11 presents the infrared spectrum of the solid residue obtained after decomposition as well as the infrared spectra for samples of potassium carbonate and potassium bicarbonate. It is evident that the main absorption bands in the spectrum of the solid residue, bands around 895, 1450, and 3220 cm⁻¹,

corresponded to the characteristic frequencies for the K_2CO_3 [20]. However, absorptions from weak to moderate intensity around 705, 833, 1010, 1600 and 2380 cm^{-1} , which are typical of the $KHCO_3$, were also observed. It is known that potassium carbonate solvents are used in hot carbonate scrubbing processes for removal of CO_2 from gas mixtures [21][22]. Hydration of the carbon dioxide with water forms carbonic acid, which in turn reacts with a carbonate ion to form two bicarbonate ions [22]. It is likely that the potassium carbonate formed during decomposition of the potassium biphenyl-2,2'-dicarboxylate acted as a trap of carbon dioxide (typical reaction product) producing a certain amount of potassium bicarbonate.

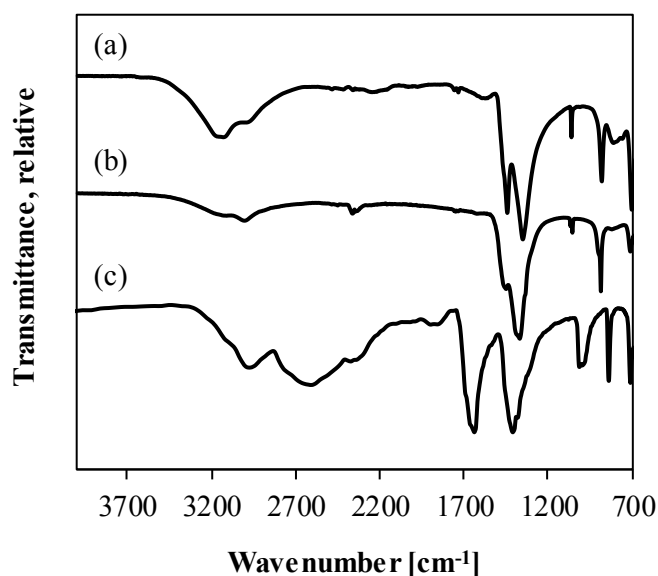


Figure 7.11. Infrared spectrum of the (a) solid residue obtained after thermal decomposition of the potassium biphenyl-2,2'-dicarboxylate when heated to $600\text{ }^\circ\text{C}$, (b) potassium carbonate, (c) potassium bicarbonate

Similar to the case of the sodium biphenyl-2,2'-dicarboxylate, the chemistry of decomposition of the potassium biphenyl-2,2'-dicarboxylate was approximated by the production of fluorenone and potassium carbonate, as the main organic and inorganic products. The mass loss associated to the formation of K_2CO_3 was calculated (Table 7.6). The $\sim 20\%$ difference between the theoretical calculation and the value experimentally obtained might be explained by the omission of potassium bicarbonate as part of the reaction products to perform

the corresponding calculations. The fact that the calculated mass loss (mass fraction, 0.48) was smaller than the experimental value (mass fraction, 0.60) supports this observation.

Decomposition of the potassium carbonate to likely potassium oxide and CO₂ started with further heating of the potassium carboxylate to 900 °C. The onset temperature of the event was 826.3 ± 8.1 °C. Thermal stability for potassium and sodium carbonates is comparable.

7.3.5 Magnesium Biphenyl-2,2'-dicarboxylate

Thermal analysis of the magnesium (II) biphenyl-2,2'-dicarboxylate revealed a very stable compound (Figure 7.12). The mass loss profile indicated events happening in three different temperature regions, I to III. Similarly, the calorigram showed four transitions, labeled *i* to *iv*, taking place. Results from the TGA and DSC analyses for this metal carboxylate are presented in Table 7.4 and Table 7.5, respectively.

According to FTIR analysis, the first region reflects the loss of water from the carboxylate structure. This process, which is seen as a small and gradual change in the mass loss profile occurring at ~65–150 °C, was perceived as a single, very wide and endothermic peak by DSC. The onset temperature is 45 ± 1.7 °C, a lower value compared to the one obtained by TGA. The energy absorbed by the system for releasing the water corresponds to 472 ± 76 kJ kg⁻¹. In this case, contrarily to the case of the alkali metal carboxylates, the calorigram showed only one wide peak associated to the loss of lattice water. The endset temperature for this event (224.7 ± 5.4 °C) indicated that the water was strongly bound to the carboxylate structure.

Further heating of the magnesium carboxylate revealed great thermal stability. Over ~2% of the original mass of compound was lost by heating from ~145 to 420 °C (Region II). It is speculated that magnesium carbonate was formed and decompose to release CO₂. According to DSC, two transitions took place over this temperature range. First, an endothermic, irreversible transition represented by a small, very broad peak, with an onset temperature of 328.1 ± 11.8°C, a peak temperature of 351.3 ± 0.8°C, and a $\Delta H = -17 \pm 1$ kJ kg⁻¹ was observed. Then, an irreversible, exothermic event with an onset temperature of 359.9 ± 1.1 °C was detected. The

energy released in this event corresponds to $28 \pm 2 \text{ kJ kg}^{-1}$. Because no mass was lost during these events, it was anticipated that they represent phase transitions. Infrared analysis of the residue left after heating the magnesium carboxylate past these transitions was recorded and is presented in Figure 7.13. After heating to 350 °C, there appeared no to be any significant changes in the carboxylate structure. However, splitting of the antisymmetric stretch, $\nu_{\text{as}}(\text{CO}_2^-)$, was observed when the carboxylate was heated to 380°C. Moreover, the evolution of a small amount of CO₂ and water was noted when the temperature increased above 350 °C. Likely, the magnesium carboxylate was slowly starting to decompose.

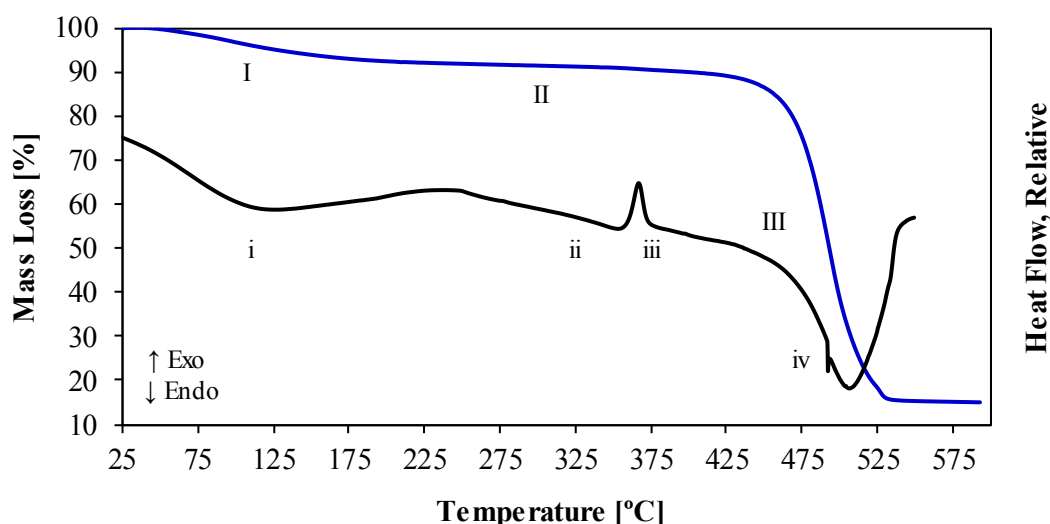


Figure 7.12. TGA mass loss profile (collected with Mettler Toledo TGA/DSC1 system) and DSC heat flow signal for decomposition of magnesium biphenyl-2,2'-dicarboxylate

Decomposition of the bulk metal carboxylate occurred at $470.2 \pm 0.9 \text{ °C}$ as a very steep step in the mass loss profile; $\sim 73\%$ of the original mass of compound was lost. In this case, the rate of mass loss with temperature, 1.73 g °C^{-1} , is an order of magnitude higher than the one calculated for the decomposition of the potassium carboxylate, 0.65 g °C^{-1} . On the other hand, a slight change in the slope of the decomposition step, which is consistent with the presence of two overlapping events in the calorigram, suggested that more than one reaction took place. The baseline of the calorigram was greatly affected by the mass loss during decomposition. No

enthalpy changes or onset temperatures associated with these events could reliably be determined.

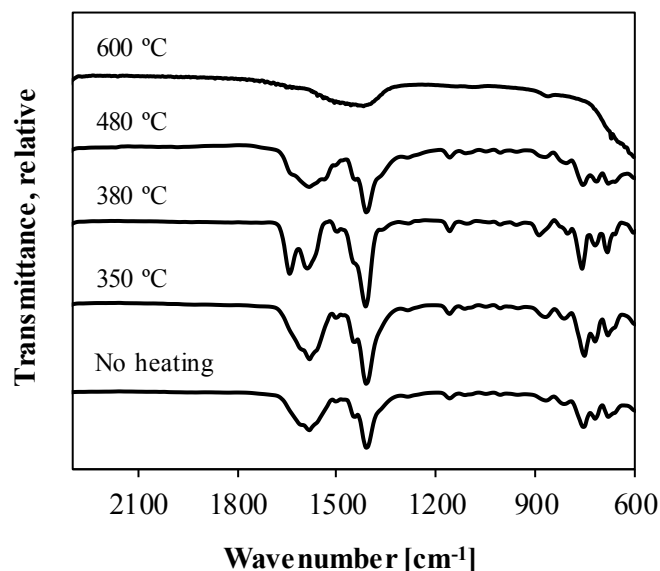
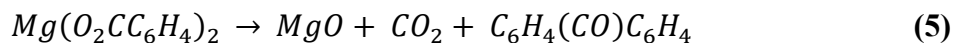


Figure 7.13. Infrared spectra of the solid residue obtained after DSC analysis of the magnesium biphenyl-2,2'-dicarboxylate

Compared to sodium or potassium carboxylates, the magnesium carboxylate was even more thermally stable. Considering that the efficiency of decarboxylation is related to the stability of the metal carboxylate, with less stable carboxylates leading to decarboxylation [4], it is clear that a magnesium based catalyst would not be a promising option to enhance the ring-opening process.

It has been reported that the decomposition of magnesium acetate tetrahydrate yields magnesium oxide as the major inorganic product [10]. It was anticipated that magnesium (II) biphenyl-2,2'-dicarboxylate would decompose to produce the same oxide, carbon dioxide and fluorenone according to Eq. (5).



The mass loss for decomposition of the magnesium carboxylate to yield MgO was calculated and corresponded well with the experimental data (Table 7.6). A difference of about 5% between the value experimentally obtained and the calculated one was observed. This difference may be related to the nature of the solid residue. XRD analysis of the solid residue obtained after heating the magnesium biphenyl-2,2'-dicarboxylate to 600 °C was not conclusive. It seemed that the solid formed after reaction was not crystalline enough to be identified as magnesium oxide by this technique. On the other hand, the infrared spectrum of the product of decomposition was measured and compared with the spectrum of a commercially available sample of MgO. Even though, the magnesium oxide does not absorb in the infrared region, the solid product of decomposition did showed a weak absorption occurring at 860 cm⁻¹ and abroad band consisting of two partially overlapped peaks absorbing at 1485 and 1427 cm⁻¹. These vibrations are characteristic of magnesium carbonate species [20].

It is speculated that the solid product of decomposition consisted of a mixture of magnesium carbonate and magnesium oxide. Formation and further decomposition of the magnesium carbonate to give magnesium oxide and carbon dioxide are plausible. The exothermic process taking place around 359 °C (transition *iii* in Figure 7.12) could be related to the decomposition of the magnesium carbonate, which has been reported to occur at >350 °C [24][25]. Production of CO₂ in this temperature range was confirmed by infrared analysis. The difference in the calculated mass loss for decomposition of the magnesium carboxylate and the value obtained by TGA can be related to the fact that magnesium carbonate was not included as part of the reaction products to perform the calculations.

Opposite to the behavior of the alkali metal carboxylates, further heating of the magnesium carboxylate to 900 °C did not revealed additional thermal events. No decomposition of the inorganic residue was observed.

7.3.6 Thermal Stability of Alkali and Alkaline Earth Biphenyl Metal Carboxylates

Thermal analysis revealed a complex and different thermal behavior between metal carboxylates. For the sodium and potassium biphenyl-2,2'-dicarboxylates, a number of

transitions occurring along the temperature range 25–550 °C were observed. Lots of very small and convoluted peaks were detected close to and during decomposition. This behavior, which in part may be attributed to the existence of the carboxylates in different polymorphic forms, was particular of the carboxylates of alkali metals, and it was not observed with the alkaline earth compound. An interesting difference regarding the thermal behavior of the sodium and potassium carboxylates is endothermic and exothermic character of the decomposition process, respectively. The cause of this difference was not elucidated in this work.

Sodium, potassium and magnesium formed thermally stable carboxylates with decomposition temperatures above 400 °C. Thermal stability depended on the metal and increased in the order alkali < alkaline earth metal carboxylates. Furthermore, sodium and potassium carboxylates decomposed to give carbonate or bicarbonate species; whereas, the magnesium carboxylate decomposed to initially form magnesium carbonate and then magnesium oxide. In all cases, production of a symmetric ketone, fluorenone, as part of the reaction products was plausible.

On the other hand, infrared spectroscopy indicated some differences in the mode of bonding depending on the metal. Sodium and potassium carboxylates existed in only one dominant configuration, likely an ionic type of interaction. Heating of the potassium carboxylate to about 170 °C resulted in splitting of the antisymmetric carboxylate stretch suggesting a partial change in the mode of bonding to a possibly a monodentate type of structure. For the magnesium carboxylate, ionic and bidentate structures are probable.

7.3.7 Generalization of Metal Carboxylates Decomposition Results

The thermal behavior of alkali metal carboxylates has been the subject of considerable research work. The phase transitions for the different alkali n-alkanoates, in the range C₁–C₂₀, have been determined using a number of analytical techniques [7]. Decomposition of lithium and potassium n-alkanoates has also been systematically studied [18][19]. In contrast, the thermal behavior of alkaline earth carboxylates has been investigated less frequently, and the available data is a bit more scattered [7][10].

Lithium, sodium, and potassium alkanoates exhibit a similar thermal behavior. The melting point of the C₁–C₄ members of the series increases with the increase in the length of the carboxylate chain; then, it stabilizes and does not change significantly for the remaining members of the series [7]. The same behavior has been observed for the temperature of decomposition of potassium and lithium alkanoates [18][19]. Moreover, when comparing the melting point or the temperature of decomposition for the Li-, Na- and K-alkanoates, it can be seen that Li- carboxylates display lower values, while Na- and K-carboxylates behave in a more similar way [7][18][19]. On the other hand, the thermal decomposition of a number of metal carboxylates indicated that thermal stability decreases in the order Na > Ca > Fe > Mn [10]. In other words, depending on the nature of the metal, the thermal stability of metal carboxylates decreases as follows: alkali > alkaline earth > transition metal carboxylates.

The findings of this work partially match with the behavior reported for other alkali and alkaline earth metal carboxylates. As in the case of the Na- and K-alkanoates, the thermal behavior of the sodium and potassium biphenyl dicarboxylates is quite similar and they decompose at very close temperatures (444.6 ± 0.1 and 440.5 ± 0.1 °C, respectively). However, these alkali metal carboxylates are less thermally stable than the magnesium biphenyl dicarboxylate, which decomposes at 471.1 ± 0.6 °C. Thus, biphenyl dicarboxylates do not follow the order of thermal stability mentioned above and the behavior of metal n-alkanoates cannot reliably be used to predict the stability of metal biphenyl dicarboxylates.

7.4 Conclusions

The thermochemistry of sodium, potassium and magnesium biphenyl metal carboxylates was investigated in order to evaluate the suitability of these metals as potential catalysts for decarboxylation. The main conclusions and observations were as follows:

- (a) The infrared spectra of the sodium and potassium carboxylates indicated only one dominant configuration, most likely an ionic type of interaction. Conversely, the infrared spectrum of the magnesium carboxylate suggested more than one type of carboxylate bonding: ionic (or bridging), and bidentate types of interactions are probable.

- (b) Sodium, potassium and magnesium formed thermally stable biphenyl metal carboxylates which decomposed at 443.3 ± 2.9 , 440.4 ± 0.5 and 470.2 ± 0.9 °C, respectively.
- (c) A series of small, convoluted, endothermic and exothermic transitions occurring close to and during decomposition were observed in the case of the alkali metal carboxylates. Rearrangements in the carboxylates structure are possible.
- (d) Formation of formic acid as a low temperature decomposition product for the sodium biphenyl-2,2'-dicarboxylate was confirmed by infrared spectroscopy. Production of this acid could be explained by ring-closure reaction through the formation of an ester, which is an undesirable side-reaction.
- (e) Infrared analysis showed that heating of the potassiumbiphenyl-2,2'-dicarboxylate to about 300 °C affected the antisymmetric stretching of a carboxylate group. Splitting of the $\nu_{as}(C=O)$ suggests a change in the mode of bonding to a monodentate type of structure.
- (f) Sodium and potassium biphenyl-2,2'-dicarboxylates decomposed through a ketonization reaction to produce carbonates and bicarbonate species. Formation of these compounds was confirmed by FTIR. It is speculated that the magnesium biphenyl-2,2'-dicarboxylate decomposed to give a mixture containing at least some magnesium carbonate and magnesium oxide.
- (g) The thermal behavior of metal *n*-alkanoates cannot reliably be used to predict the stability of metal biphenyl dicarboxylates.

7.5 References

- [1] Le Page, J.F.; Chatila, S.G.; Davidson, M. *Resid and heavy oil processing*; Editions Technip: Paris, 1992.
- [2] Montoya Sánchez, N.; De Klerk, A. Oxidative ring-opening over metal oxides. *Prepr. Pap.-Am. Chem. Soc., Div. Energy Fuels* **2014**, 59 (2), 558-561.
- [3] Montoya Sánchez, N.; De Klerk, A. Oxidative ring-opening of aromatics: Decomposition of biphenyl carboxylic acids and zinc biphenyl carboxylates. *Energy Fuels* **2015**, 29, 7910-7922.
- [4] Mars, P.; Scholten, J.J.F.; Zwietering, P. The catalytic decomposition of formic acid. *Adv. Catal.* **1693**, 14, 35-113.
- [5] Hattori, H. Catalysis by alkaline earth metal oxides. *Stud. Surf. Sci. Catal.* **1985**, 21, 319-330.
- [6] Pines, H.; Stalick, W.M. *Base-catalyzed reactions of hydrocarbons and related compounds*; Academic Press: New York, 1977.
- [7] *Thermodynamic and transport properties of organic salts*. Franzosini, P., Sanesi, M., Eds.; IUPAC Chemical Data Series 28; Pergamon Press: Oxford, 1980.
- [8] Franzosini, P.; Westrum Jr, E.F.; Plautz, W.A. Thermophysics of metal alkanoates II. Heat capacities and thermodynamic properties of sodium propanoate. *J. Chem. Thermodynamics* **1983**, 15, 609-618.
- [9] Franzosini, P.; Westrum Jr, E.F. Thermophysics of metal alkanoates III. Heat capacities and thermodynamic properties of lithium and potassium propanoates. *J. Chem. Thermodynamics*, **1984**, 16, 81-90.
- [10] Mehrotra, R.C.; Bohra, R. *Metal carboxylates*. Academic Press: New York, 1983.
- [11] Höhne, G.W.H.; Hemminger, W.F.; Flammersheim, H.-J. *Differential scanning calorimetry*. 2ed, Springer: Berlin, 2003.
- [12] Silverstein, R.M.; Bassler, G.C.; Morrill, T.C. *Spectrometric identification of organic compounds*, 4ed; John Wiley: New York, 1981.
- [13] Nakamoto, K. *Infrared and Raman spectra of inorganic coordination compounds Part B*, 6ed; Wiley: Hoboken, NJ, 2009.

- [14] Bonner, L.; Hofstadter, R. Vibration Spectra and Molecular Structure IV. The Infra-Red Absorption Spectra of the Double and Single Molecules of Formic Acid. *J. Chem. Phys.* **1938**, 6, 531- 534.
- [15] Chapman, D. The Infrared Spectra of Liquid and Solid Formic acid. *J.Chem. Soc.* **1956**, 48, 225-229.
- [16] Colthup, N. B.; Daly, L. H.; Wiberley, S. E. *Introduction to infrared and Raman spectroscopy*, 3ed; Academic Press: Boston, 1990. pp. 290, 315.
- [17] Szymanski, H. A.; Erickson, R. E. *Infrared band handbook. Vol.2. 999-29 cm⁻¹*, 2ed; IFI/Plenum: New York, 1970.
- [18] Huong Bui, L.; De Klerk, A. Lithium C₁-C₁₂ n-Alkanoates: Thermal Behavior from -30°C to 600°C. *J. Chem. Eng. Data* **2013**, 58, 1039-1049.
- [19] Huong Bui, L.; De Klerk, A. Thermal behavior of potassium C₁-C₁₂ n-alkanoates and its relevance to Fisher-Tropsch. *J. Chem. Eng. Data* **2014**, 59, 400-411.
- [20] Miller, F.A.; Wilkins, C.H. Infrared Spectra and Characteristic Frequencies of Inorganic Ions. *Anal. Chem.* **1952**, 24, 1253-1294.
- [21] Tosh, J.S.; Field, J.H.; Benson, H.E.; Haynes, W.P. *Equilibrium study of the system potassium carbonate, potassium bicarbonate, carbon dioxide, and water*; U.S. Dept. of the Interior, Bureau of Mines: Washington, 1959.
- [22] Rousseau, R.W.; Ferrell, J. K.; Staton, J. S. Conditioning coal gas with aqueous solutions of potassium carbonate: Model development and testing. *Gas Sep. Purif.* **1987**, 1, 44-54.
- [23] Ning, Y.C. *Interpretation of Organic Spectra*. John Wiley & Sons: Singapore, 2011.
- [24] Unluer, C.; Al-Tabbaa, A. Characterization of light and heavy hydrated magnesium carbonates using thermal analysis. *J. Therm. Anal. Calorim.* **2014**, 115, 595-607.
- [25] Liidakis, S.; Tsoukala, M. Environmental benefits of using magnesium carbonate minerals as new wildfire retardants instead of commercially available, phosphate-based compounds. *Environ Geochem Health*, **2010**, 32, 391-399.

8. Oxidative Ring-Opening of Aromatics: Thermochemistry of Iron, Copper and Cobalt Biphenyl Carboxylates ¹

ABSTRACT

Thermochemistry of aromatic carboxylates has received little attention in the literature, despite their relevance as intermediates in the oxidative ring-opening of aromatic compounds. The thermal behavior of selected transition metal aromatic carboxylates was studied as a way to determine the effectiveness of the metals as potential catalysts for decarboxylation. Iron, cobalt, and copper salts of biphenyl carboxylic acids were synthesized and their thermal behavior over the temperature range 25 to 600 °C was investigated. Characterization of these compounds indicated that, with exception of the copper (II) biphenyl-2-carboxylate, all metal carboxylates corresponded to homogeneous materials of different morphology. Structures in which metals might be present in more than one oxidation state or forming metal-metal bonds are possible. Infrared spectroscopy showed that all synthesized carboxylates existed in bridging configuration. In all cases, thermal analysis revealed a complicated behavior. Decomposition occurred as a multistage process and exhibited a rather complex mechanism. The decomposition of the iron and copper carboxylates resembled a cascade of reactions, i.e., the individual decomposition steps could not be resolved due to overlapping; whereas, the decomposition of the cobalt compounds followed a more stepwise type of process, i.e., the individual decomposition steps could be differentiated. Aromatic carboxylates of moderate thermal stability, with decomposition temperatures above 240 °C, were formed. Thermal stability depended on the metal and increased in the order $\text{Cu} < \text{Fe} < \text{Co}$. Production of benzoic acid during the decomposition of the copper carboxylates was observed. Production of fluorenone suggested that the Fe, Co and Cu carboxylates decomposed, at least partially, via the formation of an organic ketone and metal oxides. In the case of the copper carboxylates, the reduction of the copper by forming cuprous oxide (Cu_2O) also took place.

Keywords: Transition metals, metal carboxylates, thermal analysis, thermal decomposition, decarboxylation.

¹ Reprinted with permission from Montoya Sánchez, N.; De Klerk, A. Oxidative ring-opening of aromatics: Thermochemistry of iron, copper and cobalt biphenyl carboxylates. *Thermochim. Acta* 2018, 645, 31-42. Copyright 2018 Elsevier. <https://doi.org/10.1016/j.tca.2018.01.015>.

8.1 Introduction

Oxidative ring-opening has been explored as an alternative approach for the upgrading of heavy aromatic materials such as heavy oils, bitumens, asphalts, and coal liquids [1][2]. The overall oxidative ring-opening process involves three reaction steps: (1) oxidation of multinuclear aromatics to produce quinonoids, (2) further oxidation to form ring-opened carboxylic acids, and (3) decarboxylation to remove carboxylic acids as CO₂. During the latter step, decarboxylation competes with side-reactions, such as ketonization and dehydration, which decreases the selectivity of the reaction towards ring-opened products [2]. The use of a catalyst to favor decarboxylation is necessary.

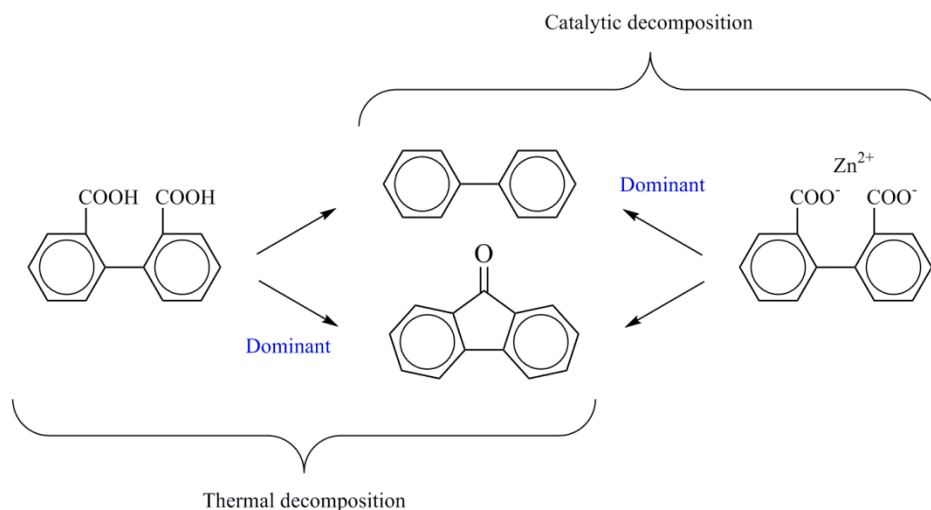


Figure 8.1. Dominant decomposition pathways of biphenyl-2,2'-dicarboxylic acid and zinc biphenyl-2,2'-dicarboxylate at around 380 °C

It has been demonstrated that metal carboxylates can be used as surrogates for the reaction of carboxylic acids over heterogeneous catalysts when investigating their catalytic decomposition [3]. This characteristic found particular application in the study of the decomposition of biphenyl carboxylic acids, which are products of the oxidative ring-opening of phenanthrene. Specifically, decomposition of zinc biphenyl carboxylates indicated that when zinc facilitated the reaction, the selectivity towards the ring-opened product, *biphenyl*, always

exceeded the selectivity towards the ring-closed product, *fluorenone* [2]. In other words, catalytic decomposition, as opposed to thermal decomposition, increased the selectivity to ring-opened products by favoring decarboxylation (Figure 8.1).

The study of zinc biphenyl carboxylates [2] highlighted the potential selectivity benefit of catalytic carboxylic acid decomposition over thermal decomposition. It also suggested that the temperature and chemistry of aromatic carboxylic acid decomposition may change depending on the metal used during the reaction. Unfortunately, there was little data in the literature about the thermal behavior and thermal stability of aromatic carboxylates that could help to predict which materials would be good candidates for carboxylic acid decomposition.

The use of alkali and alkaline earth metals for carboxylic acid decomposition was explored [4]. Thus, the thermochemistry of biphenyl-2,2'-dicarboxylates of sodium, potassium, and magnesium was investigated [4]. It was found that the strong basic properties of alkali and alkaline earth metals resulted in the formation of thermally stable carboxylates with decomposition temperatures above 400 °C. Although catalytic decomposition at such high temperatures does not preclude consideration of these materials as catalysts, it is likely that catalytic and thermal decomposition would occur in parallel, with an associated loss in selectivity to ring-opened products (e.g. biphenyl). As a result, metal carboxylates with lower decomposition temperatures to limit the contribution of thermal decomposition during catalytic decomposition were sought.

Unfortunately, there is again little information in literature on the thermochemistry of transition metal carboxylates, even for the alkanoates [5]. A couple of relevant studies are found in *this journal* [6][7][8][9][10][11]. Transition metals generally form carboxylates with lower decomposition temperatures than the corresponding carboxylates of alkali and alkaline earth metals. Thus, transition metals could be more promising candidates as decomposition catalysts.

In this study, the thermochemistry of selected transition metals biphenyl carboxylates is investigated. Iron, cobalt, and copper biphenyl-2,2'-dicarboxylates, as well as cobalt and copper biphenyl-2-carboxylates were synthesized and their thermal behavior studied. Determining the

thermochemistry of iron, copper and cobalt biphenyl carboxylates is the first step towards elucidating their decomposition reaction network by reactor studies.

8.2 Experimental Section

8.2.1 Materials

Table 8.1. Chemicals employed in this study

Compound	Formula	CASRN ^a	Mass fraction purity ^b	Supplier
Biphenyl-2,2'-dicarboxylic acid	C ₁₄ H ₁₀ O ₄	482-05-3	0.97	Sigma-Aldrich
Biphenyl-2-carboxylic acid	C ₁₃ H ₁₀ O ₂	947-84-2	0.97	Sigma-Aldrich
Metallic Iron	Fe	7439-89-6	0.99998	Alfa Aesar
Cobalt hydroxide	Co(OH) ₂	21041-93-0	0.95	Sigma-Aldrich
Copper hydroxide	Cu(OH) ₂	20427-59-2	0.57 ^c	Sigma-Aldrich
Copper (II) carbonate basic	CuCO ₃ ·Cu(OH) ₂	12069-69-1	0.57 ^c	Sigma-Aldrich
Ethanol	C ₂ H ₆ O	64-17-5	0.998	Fisher Scientific
Tetrahydrofuran	C ₄ H ₈ O	109-99-9	0.999	Fisher Scientific
Acetone	C ₃ H ₆ O	67-64-1	0.997	Fisher Scientific
Indium	In	7440-74-6	0.99999	Impag AG
Nitrogen	N ₂	7727-37-9	0.99999 ^d	Praxair
Argon	Ar	7440-37-1	0.99999 ^d	Praxair
Hydrochloric Acid	HCl	7647-01-0	^e	Ricca Chemical Company

^a CASRN: Chemical Abstracts Services Registry Number.

^b Purity of the material guaranteed by the supplier.

^c Reported as copper (II) content.

^d Mole fraction purity.

^e Hydrochloric acid solution (0.05 N).

Iron, cobalt, and copper salts of biphenyl carboxylic acids were synthesized from commercially available materials. Chemicals, calibration materials and gases used for the synthesis and the thermal analysis are listed in (Table 8.1).

8.2.2 Synthesis of Metal Carboxylates

Metal carboxylates were prepared by neutralization according to the general synthesis procedure for reaction in non-aqueous media described by Mehrotra and Bohra [12]. The corresponding metallic element or an appropriate metal-containing compound, such as hydroxide or carbonate, was mixed with a slight excess (2% molar excess) of the carboxylic acid. In this study, biphenyl-2-carboxylic acid and biphenyl-2,2'-dicarboxylic were used.

Synthesis of the iron carboxylate employed direct reaction of metallic iron and the corresponding carboxylic acid. Tetrahydrofuran was used as solvent. Synthesis of the cobalt and copper salts used ethanol as solvent, and the corresponding hydroxides as the metal-containing material. In the case of the copper biphenyl-2-carboxylate, the synthesis was carried out using both copper hydroxide and copper (II) carbonate basic. The estimated purity of the metal carboxylate obtained using the latter compound was higher, and so, it was used to perform all subsequent experimental work. In all cases, the reaction mixture was heated at 60 °C, under total reflux, and stirred for several hours until completion of the reaction. Metal carboxylates were recovered by evaporation of the solvent at reduced pressure conditions (80 kPa, absolute), using a rotary evaporator (Heidolph, Model Hei-VAP Precision with Glassware Set G3). The iron biphenyl-2-carboxylate could not be obtained under the experimental conditions employed; therefore, it is not part of the present study.

After recovery, all synthesized metal carboxylates were thoroughly washed with acetone, and then dried at approximately 100 °C until they reached constant mass. The final solid products were finely ground and stored in a desiccator.

8.2.3 Equipment and Procedure

8.2.3.1 Characterization of Metal Carboxylates

Synthesized biphenyl transition metal carboxylates were characterized. Infrared (IR) spectroscopy was used to confirm that the carboxylic acid used in the synthesis was converted into the carboxylate. Scanning electron microscopy with microanalysis by energy dispersive X-ray spectroscopy (SEM-EDS) was used to assess homogeneity and check for inorganic impurities. Elemental analysis and inductively coupled plasma optical emission spectrometry (ICP-OES) were employed to determine the metal content.

Infrared spectroscopy was employed to confirm the synthesis of the metal carboxylates. It was performed with an ABB MB3000 Fourier transform infrared spectrometer equipped with a Pike MIRacle Reflection attenuated total reflectance (ATR) diamond crystal plate and pressure clamp. The spectra were collected with Horizon MBTM FTIR Software, at a resolution of 4 cm⁻¹, using an average of 120 scans over the spectral region 4000-500 cm⁻¹.

Infrared spectroscopy was also used to estimate the amount of unreacted carboxylic acid that remained as an impurity in the metal carboxylates. Selected samples of the metal carboxylates were spiked with a known amount of the corresponding parent carboxylic acid. The IR spectra of these samples were collected and further processed to extract the semi-quantitative information that allowed for building the calibration curves (see [APPENDIX C](#)). Because the path length of light through the medium could not be fixed in the available spectrometer, the C-H bending vibrations observed in the region 1000-1300 cm⁻¹, which are typical of aromatic compounds, were used as internal standard. The IR spectra were scaled so that the peak at ~1008 cm⁻¹ had the same height relative to the baseline for all of the samples, i.e. the spectra were multiplied by a factor that made the height of this peak to be the same in the IR spectra of the parent carboxylic acid acids and the corresponding spiked samples of metal carboxylates. The relative peak height of the carbonyl vibration (C=O) in each sample was correlated with the amount of acid present, which was the main organic impurity that could affect the thermochemistry.

Scanning electron microscopy was used to investigate the morphology and homogeneity of the synthesized materials. A Zeiss Sigma Field Emission - Scanning Electron Microscope (Zeiss Sigma 300 VP-FESEM), equipped with secondary and backscattered electron detectors, as well as an in-lens electron detector, a cathodoluminescence (CL) detector and a Bruker energy dispersive X-ray spectroscopy (EDS) system was employed for this purpose. SEM micrographs were processed in ImageJ to quantify impurities. The corresponding image was converted to 8-bit TIFF and binarized employing a user-selected threshold. The number of positive and negative pixels was counted and proportions were calculated using the total amount of pixels in the original micrograph.

Elemental analysis of the metal biphenyl carboxylates was performed using a Carlo Erba Model EA1108 Elemental Analyzer for CHNS and Oxygen (Triad Scientific, Inc., Manasquan, NJ, USA). Analyses were carried out in duplicate. In addition, the metal content of the synthesized compounds was estimated by: (1) difference from elemental analysis results, (2) thermogravimetric analysis and (3) inductively coupled plasma optical emission spectrometry (ICP-OES).

Thermogravimetric analysis was performed with a Mettler Toledo TGA/DSC1 system, equipped with a LF 1100 furnace, a sample robot and a MX5 internal microbalance (5 g capacity and 1 μg readability). Experiments were conducted under air atmosphere at a constant flow rate of 100 $\text{mL}\cdot\text{min}^{-1}$. Samples of about 20 mg in size were prepared and placed in standard 70 μL alumina (Al_2O_3) crucibles. They were heated from 25 $^\circ\text{C}$ to 900 $^\circ\text{C}$ at a rate of 10 $^\circ\text{C}\cdot\text{min}^{-1}$, and then kept at 900 $^\circ\text{C}$ for two hours. Experiments were performed in triplicate. The nature of the inorganic residue (metal oxides) was confirmed by XRD analysis (see [Section 8.2.3.2](#)). The amount of metal in the synthesized compounds was calculated from the amount of metal oxide left after decomposition.

Acid treatment of the synthesized metal carboxylates was carried out prior to ICP-OES analysis. Samples of about 100 mg were mixed with a 50% molar excess of hydrochloric acid (0.05 N). The mixture was heated at 80 $^\circ\text{C}$, under total reflux, and stirred for about 5 hours until completion of the reaction. In each case, the metal element was recovered in the form of a

dissolved chloride in aqueous solution. Solutions were analyzed for metal content using an Agilent 5100 ICP-OES, with radial view configuration and equipped with a SPS-3 autosampler, an easy-fit torch, a SeaSpray nebulizer and a double-pass spray chamber. Samples were analyzed for iron, copper and cobalt; detection wavelengths were 238.204 nm, 327.395 nm, and 238.892 nm, respectively. Analyses were performed using plasma, carrier and coolant argon flow rates of 12 L·min⁻¹, 0.7 L·min⁻¹, 1.0 L·min⁻¹, respectively. Delay and read times were set at 26 s and 5 s, respectively. Each sample was measured in triplicate.

8.2.3.2 Thermal Analysis

Thermal behavior of the transition metal biphenyl carboxylates was investigated using differential scanning calorimetry (DSC) and thermogravimetric analysis (TGA). Infrared (IR) spectroscopy and X-ray diffraction (XRD) analysis assisted with the interpretation of the experimental data. The analytical approach was similar to that in a previous study [4] and it is repeated for ease of reference.

Differential scanning calorimetry was performed using a Mettler Toledo DSC 1. This heat flux calorimeter (disc-type) is equipped with FRS-5 sensor and Haake intracooler. The temperature range covered during analysis was 25 to 550 °C. In all cases a constant heating rate of 10 °C·min⁻¹ was employed. Experiments were conducted under nitrogen atmosphere. The sheathing and sample chamber nitrogen flow rates were kept constant at 100 mL·min⁻¹. Reversibility of the thermal events was verified by heating the sample just beyond the observed transition, then cooling it down and heating it again. Infrared spectroscopy was employed to monitor the changes in the nature of the solid residue left after heating the metal carboxylates to the different thermal events. Temperature and heat flow measurements were checked against an indium (In) standard and were within the specifications of the instrument. All experiments were performed in triplicate. Samples were prepared in standard 40 µL aluminum (Al) crucibles with domed aluminum lids. A single small hole was made in the lids before cold-welding the lid to the crucible by using a crucible sealing press. Samples were weighed on an analytical balance, Mettler Toledo, Model XS105, with 10 µg readability and capacity of 105 g. Sample sizes for DSC analysis were kept between 6 to 12 mg.

Visual observation of the phase transitions was conducted using an Olympus BX51 microscope and Mettler FP84HT TA Microscopy Cell (DTA/DSC sensor) with FP90 central processor. Samples of the synthesized metal carboxylates were placed in transparent glass crucibles and covered with glass covers. Crucibles and covers of 7 mm in diameter were used. Samples were heated in the temperature range 25 to 375 °C using a constant heating rate of 10 °C·min⁻¹.

Thermogravimetric analysis was performed in the Mettler Toledo TGA/DSC1 system described in [Section 8.2.3.1](#). Experiments were conducted under inert atmosphere by maintaining a nitrogen flow rate of at least 20 mL·min⁻¹. Samples of about 10 mg in size were prepared and placed in standard 70 µL alumina crucibles. The temperature range covered during analysis was 25 to 600 °C by using a heating rate of 10 °C·min⁻¹. Experiments were performed in triplicate.

The thermogravimetric analyzer was coupled with a Fourier transform infrared spectrometer in order to determine the nature of the gases produced during thermal analysis. Analysis of the gases evolved during thermal analysis was carried out in a heated gas flow cell from Pike Technologies (Model 162-20300) with a cell volume of 38.5 mL and 100 mm pathlength. The gases from the thermogravimetric analyzer were transfer to the flow cell using a line kept at 200 °C. The spectra of the gases were collected at a resolution of 4 cm⁻¹ over the spectral region of 4000-500 cm⁻¹. In reality, the non-instantaneous nature of the infrared analysis affected the way in which the experimental data had to be interpreted. The collected spectra reflect changes in the nature of the gases evolved over a temperature range and not a single temperature. According to the operating conditions of this study the infrared analysis took ~1 min to complete, which corresponds to a temperature range of 10 °C during thermal analysis.

Solid residues obtained after thermal analysis of the synthesized metal carboxylates were analyzed by X-ray diffraction. The diffractometer (Rigaku Ultima IV) was equipped with a cobalt tube (38 kV, 38 mA) and a D/Tex detector with Fe filter. Also, a silicon sample holder was employed. Samples were analyzed from 5 to 90 degrees on continuous scan, at a speed of 2.0 degrees 2-theta per minute, with a step size of 0.02 degrees. The experimental data was processed using JADE 9.5 software.

8.2.4 Calculations

Thermal analysis of the synthesized carboxylates resulted in the determination of the onset and endset temperatures, mass loss and enthalpy involved in the different thermal events. Results from TGA and DSC analysis are reported using the format in $x \pm s$, where x is the average of analyses in at least triplicate and s refers to one sample standard deviation.

8.3 Results and discussion

8.3.1 Characterization of Metal Carboxylates

8.3.1.1 Infrared Spectroscopy

Infrared spectroscopy is a well-known and widely used technique to elucidate structural features of metal carboxylates. In this study, it was employed to confirm the synthesis of the biphenyl transition metal carboxylates and to elucidate the nature of the carboxylate and metal bonding. It also helped to estimate the amount of unreacted carboxylic acids that remained as an impurity in the metal carboxylates.

8.3.1.1.1 Synthesis of Metal Carboxylates

Infrared spectroscopy confirmed the chemical identity of the synthesized metal carboxylates. The observed characteristic symmetric, $\nu_s(\text{CO}_2)^-$, and asymmetric, $\nu_{as}(\text{CO}_2)^-$, stretching bands are listed in [Table 8.2](#). Similarly, the infrared spectra of the synthesized metal carboxylates as well as the spectra of the parent carboxylic acids are presented in [Figure 8.2](#).

Spectroscopic studies of a number of carboxylic acids have shown that the carboxyl group displays five characteristic absorptions, and among those, the C=O stretching band at $\sim 1700 \text{ cm}^{-1}$ and O-H stretching vibrations in the $\sim 3300\text{-}2500 \text{ cm}^{-1}$ region are considered the most important ones. [Figure 8.2](#) shows that for all synthesized compounds the strong absorption bands of the carbonyl group, $\nu_{as}(\text{C}=\text{O})$, of the biphenyl-2,2'-dicarboxylic acid and the biphenyl-2-carboxylic

acid at 1674 and 1681 cm^{-1} , respectively, as well as O-H stretching vibrations occurring at $\sim 3300\text{-}2500\text{ cm}^{-1}$ disappeared and were replaced with the characteristic carboxylate vibrations.

Table 8.2. Strong carboxylate stretching vibrations in the infrared spectra of the synthesized metal carboxylates

Metal	Carboxylate stretching vibrations, [cm^{-1}]		$\Delta\nu$, [cm^{-1}] ^a		
	Asymmetric, $\nu_{\text{as}}(\text{CO}_2^-)$	Symmetric, $\nu_{\text{s}}(\text{CO}_2^-)$	Standard	Alternate	
Metal carboxylate = Biphenyl-2,2'-dicarboxylates					
Iron	1573 ^b	1523	1396	177	127
Copper	1589 ^b	1542	1396	193	146
Cobalt	1575	1533 ^b	1394	139	181
Metal carboxylate = Biphenyl-2-carboxylates					
Copper	1589 ^b	1541 ^c	1396	193	145
Cobalt	1587	1552 ^b	1396	156	191

^a $\Delta\nu = \nu_{\text{as}}(\text{CO}_2^-) - \nu_{\text{s}}(\text{CO}_2^-)$.

^b Characteristic carboxylate stretch exhibiting the strongest intensity and used to calculate the standard $\Delta\nu$.

^c Absorption band observed as a very small shoulder.

The shape and relative intensity of the characteristic carboxylate stretching bands were different between the synthesized metal carboxylates. A single very strong band at $\sim 1396\text{ cm}^{-1}$ describes the symmetric stretch; whereas, a weaker split band, located in the region $1589\text{-}1523\text{ cm}^{-1}$ of the spectra represented the asymmetric stretch in all cases. The splitting of the bands indicated that nonsymmetrical structures exhibiting more than one type of bonding mode are possible for this group of compounds [12].

A slight increase in the frequency of the asymmetric stretch was observed when the size of the transition metal atom increased. The separation of the characteristic bands ($\Delta\nu$) went from 127 cm^{-1} to 139 cm^{-1} , and then to 146 cm^{-1} in the order iron, cobalt, and copper biphenyl dicarboxylates. The same behavior was observed in the case of the cobalt and copper salts of the biphenyl monocarboxylic acid.

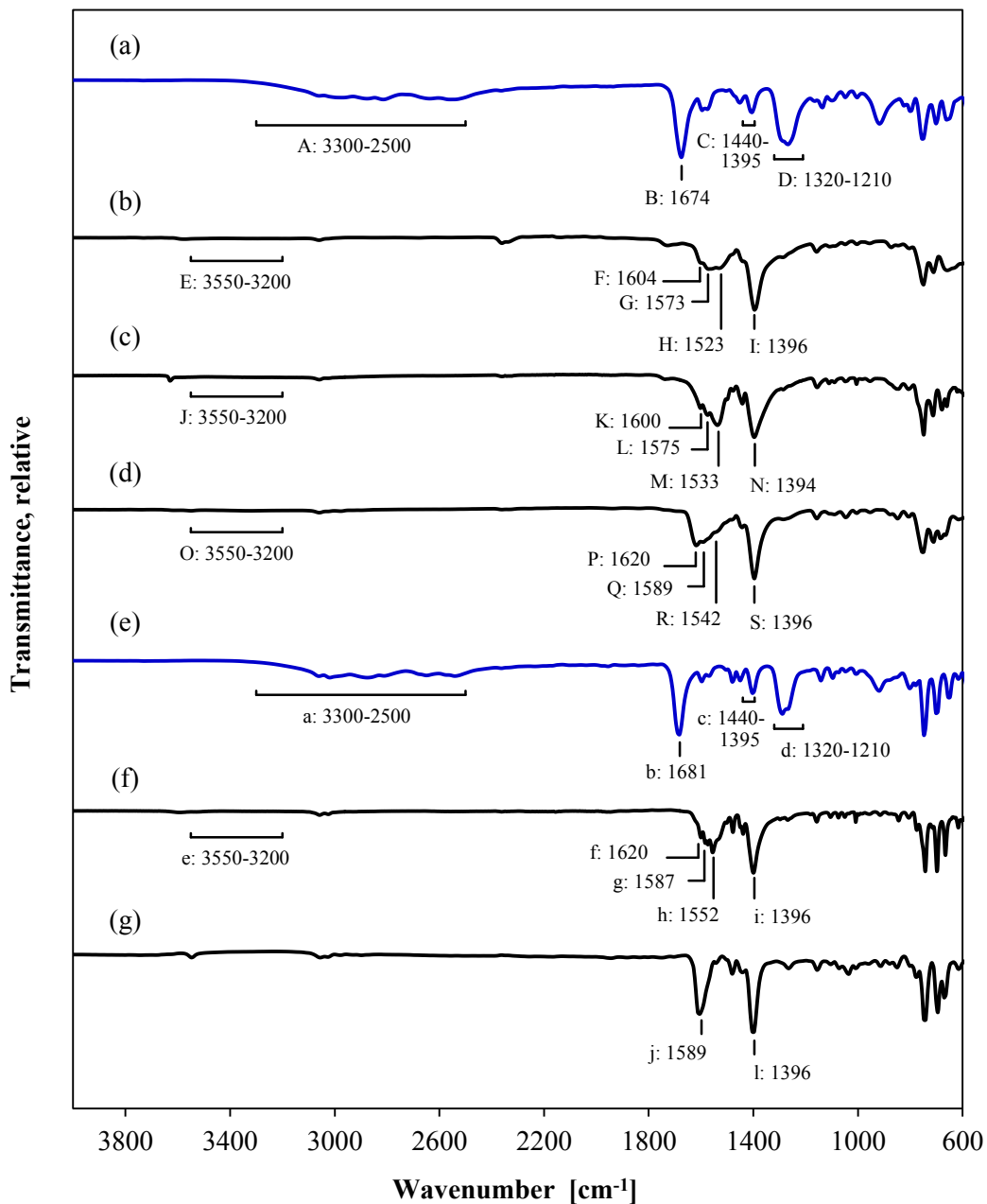


Figure 8.2. Infrared spectra of (a) biphenyl-2,2'-dicarboxylic acid, (b) iron, (c) cobalt, (d) and copper biphenyl-2,2'-dicarboxylates, (e) biphenyl-2-carboxylic acid, (f) cobalt, and (g) copper biphenyl-2-carboxylates. A, a: O–H stretching; B, b: $\nu_{as}(\text{C}=\text{O})$ stretching; C, c: O–H bending; D, d: C–O stretching; E, J, O, e: OH stretching for lattice water; F, K, P, f: HOH bending for lattice water; G, H, L, M, Q, R, g, h, j, k: $\nu_{as}(\text{CO}_2^-)$ stretching; I, N, S, i, l: $\nu_s(\text{CO}_2^-)$ stretching

The presence of lattice water in the crystalline structure of the synthesized metal carboxylates was investigated. Results from infrared analysis were inconclusive. Bands of moderate to weak intensity displaying the characteristic HOH bending around 1630-1600 cm^{-1} were observed in all cases, except for the copper biphenyl-2-carboxylate. However, the corresponding antisymmetric and symmetric -OH stretching in the region 3550-3200 cm^{-1} [13] was not evident. Results from TGA-FTIR analysis showed that water was present in the carboxylates structure (see Section 8.3.2).

Note that the two small absorption bands occurring around 2340 cm^{-1} in the spectrum of the iron biphenyl-2,2'-dicarboxylate are not due to the compound but are attributed to some background CO_2 concentration at the time of recording the spectrum.

8.3.1.1.2 Nature of the Carboxylate Bonding

Carboxylate ions can coordinate to a metal in four different configurations (Figure 8.3). Ionic or uncoordinated structures, typical of highly electropositive elements, exhibit resonance between the two C-O bonds of the carboxylate anion. On the other hand, monodentate structures use only one of the oxygen atoms from the carboxylate moiety to attach to the metal, whereas bridging and bidentate complexes use both oxygen atoms for bonding [12][13]. Complexes with bridging configuration are common, particularly for carboxylates of transition metals. Conversely, bidentate structures are unusual because that is the least favored mode of bonding [12].

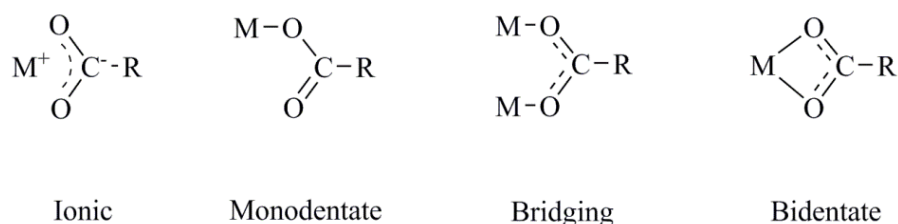


Figure 8.3. Bonding configurations for metal carboxylates

The work of Nakamoto [13] showed that it is possible to infer the nature of the carboxylate bonding according to the wavenumber difference, $\Delta\nu$, between the asymmetric, $\nu_{\text{as}}(\text{CO}_2^-)$, and symmetric, $\nu_{\text{s}}(\text{CO}_2^-)$, stretchings of a carboxylate (Eq. 1). The $\Delta\nu$ value for ionic and bridging configurations is close, and therefore, these structures cannot be distinguished. For monodentate configurations, the $\Delta\nu$ value is much larger than the $\Delta\nu$ for ionic structures. Values of $\Delta\nu$ in the range of 200 to 300 cm^{-1} are typical for monodentate complexes. In contrast, bidentate complexes exhibit significantly smaller $\Delta\nu$ compared to the ionic structures, usually $< 100 \text{ cm}^{-1}$.

$$\Delta\nu = \nu_{\text{as}}(\text{CO}_2^-) - \nu_{\text{s}}(\text{CO}_2^-) \quad (1)$$

Table 8.2 shows that for all synthesized biphenyl metal carboxylates both a standard and an alternate $\Delta\nu$ value were calculated. Furthermore, all $\Delta\nu$ values fall in the range typical of bridging or ionic configurations. Even though, initially the splitting of the $\nu_{\text{as}}(\text{CO}_2^-)$ absorption suggested that two configurations were present, the nature of the carboxylate bonding was retained in all cases. The formation of bridging complexes by iron, cobalt and copper is very likely. For example, it was reported that the copper in copper (II) acetate occurred as Cu–Cu dimers, which were coordinated in a bridged fashion by the carboxylate ions [14]. It has also been reported that in copper and cobalt formates the ligand behaves as a bridging group, which forms polymeric species and crystallographic studies have shown that most of the copper (II) carboxylates are actually carboxylate-bridged dimers [12].

In this work it was found that the carboxylates were sparsely soluble to insoluble in water, tetrahydrofuran, toluene, and dimethyl sulfoxide, which suggested that the carboxylates formed bridging polymeric species. This made analysis by UV-vis spectroscopy difficult and absorption in the visible range was weak due to poor solubility, despite the compounds being colored.

Co^{2+} forms both tetrahedral and octahedral complexes. Octahedral Co^{2+} is usually pink to violet in color, whereas tetrahedral complexes are blue [15]. Cobalt biphenyl-2,2'-dicarboxylate was violet in color, and cobalt diphenyl-2-carboxylate was deep Prussian blue. Hence, it appears that the Co^{2+} in the dicarboxylate was in an octahedral configuration, whereas the Co^{2+} in the mono-carboxylate was in a tetrahedral configuration.

Analysis using XRD indicated that the compounds were amorphous, the exception being copper biphenyl-2-carboxylate, providing further support for the carboxylates forming bridging polymeric structures. This is important, because it affects the interpretation of the thermochemistry, as well as the way in which the thermochemistry would represent catalytic decomposition.

8.3.1.2 Purity of Metal Carboxylates

It was realized that the presence of unreacted carboxylic acids, residual inorganic matter and occluded organic solvent affected the purity of the synthesized metal carboxylates. Quantification of these contaminants was carried out using a combination of analytical techniques. The amount of unreacted acid was estimated using infrared spectroscopy. Residual inorganic matter (when present) was quantified by processing of SEM micrographs (see [Section 8.3.1.3](#)). Residual solvent (when present) was evaporated at low temperature and accounted for during thermogravimetric analysis (see [Section 8.3.2](#)). [Table 8.3](#) presents the estimated purity of the synthesized metal carboxylates. Details on the specific contaminants present in each compound are given in the [APPENDIX C](#).

Table 8.3. Fractional purity of the synthesized metal carboxylates

Compound	Mass fraction purity ^a
Iron biphenyl-2,2'-dicarboxylate	0.96
Copper (II) biphenyl-2,2'-dicarboxylate	0.93
Cobalt biphenyl-2,2'-dicarboxylate	0.98
Copper (II) biphenyl-2-carboxylate	0.85
Cobalt biphenyl-2-carboxylate	0.96

^a The purity of the metal carboxylates reflects the presence of unreacted carboxylic acids, residual inorganic matter and occluded organic solvent from the synthesis process.

^b Purity of the metal carboxylates is expressed on a free water basis.

With exception of the copper (II) biphenyl-2-carboxylate, materials of acceptable purity were obtained. It is speculated that the polymeric nature of the synthesized compounds affected,

to some extent, their purity; contaminants were trapped in the carboxylates structure. The presence of the impurities was taken into account when interpreting the thermal behavior of each compound.

8.3.1.3 Scanning Electron Microscopy

Once the synthesis of the transition metal biphenyl carboxylates was confirmed by FTIR analysis, the morphology and homogeneity of these materials were examined by scanning electron microscopy. SEM micrographs revealed materials of very different morphology (Figure C.3-C7 in the APPENDIX C). Iron biphenyl-2,2'-dicarboxylate consisted of a series of irregular and sharp-edged particles. Copper (II) biphenyl-2,2'-dicarboxylate showed a densely packed, plate-like morphology. Cobalt biphenyl-2,2'-dicarboxylate formed a needle-type of structure. Cobalt biphenyl-2-carboxylate formed irregular particles, and copper (II) biphenyl-2-carboxylate showed a fine, granulated, sand-like structure.

SEM micrographs also confirmed that in all cases, except in the one of the copper biphenyl-2-carboxylate, homogeneous materials were obtained. Backscattered electron imaging of the copper biphenyl-2-carboxylate (Figure C.8 in the APPENDIX C) pointed to the presence of a second compound. According to microanalysis by energy dispersive X-ray spectroscopy (EDS), it corresponded to a copper-based compound exhibiting a copper to oxygen ratio of 1.82. Copper hydroxide, which participated as a reagent in the synthesis of the copper carboxylate in question, has a copper to oxygen ratio of 1.98. Therefore, after processing of the backscattered electron image, it is suggested that the copper (II) biphenyl-2-carboxylate is contaminated with approximately 10 wt% of copper hydroxide. The presence of copper hydroxide in the copper (II) biphenyl-2-carboxylate does not prevent the study of its thermochemistry; however, it should be considered in the interpretation of the results.

8.3.1.4 Elemental Analysis

Elemental analysis of the transition metal biphenyl carboxylates was performed as part of the characterization process (Table 8.4). In all cases, the elemental composition was adjusted to

account for the amount of the corresponding parent carboxylic acid found as impurity by FTIR analysis, as well as for the amount of lattice water and/or solvent present in the carboxylates structure indicated by TGA-FTIR analysis (see [Section 8.3.2](#)). In the case of the copper biphenyl-2-carboxylate, the amount of copper hydroxide present as impurity was also considered. Calculations are described in the [APPENDIX C](#).

Table 8.4. Elemental composition of the synthesized metal carboxylates

	Elemental composition, [wt%]					
	C		H		O	
	Calc. ^a	Exp. ^{b,c}	Calc. ^a	Exp. ^{b,c}	Calc. ^a	Exp. ^{b,c}
Metal carboxylate = Biphenyl-2,2'-dicarboxylates						
Fe	56.8	57.0	2.7	3.0	21.6	22.1
Cu	55.3	52.9	2.6	2.6	21.1	22.5
Co	56.2	51.5	2.7	2.8	21.4	22.5
Metal carboxylate = Biphenyl-2-carboxylates						
Cu	68.2	68.6	3.9	3.8	14.0	14.3
Co	68.9	64.4	4.0	4.0	14.1	15.4

^a For calculation purposes, it was assumed that the synthesis process yielded salts of biphenyl carboxylic acids in which the transition metal exhibited an oxidation state of 2⁺.

^b Elemental composition was measured in duplicate.

^c The elemental composition of all metal carboxylates was adjusted to account for acid impurities as well as water and/or solvent present in the carboxylate structure.

For calculation purposes, it was assumed that the synthesis process yielded metals carboxylates in which the corresponding metal element displayed an oxidation state of 2⁺. The carbon, hydrogen and oxygen contents calculated under this assumption corresponded well with the experimental data. Differences of less than 10% between the expected and experimental compositions were observed ([Table 8.4](#)).

8.3.1.5 Metal Content

Evaluation of the purity of the biphenyl transition metal carboxylates was also approached from the inorganic side by determining the metal content. Three different methods were used. First, it was estimated by difference from the elemental analysis results (see [Section 8.3.1.3](#)). Second, it was determined using thermogravimetric analysis. Iron, cobalt, and copper carboxylates were decomposed in air atmosphere by heating to 900 °C for 2 hours. The formation of Fe₂O₃, Co₃O₄ and CuO as the corresponding inorganic residue was confirmed by XRD analysis ([Figure C.9-C13](#) in the [APPENDIX C](#)). The metal content was estimated from the amount of residue obtained in each case. Third, the metal content was measured by ICP-OES analysis. Results are presented in [Table 8.5](#).

Transition metal ions can exhibit different oxidation states depending on the specifics of the coordination complexes. Nevertheless, in order to calculate the theoretical metal content for all synthesized metal carboxylates, it was assumed that the carboxylate ions coordinated to transition metals exhibiting an oxidation state of 2⁺, as in [Section 8.3.1.3](#).

In the case of the iron biphenyl-2,2'-dicarboxylate, the measured metal content (18.0 wt% and 16.4 wt%, by elemental analysis and TGA, respectively) is lower than the calculated one (18.9 wt%). This suggests that even though iron in an oxidation state of 2⁺ might be the predominant metal species in the synthesized metal carboxylate, iron in a different oxidation state might also be present. The theoretical metal content for an iron biphenyl-2,2'-dicarboxylate in which iron is present in an oxidation state of 3⁺ is 13.4 wt%. Considering that the experimental metal content of the iron biphenyl-2,2'-dicarboxylate synthesized in this study lies in between the theoretical values for carboxylates having iron in 2⁺ and 3⁺ oxidation states, it is suggested that at least some of the iron in the synthesized compound is present as iron 3⁺. Oxidation states of 2⁺ and 3⁺ are the most common ones for this metal.

Table 8.5. Metal content of the synthesized metal carboxylates

Metal content, [wt%]					
Calculated ^a	Experimental			Comments	
	By Elemental Analysis ^b	By TGA ^c	By ICP		
Metal carboxylate = Biphenyl-2,2'-dicarboxylates					
Fe	18.9	18	16.4	^d	Iron mostly present as Fe ²⁺
Cu	20.9	22.5	21.2	20.7	Copper present as Cu ²⁺
Co	19.7	23.1	22	21.7	Cobalt mostly present as Co ²⁺ Co-Co bonds are possible
Metal carboxylate = Biphenyl-2-carboxylates					
Cu ^e	13.9	13.3	12.9	12.1	Copper present as Cu ²⁺
Co	13	16.3	15.2	14.7	Cobalt mostly present as Co ²⁺ Co-Co bonds are possible

^a For calculation purposes, it was assumed that the synthesis process yielded salts of biphenyl carboxylic acids in which the transition metal exhibited an oxidation state of 2⁺.

^b The amount of metal present in the synthesized carboxylates was determined by difference according to the results from elemental analysis.

^c The amount of metal present in the synthesized carboxylates was calculated based on the amount of metal oxide residue obtained after their decomposition in air atmosphere by heating to 900 °C for 2 hours.

^d Even though the acid digestion of the metal carboxylates was conducted under the same conditions (Acid = HCL, 0.05 N, 50% molar excess, T=80 °C, t=5 h), in the case of the iron biphenyl-2,2'-dicarboxylate the experimental procedure was not successful. The compound could not be properly dissolved.

^e The amount of copper measured experimentally for this metal carboxylate was adjusted to account for the copper hydroxide present as impurity.

Even though the experimental values for metal content varied a little between analytical techniques, they indicated that the amount of metal present in the synthesized cobalt carboxylates is a little higher than the one expected for biphenyl metal carboxylates having cobalt in a 2⁺ oxidation state. Differences between the experimental and the calculated metal contents are above 10%. The formation of metallic bonds might explain the observed additional amount of cobalt. Infrared analysis demonstrated that cobalt carboxylates exhibited a bridging type of

configuration (see [Section 8.3.1.1.2](#)). It is known that metal carboxylates with bidentate bridging groups can exist in the *syn-syn* geometry; metal atoms in this arrangement are close enough to form structures with metal-metal bonds [12][10]. Complexes having bidentate, bridging symmetrical carboxylate groups have been observed for metals of the transition series, e.g. dimeric complexes of copper, chromium, titanium, vanadium and cobalt, among others [12].

The calculated metal content for the copper carboxylates corresponded well with the experimentally observed values. This suggests that salts of the corresponding biphenyl carboxylic acids having copper in an oxidation state of 2^+ were formed.

8.3.1.6 Remarks

With exception of the copper (II) biphenyl-2-carboxylate, all synthesized metal carboxylates corresponded to homogeneous materials of different morphology. Characterization of these compounds suggested the formation of complex structures in which metals might be present in more than one oxidation state. According to infrared spectroscopy, the ligands are coordinated to the metals in bridging modes. Even more, the poor solubility of the synthesized compounds in solvents such as water, tetrahydrofuran, and dimethyl sulfoxide suggested that the metal carboxylates formed bridging polymeric species. In the case of the cobalt carboxylates, the metal content of the carboxylate species suggested that not only the oxygen atoms of the carboxylate moiety are involved in forming the carboxylate bridges but also metal-metal bonds are possible [10].

Determining these characteristics is relevant not only as part of the characterization process but also from a thermochemistry point of view. As discussed later on in the next sections, the thermal response for all metal carboxylates is quite complex. It is speculated that, at least in part, this behavior might be related to the existence of multiple oxidation states, as well as the ability of these metals to be oxidized or reduced during decomposition, for which experimental evidence is provided.

The complex nature of the synthesized transition metal biphenyl carboxylates does not prevent consideration of these materials as surrogates for the reaction of carboxylic acids over heterogeneous catalysts to investigate their catalytic decomposition, as suggested in literature [4]. However, it is doubtful that all of the thermochemical features would be relevant when the nature of carboxylate formation is restricted to the modes of chemisorption possible on a catalytic surface.

8.3.2 Thermochemistry of Metal Carboxylates

8.3.2.1 Thermochemistry of Iron Biphenyl-2,2'-Dicarboxylate

Thermal analysis of the iron biphenyl-2,2'-dicarboxylate revealed complex thermal behavior. According to thermogravimetric analysis, thermal events occurred in four temperature regions, labeled I to IV, over the temperature range 25 to 600 °C (Figure 8.4). The onset temperature, the amount of mass loss and the nature of the gaseous products released and associated to each temperature region are listed in Table 8.6. On the other hand, analysis by differential scanning calorimetry revealed a series of endothermic transitions, labeled *i* to *iv* (Figure 8.4). The onset, endset and peak temperatures as well as the energy associated to these transitions are presented in Table 8.7

The first transition corresponded to a small and gradual change in the mass loss profile which took place over the temperature range ~27 to 150 °C. Approximately 2% of the original mass of the iron carboxylate was lost in this event. Infrared analysis of the gaseous products indicated the release of water from the carboxylate structure (Figure 8.5). According to DSC analysis, the loss of water was perceived as a single wide peak with onset and endset temperatures of 50.0 ± 22.3 °C and 102.0 ± 21.8 °C, respectively. It is common for metal carboxylates to release any adduct molecules, especially water, upon initial heating [12]. In this case, about $26 \text{ kJ}\cdot\text{kg}^{-1}$ of energy were required to remove the water from the carboxylate structure.

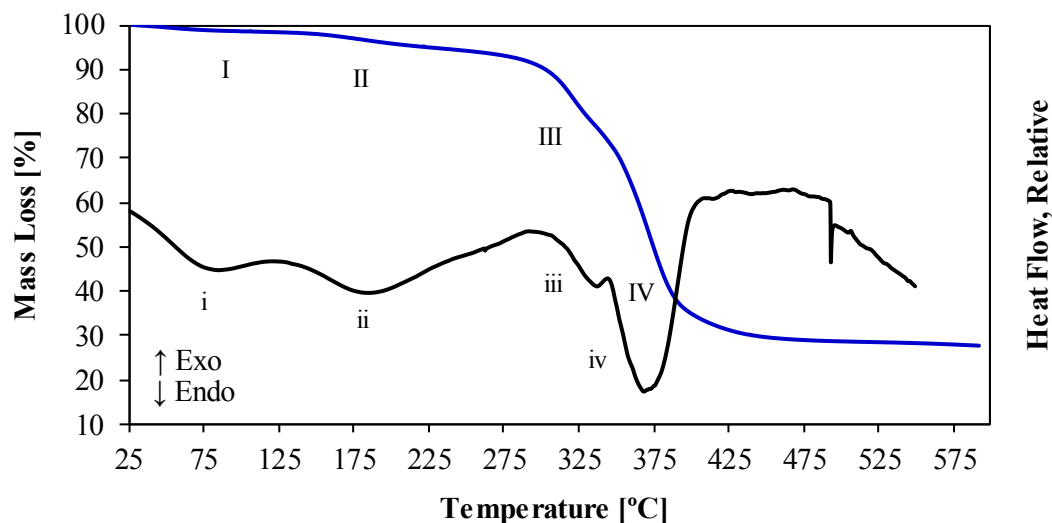


Figure 8.4. TGA mass loss profile and DSC signal for decomposition of iron biphenyl-2,2'-dicarboxylate

Further heating of the iron biphenyl-2,2'-dicarboxylate resulted in the second thermal event. TGA showed that the mass loss commenced at 150.5 ± 3.7 °C and proceeded slowly until 207.4 ± 3.6 °C (Region II in Figure 8.4). A little over 2% of the original mass of the iron carboxylate was lost in this temperature range. The same event was detected by DSC as a wide and gradual endothermic peak (transition *ii*) with an onset temperature of 141.9 ± 1.0 °C, which correlated well with the value observed by TGA, and $\Delta H = -37 \pm 0$ kJ·kg⁻¹. Infrared analysis of the gases released during transition *ii* confirmed production of water and a small amount of carbon dioxide. These two are logical and expected products of decomposition; thus, reaction occurring at a low rate is reasonable. In addition, comparison of the IR spectrum of the gases evolved when heating the iron biphenyl-2,2'-dicarboxylate to around 205 °C and the IR spectrum of gas phase tetrahydrofuran [16] confirmed the presence of the latter as part of the gaseous products (Figure C.14 in APPENDIX C). It is speculated that some of the tetrahydrofuran used in the synthesis process was trapped in the crystalline structure. Comparison of the boiling point of this solvent, ~66 °C [16], and the temperature associated to its release, suggests that the solvent was strongly associated with the carboxylate structure.

Table 8.6. Thermal decomposition and mass loss profile of the synthesized metal carboxylates studied by TGA and TGA-FTIR analyses

Metal	Region ^{a,b}	Temperature (T _{onset} - T _{endset})		Mass loss	$\Delta m / \Delta T$	Gaseous Products
		[°C]	[°C]	[%]	[g/°C]	
Metal carboxylate = Biphenyl-2,2'-dicarboxylates						
Fe	I	27.2 ± 1.4	150.5 ± 3.7	2.2 ± 0.3	0.02	Water
	II	150.5 ± 3.7	207.4 ± 3.6	2.1 ± 1.2	0.04	Water, CO ₂ , tetrahydrofuran
	III	303.8 ± 0.9	328.8 ± 1.2	11.3 ± 0.3	0.45	Water, CO ₂
	IV	356.1 ± 0.5	395.2 ± 0.3	39.3 ± 1.2	1.00	Water ^c , CO ₂ , fluorenone
Cu	I	79.1 ± 9.6	200.1 ± 0.1	4.9 ± 0.3	0.04	Water, Ethanol
	II	250.5 ± 0.9	268.8 ± 0.5	10.2 ± 0.6	0.56	Water, CO ₂ , benzoic acid, fluorenone
	III	288.4 ± 1.1	300.4 ± 0.4	18.6 ± 0.6	1.55	
	IV	335.0 ± 3.5	409.9 ± 3.5	16.4 ± 0.6	0.22	
Co	I	46.7 ± 1.9	130.5 ± 21.8	3.2 ± 0.3	0.04	Water
	II	130.5 ± 21.8	319.7 ± 1.8	4.1 ± 0.6	0.02	Water, CO ₂
	III	319.7 ± 1.8	354.0 ± 0.8	11.0 ± 0.8	0.32	Water, CO ₂
	IV	398.8 ± 0.9	441.6 ± 0.4	48.0 ± 0.9	1.12	Water, CO ₂ , fluorenone
	V	515.6 ± 1.5	615.4 ± 7.8	5.3 ± 4.6	0.05	Water, CO ₂ , CO, fluorenone
Metal carboxylate = Biphenyl-2-carboxylates						
Cu	I	169.8 ± 0.5	202.0 ± 0.8	3.5 ± 0.1	0.11	Ethanol
	II	242.5 ± 0.0	254.3 ± 0.3	6.6 ± 0.4	0.56	Water, CO ₂
	III	287.5 ± 0.7	307.5 ± 0.3	28.2 ± 0.1	1.41	Water, CO ₂ , benzoic acid, fluorenone
	IV	327.1 ± 2.9	363.9 ± 1.3	15.2 ± 0.3	0.41	
Co	I	59.5 ± 0.5	122.4 ± 0.6	2.2 ± 0.2	0.03	Water, CO ₂ ^d
	II	275.1 ± 1.7	299.1 ± 11.6	1.3 ± 0.4	0.05	Water, CO ₂
	III	352.3 ± 2.6	373.3 ± 3.1	3.5 ± 0.1	0.17	Water ^c , CO ₂
	IV	419.3 ± 5.1	453.5 ± 8.5	62.7 ± 0.4	1.84	Water, CO ₂ , fluorenone
	V	453.5 ± 8.5	469.1 ± 6.8	0.8 ± 0.2	0.05	Water, CO ₂ , CO, fluorenone

^a All experiments were conducted in nitrogen atmosphere (100 mLmin⁻¹). The experimental pressure corresponds to the atmospheric pressure, which for typical laboratory conditions is 0.1 MPa.

^b Mass loss profiles of the synthesized transition metal carboxylates were conveniently described in terms of temperature regions containing the main thermal events. These regions do not necessarily cover the whole temperature range of analysis.

^c The intensity of the vibrations indicating the presence of water in the IR spectra of the gases was really low compared to the other products.

^d Some background CO₂ was observed in the reference spectrum collected before analysis.

Table 8.7. Thermal decomposition of the synthesized metal carboxylates studied by DSC analysis

Metal	Transition ^a	Onset Temperature [°C] ^c	Endset Temperature [°C] ^c	Peak Temperature [°C] ^d	Enthalpy of transition [kJ/kg] ^e
Metal carboxylate = Biphenyl-2,2'-dicarboxylates					
Fe	<i>i</i>	50.0 ± 22.3	102.0 ± 21.8	75.0 ± 0.9	-26 ± 7
	<i>ii</i>	141.9 ± 1.0	238.6 ± 1.0	184.4 ± 1.4	-37 ± 0
	<i>iii</i>	310.0 ± 1.6	-	-	^f
	<i>iv</i>	346.2 ± 0.6	-	-	^f
Cu	<i>i</i>	48.9 ± 11.8	133.5 ± 3.2	93.5 ± 1.7	-13 ± 6
	<i>ii</i>	178.8 ± 0.5	198.2 ± 2.5	186.3 ± 1.3	-12 ± 1
	<i>iii</i>	261.4 ± 1.3	-	281.3 ± 0.3	^f
	<i>iv</i>	286.3 ± 1.0	-	306.0 ± 3.9	^f
	<i>v</i>	309.9 ± 2.7	-	-	^f
Co	<i>i</i>	312.2 ± 2.5	357.8 ± 11.4	344.7 ± 0.8	-53 ± 5
	<i>ii</i>	379.0 ± 6.9	-	-	^f
	<i>iii</i>	419.0 ± 3.9	-	-	^f
Metal carboxylate = Biphenyl-2-carboxylates					
Cu	<i>i</i>	161.6 ± 0.6	195.5 ± 1.2	186.8 ± 1.1	-63 ± 5 ^g
	<i>ii</i>	233.8 ± 0.3	238.0 ± 0.3	235.0 ± 0.2	-55 ± 2
	<i>iii</i>	250.1 ± 1.9	278.9 ± 0.3	265.5 ± 0.5	-24 ± 6
	<i>iv</i>	302.6 ± 0.9	313.6 ± 0.1	305.0 ± 0.6	-37 ± 9
	<i>i</i>	69.2 ± 0.5	88.1 ± 0.1	82.3 ± 0.6	-4 ± 0
Co	<i>ii</i>	94.1 ± 0.3	121.0 ± 0.1	107.3 ± 2.6	-11 ± 0
	<i>iii</i>	146.6 ± 0.3	168.3 ± 1.5	157.7 ± 1.9	24 ± 1
	<i>iv</i> ^b	278.7 ± 0.2	286.2 ± 0.5	283.6 ± 0.4	-30 ± 1
	<i>v</i>	349.8 ± 2.9	-	-	^f
	<i>vi</i>	415.8 ± 0.1	-	-	^f

^a All experiments were conducted in nitrogen atmosphere (100 mLmin⁻¹). The experimental pressure corresponds to the atmospheric pressure, which for typical laboratory conditions is 0.1 MPa.

^b This is a reversible event (the opposite transition was observed upon dynamic cooling by DSC analysis).

^c Onset and endset temperatures were estimated but were ill-defined. Transitions consisted of multiple convoluted peaks and the behavior of the baseline was greatly affected by the mass loss.

^d The peak temperature reported here corresponds to the main thermal event when convoluted peaks are observed.

^e Energy changes: endothermic values are negative, exothermic values are positive.

^f The enthalpy of transition was not estimated due to the complexity of the calorigram.

^g The enthalpy value describes both the loss of ethanol from the carboxylate structure and the decomposition of the copper hydroxide present as impurity.

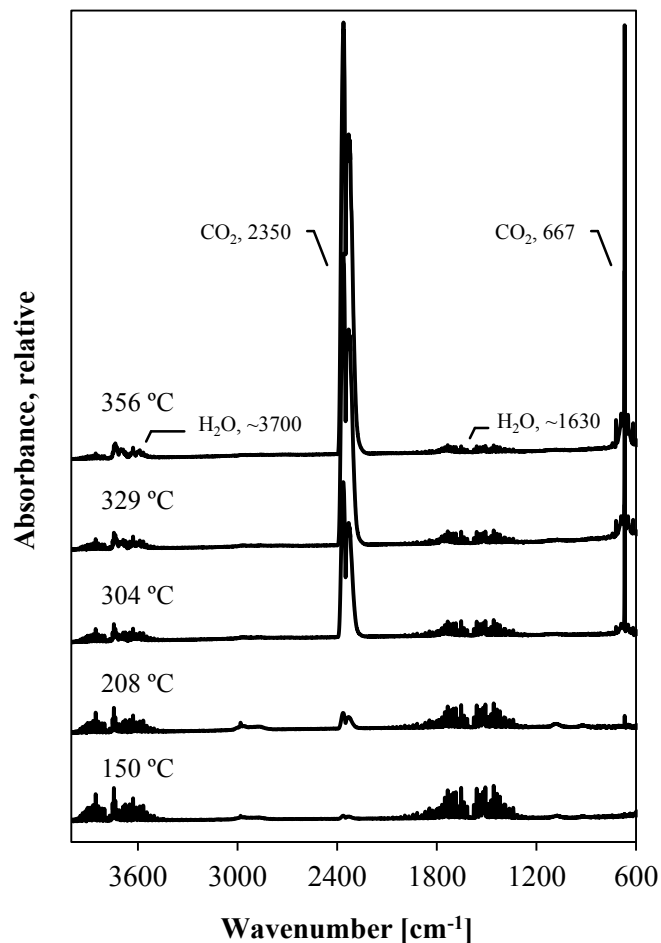


Figure 8.5. Infrared spectra of the gaseous products evolved during thermogravimetric analysis of the iron biphenyl-2,2'-dicarboxylate

Decomposition of the iron biphenyl-2,2'-dicarboxylate became significant and extremely rapid when the temperature increased to about 300 °C (Figure 8.4). As of this point, almost 50% of the original mass of compound was lost. The mass loss profile indicated that the process occurred in two main stages, with onset temperatures of 303.8 ± 0.9 °C and 356.1 ± 0.5 °C, respectively. According to DSC analysis, two partially overlapping endothermic peaks represented these stages in the calorigram. They have onset temperatures of 310.0 ± 1.6 °C and 346.2 ± 0.6 °C, respectively, which are in good agreement with the temperatures observed by TGA. Despite of being convoluted, it seems that the first peak, transition *iii*, is considerably smaller than the second one, transition *iv*, which in turn correlates well with the corresponding

mass losses observed for regions III and IV in the mass loss profile ($11.3 \pm 0.3\%$ and $39.3 \pm 1.2\%$, respectively). The enthalpy associated to these transitions was not determined because there was too much uncertainty in the baseline, which changed due to the mass loss. Production of CO_2 and water as gaseous products was confirmed (Figure 8.5).

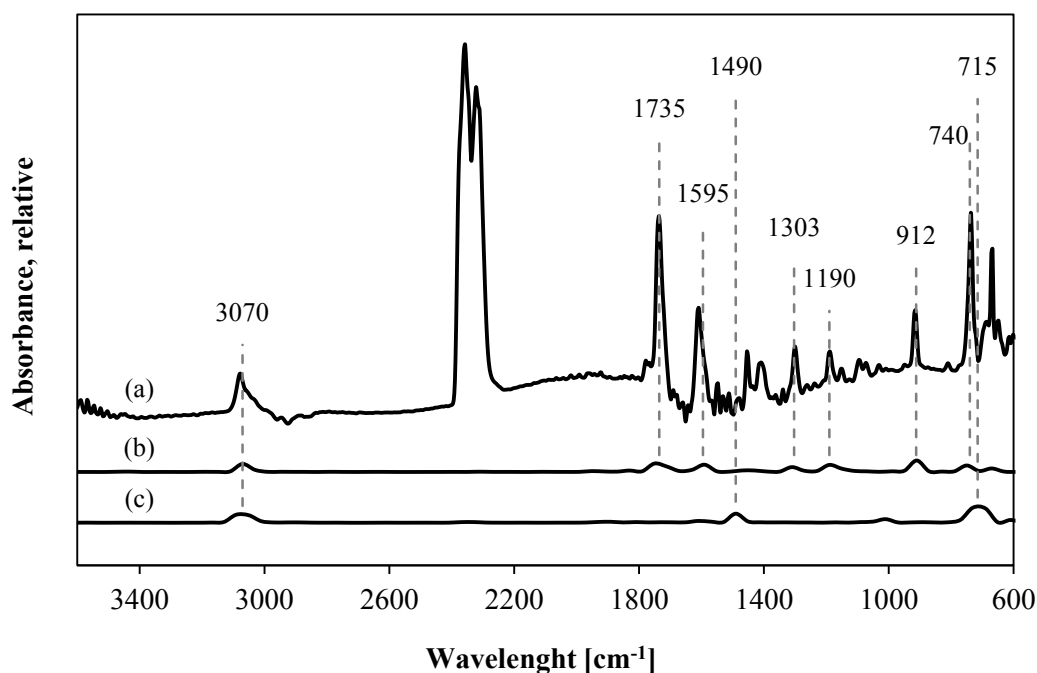


Figure 8.6. Infrared spectra of (a) gases evolved during heating of the iron biphenyl-2,2'-dicarboxylate at 385 °C, (b) gas phase fluorenone, and (c) gas phase biphenyl

Production of additional volatile compounds during the last step of decomposition was noticed. It has been demonstrated that decomposition of zinc biphenyl carboxylates yields fluorenone and biphenyl as the main products [2]. Assuming that the chemistry of decomposition of zinc and iron biphenyl carboxylates is to some extent similar, production of these two compounds is possible when decomposing the iron dicarboxylate. Figure 8.6 shows the IR spectrum of the gases evolved when heating the iron biphenyl-2,2'-dicarboxylate to 385 °C as well as the infrared spectra of gas phase fluorenone and gas phase biphenyl, for comparison purposes [16]. The correspondence of the absorption bands occurring in the $\sim 1750\text{--}700\text{ cm}^{-1}$ region pointed to the production of fluorenone as part of the decomposition products for the iron

biphenyl-2,2'-dicarboxylate. Ketonic decarboxylation over iron oxides and iron containing compounds (e.g. iron-containing graphite) have been reported [17][18]. On the other hand, production of biphenyl is doubtful. The expected absorptions bands at 1490 and 715 cm^{-1} were not observed.

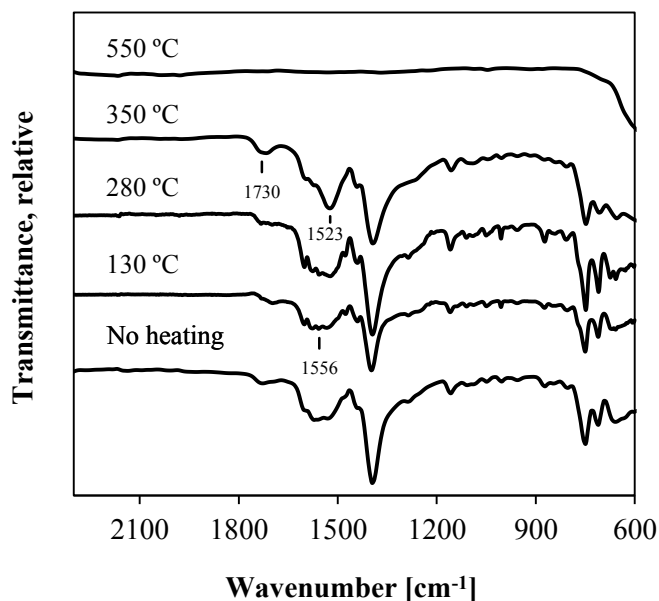


Figure 8.7. Infrared spectra of the solid residue obtained after DSC analysis of the iron biphenyl-2,2'-dicarboxylate to different temperatures

The residue left when heating the iron biphenyl-2,2'-dicarboxylate past the transitions observed in DSC was cooled down in the calorimeter, collected and analyzed by infrared spectroscopy. Changes in the carboxylate structure and information regarding the nature of the reaction products were extracted from the IR spectra (Figure 8.7). Heating up to 350 °C did not cause significant changes in the characteristic carboxylate symmetric stretch. In fact, the shape and intensity of this vibration remained relatively constant. In contrast, heating of the iron carboxylate affected the region of the spectra surrounding the asymmetric stretch. After the loss of water, the $\nu_{\text{as}}(\text{CO}_2^-)$ consisted of what appear to be four instead of three partially overlapped peaks. The end of an absorption band located at 1556 cm^{-1} was observed. The same four peaks became more defined when the temperature increased and was high enough to release the trapped tetrahydrofuran from the carboxylate structure. Furthermore, heating of the iron

carboxylate slowly promoted changes in the mode of carboxylate bonding. The characteristic asymmetric stretch located at 1523 cm^{-1} became quite strong during decomposition. The bridging configuration described by the $\Delta\nu$ value of 127 cm^{-1} (alternate value in Table 8.2) dominated the carboxylate structure at this point. The solid residue obtained at the end of the decomposition process does not absorb in the infrared region of the light spectrum.

The IR spectrum of the solid residue collected after heating the iron carboxylate to $350\text{ }^\circ\text{C}$, temperature at which the decomposition process was in an advanced stage, showed a relatively wide absorption band occurring at $\sim 1730\text{ cm}^{-1}$ (Figure 8.7). Vibrations in this region of the infrared spectrum point to carbonyl groups ($\text{C}=\text{O}$). Considering that IR analysis of the gaseous products pointed to production of fluorenone, it is reasonable to think that this band indicates the presence of some fluorenone remaining in the solid product.

XRD analysis of the solid residue left after decomposition of the iron carboxylate confirmed the presence of a mixture of iron oxides, $\text{FeO} \cdot \text{Fe}_2\text{O}_3$ or Fe_3O_4 . These type of species have also been observed during decomposition of the Mn(II) and Co(II) acetates, which decompose to produce M_2O_3 and then M_3O_4 oxides ($\text{M} = \text{metal}$) [12].

8.3.2.2 Thermochemistry of Copper (II) Biphenyl-2,2'-Dicarboxylate and Copper Biphenyl-2-Carboxylate

Copper biphenyl carboxylates exhibited a very interesting and complex thermal behavior. Typical mass loss profiles for the copper (II) biphenyl-2,2'-dicarboxylate and the copper biphenyl-2-carboxylate are presented in Figure 8.8. In both cases, events associated with some mass loss occurred in four distinct temperature regions, labeled I to IV. To provide a more complete picture of their thermal behavior, the calorigrams obtained during DSC analysis of these compounds are also included in Figure 8.8. It is evident that decomposition was, by far, the most relevant thermal event: a multistage process with a rather complicated mechanism. As for the mass loss curves, the amount of mass loss, the nature of the gaseous products released upon heating and the onset and endset temperatures for each characteristic temperature region are

listed in Table 8.6. Similarly, the temperature and enthalpy determinations for the thermal events observed by DSC analysis are presented in Table 8.7.

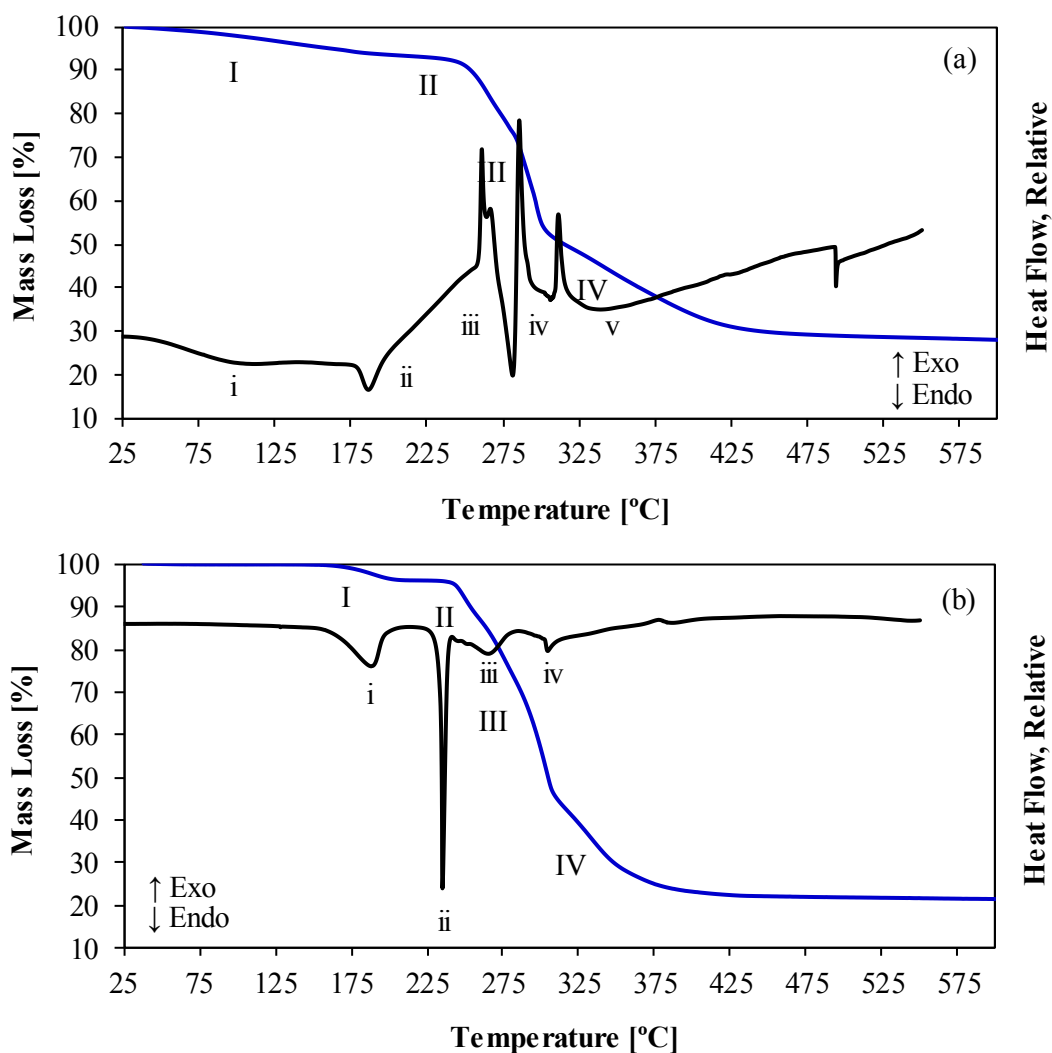


Figure 8.8. TGA mass loss profile and DSC signal for decomposition of **(a)** copper (II) biphenyl-2,2'-dicarboxylate **(b)** copper (II) biphenyl-2-carboxylate

8.3.2.2.1 Decomposition of Copper (II) Biphenyl-2,2'-Dicarboxylate

Thermogravimetric analysis of the copper (II) biphenyl-2,2'-dicarboxylate showed that close to 5% of the original mass of compound was gradually lost over the temperature range ~79-200 °C (Figure 8.8a). DSC analysis indicated that two endothermic events took place in this

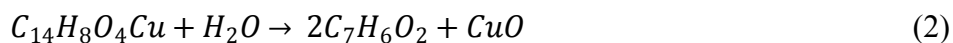
temperature range. Transition *i* corresponded to a very wide and rounded peak, with an onset temperature of 48.9 ± 11.8 °C, an endset temperature of 133.5 ± 3.2 °C, and a $\Delta H = -13 \pm 6$ kJ/kg. The evolution of water during this transition was confirmed by infrared analysis of the gaseous products. On the other hand, transition *ii*, corresponded to a small and relatively sharp peak, with onset and endset temperatures of 178.8 ± 0.5 °C and 198.2 ± 2.5 °C, respectively. Besides water the evolution of ethanol was observed by FTIR (Figure C.15 in the APPENDIX C). It is speculated that part of the ethanol used as solvent in the synthesis process was trapped in the carboxylate structure. The onset temperature for transition *ii*, ~ 180 °C, is significantly higher than the ethanol boiling point, ~ 76 °C [16], suggesting that this alcohol was strongly associated.

Further heating of the copper (II) biphenyl-2,2'-dicarboxylate to ~ 250 °C resulted in thermal decomposition. Rapid and continuous changes in the slope of the mass loss profile pointed out to a rather complicated process involving at least three major stages (Figure 8.8a). The estimated onset temperatures for these stages are 250.5 ± 0.9 °C, 288.4 ± 1.1 °C and 335.0 ± 3.5 °C, respectively. In this case, increasing the temperature by just 40–50 °C influenced the way in which the decomposition was taking place. The calculated rate of mass loss with temperature ($\Delta m/\Delta T$) indicated that the phenomena occurring in region III was the process resulting in the fastest mass loss. Thus, the $\Delta m/\Delta T$ for region III ($1.55 \text{ g}\cdot\text{°C}^{-1}$) is an order of magnitude higher than the values obtained for regions II and IV (0.56 and $0.22 \text{ g}\cdot\text{°C}^{-1}$, respectively). Significant mass loss was observed in every step, with a total of $\sim 45\%$ of the original mass of compound lost due to decomposition.

According to DSC, the above-mentioned changes in the mass loss profile correlated rather well with a series of endothermic thermal events. Despite of being poorly resolved, the onset temperatures for these transitions were estimated. Transition *iii* had an onset temperature of 261.4 ± 1.3 °C, and consisted of two convoluted peaks with peak temperatures of 264.0 ± 1.0 and 281.3 ± 0.3 °C respectively. Transition *iv* had an onset temperature of 286.3 ± 1.0 °C and a peak temperature of 306.0 ± 3.9 °C. Transition *v*, which corresponded to a slightly rounded and wide peak, had an onset temperature of 309.9 ± 2.7 °C. The behavior of the baseline was greatly affected due to the rapid mass loss during decomposition, making the analysis quite difficult. Hence, these temperatures should be understood just as an indication of where decomposition

took place. No enthalpies of transition were determined due to the uncertainty associated with the baseline of the calorigram.

Infrared analysis of the gas phase products showed production of CO₂ and water in all three stages of decomposition. It also indicated formation of additional volatile compounds. Comparison of the IR spectrum of the gas phase products with the IR spectrum of vapor phase benzoic acid [16] confirmed production of the latter (Figure 8.9). The strong band located at 1768 cm⁻¹ represents the C=O stretch of the carboxylic acid functionality [19]. As for the O-H vibrations, the O-H stretching is observed around 3070 cm⁻¹. The O-H bending, typically found in the 1440-1395 cm⁻¹ region [19], is not visible due to the presence of water. The absorption bands observed in the 1300-1000 cm⁻¹ region corresponded to the in-plane ring C-C-H bending. The out-of-plane ring C-C-H bending bands occurring in the lower frequency region (900-675 cm⁻¹) were hidden by the presence of CO₂ [19][20]. Reaction of the copper biphenyl-2,2'-dicarboxylate with water produces benzoic acid (see Eq. 2).



Same as in the case of the iron dicarboxylate, production of fluorenone and biphenyl was investigated. Peaks occurring at 1595, 1310, 910 and 742 cm⁻¹ in the IR spectrum of the gas phase products suggest that decomposition of the copper biphenyl dicarboxylate also yielded some fluorenone (Figure 8.9). The presence of biphenyl could not be confirmed. Absorption bands from water, carbon dioxide, and benzoic acid interfere with the characteristic peaks from biphenyl.

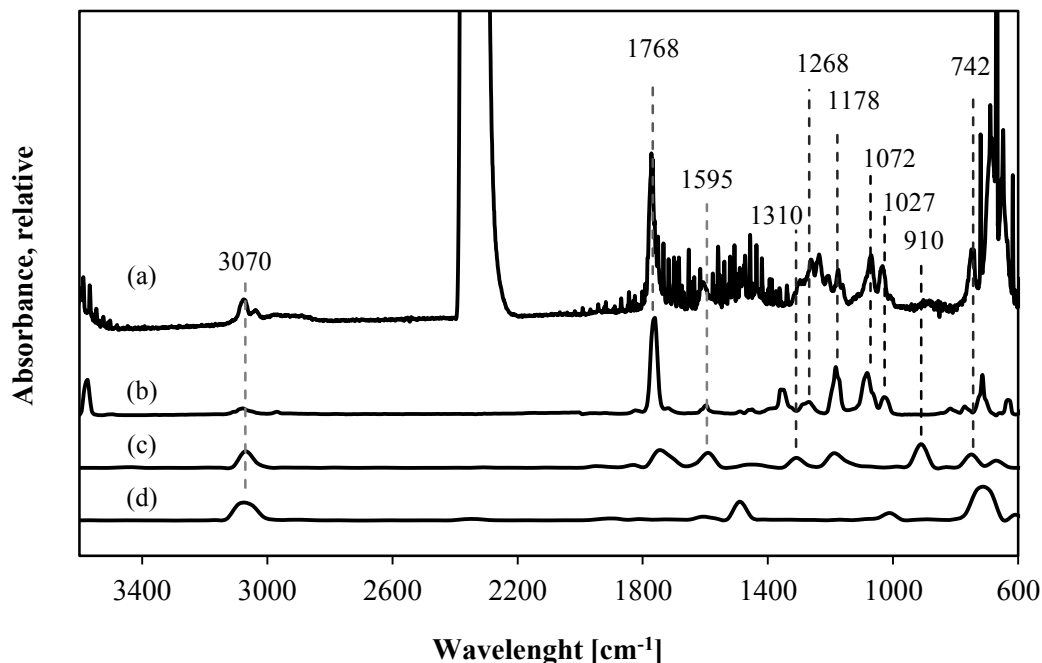


Figure 8.9. Infrared spectra of **(a)** the gases evolved during heating of the copper (II) biphenyl-2,2'-dicarboxylate at 281 °C, and **(b)** vapor phase benzoic acid at 160 °C **(c)** gas phase fluorenone, and **(d)** gas phase biphenyl

8.3.2.2.2 Decomposition of Copper (II) Biphenyl-2-Carboxylate

Thermal behavior of the copper (II) biphenyl-2-carboxylate is similar to the one observed for its dicarboxylate counterpart. Thus, a rapid decomposition, starting at a relatively low temperature, and correlating well with a series of endothermic events was found (Figure 8.8b).

The loss of ethanol (solvent used during synthesis) from the monocarboxylate structure in combination with the decomposition of the copper hydroxide present as impurity corresponded to the first thermal event (transition *i*). These phenomena were detected as a small and relatively sharp endothermic peak with an onset temperature of 161.6 ± 0.6 °C and $\Delta H = -63 \pm 5$ kJ·kg⁻¹. They were also seen in the mass loss profile as a small step change occurring at 169.8 ± 0.5 °C and accompanied by a mass loss of about 3.5% of the original mass of carboxylate. Once again, the relatively high onset temperature for this event indicates that ethanol was strongly associated

with the carboxylate structure. On the other hand, it is worth to mention that DSC analysis of copper hydroxide revealed an endothermic event with onset and endset temperatures of 171.5 ± 0.8 °C and 186.1 ± 1.5 °C, respectively, which are contained in the temperature range of transition *i*.

The second thermal event, transition *ii*, is represented by a well-defined and quite sharp peak. It has an onset temperature of 233.8 ± 0.3 °C with $\Delta H = -55 \pm 2$ kJ·kg⁻¹. DSC-microscopy and calorimetry were employed to study the behavior of this transition. On one hand, DSC-microscopy showed that melting of the carboxylate took place. A liquid phase was formed upon heating; then, while cooling down, the material exhibited a series of “fractures” in the surface suggesting the formation of a solid phase. DSC analysis showed this event was irreversible, i.e. under dynamic cooling the reverse transition with the same enthalpy change was not observed. It is speculated that besides melting of the copper (II) biphenyl-2-carboxylate, some chemical change also took place.

Transition *ii* is particular to the copper (II) biphenyl-2-carboxylate and it was not observed during thermal analysis of its dicarboxylate counterpart. However, after transition *ii* occurs, the way in which both copper carboxylates decompose is quite similar. A change in the structure of the copper biphenyl-2-carboxylate was suspected. Samples of both copper carboxylates were heated to 235 °C (peak temperature of transition *ii*) and compared. Visual observation confirmed that the color of the copper monocarboxylate changed, from bright turquoise to dark green, and matched the color exhibited by the copper dicarboxylate sample. The true nature of transition *ii* was not elucidated in this work.

Heating of the copper (II) biphenyl-2-carboxylate to ~240 °C triggered the decomposition process. Three rapid and consecutive changes in the slope of the mass loss profile were observed. The first stage of decomposition started at 242.5 ± 0.0 °C and was accompanied with a mass loss of approximately 7% of the original mass of metal carboxylate. A small endothermic transition (transition *iii*) consisting of three convoluted peaks was observed by DSC during this first step of reaction. Transition *iii* has an onset temperature of 250.1 ± 1.9 °C and peak temperatures of 244.5 ± 0.6 °C, 250.8 ± 0.4 °C and 265.5 ± 0.5 °C, respectively. The second stage of

decomposition took place between 287.5 ± 0.7 °C and 307.5 ± 0.3 °C. It was accompanied by a mass loss of nearly 28% of the original mass of copper carboxylate, and exhibited the highest rate of mass loss with temperature, $\Delta m/\Delta T = 1.41$ g·°C⁻¹. The last step of reaction commenced at 327.1 ± 2.9 °C and involved the loss of close to 15% of the original mass of carboxylate.

Same as in the case of the copper dicarboxylate, infrared analysis of the gaseous products pointed to the production of CO₂, water, benzoic acid and fluorenone during all three stages of decomposition. Production of biphenyl could not be confirmed by this technique.

8.3.2.2.3 Comparison of the Decomposition of the Copper Carboxylates

DSC analysis of the copper biphenyl carboxylates revealed a number of transitions displaying similar peak temperatures. In order to compare the decomposition process of the two compounds, samples of both copper biphenyl carboxylates were heated to these peaks temperatures. Then, the IR spectra of the gaseous products and solid residues were recorded and interpreted.

Figure 8.10 presents the infrared spectra of the gases released when heating the copper biphenyl carboxylates to 235, 265, 281 and 305 °C. The similarity between the IR spectra of the gases produced by the two compounds at the same temperatures is clear. Before decomposition became significant, absorption bands indicating production of some water and CO₂ were observed (Figure 8.10a). The increase in temperature to 240–250 °C triggered the decomposition processes. As of this point, CO₂ was the main gas product. Production of some benzoic acid along the different stages of reaction was also observed (Figure 8.10b-d).

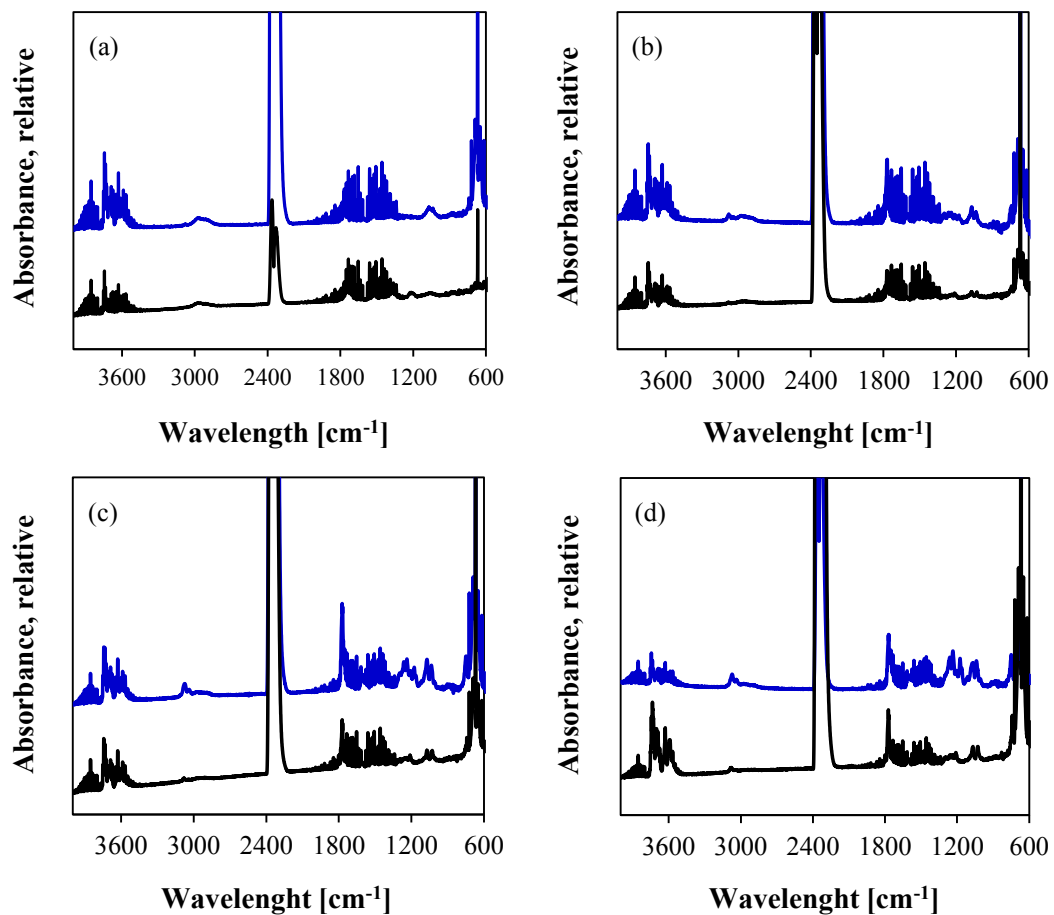


Figure 8.10. Infrared spectra of **(a)** the gases evolved during heating of the copper (II) biphenyl-2,2'-dicarboxylate at 281 °C, and **(b)** vapor phase benzoic acid at 160 °C **(c)** gas phase fluorenone, and **(c)** gas phase biphenyl

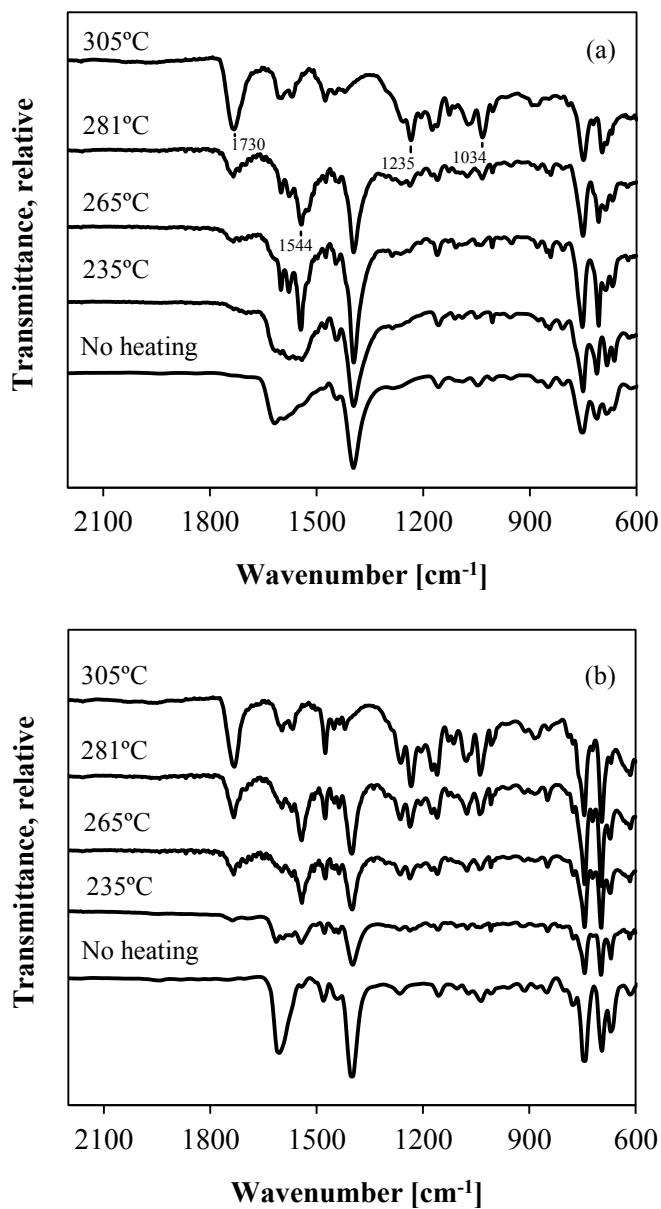


Figure 8.11. Infrared spectra of the solid residue left after heating the (a) copper (II) biphenyl-2,2'-carboxylate (b) copper (II) biphenyl-2-carboxylate

Figure 8.11 shows the IR spectra of the solid residues left after heating the copper biphenyl carboxylates to the same temperatures. With exception of the IR spectra recorded at 305 °C, heating of the copper compounds did not have a major effect on the characteristic symmetric stretch, $\nu_s(\text{CO}_2^-)$. On the other hand, significant changes were observed on the spectral region

surrounding the characteristic asymmetric stretch, $\nu_{\text{as}}(\text{CO}_2^-)$. Some general comments can be made:

- (a) Heating of the copper biphenyl-2-carboxylate up to 235 °C resulted in the splitting of the asymmetric stretch. Instead of displaying one sharp peak with a small shoulder as it was the initial configuration, the $\nu_{\text{as}}(\text{CO}_2^-)$ consisted of five small and overlapped peaks absorbing at 1616, 1595, 1580, 1568 and 1541 cm^{-1} . Heating the copper (II) biphenyl-2,2'-dicarboxylate to the same temperature had a similar effect in the $\nu_{\text{as}}(\text{CO}_2^-)$. Thus, absorption bands occurring at 1616, 1600, 1578, 1558 and 1541 cm^{-1} were observed. It is speculated that the copper monocarboxylate went through some structural change, which made it more similar to its dicarboxylate counterpart.
- (b) Changes in the mode of bonding accompanied the decomposition process of the copper carboxylates. After heating to 265 and 281 °C, a strong absorption band located at 1544 cm^{-1} seemed to represent the asymmetric stretch for both copper compounds. A bridging configuration described by a $\Delta\nu$ value of 151 cm^{-1} , an intermediate value between the standard and alternate $\Delta\nu$ values initially determined (Table 8.2), was observed during the two initial stages of decomposition.
- (c) Decomposition was significant at 305 °C. The characteristic carboxylate stretchings disappeared and two changes related to carbon-oxygen bond formation became noticeable. On one hand, a strong absorption, which is typical of the carbonyl group (C=O), developed at 1730 cm^{-1} . Since decomposition of similar biphenyl metal carboxylates proceeded, at least partially, through a ketonization reaction [2][4], this band should be indicative of fluorenone or a fluorenone derivative. Production of this ketone was also suggested by IR analysis of the gaseous products (see Section 8.3.2.2.1). On the other hand, the development of absorption bands near 1235 cm^{-1} and 1034 cm^{-1} suggested the formation of an aromatic ether. Peaks in this region of the spectrum are characteristic of the C-O-C stretchings [19]. It is speculated that dibenzofuran was formed as product, as discussed in the next section.

It not uncommon for copper carboxylates to decompose in multi-stage processes displaying rather complicated decomposition mechanisms [21][22]. Also, thermal behavior of copper (II) carboxylates is different to other carboxylates due to their dimeric nature and tendency to produce copper (I) carboxylates in an intermediate step and copper (I) oxides or salts as inorganic products [12]. For instance, decomposition of cupric mono-, di-, and tri-chloroacetates in nitrogen atmosphere yielded cuprous chloride as the solid inorganic residue [21]. Similarly, decomposition of $\text{Cu}(\text{XC}_6\text{H}_4\text{CO}_2) \cdot n\text{H}_2\text{O}$ and $\text{Cu}(\text{XC}_6\text{H}_4\text{CO}_2)_2 \cdot \text{Cu}(\text{OH})_2$, where $\text{X} = \text{Cl}, \text{Br}, \text{I}$ and $n = 1, 2$, yielded Cu (I) halides [12]. In this study, XRD analysis confirmed reduction of the copper to form cuprous oxide, Cu_2O , during decomposition of the copper biphenyl carboxylates in nitrogen atmosphere.

8.3.2.2.4 Decomposition Chemistry of Copper Carboxylates

The nature of the products observed during decomposition of the copper biphenyl carboxylates offers some insights into the chemistry taking place. On one hand, IR analysis of the gaseous products confirmed that the organic moiety of the carboxylates decomposed, at least partially, to produce benzoic acid. Formation of benzoic acid through a reaction with water was shown in Eq. 1. On the other hand, the formation of ketone and ether functional groups was supported by IR analysis of solid residues. Also, production of cuprous oxide showed reduction of copper. Copper's oxidation state changed from 2^+ when present in the metal carboxylates to 1^+ on the oxide residues. Based on this findings, a potential reaction pathway for decomposition of copper (II) biphenyl-2,2'-dicarboxylate is presented in Figure 8.12.

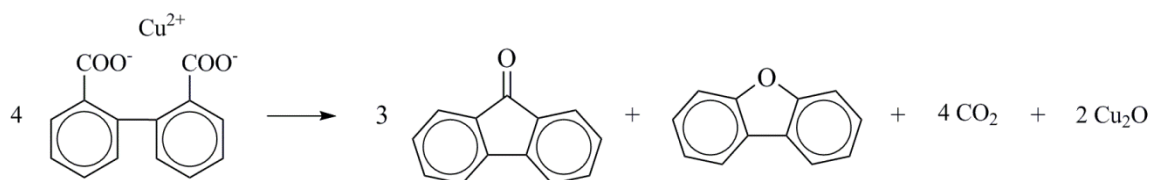


Figure 8.12. Possible reaction pathway leading copper reduction during decomposition of copper (II) biphenyl-2,2'-dicarboxylate

8.3.2.3 Thermochemistry of Cobalt Biphenyl-2,2'-Dicarboxylate and Cobalt Biphenyl-2-Carboxylate

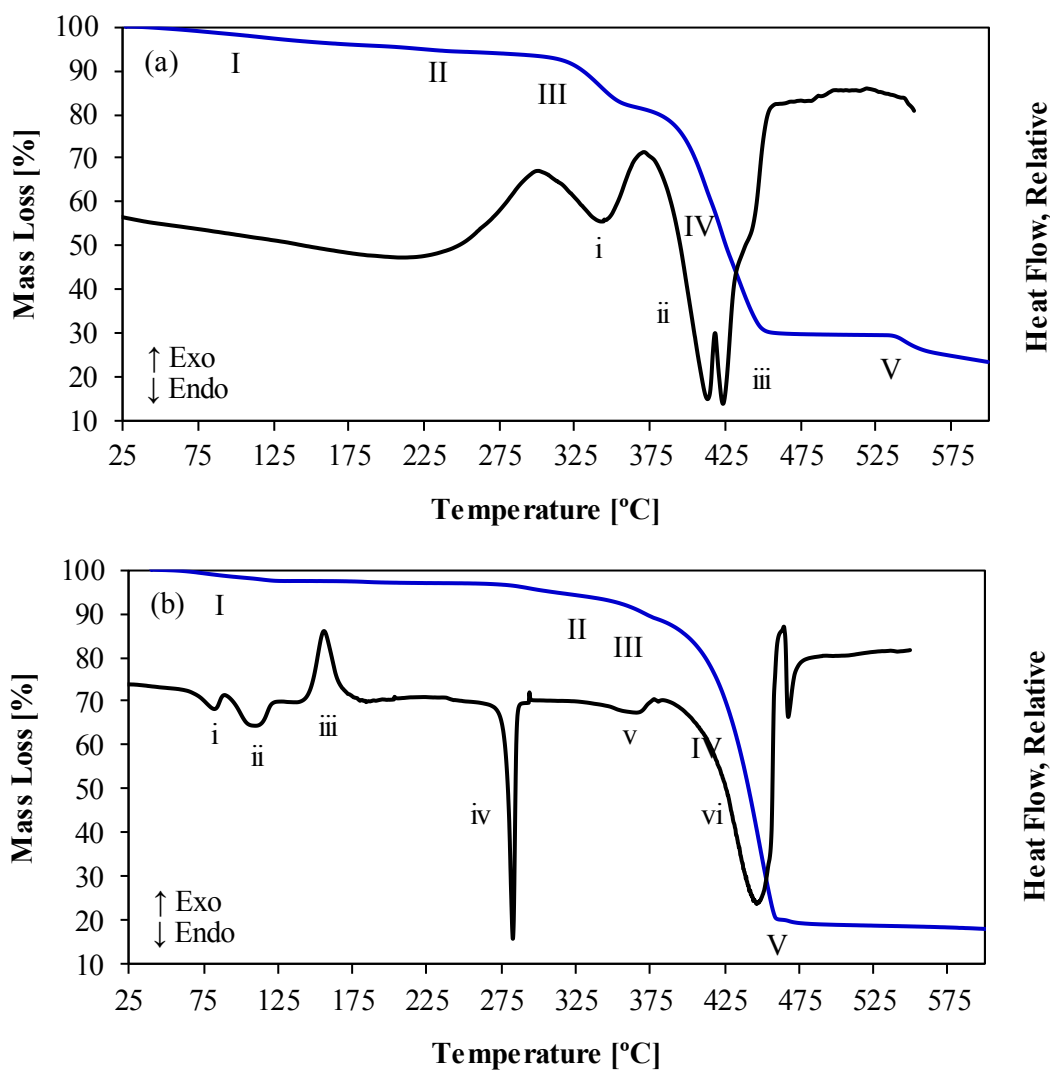


Figure 8.13. TGA mass loss profile and DSC signal for decomposition of (a) cobalt biphenyl-2,2'-dicarboxylate (b) cobalt biphenyl-2-carboxylate

Thermogravimetric analysis of the cobalt biphenyl-2,2'-dicarboxylate and the cobalt biphenyl-2-carboxylate over the temperature range 25 to 600 °C resulted in mass losses that could be classified in five temperature regions, labeled I to V (Figure 8.13). The mass loss profiles indicated that when cobalt catalyzes the reaction, decomposition occurred as a stepwise

process (well-defined individual decomposition steps) rather than as a cascade of reactions, as it was the case of the iron and copper biphenyl carboxylates (individual decomposition steps could not be resolved). On the other hand, DSC analysis suggested a somewhat complicated behavior in both cases. The onset and endset temperatures, the amount of mass loss, the nature of the gaseous products and the enthalpies of the different thermal events were determined and are presented in [Table 8.6](#) and [Table 8.7](#).

8.3.2.3.1 Decomposition of Cobalt Biphenyl-2,2'-Dicarboxylate

Heating of the cobalt biphenyl-2,2'-dicarboxylate up to ~ 320 °C resulted in a continuous mass loss ([Figure 8.13a](#)). Close to 3.2% of the original mass of metal carboxylate was lost as water over the temperature range ~ 47 -130 °C. Similarly, about 4% of the original mass of metal carboxylate was lost as water and CO₂ over the temperature range ~ 130 -230 °C. The constant mass loss affected the behavior of the baseline during DCS analysis by creating a negative slope.

Heating of the cobalt biphenyl-2,2'-dicarboxylate above ~ 320 °C triggered the decomposition process. Three consecutive and well-defined steps in the mass loss profile were observed. The first stage of decomposition started at 319.6 ± 1.8 °C and was accompanied by a mass loss of approximately 11% of the original mass of metal carboxylate. This stage was perceived as an endothermic and relatively wide peak in the calorigram (transition *i* in [Figure 8.13a](#)). According to DSC analysis, transition *i* has an onset temperature of 312.2 ± 2.5 °C, a temperature slightly lower than the one determined by TGA, and $\Delta H = -53 \pm 5$ kJ/kg. IR analysis confirmed the evolution of water and CO₂. The presence of other volatile products was not detected.

Reaction became more significant during the second stage of decomposition. A pronounced step starting at 398.8 ± 0.9 °C and involving the loss of $\sim 48\%$ of the original mass of metal carboxylate was observed in the mass loss profile. Even though thermogravimetric analysis showed this stage as single and clearly defined event, two energy changes in the form of convoluted peaks were associated with it. Thus, transitions *ii* and *iii* pointed to more than one phenomenon taking place. The last step of decomposition commenced at 515.6 ± 1.5 °C and

involved a mass loss of a little over 5% of the original mass of metal carboxylate. This step-wise decomposition process resembles the behavior observed during decomposition of the zinc biphenyl dicarboxylate [2]. On the other hand, IR analysis of the gaseous products confirmed formation of carbon dioxide and water in the last two stages of decomposition. It also indicated the evolution of carbon monoxide in the last step of reaction. Same as in the case of copper and iron dicarboxylates, it supported the production of fluorenone as part of the products (Figure 8.14). Formation of other products, such as biphenyl, could not be confirmed because of peaks interference.

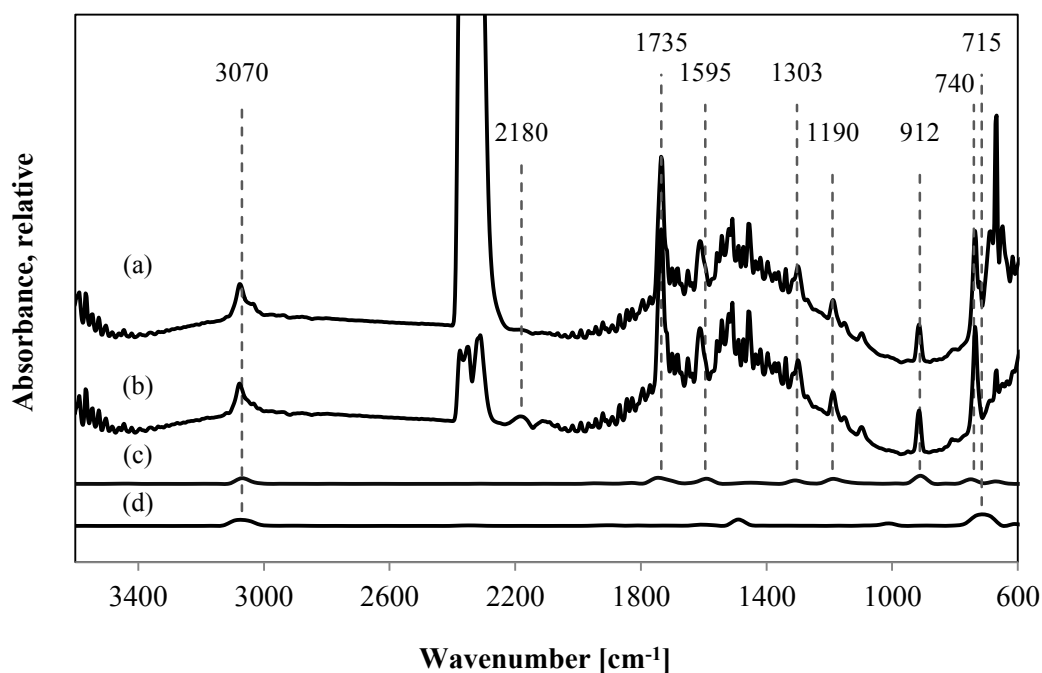


Figure 8.14. Infrared spectra of the gases evolved during heating of the cobalt biphenyl-2,2'-dicarboxylate **(a)** 430 °C, **(b)** 550 °C, as well as **(c)** gas phase fluorenone, and **(d)** gas phase biphenyl

It is common for metal carboxylates of the transition metal elements to decompose via the formation of an organic component, a ketone, and metal oxides [12][10]. Figure 8.15 shows two potential reaction pathways that accommodate the observed decomposition products as well as the possible ways in which cobalt might be coordinated to the carboxylate structure. Note that

determination of the metal content indicated that the cobalt in the cobalt biphenyl-2,2'-dicarboxylate was present mostly as Co^{2+} but Co-Co bonds were also possible. Direct elimination of one of the carboxylate groups as CO_2 or CO would result in intramolecular ketonization.

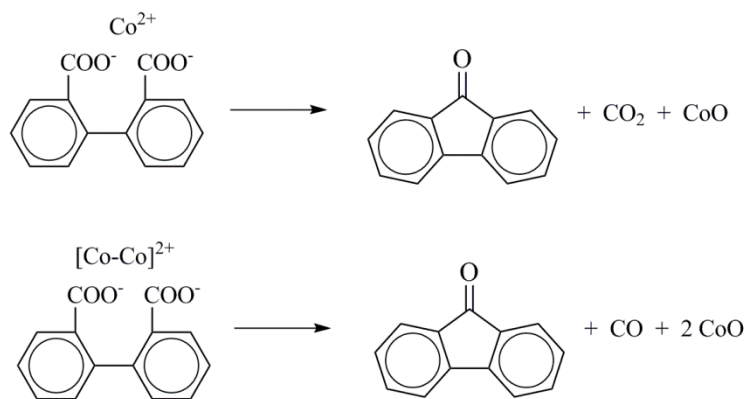


Figure 8.15. Possible reaction pathway leading fluorenone during decomposition of cobalt biphenyl-2,2'-dicarboxylate

Cobalt biphenyl-2,2'-dicarboxylate proved to be thermally stable up to high temperatures. Heating of this compound below $425\text{ }^\circ\text{C}$ did not have a significant effect on the characteristic carboxylate vibrations (Figure 8.16). Unlike its iron and copper counterparts, splitting of the asymmetric stretch was not observed. The shape and intensity of the symmetric stretch, $\nu_s(\text{CO}_2^-)$, remained essentially constant even at an advanced stage of the decomposition.

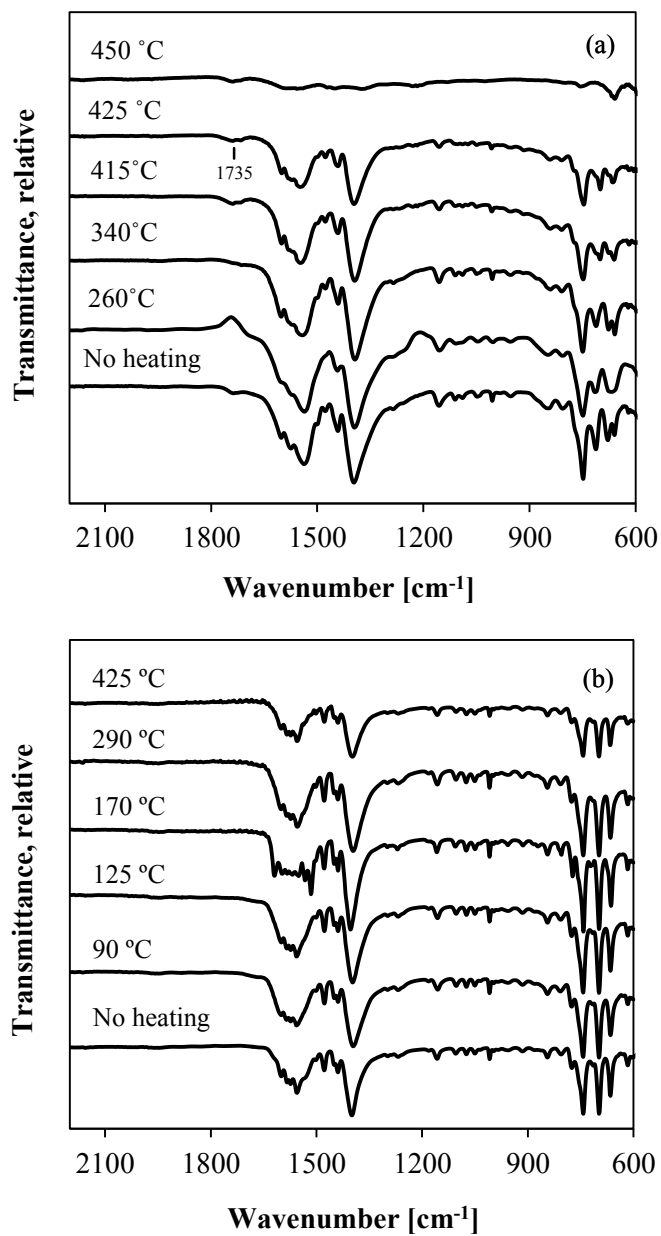


Figure 8.16. Infrared spectra of the solid residue obtained after DSC analysis of the **(a)** cobalt biphenyl-2,2'-dicarboxylate, **(b)** cobalt biphenyl-2-carboxylate

8.3.2.3.2 Decomposition of Cobalt Biphenyl-2-Carboxylate

Although thermogravimetric analysis of the cobalt biphenyl-2-carboxylate indicated that decomposition was by far the most significant thermal event, DSC analysis revealed multiple transitions taking place over the studied temperature range (Figure 8.13b).

Initial heating of the cobalt biphenyl-2-carboxylate over the region ~ 59 - 122 °C resulted in the loss of $\sim 2\%$ of the original mass of metal carboxylate. IR analysis confirmed the evolution of some water in the gas phase. Furthermore, DSC analysis pointed out to the presence of two small endothermic transitions occurring in this temperature range. Transition *i* has an onset temperature of 69.2 ± 0.5 °C and $\Delta H = -4 \pm 0$ kJ·kg⁻¹. The infrared spectrum of the solid residue obtained after heating the cobalt carboxylate pass transition *i* showed a slight decrease in the intensity of the asymmetric stretch absorbing at 1552 cm⁻¹ (Figure 8.16b). DSC-microscopy did not show evident changes in the physical appearance of the material. The loss of water might be responsible for this first energy change.

Transition *ii* takes place in the temperature range 94.1 ± 0.3 to 121.0 ± 0.1 °C and involved an energy change of -11 ± 0 kJ·kg⁻¹. It was speculated that transition *ii* could be related to the melting of the biphenyl-2-carboxylic acid remaining as an impurity after the synthesis of the cobalt carboxylate (Table 8.3). After all, melting of this acid was determined to occur between 110.6 ± 1.3 and 116.1 ± 0.8 °C ($\Delta H = -101.0 \pm 0.2$ kJ·kg⁻¹). Assuming that the energy absorbed by the system was related only to the melting of the acid, it was estimated that the cobalt biphenyl-2-carboxylate would be contaminated with approximately 10% of biphenyl-2-carboxylic acid. This value is higher than the one expected from IR analysis (Table 8.3). It is speculated that melting of the acid impurity was not the only phenomenon taking place. Visual observation of transition *ii* through DSC-microscopy showed that a solid-liquid transition took place (Figure 8.17). Formation of a liquid phase became noticeable around 107 °C.

Further heating of the cobalt carboxylate resulted in transition *iii*, a well-defined, exothermic event with an onset temperature of 146.6 ± 0.3 °C and $\Delta H = 24 \pm 1$ kJ·kg⁻¹. Because no mass loss was associated with this transition, a phase change was suspected. The exothermic character

of the event pointed to a crystallization process. DSC-microscopy confirmed the formation of a solid phase. The growth of a series of small, needle-like crystals was observed (Figure 8.17). Reversibility of transition *iii* was investigated by DSC analysis using the following temperature program: samples of the cobalt carboxylate were heated just beyond the endset temperature of transition *iii*; then, they were cooled down to -20 °C and heated again close to the onset temperature of transition *iv*. The reverse transition was found to occur at a much higher onset temperature (205.4 ± 0.3 °C).

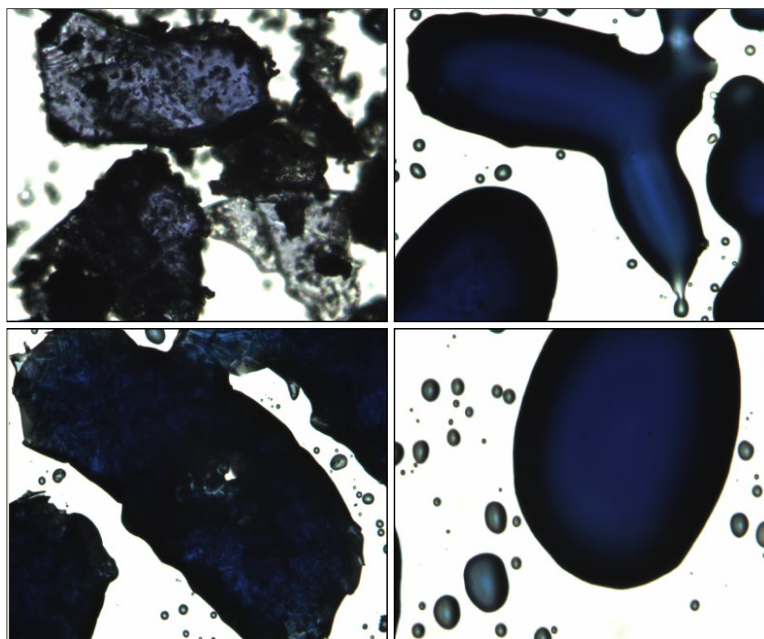


Figure 8.17. DSC-microscopy images of cobalt biphenyl-2-carboxylate to show the solid (up-left), transition *ii* (up-right), transition *iii* (bottom-left) and transition *iv* (bottom-right)

Infrared spectroscopy revealed a change in the mode of bonding of the cobalt carboxylate as a consequence of transition *iii*. The characteristic asymmetric stretch, $\nu_{as}(\text{CO}^-)$, was greatly modified (Figure 8.16b). Two absorption bands of moderate intensity occurring at 1533 and 1515 cm^{-1} gave $\Delta\nu$ values of 134 and 119 cm^{-1} , respectively. Hence, new bridging configurations are possible [13].

The increase in temperature to about 275 °C resulted in a small mass loss (approximately 1% of the original mass of carboxylate) in the form of gaseous water and CO₂. Decomposition of the metal carboxylate taking place at a very slow reaction rate is possible. Heating of the carboxylate also resulted in transition *iv*. DCS analysis showed an endothermic thermal event represented by a well-defined and very sharp peak occurring between 278.7 ± 0.2 and 286.2 ± 0.5 °C, and $\Delta H = -30 \pm 1$ kJ/kg. DSC-microscopy confirmed the formation of a liquid phase (Figure 8.17). Reversibility of transition *iv*, which was confirmed by DSC analysis, suggests that this event corresponded to the melting point of the metal carboxylate. Furthermore, the IR spectrum of the solid residue obtained after heating the cobalt carboxylate past transition *iv* showed that the structural changes caused due to transition *iii* were overturned.

Based on the information gathered from DSC-microscopy and IR analysis, it is speculated that transitions *ii*, *iii* and *iv* are all related to structural changes. It is speculated that heating of the cobalt biphenyl-2-carboxylate caused the structure to change from a low-melting meta-stable configuration (transition *ii*) to a high-melting stable state (transition *iv*). The acid impurity might have had a role in stabilizing the meta-stable configuration. Once the compound in the metastable configuration melted, the system re-arranged to a different and more stable configuration. This re-arrangement required the release of energy (transition *iii*).

Heating of the cobalt biphenyl-2-carboxylate between ~352-373 °C resulted in a mass loss close to 3.5% of the original mass of metal carboxylate. Production of CO₂ and water was verified by FTIR. A small and wide endothermic peak (transition *v*) accompanied this change in mass. On the other hand, decomposition became significant when the temperature rose to about 420 °C (region IV in Figure 8.13b). As of this point, ~63% of the original mass of carboxylate was lost. A single endothermic event with an onset temperature of 349.8 ± 2.9 °C correlated well with this stage of decomposition. Water and CO₂ became the main gaseous products. IR analysis suggested production of some fluorenone.

Spectroscopic evidence confirmed the high thermal stability of the cobalt carboxylate (Figure 8.16b). The characteristic carboxylate absorption bands were observed even at an

advance stage of decomposition. No evidence of carbonyl groups being formed, as part of a ketonization reaction, was observed in the IR spectrum of the solid residues.

8.3.2.4 Thermal Stability of Transition Metal Carboxylates

Thermal analysis of the iron, copper and cobalt carboxylates (carboxylates of transition metals) indicated that decomposition was the most relevant thermal event. In all cases, decomposition occurred as a multistage process with a rather complicated mechanism. Decomposition of the iron and copper carboxylates was perceived as a series of rapid and continuous changes in the slope of the mass loss profile, which correlated well with a series of endothermic and partially overlapped peaks in the corresponding calorigram. For these metal carboxylates, a cascade of reactions took place. On the other hand, decomposition of the cobalt carboxylates occurred in a more stepwise manner.

It is likely that the complexity of decomposition is at least partly due to the ability of the carboxylates to form polymeric species by bridging. Even though the materials were chemically of good purity (Table 8.3), diversity was introduced by bridging between metal centres. This interpretation is supported by the observed amorphous nature of most of the carboxylates. These observations also affect the interpretation of the onset of decomposition related to the application of this work to catalysis. Metal carboxylates formed on a heterogeneous catalyst surface are less likely to form bridged polymeric species.

Thermal stability depended on the metal and increased in the order $\text{Cu} < \text{Fe} < \text{Co}$. These metals formed carboxylates of moderate thermal stability with temperatures of decomposition above 250 °C. Copper, iron and cobalt salts of the biphenyl-2,2'-dicarboxylic acid exhibited a temperature of decomposition close to 250, 300, 320 °C, respectively. Similarly, the copper and cobalt salts of the biphenyl-2-carboxylic acid decomposed around 240 and 350 °C. The transition metals studied in this work formed aromatic carboxylates with lower decomposition temperatures compared to those of the corresponding aromatic carboxylates of alkali and alkaline earth metals, which were previously studied [4]. For the oxidative ring-opening of multinuclear aromatics, catalysts that facilitate decomposition of carboxylic acid species at lower temperatures

are preferred. There is a selectivity benefit when decreasing the temperature of reaction because the contribution of free radical chemistry is limited [2].

Regarding the decomposition products, metal oxides were formed as the inorganic products in all cases. Production of CO₂ and water was observed in all cases; whereas, CO was only formed when decomposing the cobalt carboxylates. Production of benzoic acid during decomposition of the copper carboxylates was confirmed by infrared spectroscopy. The change in the copper's oxidation state (it was reduced) was indicative of complex chemistry taking place. In addition, production of fluorenone was common to all synthesized metal carboxylates. Formation of this compound indicated that even during catalytic decomposition, ketonization of carboxylic acids remained as a potential reaction pathway. Preventing or controlling the extent of this type of reaction is vital in the success of the oxidative ring-opening of multinuclear aromatics [2]. Production of biphenyl, a desirable ring-opened product formed by decomposition through decarboxylation, could not be confirmed in this study. The presence of natural products of decomposition, such as water and carbon dioxide, interferes with the identification of this compound through infrared spectroscopy.

A reactor study in which decomposition of the synthesized metal carboxylates would offer information regarding the selectivity of reaction towards ketonization and decarboxylation can benefit from the thermochemistry determined in this study.

8.4 Conclusions

Iron, cobalt, and copper salts of biphenyl carboxylic acids, namely biphenyl-2,2'-carboxylic acid and biphenyl-2-carboxylic acid, were synthesized. The thermal behavior of these aromatic carboxylates was studied, over the temperature range 25 to 600 °C, as a first step to determine the suitability of the transition metals as potential catalytic materials for decarboxylation. The main observations of this work are as follows:

- (a) The infrared spectra of the iron, cobalt and copper carboxylates suggested that all synthesized compounds exhibited one type of dominant configuration, most likely a bridging type of carboxylate bonding.
- (b) Synthesized transition metal biphenyl carboxylates were homogeneous materials (with exception of the copper biphenyl-2-carboxylate). It was further found that the carboxylates were of complex structure in which the polymeric nature, the presence of metals in more than one oxidation state or forming metal-metal bonds are possible features.
- (c) Thermal stability depended on the metal and it increased in the order $\text{Cu} < \text{Fe} < \text{Co}$. Decomposition of the carboxylates started at 240 and 250 °C for Cu, 300 °C Fe and 320 and 352 °C for Co compounds.
- (d) For all metal carboxylates, decomposition was the most important thermal event: a multistage process with a rather complicated mechanism. Decomposition of the iron and copper compounds resembled a cascade of reactions, whereas decomposition of the cobalt compounds occurred in a more stepwise manner.
- (e) Spectroscopic evidence suggested that iron, copper and cobalt carboxylates decomposed, at least partially, through a ketonization reaction to give fluorenone.
- (f) Infrared spectroscopy showed that heating of the iron and copper compounds promoted a gradual change in the mode of bonding. Although, splitting of the asymmetric stretch $\nu_{\text{as}}(\text{CO}^-)$ resulted in different $\Delta\nu$ values, the nature of the carboxylate bonding was retained in all cases.
- (g) Copper carboxylates decomposed to give benzoic acid and cuprous oxide (Cu_2O) as a part of the reaction products. The change in the copper's oxidation state, it was reduced, indicated a complex chemistry taking place.

(h) Thermal behavior of the copper and cobalt biphenyl-2-carboxylates involved phase transitions before decomposition, which included melting and the formation of some metastable phases. These transitions were not observed during the analysis of their dicarboxylate counterparts.

8.5 References

- [1] Montoya Sánchez, N.; De Klerk, A. Oxidative ring-opening over metal oxides. *Prepr. Pap.-Am. Chem. Soc., Div. Energy Fuels* **2014**, 59(2), 558-561.
- [2] Montoya Sánchez, N; De Klerk, A. Oxidative ring-opening of aromatics: Decomposition of biphenyl carboxylic acids and zinc biphenyl carboxylates, *Energy Fuels*, **2015**, 29, 7910-7922.
- [3] Mars, P.; Scholten, J.J.F.; Zwietering, P. The catalytic decomposition of formic acid. *Adv. Catal.*, **1963**, 14, 35-113.
- [4] Montoya Sánchez, N; De Klerk, A. Oxidative ring-opening of aromatics: Thermochemistry of sodium, potassium and magnesium biphenyl carboxylates. *Thermochim. Acta*, **2016**, 645, 31-42.
- [5] *Thermodynamic and transport properties of organic salts (IUPAC Chemical Data Series 28)*; Franzosini, P., Sanesi, M. Eds.; Pergamon Press: Oxford, 1980.
- [6] Jewur, S.S.; Kuriacose, J.C. Studies on the thermal decomposition of ferric acetate. *Thermochim. Acta*, **1977**, 19, 195-200.
- [7] Kalsi, P.C.; Bassi, P.S.; Khajuria, C.M. Kinetics of the isothermal decomposition of Cu(II) butyrate. *Thermochim. Acta*, **1980**, 41, 265-268.
- [8] Burrows, H.D.; Ellis, H.A. The thermal behavior and spectral properties of some long chain copper(II) carboxylates. *Thermochim. Acta*, **1982**, 52, 121-129.
- [9] Bassi, P.S.; Randhawa, B.S.; Jamwal, H.S. Mössbauer study of the thermal decomposition of some iron(III) monocarboxylates. *Thermochim. Acta*, **1983**, 62, 209-216.
- [10] Bassi, P.S.; Randhawa, B.S.; Jamwal, H.S. Mössbauer study of the thermal decomposition of some iron(III) dicarboxylates. *Thermochim. Acta*, **1983**, 65, 1-8.

- [11] Bassi, P.S.; Jamwal, H.S.; Randhawa, B.S. Comparative study of the thermal analyses of some transition metal(II) propionates. Part I. *Thermochim. Acta*, **1963**, 71, 15-24.
- [12] Mehrotra, R. C.; Bohra, R. *Metal Carboxylates*; Academic Press: New York, 1983.
- [13] Nakamoto, K. *Infrared and Raman Spectra of Inorganic Coordination Compounds Part B*, 6th Edition; Wiley: Hoboken, NJ, 2009.
- [14] Doedens, R.J. Structure and metal-metal interactions in copper(II) carboxylate complexes. *Prog. Inorg. Chem.*, **1976**, 21, 209-231.
- [15] Greenwood, N. N.; Earnshaw, A. *Chemistry of the elements*, 2ed; Butterworth-Heinemann: Oxford, 1997.
- [16] P.J. Linstrom, W.G. Mallard (Eds.), NIST Chemistry WebBook, NIST Standard Reference Database Number 69, National Institute of Standards and Technology, Gaithersburg MD, 20899, <http://webbook.nist.gov>, (retrieved June, 2017).
- [17] Renz, M. Ketonization of Carboxylic Acids by Decarboxylation: Mechanism and Scope. *Eur. J. Org. Chem.* **2005**, 979-988.
- [18] Rajadurai, S. Pathways for Carboxylic Acid Decomposition on Transition Metal Oxides. *Catal. Rev.- Sci. Eng.*, **1944**, 36, 385-403.
- [19] Silverstein, R. M.; Bassler, G. C.; Morrill, T. C. *Spectrometric Identification of Organic Compounds*, 4Edition; John Wiley: New York, 1981
- [20] Bakker, J. M.; Mac Aleese, L.; Von Helden, G.; Meijer, G. The infrared absorption spectrum of the gas phase neutral benzoic acid monomer and dimer. *J. Chem. Phys.*, **2003**, 119, 11180-11185.
- [21] Judd, M.D.; Plunkett, B.A.; Pope, M.I. The structures and thermal decomposition of cupric mono, di and trichloroacetates. *J. Therm. Anal.*, **1976**, 9, 83-92.
- [22] Judd, M.D.; Plunkett, B.A.; Pope, M.I. The thermal decomposition of calcium, sodium, silver and copper(II) acetates. *J. Therm. Anal.*, **1974**, 6, 555-563.

9. CONCLUSIONS

9.1 Introduction

Given the increased production of heavy and extra-heavy oils, refineries need to prepare to process feedstocks of increasingly lower quality and reduced yield of light fractions [1]. Heavy aromatic-rich materials will become a regular feed for refineries in the future. To respond to this situation, industry and academia are actively working on process development that focuses on the effective conversion of heavy materials. Even though traditional upgrading technologies, e.g. hydrogen addition and thermal processes, are still applicable for this purpose, they have shown limitations when dealing with heavier oils [2]. Therefore, to move beyond process improvement of existing technologies there is a need to develop new approaches to the upgrading of heavier oils.

The objective of this investigation was to explore the oxidation of multinuclear aromatics using oxygen (in air) as oxidant to produce ring-opened hydrocarbon products. In other words, this investigation dealt with the proof of concept of the conversion chemistry involved in an oxidative approach for potential upgrading of heavy aromatic-rich materials. The main observations and findings of scientific value derived from this work are presented in the following section.

9.2 Significance, Major Conclusions and Insights

It was recognized that the success of the oxidative upgrading strategy investigated in this work, i.e., the oxidative ring-opening of multinuclear aromatics, relied on a deep understanding of the fundamentals of aromatic oxidation. As a result, the literature concerning selective oxidation of atoms that are part of an aromatic ring structure was critically reviewed. It was found that when oxidation of multinuclear aromatics takes place on carbocyclic rings which do not contain heteroatoms, the structure of the hydrocarbon dictates the possible interaction with

oxygen. Thus, oxidation chemistries which are fundamentally different are possible, i.e., transannular oxygen addition, oxygen addition to a carbon-carbon double bond, or free radical chemistry. Interestingly, regardless of the type of oxidation chemistry taking place, the initiation step does not involve hydrogen abstraction as it is the case for aliphatic autoxidation. On the other hand, when oxidation takes place on heterocyclic aromatics the chemistry observed is influenced by the nature of the heteroatom present in the hydrocarbon structure.

It was also found that non-selective oxidation of multinuclear aromatics leads to addition and combustion products. In fact, selective formation of oxygenates accompanied by the cleavage of the aromatic rings has only been successful at industrial scale when catalyzed by metal oxides. From these observations it became clear that the only realistic strategy for oxidative ring-opening of heavy aromatic-rich materials is to perform catalytic oxidation. The use of a catalyst would limit the contribution of free radical chemistry and total combustion. In addition, the selectivity of reaction would benefit from the reduction of the temperature of reaction as well as the different nature of the transition states enabled by catalysis.

While reviewing the literature on aromatic oxidation, some patents dealing with low-temperature oxidative liquefaction of heavy feedstocks were found. According to these patents, the non-catalytic air oxidation of asphaltenes (the paraffin insoluble fraction of heavy oils) at low temperature is able to produce partially upgraded products, i.e., liquid products of petrochemical value. The validity of these claims was questioned. After all, the study of the fundamentals of aromatic oxidation highlighted the importance of adopting a catalytic approach for selective oxidation to avoid side-reactions typically found during low temperature free radical oxidation. Results from a concrete experimental study demonstrated that low-temperature air oxidation of asphaltenes on its own was not a plausible upgrading strategy as suggested by the patent literature. Instead of increasing the yield of the maltenes fraction, mild oxidation of industrially obtained asphaltenes resulted in the formation additional *n*-pentane insoluble material. These findings reinforced the idea of using a catalytic approach during the oxidative process, although it was analytically difficult to determine the exact nature of the reactions that occurred.

These analytical challenges associated with heavy oils and asphaltenes emphasized the need of conducting a study using model compounds, i.e. feeds of less complex nature, to understand what can actually be achieved through the catalytic process.

Liquid-phase autoxidation (air atmosphere) and catalytic oxidation (nitrogen atmosphere) of anthracene and 9,10-anthraquinone in combination with a number of metal oxides (V_2O_5 , MoO_3 , Fe_2O_3 and NiO) were investigated. V_2O_5 showed the highest catalytic contribution by significantly accelerating the autoxidation of both aromatic compounds. Furthermore, reaction under nitrogen atmosphere confirmed that V_2O_5 was also capable of using the lattice oxygen to oxidize anthracene (first oxidation step) and oxidize 9,10-anthraquinone (second oxidation step) in the liquid-phase. The nature of the reaction products demonstrated that oxidative ring-opening of multinuclear aromatics by transfer of lattice oxygen from appropriate metal oxide catalysts was technically feasible. A Mars-Van Krevelen mechanism was likely. Unfortunately, production of ring-opened products was obscured by the contribution of thermal cracking and the equilibrium of ring-opening and ring-closure reactions. It became evident that catalytic oxidation was not enough as upgrading strategy and additional work needed to be done to improve the selectivity of the reaction towards ring-opened products.

In order to understand how to provide additional driving force for the oxidative ring-opening to happen, thermal decomposition of biphenyl carboxylic acids, which are key intermediates in the catalytic oxidation of phenanthrene, was investigated. After all, the effective removal of the carboxylic acid functionality as CO_2 was essential to produce ring-opened hydrocarbon products. The analysis of the reaction network derived from the thermal decomposition study showed that decarboxylation competes with ketonization and dehydration, decreasing the selectivity of the reaction towards the ring-opened products. It was also found that ketonization was the preferred thermal reaction pathway; therefore, the possibility of favoring production of ring-opened products after thermal decomposition was low. The need for a strategy to modify the reaction selectivity became evident. Since the reaction pathways leading to ring-closed products were accompanied by elimination of water, whereas, that to the desired ring-opened product required elimination of CO_2 , two strategies were considered: (i) carboxylic acid decomposition using a

catalyst that favors decarboxylation, and (ii) decomposition in the presence of water to suppress reactions involving dehydration.

Catalytic decomposition of biphenyl carboxylic acids was studied using metal carboxylates as catalytic surrogates. Compared to thermal decomposition of the acids, a clear change in the reaction selectivity was achieved. When zinc facilitated the decomposition, the selectivity towards the ring-opened product always exceeded the selectivity towards the ring-closed one. Furthermore, the contribution of free radical chemistry was controlled by lowering the onset temperature of decomposition. These findings highlighted the potential selectivity benefit of catalytic carboxylic acid decomposition over thermal decomposition. They also suggested that the temperature and chemistry of aromatic carboxylic acid decomposition would change depending on the metal used during the reaction.

As a natural consequence of the previous findings, the use of alkali, alkaline earth and transition metals for carboxylic acid decomposition was investigated. The thermal behavior and thermal stability of a series of biphenyl metal carboxylates was studied in order to gain an understanding of the steps involved during the decomposition process and to determine the temperature window associated with such steps. These studies contributed to expand the base knowledge for the catalytic behavior of very specific metals. They also helped to realize that there is a “gap” in the literature regarding the chemistry of catalytic decarboxylation of carboxylic acids. There is still a lot of work to be done in order to have a systematic approach to predict which materials are suitable for carboxylic acid decarboxylation, i.e., which materials will be active and selective to this specific decomposition pathway.

In order to facilitate the decarboxylation step of the ring-opening process, decomposition of biphenyl carboxylic acids in the presence of water was also investigated. Compared to thermal decomposition, reaction in the presence of water had a positive impact on the reaction selectivity. Production of ring-opened products was favored. It seemed that water might participate as an intermediary to facilitate the proton or hydrogen transfer during decarboxylation; however, no direct proof of this interpretation was provided in this study. On the other hand, an interesting finding was that the reaction selectivity was sensitive to the mass transport of water. The

implication of this observation for the overall ring-opening concept is far reaching. It highlights that the success of the strategy relies not only on the conversion chemistry, but also on the way in which the reaction engineering is done.

The work conducted on the present investigation showed that oxidative ring-opening of multinuclear aromatics is a strategy able to form products of a simpler structure, i.e., products with less cyclic molecules compared to the initial feed, which have a higher H:C ratio. It has the benefit of not relying on severe reaction conditions, specialized oxidants or expensive metals for catalysis. This investigation dealt with the proof of concept of the conversion chemistry involved in this oxidative approach, however, the development of the process to turn it into a technology will require extensive additional work.

9.3 Recommended Work

9.3.1 Future Work on Process Development of Oxidative Ring-Opening of Multinuclear Aromatics

- (a)** Results from the water-assisted decomposition of biphenyl carboxylic acids highlighted the existence of mass transfer limitations and therefore, the high sensitivity of the reaction to the type of reactor employed. In addition, from the metal carboxylates studies it is clear that catalytic decomposition of the biphenyl carboxylic acids needs to be, ultimately, studied using promising heterogeneous catalysts. The use of a flow reactor, e.g. packed-bed reactor, to investigate the decomposition of aromatic carboxylic acids with the incorporation of water as a co-feed and using a heterogeneous catalyst to favor decarboxylation is suggested. Valuable selectivity and conversion data can be generated.

- (b)** Different catalysts favor oxidation and decarboxylation. The use of a flow reactor system will also help to investigate whether it is possible to combine the conversion chemistries of the oxidation and decarboxylation reactions in a single unit, i.e., evaluation of the entire oxidative ring-opening concept.

- (c) Testing of the oxidative conversion chemistry studied in this work using a real feed material, i.e. a heavy aromatic-rich material, is worthwhile. Yet, this transition should be carefully approached. Real feeds add new complexities that may cause problems which are not necessarily related to the actual oxidative ring-opening process. For instance, a metal may work well as decarboxylation catalyst for a feed consisting of C, H and O; however, when S- or N-containing compounds are added to the feed, the metal could deactivate because of such compounds. As a result, the selection of a metal now has to consider another reaction that could undermine the primary function and catalyst selection is no longer based just on decarboxylation performance.
- (d) Even though there is still a lot of work to be done to turn the oxidative ring-opening concept into a technology, it is possible to envision an initial techno-economic evaluation to determine the extent of economic incentive relative to other traditional upgrading technologies, as well as to highlight areas of economic sensitivity in the conceptual design. An estimate of the possible costs associated to the oxidative ring-opening strategy would be useful to guide future development work from an economic perspective.

9.3.2 Future Work on Selective Decarboxylation Catalysis

- (a) Dealing with carboxylic acid decomposition is an essential part of the oxidative ring-opening strategy. It is also important for the upgrading of liquid products derived from biomass conversion [3][4][5] and coal processing [5]. Chemistries to remove the acid functionality, i.e., ketonization and hydrodeoxygenation (HDO), have been extensively studied. A variety of mechanistic explanations for these reactions have been discussed, and a large number of catalysts have been tested [3][6][7]. However, this is not the case for catalytic decarboxylation. Despite being a relevant chemistry to produce ring-opened hydrocarbon products, and to effectively reduce the oxygen content of bio-oils and coal liquids, catalytic decarboxylation received little systematic study. Studies on decarboxylation, including those reported here, were mainly empirical in nature and failed to uncover the fundamental properties required by a catalytic material that is required for decarboxylation opposed to decomposition by ketonization. This gap in our

fundamental understanding of decarboxylation catalysis remains and presents an opportunity for future fundamental study.

9.4 Presentations and Publications

A list of the publications and presentations in conferences related to the work developed in the current research project is presented in the following:

- Montoya Sánchez, N.; De Klerk, A. Oxidative ring-opening over metal oxides. *Prepr. Pap.-Am. Chem. Soc., Div. Energy Fuels* **2014**, 59(2), 558-561.
(Presented at the 248th ACS National Meeting, 2014, San Francisco, CA, US).
- Montoya Sánchez, N.; De Klerk, A. Oxidative ring-opening: new upgrading strategy. (Presented at Oil Sands 2014 Conference, 2014, Edmonton Alberta).
- Montoya Sánchez, N.; De Klerk, A. Oxidative ring-opening of aromatics: Decomposition of biphenyl carboxylic acids and zinc biphenyl carboxylates. *Energy Fuels* **2015**, 29, 7910-7922.
- Montoya Sánchez, N.; De Klerk, A. Oxidative ring-opening as upgrading strategy: fact or fiction?.
(Presented at C⁵MPT Stewardship Day, 2015, Edmonton, Canada).
- Montoya Sánchez, N.; De Klerk, A. Low-temperature oxidative asphaltenes liquefaction for petrochemicals: fact or fiction? *Appl. Petrochem. Res.* **2016**, 6, 97-106.
- Oxidative ring-opening of aromatics: Effect of Water on Reaction Selectivity. *Prepr. Pap.-Am. Chem. Soc., Div. Energy Fuels* **2016**, 61(1), 489-492.
(Presented at the 251st ACS National Meeting, 2016, San Diego, CA, US)

- Montoya Sánchez, N.; De Klerk, A. Oxidative ring-opening of aromatics: Thermochemistry of sodium, potassium and magnesium biphenyl carboxylates. *Thermochim. Acta* **2016**, 645, 31-42.
- Montoya Sánchez, N.; De Klerk, A. Autoxidation of Aromatics: An Interpretative Review.
(*Paper accepted for publication in Applied Petrochemical Research*).
- Montoya Sánchez, N.; De Klerk, A. Oxidative ring-opening of aromatics: Thermochemistry of iron, copper and cobalt biphenyl carboxylates. *Thermochim. Acta* **2018**, 662, 23-40.
- Montoya Sánchez, N.; De Klerk, A. Oxidative ring-opening as upgrading strategy.
(*Presented at 67th Canadian Chemical Engineering Conference, 2017, Edmonton, Canada*).

9.5 References

- [1] Ancheyta, J.; Trejo, F.; Rana Singh, M. *Asphaltenes: Chemical Transformation during Hydroprocessing of Heavy Oils*; CRC Press: Boca Raton, FL, 2010.
- [2] Castañeda, L. C.; Muñoz, J. A. D.; Ancheyta, J. Current situation of emerging technologies for upgrading of heavy oils. *Catalysis Today* **2014**, 220-222, 248-273.
- [3] He, Z.; Wang, Xianqin. Hydrocarbon production from carboxylic acids via catalytic deoxygenation: required catalytic properties. In *Novel Materials for Catalysis and Fuels Processing*; Bravo-Suárez, J.J., Kidder, M. K., Schwartz, V. Eds.; ACS Symposium Series; American Chemical Society: Washington, DC, 2013.
- [4] Gaertner, C. A.; Serrano-Ruiz, J. C.; Braden, D. J.; Dumesic, J. A. Ketonization reactions of carboxylic acids and esters over ceria-zirconia as biomass-upgrading processes. *Ind. Chem. Chem. Res.* **2010**, 49, 6027-6033.

- [5] Artok, L.; Schobert, H. H. Reaction of carboxylic acids under coal liquefaction conditions 1. Under nitrogen atmosphere. *J Anal Appl Pyrolysis* **2000**, 54, 215-233.
- [6] Pham, T. N.; Sooknoi, T.; Crossley, S. P.; Resasco, D. E. Ketonization of Carboxylic Acids: Mechanisms, Catalysts, and Implications for Biomass conversion. *ACS Catal.* **2013**, 3, 2456-2473.
- [7] Rajadurai, S. Pathways for carboxylic acid decomposition on transition metal oxides. *Catal. Rev.: Sci. Eng.* 1994, 36, 385–403

REFERENCES

- Akiya, N.; Savage, P. Role of Water in Formic Acid Decomposition. *AIChE J.* **1998**, *44*, 406-415.
- Ancheyta, J.; Speight, J. G. *Hydroprocessing of Heavy Oils and Residua*; CRC Press: Boca Raton, FL, 2007.
- Ancheyta, J.; Trejo, F.; Singh Rana, M. In *Asphaltenes: chemical transformation during hydroprocessing of heavy oils*; CRC Press: Boca Raton, FL, 2009.
- Anderson, K. B.; Crelling, J. C.; Huggett, W. W.; Perry, D.; Fullinghim, T.; McGill, P.; Kaelin, P. Oxidative hydrothermal dissolution (OHD) of coal and biomass. *Prepr. Pap.-Am. Chem. Soc., Div. Fuel Chem.* **2011**, *56* (2), 310-311.
- Andersson, T.; Hartonen, K.; Riekkola, M. Solubility of Acenaphthene, Anthracene, and Pyrene in Water At 50 °C to 300 °C. *J. Chem. Eng. Data* **2005**, *50*, 1177-1183.
- Ashida, R.; Painter, P.; Larsen, J. W. Kerogen chemistry. 4. Thermal decarboxylation of kerogen. *Energy Fuels* **2005**, *19*, 1954-1961.
- Artok, L.; Schobert, H. H. Reaction of carboxylic acids under coal liquefaction conditions 1. Under nitrogen atmosphere. *J Anal Appl Pyrolysis* **2000**, *54*, 215-233.
- Attar, A.; Corcoran, W.H. Desulfurization of organic sulfur compounds by selective oxidation. 1. Regenerable and nonregenerable oxygen carriers, *Ind. Eng. Chem. Prod. Res. Dev.*, **1978**, *17*, 102.
- Babu, D. R.; Cormack, D. E. Effect of oxidation on the viscosity of Athabasca bitumen. *Can. J. Chem. Eng.* **1984**, *62*, 562-564.
- Badovskaya, L.A.; Povarova, L.V. Oxidation of furans (Review). *Chemistry of Heterocyclic Compounds* **2009**, *45*, 1023-1034.
- Bakker, J. M.; Mac Aleese, L.; Von Helden, G.; Meijer, G. The infrared absorption spectrum of the gas phase neutral benzoic acid monomer and dimer. *J. Chem. Phys.* **2003**, *119*, 11180-11185.
- Balaban, A. T. Clar Formulas: How to draw and how not to draw formulas of polycyclic aromatic hydrocarbons. *Polycyclic Aromatic Compounds* **2004**, *24*, 83-89.

- Balster, L. M.; Zabarnick, S.; Striebitch, R. C.; Shafer, L. M.; West, Z. J. Analysis of polar species in jet fuel and determination of their role in autoxidative deposit formation. *Energy Fuels* **2006**, 20, 2564-2571.
- Bansal, R. K. *Heterocyclic chemistry 4th ed.* Anshan Ltd: Tunbridge Wells, 2008.
- Barker, R. S.; Halcon International, Inc. Method of oxidizing benzene to maleic anhydride using a vanadium, molybdenum, boron, containing catalyst. Pat. Appl. US 3867412, 1975.
- Bassi, P.S.; Jamwal, H.S.; Randhawa, B.S. Comparative study of the thermal analyses of some transition metal(II) propionates. Part I. *Thermochim. Acta*, **1983**, 71, 15-24.
- Bassi, P.S.; Randhawa, B.S.; Jamwal, H.S. Mössbauer study of the thermal decomposition of some iron(III) monocarboxylates. *Thermochim. Acta* **1983**, 62, 209-216.
- Bassi, P.S.; Randhawa, B.S.; Jamwal, H.S. Mössbauer study of the thermal decomposition of some iron(III) dicarboxylates. *Thermochim. Acta* **1983**, 65, 1-8.
- Bayne, J.; King, I. R.; Richard, M.; Laporte Industries Limited. Vapor Phase oxidation of benzene to maleic anhydride using an aluminum phosphate supported catalyst. Pat. Appl. US 3697550, 1972.
- *Benzene and its industrial derivatives*; Hancock, E. G. Ed.; Ernest Benn: London, 1975.
- Bielański, A; Haber, J. *Oxygen in Catalysis*; Marcel Dekker, Inc: New York, 1991.
- Bielański, A.; Najbar, M. V₂O₅-MoO₃ catalysts for benzene oxidation. *Applied Catalysis A: General* **1997**, 157, 223-261.
- Bonner, L.; Hofstadter, R. Vibration Spectra and Molecular Structure IV. The Infra-Red Absorption Spectra of the Double and Single Molecules of Formic Acid. *J. Chem. Phys.* **1938**, 6, 531- 534.
- Brooks, J. D. The catalytic oxidation of phenanthrene. *J. Appl. Chem.* **1955**, 5, 250-260.
- Brückner, A.; Baerns, M. Selective gas-phase oxidation of polycyclic aromatic hydrocarbons on vanadium oxide-based catalysts. *Applied Catalysis A: General.* **1997**, 157, 311-334.
- Burrows, H.D.; Ellis, H.A. The thermal behavior and spectral properties of some long chain copper(II) carboxylates. *Thermochim. Acta* **1982**, 52, 121-129.
- Calderbank, P. H. *Ind. Chemist* **1952**, 28, 291.

- Castañeda, L. C.; Muñoz, J. A. D.; Ancheyta, J. Current situation of emerging technologies for upgrading of heavy oils. *Catalysis Today* **2014**, 220-222, 248-273.
- Cavani, F.; Trifirò, F. Some innovative aspects in the production of monomers via catalyzed oxidation processes. *Applied Catalysis A: General* **1992**, 88, 115-135.
- Centi, G.; Cavani, F.; Trifiro, F. *Selective Oxidation by Heterogeneous Catalysis*; Kluwer Academic/Plenum Publishers: New York, 2001.
- Chapman, D. The Infrared Spectra of Liquid and Solid Formic acid. *J.Chem. Soc.* **1956**, 48, 225-229.
- Chemical feedstocks from coal; Falbe, J. Ed; John Wiley & Sons: New York, 1982.
- Clar, E. Polycyclic Hydrocarbons (Vol 1). Academic Press: London, 1964.
- Clar, E. *The aromatic sextet*; John Wiley & Sons: London, 1972.
- Clark, J.; Nimlos, M.; Robichaud, D. Bimolecular decomposition pathways for carboxylic acids of relevance to biofuels. *J. Phys. Chem. A* **2015**, 119, 501-516.
- Cofrancesco, A. J. Anthraquinone. In Kirk-Othmer Encyclopedia of Chemical Technology; John Wiley & Sons, Inc. 2000.
- Colthup, N. B.; Daly, L. H.; Wiberley, S. E. *Introduction to Infrared and Raman Spectroscopy*, 3rd Edition; Academic Press: Boston, 1990.
- Cullis, C. F.; Fish, A. Carbonyl-forming oxidations. In *The Chemistry of the Carbonyl Group*; Patai, S., Ed.; Interscience: London, 1966; pp 79–176.
- Dabestani, R.; Britt, P. F.; Buchanan, A. C., III. Pyrolysis of aromatic carboxylic acid salts: Does decarboxylation play a role in cross-linking reactions? *Energy Fuels* **2005**, 19, 365–373.
- Dálessandro, A.F.; Farkas, J. The kinetics of the catalytic oxidation of naphthalene. *Coll. Sci.* **1956**, 11, 653-670.
- Dao-Huy, T.; Haider, M.; Glatz, F.; Schnürch, M.; Milhovilovic, M. D. Direct arylation of benzo[b]furan and other benzo-fused heterocycles. *Eur. J. Org. Chem.* **2014**, 8119–8125.
- David, B.; Boule, P. Phototransformation of PAHs adsorbed on SiO₂ in aqueous suspension. In *Polycyclic aromatic compounds. Synthesis, properties, analytical measurements, occurrence and biological effects*; Garrigues, P., Lamotte, M. Eds.; Gordon and Breach Science Publishers: Amsterdam, 1993, p. 127-133.

- Davies, D. T. *Aromatic heterocyclic chemistry*. Oxford University Press: Oxford, 1992.
- De Klerk, A. Continuous-mode thermal oxidation of Fischer-Tropsch waxes. *Ind. Eng. Chem. Res.* **2003**, 42, 6545-6548.
- De Klerk, A.; Gray, M.; Zerpa, N. Unconventional Oil and Gas: Oilsands. In *Future Energy*, 2ed; Letcher, T. Ed; Elsevier: Amsterdam, 2014, pp 95-115.
- De Maria, F.; Longfield, J. E.; Butler, G. Catalytic Reactor Design. *Ind. Eng. Chem.* **1961**, 53, 259-266.
- Denisov, E. T.; Mitskevich, N. I.; Agabekov, V. E. *Liquid-phase oxidation of oxygen-containing compounds*; Consultants Bureau: New York, 1977.
- Dias, H. P.; Gonçalves, G. R.; Freitas, J. C. C.; Gomes, A. O.; Eustáquio, V. R.; De Castro, E. V. R.; Vaz, B. G.; Aquije, G. M. F. V.; Romão, W. Catalytic decarboxylation of naphthenic acids in crude oils. *Fuel* **2015**, 158, 113–121.
- Di Cio, A.; Vitali, A.; Prolizenz AG. Oxidation of benzene to maleic anhydride using a new catalyst. Pat. Appl. US 3917655, 1975.
- Diels, O.; Kassebart, R. Polymerization processes produced by pyridine. II. The formation of a blue-colored 1,2,3-triketone from phenanthraquinone (in Ger.). *Justus Liebigs Ann. Chem.* **1938**, 536, 78–88.
- Ding, L.; Rahimi, P.; Hawkins, R.; Bhatt, S.; Shi, Y. Naphthenic acid removal from heavy oils on alkaline earth-metal oxides and ZnO catalysts. *Appl. Catal., A* **2009**, 371, 121–130.
- Dixon, J. K.; Longfield, J. E. Hydrocarbon oxidation. In *Catalysis. Vol. VII. Oxidation, hydration, dehydration and cracking catalysts*; Emmett, P.H. Ed.; Reinhold: New York, 1960, p. 183-280.
- Doedens, R.J. Structure and metal-metal interactions in copper(II) carboxylate complexes. *Prog. Inorg. Chem.* **1976**, 21, 209-231.
- Do, H.-Q.; Daugulis, O. An aromatic Glaser-Hay reaction. *J. Am. Chem. Soc.* **2009**, 131, 17052–17053.
- Dunn, J. B.; Burns, M. L.; Hunter, S. E.; Savage, P. E. Hydrothermal stability of aromatic carboxylic acids. *J. Supercrit. Fluids* **2003**, 27, 263–274.
- Duyvesteyn, Willem P. C.; Morley, Raymond L. Oxidation of asphaltenes. US Patent 7,811,444 B2, October 12, 2010.

- Dwight, T. A.; Rue, N. R.; Charyk, D.; Josselyn, R.; DeBoef, B. C-C bond formation via double C-H functionalization: Aerobic oxidative coupling as a method for synthesizing heterocoupled biaryls. *Org. Lett.* **2007**, 9, 3137–3139.
- Dzik, W. I.; Lange, P. P.; Gooßen, L. J. Carboxylates as sources of carbon nucleophiles and electrophiles: comparison of decarboxylative and decarbonylative pathways. *Chem. Sci.* **2012**, 3, 2671–2678.
- Emanuel, N.M.; Denisov, E. T.; Maizus, Z. K. *Liquid-Phase Oxidation of Hydrocarbons*; Plenum Press: New York, 1967; translated by B.J. Hazzard.
- Eskay, T. P.; Britt, P. F.; Buchanan, A. C., III. Does decarboxylation lead to cross-linking in low-rank coals? *Energy Fuels* **1996**, 10, 1257–1261.
- Eskay, T. P.; Britt, P. F.; Buchanan, A. C., III. Pyrolysis of aromatic carboxylic acids: Potential involvement of anhydrides in retrograde reactions in low-rank coal. *Energy Fuels* **1997**, 11, 1278–1287.
- Ford, J.F.; Rayne, T.A.; Adlington, D.G. Desulfurization of hydrocarbons using oxidative and hydro-treatments. U.S. Patent 3,341,448, 1967.
- Franzosini, P.; Westrum Jr, E.F.; Plautz, W.A. Thermophysics of metal alkanoates II. Heat capacities and thermodynamic properties of sodium propanoate. *J. Chem. Thermodynamics* **1983**, 15, 609-618.
- Franzosini, P.; Westrum Jr, E.F. Thermophysics of metal alkanoates III. Heat capacities and thermodynamic properties of lithium and potassium propanoates. *J. Chem. Thermodynamics*, **1984**, 16, 81-90.
- Fu, J.; Savage, P. E.; Lu, X. Hydrothermal decarboxylation of pentafluorobenzoic acid and quinolinic acid. *Ind. Eng. Chem. Res.* **2009**, 48, 10467–10471.
- Fu, X.; Dai, Z.; Tian, S.; Long, J.; Hou, S.; Wang, X. Catalytic decarboxylation of petroleum acids from high acid crude oils over solid acid catalysts. *Energy Fuels* **2008**, 22, 1923–1929.
- Gaertner, C. A.; Serrano-Ruiz, J. C.; Braden, D. J.; Dumesic, J. A. Ketonization reactions of carboxylic acids and esters over ceria-zirconia as biomass-upgrading processes. *Ind. Chem. Chem. Res.* **2010**, 49, 6027-6033.
- García Zapata, J. L.; De Klerk, A. Viscosity changes during mild oxidation of oilsands derived bitumen: Solvent effects and selectivity. *Energy Fuels* **2014**, 28, 6242-6248.

- Gizir, A.; Clifford, A. Solubility of polycyclic aromatic hydrocarbons in subcritical water from 298 K to 498 K. *J. Chem. Eng. Data* **1998**, *43*, 1043-1047.
- Gonzalez, V.; De Klerk, A. Influence of acid chemistry on bitumen viscosity. *Prepr. Pap.-Am. Chem. Soc. Div. Energy Fuels* **2015**, *60*(1), 9-12.
- *Graphene Chemistry: Theoretical Perspectives, First Edition*; Jiang, D.; Chen, Z. Ed.; John Wiley & Sons: United Kingdom, 2013.
- Gray, M.R.; Ayasse, A.R.; Chan, E.W.; Veljkovic, M. Kinetics of hydrodesulfurization of thiophenic and sulfide sulfur in Athabasca bitumen. *Energy Fuels* **1995**, *9*, 500–506.
- Grey, M. R. *Upgrading Oilsands Bitumen and Heavy Oil*. University of Alberta Press: Edmonton, AB. 2015.
- Greenwood, N. N.; Earnshaw, A. *Chemistry of the elements*, 2ed; Butterworth-Heinemann: Oxford, 1997.
- Grzybowski, M.; Skonieczny, K.; Butenschön, H.; Gryko, D.T. Comparison of oxidative aromatic coupling and the Scholl reaction. *Angew. Chem. Int. Ed.* **2013**, *52*, 9900-9930.
- *Handbook of advanced methods and processes in oxidation catalysis. From laboratory to industry*; Duprez, D., Cavani, F. Eds.; Imperial College Press: London, 2014.
- Hardy, D. R.; Wechter, M. A. Characterization of soluble macromolecular oxidatively reactive species (SMORS) from middle distillate diesel fuels: Their origin and role in instability. *Energy Fuels* **1994**, *8*, 782–787.
- Hattori, H. Catalysis by alkaline earth metal oxides. *Stud. Surf. Sci. Catal.* **1985**, *21*, 319-330.
- Hayashi, J.; Matsuo, Y.; Kusakabe, K.; Morooka, S. Depolymerization of lower rank coals by low-temperature O₂ oxidation. *Energy Fuels* **1997**, *11*, 227-235.
- Hayatsu, R.; Scott, R. G.; Winans, R. E. Oxidation of coal. In *Oxidation in organic chemistry. Part D*; Trahanovsky, W. S. Ed.; Academic Press: New York, 1982, p. 279-354.
- He, Z.; Wang, Xianqin. Hydrocarbon production from carboxylic acids via catalytic deoxygenation: required catalytic properties. In *Novel Materials for Catalysis and Fuels Processing*; Bravo-Suárez, J.J., Kidder, M. K., Schwartz, V. Eds.; ACS Symposium Series; American Chemical Society: Washington, DC, 2013.

- Herrington, P. R. Oxidation of bitumen in the presence of a constant concentration of oxygen. *Petrol. Sci. Technol.* **1998**, 16, 1061-1084.
- Herron, J. T. Thermochemistry of sulfoxides and sulfones. In *The chemistry of sulphones and sulfoxides*; Pata, S., Rappoport, Z., Stirling, C. Eds.; John Wiley & Sons: Chichester, 1988, p 95-106.
- *Heterogeneous hydrocarbon oxidation* (ACS Symp. Ser. 638); Warren, B. K., Oyama, S. T. Eds.; American Chemical Society: Washington DC, 1996.
- Höhne, G.W.H.; Hemminger, W.F.; Flammersheim, H.-J. *Differential scanning calorimetry*. 2ed, Springer: Berlin, 2003.
- Hucknall, D. J. *Selective oxidation of hydrocarbons*; Academic Press: London, 1974, pp 147-150.
- Hudlický, M. Oxidations in organic chemistry (ACS Monograph Ser. 186); American Chemical Society: Washington DC, 1990.
- Huong Bui, L.; De Klerk, A. Lithium C₁-C₁₂ n-Alkanoates: Thermal Behavior from -30°C to 600°C. *J. Chem. Eng. Data* **2013**, 58, 1039-1049.
- Huong Bui, L.; De Klerk, A. Thermal behavior of potassium C₁-C₁₂ n-alkanoates and its relevance to Fisher-Tropsch. *J. Chem. Eng. Data* **2014**, 59, 400-411.
- Ishihara, A.; Wang, D.; Dumeignil, F.; Amano, H.; Qian, E. W.; Kabe, T. Oxidative desulfurization and denitrogenation of a light gas oil using an oxidation/adsorption continuous flow process. *Appl. Catal., A* **2005**, 279, 279-287.
- Ismagilov, Z.; Yashnik, M. Kerzhentsev, M.; Parmon, V.; Bourane, A.; Al-Shahrani, F. M.; Hajji, A. A, Koseglo, O.R. Oxidative Desulfurization of Hydrocarbon Fuels. *Catalysis Reviews* **2011**, 53, 199-255.
- Ioffe, I. I.; Sherman, Y. G. *J. Phys. Chem. (U.S.S.R.)* 1954, 28, 2095.
- Javadli, R.; De Klerk, A. Desulfurization of heavy oil. *Appl. Petrochem. Res.* **2012**, 1, 3-19.
- Javadli, R.; De Klerk, A. Desulfurization of Heavy Oils. Oxidative Desulfurization (ODS) As Potential Upgrading Pathway for Oil Sands Derived Bitumen. *Energy Fuels* **2012**, 26, 594-602.
- Jewur, S.S.; Kuriacose, J.C. Studies on the thermal decomposition of ferric acetate. *Thermochim. Acta* **1977**, 19, 195-200.

- Jones, R.A.; Bean, G.P. *The chemistry of Pyrroles*; Academic Press: London, 1977.
- Jones, R.A. *Pyrroles*. Wiley: New York, 1990.
- Joule, J.A.; Mills, K. *Heterocyclic Chemistry, 5th ed.* Wiley: Chichester, U.K., 2010.
- Judd, M.D.; Plunkett, B.A.; Pope, M.I. The structures and thermal decomposition of cupric mono, di and trichloroacetates. *J. Therm. Anal.* **1976**, 9, 83-92.
- Judd, M.D.; Plunkett, B.A.; Pope, M.I. The thermal decomposition of calcium, sodium, silver and copper(II) acetates. *J. Therm. Anal.* **1974**, 6, 555-563.
- Kalsi, P.C.; Bassi, P.S.; Khajuria, C.M. Kinetics of the isothermal decomposition of Cu(II) butyrate. *Thermochim. Acta* **1980**, 41, 265-268.
- Katritzky, A. R.; Lagowski, J. M. *Chemistry of the heterocyclic N-Oxides*; Academic Press: London, 1971.
- Katritzky, A. R. *Handbook of Heterocyclic Chemistry, 1th ed.* Pergamon Press: Oxford, 1985.
- Kim, K. S.; Barteau, M. A. Pathways for carboxylic acid decomposition on TiO₂. *Langmuir* **1988**, 4, 945–953.
- Klein, D.J.; Rosenfeld, V. Forcing, Freedom, & Uniqueness in Graph Theory & Chemistry. *Croatica Chemica Acta* **2014**, 87, 49-59.
- Kluger, R.; Howe, G. W.; Mundle, S. O. C. Avoiding CO₂ in catalysis of decarboxylation. *Adv. Phys. Org. Chem.* **2013**, 47, 85–128.
- Kreile, D. R; Slavinskaya, V.A.; Shimanskaya, M. V.; Lukevits, E. Y. The reactivity of furan compounds in vapor-phase catalytic oxidation. *Chemistry of Heterocyclic Compounds* **1969**, 5, 579-581.
- Lee, D. G.; Noureldin, N. A.; Effect of water on the low-temperature oxidation of heavy oil. *Energy Fuels* **1989**, 3, 713-715.
- Lee-Ruff, E.; Wang, C. Photooxydation of 6-methylbenzo[a]pyrene and related compounds. In *Polycyclic aromatic compounds. Synthesis, properties, analytical measurements, occurrence and biological effects*; Garrigues, P., Lamotte, M. Eds.; Gordon and Breach Science Publishers: Amsterdam, 1993, p. 93-101.
- Le Page, J. F. *Applied heterogeneous catalysis*; Technip: Paris, 1987, pp 366-401.
- Le Page, J.F.; Chatila, S.G.; Davidson, M. *Resid and heavy oil processing*; Editions Technip: Paris, 1992.

- Linhares, M.; Rebelo, S. L.; Simões, M. M. Q.; Silva, A. M. S.; Graça, M.; Neves, P. M. S.; Cavaleiron, J. A. S.; Freire, C. Biomimetic oxidation of indole by Mn(III)porphyrins. *App. Catal. A*, **2014**, 470, 427-433.
- Liodakis, S.; Tsoukala, M. Environmental benefits of using magnesium carbonate minerals as new wildfire retardants instead of commercially available, phosphate-based compounds. *Environ Geochem Health*, **2010**, 32, 391-399.
- Liquid phase oxidation via heterogeneous catalysis. Organic synthesis and industrial applications; Clerici, M. G., Kholdeeva, O. A. Eds.; Wiley: Hoboken, NJ, 2013.
- Lohbeck, K.; Haferkorn, H.; Fuhrmann, W.; Fedtke, N. Maleic and Fumaric acids. In *Ullman's Encyclopedia of Industrial Chemistry*; Wiley-VCH Verlag GmbH & Co, Weinheim, 2012.
- Lorz, P. M.; Towae, F. K.; Enke, W.; Jäckh, R.; Bhargava, N; Hillesheim, W. Phthalic Acid and Derivatives. In *Ullmann's Encyclopedia of Industrial Chemistry*. Wiley-VCH Verlag GmbH & Co, Weinheim, 2007.
- Lugo-José, Y. K.; Monnier, J. R.; Williams, C. T. Gas-phase, catalytic hydrodeoxygenation of propanoic acid, oversupported group VIII noble metals: Metal and support effects. *Appl. Catal., A* **2014**, 469, 410–418.
- Lücke, B.; Martin, A. The Future Role of Aromatics in Refining and Petrochemistry, Proc. Of the DGMK-Conference on Petrochemistry, Erlangen, Germany, 1999, p 139.
- Lücke, B.; Narayana, K.V.; Martin, A.; Jähnisch, K. Oxidation and Ammoxidation of Aromatics. *Adv. Synth. Catal.* **2004**, 346, 4107-1424.
- Ma, X.; Sakanishi, K.; Mochida, I. Hydrodesulfurization Reactivities of Various Sulfur Compounds in Vacuum Gas Oil. *Ind. Eng. Chem. Res.*, **1996**, 35, 2487-2494.
- Ma, X; Zhou, A.; Song, C. A novel method for oxidative desulfurization of liquid hydrocarbon fuels based on catalytic oxidation using molecular oxygen coupled with selective adsorption. *Catal. Today*. **2007**, 123, 276-284.
- Manion, J. A.; McMillen, D. F.; Malhotra, R. Decarboxylation and coupling reactions of aromatic acids under coal-liquefaction conditions. *Energy Fuels* **1996**, 10, 776–788.
- Marek, L. F.; Hahn, D. A. *The catalytic oxidation of organic compounds in the vapor phase*; Chemical Catalogue Company: New York, 1932.

- Mars, P.; Scholten, J. J F.; Zwietering, P. The catalytic decomposition of formic acid. *Adv. Catal.* **1963**, 14, 35–113.
- Mars, P.; Van Krevelen, D. W. Oxidations carried out by means of vanadium oxide catalysts. *Chem. Eng. Sci. Special Suppl.*, **1954**, 3, 41-59.
- Mason, R.T. Naphthalene. In *Kirk-Othmer Encyclopedia of Chemical Technology*; John Wiley & Sons, Inc. 2002.
- Mehrotra, R. C.; Bohra, R. *Metal Carboxylates*; Academic Press: New York, 1983.
- Mensah, T. A.; Ho, C.; Chang, S. S. Products identified from photosensitized oxidation of selected furanoid flavor compounds. *J. Agric. Food Chem.*, **1936**, 34, 336-338.
- Milas, N. A.; Walsh, W.L. Catalytic oxidations I. Oxidations in the furan series. *J. Am. Chem. Soc.*, **1935**, 57, 1389-1393.
- Miller, F.A.; Wilkins, C.H. Infrared Spectra and Characteristic Frequencies of Inorganic Ions. *Anal. Chem.* **1952**, 24, 1253-1294.
- Montoya Sánchez, N.; De Klerk, A. Low-temperature oxidative asphaltenes liquefaction for petrochemicals: fact or fiction? *Appl. Petrochem. Res.* **2016**, 6, 97-106.
- Montoya Sánchez, N.; De Klerk, A. Oxidative ring-opening of aromatics: Decomposition of biphenyl carboxylic acids and zinc biphenyl carboxylates. *Energy Fuels* **2015**, 29, 7910-7922.
- Montoya Sánchez, N.; De Klerk, A. Oxidative ring-opening of aromatics: Thermochemistry of sodium, potassium and magnesium biphenyl carboxylates. *Thermochim. Acta* **2016**, 645, 31-42.
- Montoya Sánchez, N.; De Klerk, A. Oxidative ring-opening over metal oxides. *Prepr. Pap.-Am. Chem. Soc., Div. Energy Fuels* **2014**, 59(2), 558-561.
- Mundle, S. O. C.; Kluger, R. Decarboxylation via addition of water to a carboxyl group: Acid catalysis of pyrrole-2-carboxylic acid. *J. Am. Chem. Soc.* **2009**, 131, 11674–11675.
- Mundle, S. O. C.; Lacrampe-Couloume, G.; Sherwood Lollar, B.; Kluger, R. Hydrolytic decarboxylation of carboxylic acids and the formation of protonated carbonic acid. *J. Am. Chem. Soc.* **2010**, 132, 2430–2436.
- Murata, S.; Murata, K.; Kidena, K.; Nomura, M. A novel oxidative desulfurization system for diesel fuels with molecular oxygen in the presence of cobalt catalysts and aldehydes. *Energ. Fuel.* **2004**, 18, 116-121.

- Mustafa, A. *Benzofurans* (The chemistry of heterocyclic compounds Vol. 29); Wiley: New York, 1974.
- Nakamoto, K. *Infrared and Raman Spectra of Inorganic Coordination Compounds Part B*, 6th Edition; Wiley: Hoboken, NJ, 2009.
- Niizuma, S.; Steele, C. T.; Gunning, H. E.; Strausz, O.P. Electron spin resonance study of the free radicals in Athabasca asphaltene. *Fuel* **1977**, 56, 249-256.
- Ning, Y.C. *Interpretation of Organic Spectra*. John Wiley & Sons: Singapore, 2011.
- Oh, H.-Y.; Park, J.-H.; Rhee, Y.-W.; Kim, J.-N. Decarboxylation of naphthenic acid using alkaline earth metal oxide. *J. Ind. Eng. Chem.* **2011**, 17, 788–793.
- Oswald, A. A.; Noel, F. Role of pyrroles in fuel instability. *J. Chem. Eng. Data*, **1961**, 6, 294-301.
- Paniv, P.M.; Pysh'ev, S.V.; Gaivanovich, V.I.; Lazorko, O.I. Current Problems, Nontraditional Technologies, Noncatalytic oxidation desulfurization of the kerosene cut, *Chem. Tech. Fuels. Oils*, **2006**, 42, 159-166.
- Petersen, J. C. Asphalt oxidation - an overview including a new model for oxidation proposing that physicochemical factors dominate the oxidation kinetics. *Fuel Sci. Technol. Int.* **1993**, 11, 57-87.
- Petroleum Refining Vol. 3 Conversion Processes; Leprince, P. Ed; EditionsTechnip: Paris, 2001, p. 381-407.
- Pham, T. N.; Sooknoi, T.; Crossley, S. P.; Resasco, D. E. Ketonization of Carboxylic Acids: Mechanisms, Catalysts, and Implications for Biomass conversion. *ACS Catal.* **2013**, 3, 2456-2473.
- Pines, H.; Stalick, W.M. Base-catalyzed reactions of hydrocarbons and related compounds; Academic Press: New York, 1977.
- Pitchford, Armin C. Asphaltene oxidation. US Patent 3,484,365, December 16, 1969.
- P.J. Linstrom, W.G. Mallard (Eds.), NIST Chemistry WebBook, NIST Standard Reference Database Number 69, National Institute of Standards and Technology, Gaithersburg MD, 20899, <http://webbook.nist.gov>, (retrieved June, 2017).
- Prado, G. H. C.; Rao, Y.; De Klerk, A. Nitrogen removal from oil: a review. *Energy Fuels* **2017**, 31, 14-36.

- Pyatnitskii, Y. I. Heterogeneous catalytic oxidation of aromatic hydrocarbons in the gas phase. *Russian Chemical Reviews* **1976**, 45 (8), 762-776.
- Rajadurai, S. Pathways for carboxylic acid decomposition on transition metal oxides. *Catal. Rev.: Sci. Eng.* **1994**, 36, 385–403.
- Renz, M. Ketonization of Carboxylic Acids by Decarboxylation: Mechanism and Scope. *Eur. J. Org. Chem.* **2005**, 979-988.
- Rousseau, R.W.; Ferrell, J. K.; Staton, J. S. Conditioning coal gas with aqueous solutions of potassium carbonate: Model development and testing. *Gas Sep. Purif.* **1987**, 1, 44-54.
- Ruiz-Morales, Y.; Mullins, O. Polycyclic Aromatic Hydrocarbons of Asphaltenes Analyzed by Molecular Orbital Calculations with Optical Spectroscopy. *Energy Fuels* **2007**, 21, 256-265.
- Satchell, D. P. N.; Satchell, R. S. Substitution in the groups COOH and COOR. In *The Chemistry of Carboxylic Acids and Esters*; Patai, S., Ed.; Interscience: London, 1969; pp 375–452.
- Sheldon. R. A.; Kochi, J. K. *Metal-Catalyzed Oxidations of Organic Compounds*; Academic Press: New York, 1981.
- Shiraishi, Y.; Tachibana, K.; Hirai, T.; Komasa, I. Desulfurization and denitrogenation process for light oils based on chemical oxidation followed by liquid-liquid extraction. *Ind. Eng. Chem. Res.* **2002**, 41, 4362–4375.
- Siddiquee, M. N.; De Klerk, A. Continuous and prolonged oxidation of bitumen for upgrading by microbial digestion. *Prepr. Pap.-Am. Chem. Soc., Div. Energy Fuels* **2013**, 58 (2), 649-651.
- Siddiquee, M. N.; De Klerk, A. Heterocyclic addition reactions during low temperature autoxidation. *Energy Fuels* **2015**, 29, 4236-4244.
- Siddiquee, M. N.; De Klerk, A. Hydrocarbon Addition Reactions during Low-Temperature Autoxidation of Oilsands Bitumen. *Energy Fuels* **2014**, 28, 6848-6859.
- Silverstein, R. M.; Webster, F. X.; Kiemle, D. J. *Spectroscopic Identification of Organic compounds, 7th Edition*; John Wiley: New York, 2005.
- Silverstein, R. M.; Bassler, G. C.; Morrill, T. C. *Spectrometric Identification of Organic Compounds, 4Edition*; John Wiley: New York, 1981.

- Sittig, M. *Combine oxygen and hydrocarbons for profit*; Gulf Publishing Company: Houston, TX, 1962.
- Smith, B. H. *Bridged Aromatic Compounds*; Academic Press: New York, 1964; pp 100–104.
- Solà, M. Forty years of Clar's aromatic π -sextet rule. *Frontiers in Chemistry* **2013**, 1 (22), 1-8.
- Song, N.; Zhang, D.; Huang, H.; Zhao, H.; Tian, F. Behavior of vanadium–phosphorus-oxides catalyst for butane oxidation to maleic anhydride in a single-tube packed bed reactor. *Catalysis Today* **1999**, 51, 85-91.
- Stock, L. M.; Obeng, M. Oxidation and decarboxylation. A reaction sequence for the study of aromatic structural elements in Pocahontas No. 3 coal. *Energy Fuels* **1997**, 11, 987-997.
- Strausz, O. P.; Lown, E. M. *The chemistry of Alberta oil sands, bitumens and heavy oils*; Alberta Energy Research Institute: Calgary, AB, 2003.
- Szymanski, H. A.; Erickson, R. E. *Infrared band handbook. Vol.2. 999-29 cm⁻¹*, 2ed; IFI/Plenum: New York, 1970.
- Takemura, Y.; Nakamura, A.; Taguchi, H.; Ouchi, K. Catalytic decarboxylation of benzoic acid. *Ind. Eng. Chem. Prod. Res. Dev.* **1985**, 24, 213–215.
- *The chemistry of the quinonoid compounds* (2 Parts); Patai, S. Ed.; John Wiley & Sons: London, 1974.
- *Thermodynamic and transport properties of organic salts*. Franzosini, P., Sanesi, M., Eds.; IUPAC Chemical Data Series 28; Pergamon Press: Oxford, 1980.
- Tipson, R. S. *Oxidation of polycyclic aromatic hydrocarbons. A review of the literature* (National Bureau of Standards Monograph 87); US Government Printing Office: Washington DC, 1965.
- Trivedi, B. C.; Culbertson, B. M. *Maleic Anhydride*; Plenum Press: New York, 1982.
- Tolman, C. A.; Druliner, J. D.; Nappa, M. J.; Herron, N. Alkane oxidation studies in Du Pont's central research department. *In Activation and functionalization of alkanes*; Hill, C. L. Ed.; John Wiley & Sons.: New York, 1989, p. 303-360.

- Tosh, J.S.; Field, J.H.; Benson, H.E.; Haynes, W.P. *Equilibrium study of the system potassium carbonate, potassium bicarbonate, carbon dioxide, and water*; U.S. Dept. of the Interior, Bureau of Mines: Washington, 1959.
- Unluer, C.; Al-Tabbaa, A. Characterization of light and heavy hydrated magnesium carbonates using thermal analysis. *J. Therm. Anal. Calorim.* **2014**, 115, 595-607.
- *Vanadia catalysts for processes of oxidation of aromatic hydrocarbons*. Grzybowska-Świerkosz, B. Ed.; Polish Scientific Publishers: Warsaw, 1984.
- Vandersteen, A. A.; Mundle, S. O. C.; Kluger, R. Protonated carbonic acid and reactive intermediates in the acidic decarboxylation of indolecarboxylic acids. *J. Org. Chem.* **2012**, 77, 6505–6509.
- Vogel, A. Anthraquinone. In *Ullman's Encyclopedia of Industrial Chemistry*. Wiley-VCH Verlag GmbH & Co, Weinheim, 2012.
- Vrbaski, T. Oxidation of aromatic compounds. U.S. Patent 3,306,915, 1963.
- Waack, R. The Stability of the “Aromatic Sextet”. *Journal of Chemical Education* **1962**, 39, 469-472.
- Wainwright, M. S.; Foster, N. Catalysts, Kinetics and Reactor Design in Phthalic Anhydride Synthesis. *Catal. Rev. – Sci. Eng.* **1979**, 19, 211-292.
- Weh, R.; De Klerk, A. Thermochemistry of sulfones relevant to oxidative desulfurization. *Energy Fuels*, **2017**, 31, 6607-6614
- Wender, I.; Heredy, L.A.; Neuworth, M.B.; Dryden, I.G.C. Chemical reactions and the constitution of coal. In *Chemistry of coal utilization. Second supplementary volume*; Elliott, M.A. Ed.; Wiley: New York, 1981, p. 425-521.
- Wiehe, I. A.; A Phase-separation kinetic model for coke formation. *Ind. Eng. Chem. Res.* **1993**, 32, 2447-2454.
- Wiehe, I. A.; A Solvent-resid phase diagram for tracking resid conversion. *Ind. Eng. Chem. Res.* **1992**, 31, 530-536.
- Wiehe, I. A. *Process chemistry of petroleum macromolecules*; CRC Press: Boca Raton, FL, 2008.
- Witkop, B.; Patrick, J.B.; Rosenblum, M. Ring effects in autoxidation. A new type of Camps reaction. *J. Am. Chem. Soc.* **1951**, 73, 2641-2647.

- Xu, X.; Moulijn, J. A.; Ito, E.; Wagemans, R.; Makke, M. Deep desulfurization of fossil fuels by air in the absence of a catalyst. *Chem. Sustain.* **2008**, 1, 817-819.
- You, N.; Kim, M. J.; Jeong, K.; Jeong, S.; Park, Y.; Jeon, J. Catalytic Removal of Sulfur Dioxide from Dibenzothiophene Sulfone Over Mg-Al Mixed Oxides Supported on Mesoporous Silica. *Journal of Nanoscience and Nanotechnology* **2010**, 5, 3663-3666.

APPENDIXES

APPENDIX A.

Oxygen balance for the catalytic oxidation of anthracene

The catalytic oxidation of anthracene to produce anthraquinone using a metal oxide is described by Eq. A1. The stoichiometry of the reaction for the different selected metal oxide catalysts was calculated and is summarized in Table A.1.

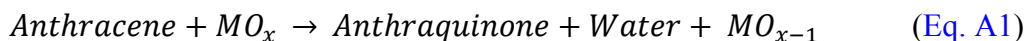


Table A.1. Reaction stoichiometry for the catalytic oxidation of anthracene

	Compound	Stoichiometric Coefficient	Oxygen required ^a [mol]	Oxygen provided ^b [mol]
Reactants	C ₁₄ H ₁₀	1		
	V ₂ O ₅	3		
	C ₁₀ H ₈ O ₂	1	15	5
Products	H ₂ O	1		
	VO ₂	6		
Reactants	C ₁₄ H ₁₀	1		
	MoO ₃	3		
	C ₁₀ H ₈ O ₂	1	9	3
Products	H ₂ O	1		
	MoO ₂	3		
Reactants	C ₁₄ H ₁₀	1		
	Fe ₂ O ₃	3		
	C ₁₀ H ₈ O ₂	1	9	3
Products	H ₂ O	1		
	FeO	6		
Reactants	C ₁₄ H ₁₀	1		
	NiO	3		
	C ₁₀ H ₈ O ₂	1	3	1
Products	H ₂ O	1		
	Ni	3		

^a Oxygen required for complete conversion of 1 mol of anthracene.

^b Oxygen provided by using 1 mol of metal oxide for reaction of 1 mol of anthracene.

Experiments presented in Chapter 4 were performed using a molar ratio of 1:1, i.e., one mol of anthracene reacted with one mol of metal oxide. It should be noted that in all cases, this ratio provided insufficient oxygen for complete conversion of anthracene to anthraquinone.

APPENDIX B.

Supporting Information of Oxidative Ring-Opening of Aromatics: Decomposition of Biphenyl Carboxylic Acids and Zinc Biphenyl Carboxylates

B.1. Chromatograms of decomposition products

Chromatograms of the products from thermal decomposition of biphenyl-2,2'-dicarboxylic acid (Figure B.1), zinc(II) biphenyl-2,2'-dicarboxylate (Figure B.2), and zinc(II) biphenyl-2-carboxylate (Figure B.3) are shown. The chromatograms of the thermal decomposition products of biphenyl-2,2'-dicarboxylic acid were included as Figure 2 in the manuscript.

The numbers refer to the compounds as identified in Table 5.1 and Table 5.2 in Chapter 5.

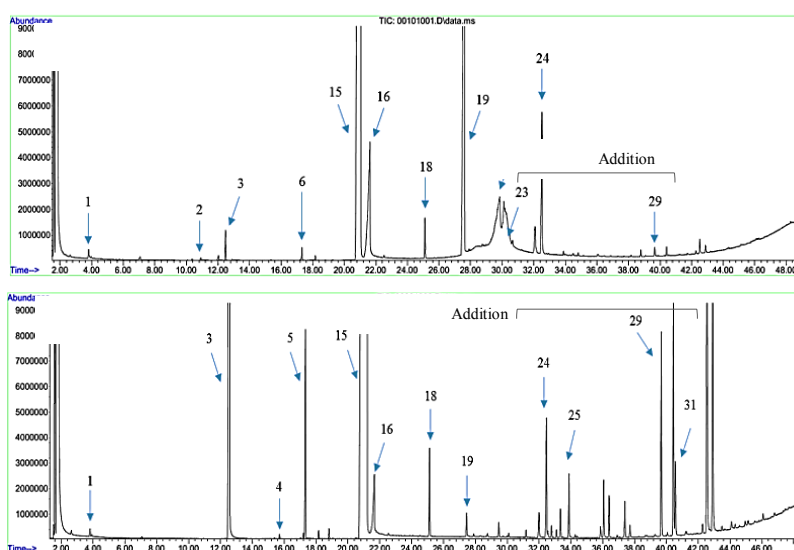


Figure B.1. Chromatogram of biphenyl-2,2'-dicarboxylic acid decomposition products after reaction at 4MPa of nitrogen, during 20 min at (a) 340 °C, and (b) 400 °C

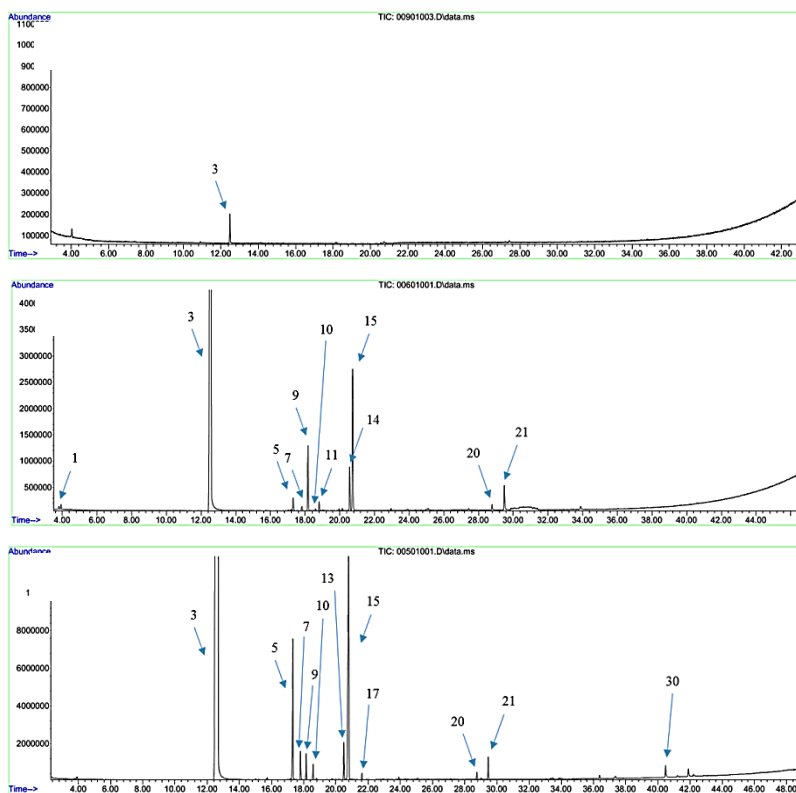


Figure B.2. Chromatogram of zinc(II) biphenyl-2,2'-dicarboxylate decomposition products after reaction under nitrogen atmosphere at **(a)** 263 °C, **(b)** 380 °C, and **(c)** 435 °C

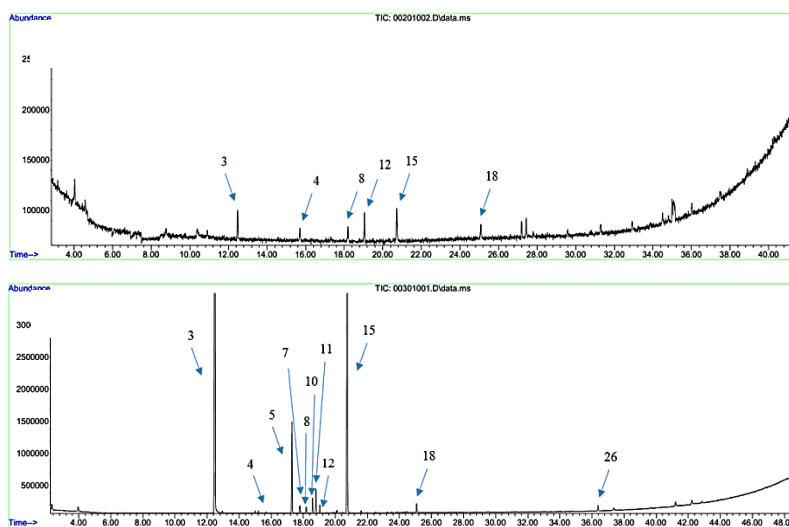


Figure B.3. Chromatogram of zinc(II) biphenyl-2-carboxylate decomposition products after reaction under nitrogen atmosphere at **(a)** 350 °C, and **(b)** 390 °C

APPENDIX C.

Supporting Information of Oxidative Ring-Opening of Aromatics: Thermochemistry of Iron, Copper and Cobalt Biphenyl Carboxylates

C.1. Purity of metal carboxylates

The presence of unreacted carboxylic acids, residual inorganic matter and occluded organic solvent affected the purity of the metal carboxylates. The impurities remaining in the synthesized compounds were quantified using a combination of analytical techniques, i.e., infrared spectroscopy, scanning electron microscopy and thermogravimetric analysis.

Table C.1 presents the estimated purity of the synthesized metal carboxylates. The amount of contaminants is also included.

Table C.1. Purity and contaminants of the synthesized metal carboxylates

Compound	Purity [wt%]	Contaminants, [wt%]		
		Carboxylic Acid	Inorganic Matter	Solvent
Iron biphenyl-2,2'-dicarboxylate	96.0	1.9	0	2.1
Copper (II) biphenyl-2,2'-dicarboxylate	93.3	1.8	0	4.9
Cobalt biphenyl-2,2'-dicarboxylate	97.9	2.1	0	0
Copper (II) biphenyl-2-carboxylate	85.3	1.2	10.0	3.5
Cobalt biphenyl-2-carboxylate	95.7	4.3	0	0

Regarding the presence of unreacted acids, the calibration curve used to estimate the amount of biphenyl carboxylic acid remaining as an impurity in the iron, copper and cobalt salts of the biphenyl-2,2'-dicarboxylic acid was built by adding a known amount of the dicarboxylic acid to samples of the iron biphenyl-2,2'-dicarboxylate. Similarly, the calibration curve used to assess the purity of the copper and cobalt salts of the biphenyl-2-carboxylic acid was derived from the

addition of a known amount of the monocarboxylic acid to samples of the copper biphenyl-2-carboxylate.

The IR spectra of the samples spiked with the acids were collected, and after processing (see [Section 8.2.3.1](#) in [Chapter 8](#)), the amount of acid present in each sample was correlated with the relative peak height of the carbonyl (C=O) vibration. The amount of acid present in the synthesized metal carboxylates was estimated using the correlations showed in [Figure C.1](#) and [Figure C.2](#).

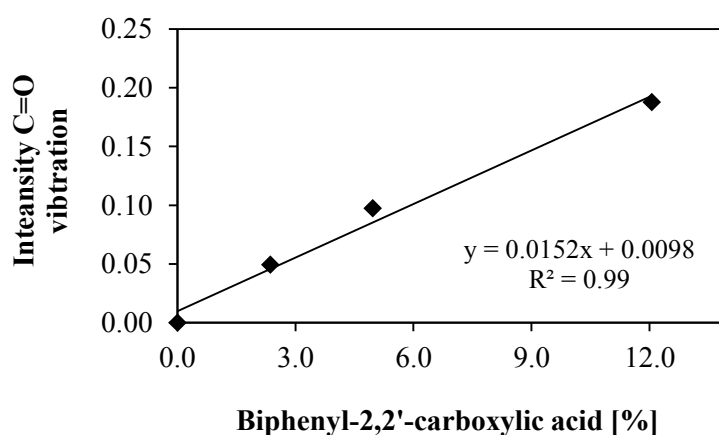


Figure C.1. Calibration curve to estimate purity of biphenyl-2,2'-dicarboxylates

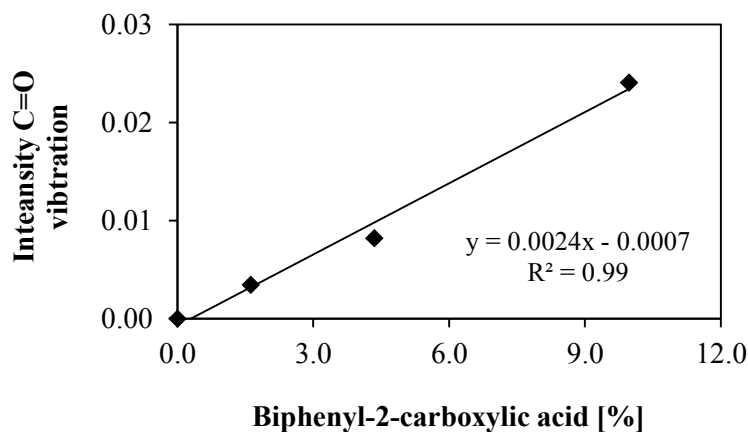


Figure C.2. Calibration curve to estimate purity of biphenyl-2-carboxylates

The presence of residual inorganic matter was explored using scanning electron microscopy. SEM micrographs confirmed that in all cases, except in the one of the copper (II) biphenyl-2-carboxylate, homogeneous materials were obtained. Processing of the backscattered electron image obtained for the copper biphenyl-2-carboxylate (Figure C.8) suggested that this compound was contaminated with 10 wt% of copper hydroxide. The corresponding image was converted to 8-bit TIFF and binarized employing a user-selected threshold. The number of positive and negative pixels was counted and proportions were calculated using the total amount of pixels in the original micrograph.

Residual organic solvent (when present) was estimated by TGA-FTIR. With exception of the copper (II) biphenyl-2-carboxylate, solvents were released in combination with water. However, the experimental set-up did not allow to distinguish how much of the mass loss was due to the release of solvent or water. For calculation purposes, the amount of residual solvent was taken as the total mass loss observed in the thermal event where the solvent was released (this would result in the most conservative scenario).

Note that calculations were performed in a free water basis because there was uncertainty regarding its origin, i.e. it could not be determined how much of the water detected corresponded to crystal water, water from reaction, water from the environment.

C.2. Scanning Electron Microscopy Analysis of Biphenyl Transition Metal Carboxylates

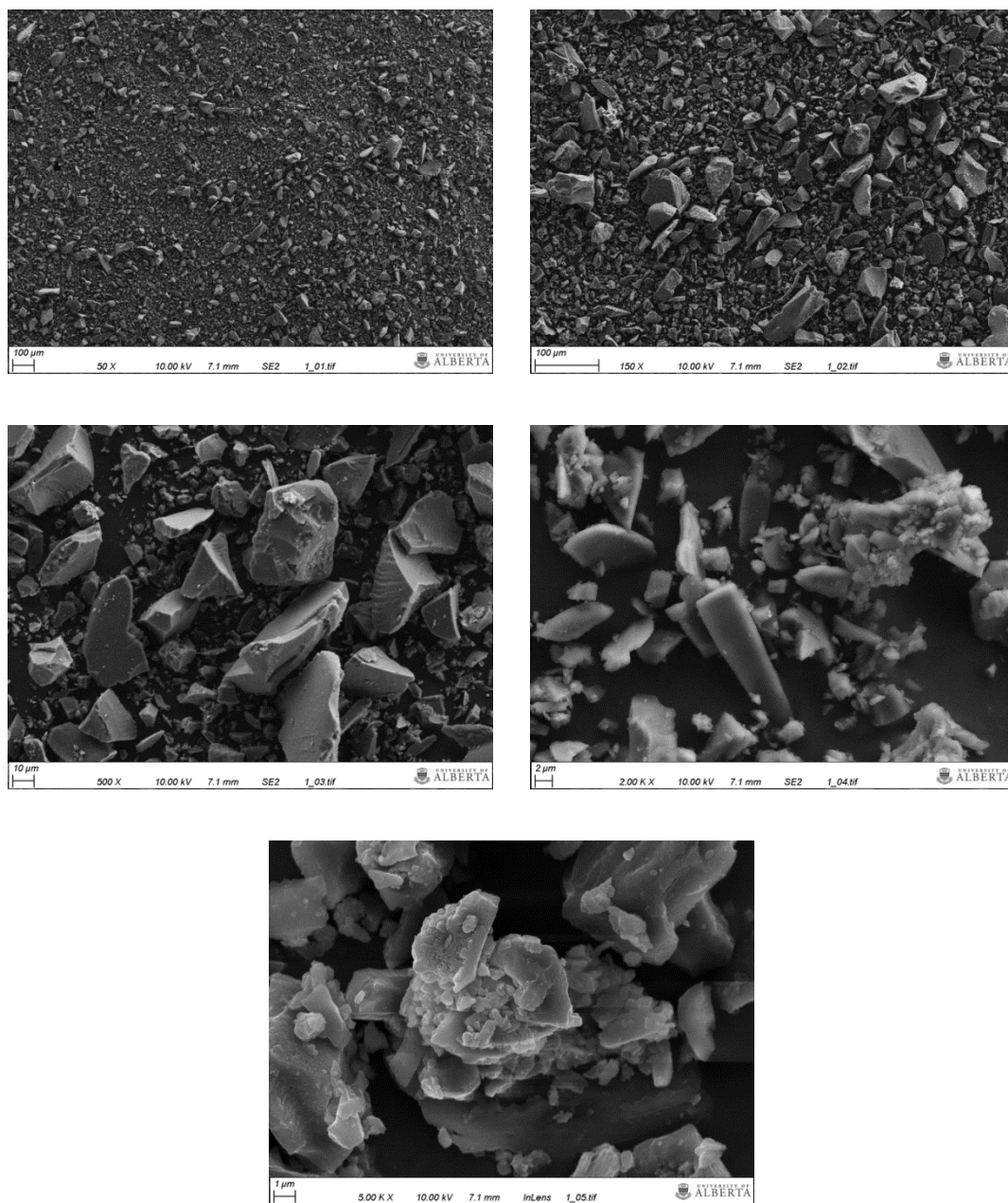


Figure C.3. SEM micrograph of iron biphenyl-2,2'-dicarboxylate

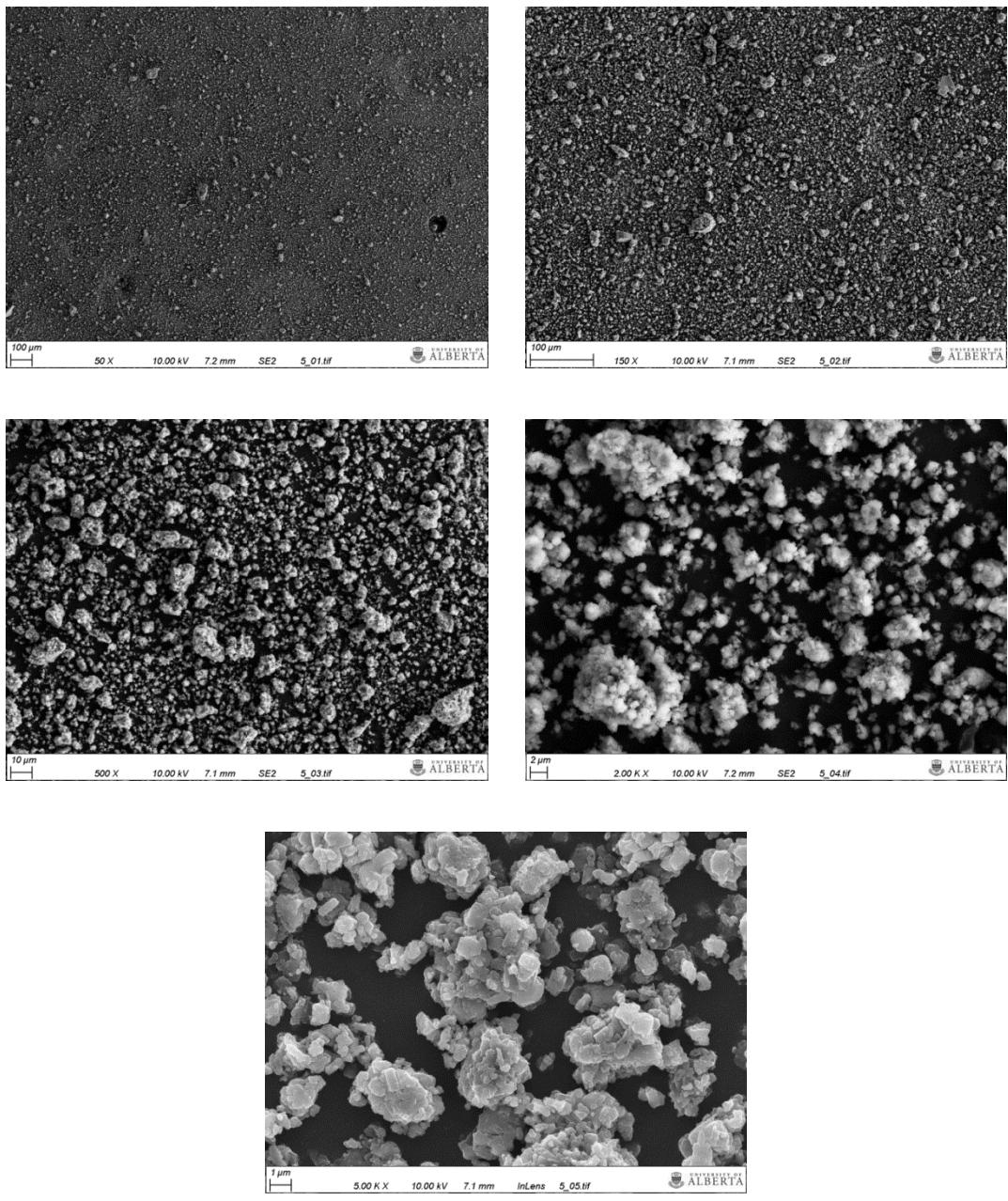


Figure C.4. SEM micrograph of copper biphenyl-2,2'-dicarboxylate

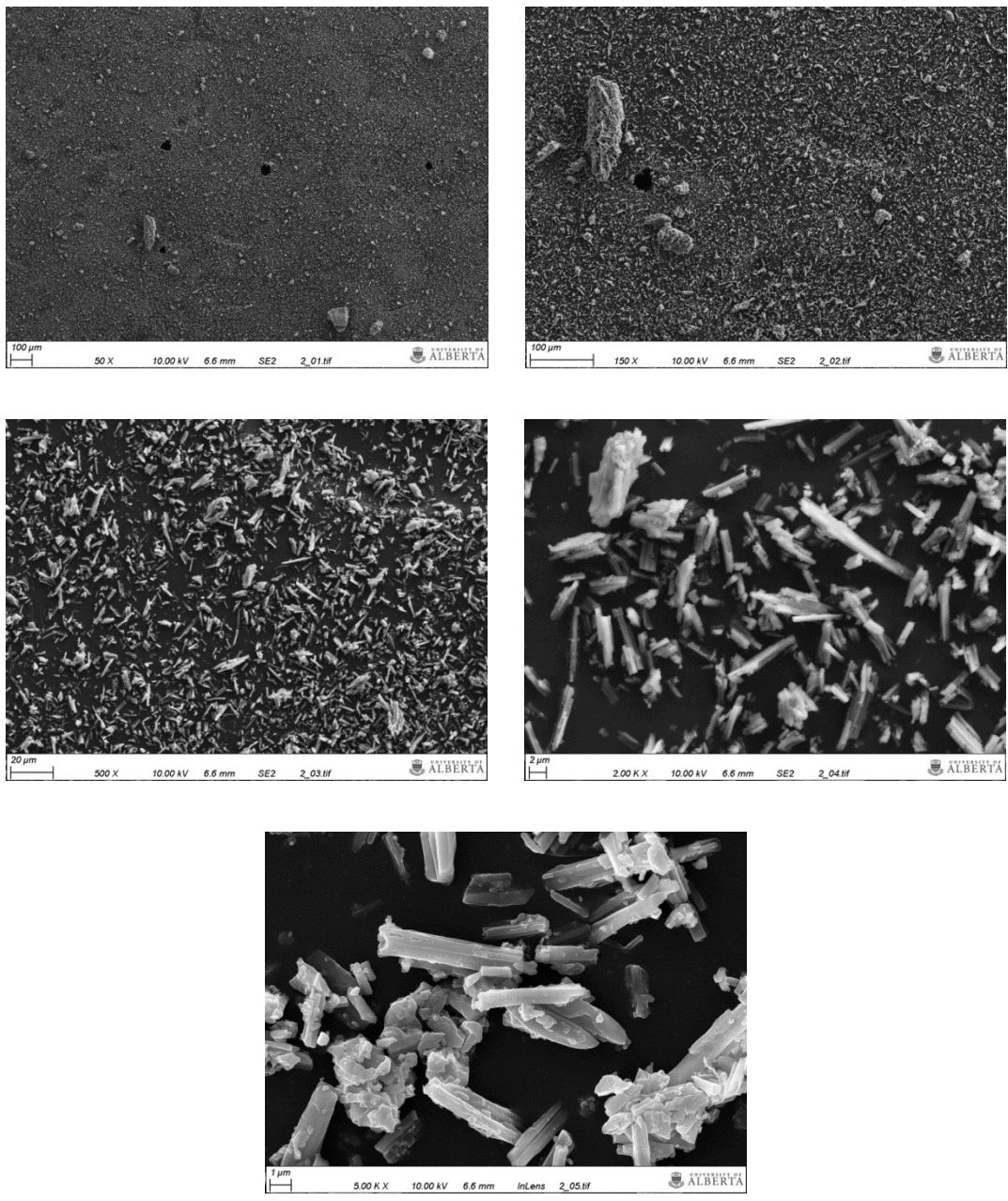


Figure C.5. SEM micrograph of cobalt biphenyl-2,2'-dicarboxylate

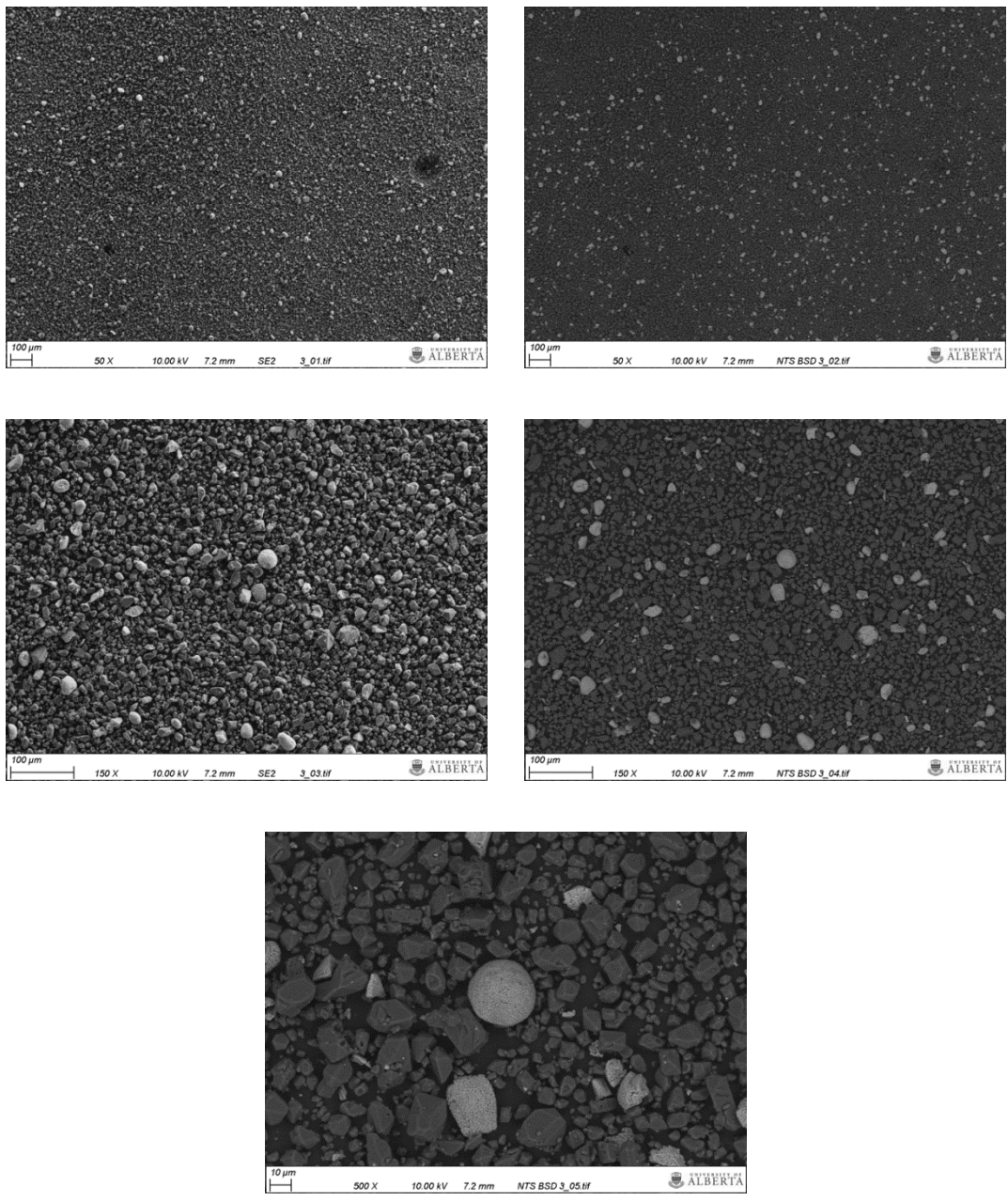


Figure C.6. SEM micrograph of copper biphenyl-2-carboxylate

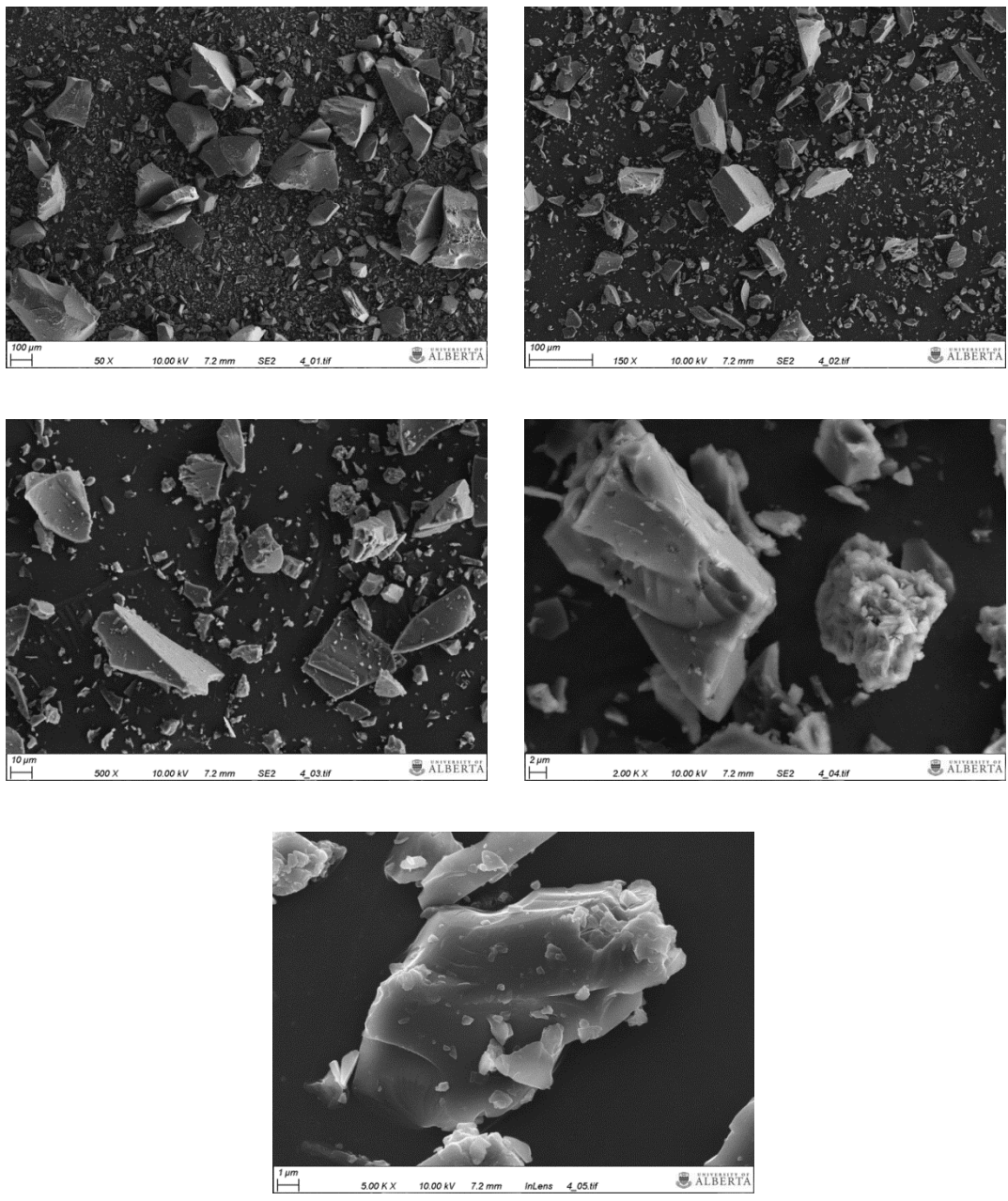


Figure C.7. SEM micrograph of cobalt biphenyl-2-carboxylate

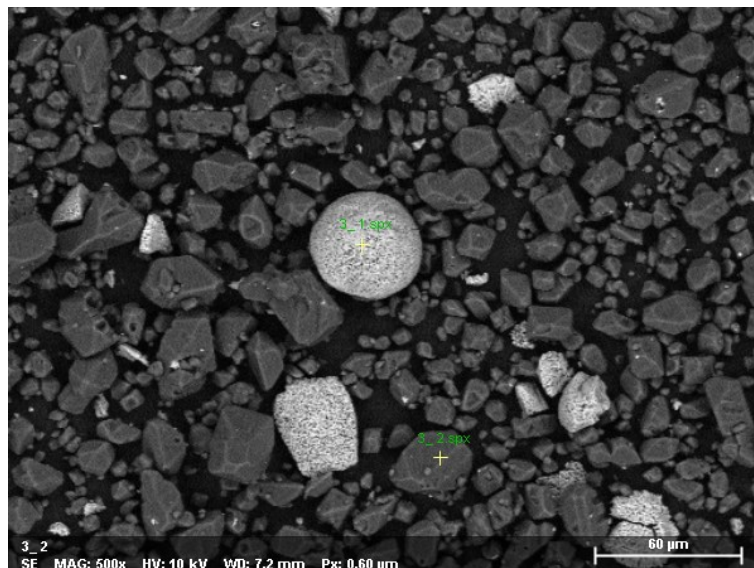


Figure C.8. Backscattered electron micrograph of copper biphenyl-2-carboxylate with points of microanalysis indicated (3_1: Copper hydroxide, 3_2: Copper biphenyl-2-carboxylate)

C.3. Elemental Analysis - Sample Calculation

Elemental analysis of the metal biphenyl carboxylates was performed using a Carlo Erba Model EA1108 Elemental Analyzer for CHNS and Oxygen (Triad Scientific, Inc., Manasquan, NJ, USA). Measurements were performed in duplicate and each sample was analyzed two times. Experimental results were adjusted to account for impurities as well as for the lattice water and/or solvent present in the carboxylates structure. Copper biphenyl-2-carboxylate will be used as example to illustrate the calculations performed to adjust the elemental composition of the synthesized metal carboxylates. Calculations steps are as follow:

1. Average composition from elemental analysis results was calculated.

Table C.2. Results from elemental analysis of the copper biphenyl-2-carboxylate

Sample	Measurement	Elemental composition, [%]			
		C	H	O	Metal ^a
Copper	1	60.68	4.03	17.33	17.96
		60.37	4.02	17.30	18.30
biphenyl-2-carboxylate	2	61.11	4.04	16.86	18.00
		60.76	4.03	17.07	18.14
	Average	60.73	4.03	17.14	18.10

^a Metal content was determined by difference

2. The amount of C, H, O and metal (if applicable) associated to impurities, lattice water and/or solvent present in the carboxylate structure were calculated and subtracted from the average composition found in step 1. Then, values were normalized to total 100%.

Table C.3. Elemental composition (adjusted) of the copper biphenyl-2-carboxylate

Compound	Amount [g]	Elemental composition, [%]			
		C	H	O	Metal
Copper biphenyl-2-carboxylate	100.0	60.7	4.0	17.1	18.1
Biphenyl-2-carboxylic acid	1.2	1.2	0.1	0.2	0.0
Copper hydroxide	10.0	0.0	0.2	3.3	6.5
Ethanol	3.5	0.0	0.5	1.2	0.0
Copper biphenyl-2-carboxylate (without impurities and solvent)	-	59.5	3.3	12.4	11.6
				Total	86.8
Copper biphenyl-2-carboxylate (normalized composition)	-	68.6	3.8	14.3	13.3
				Total	100.0

Note. FTIR and SEM-EDS analyses indicated that copper biphenyl-2-carboxylate was contaminated with 10 wt% of copper hydroxide and 1.2 wt% of biphenyl-2-carboxylic acid. On the other hand, TGA-FTIR analysis showed that 3.5% of the mass of carboxylate corresponded to ethanol present in the carboxylate structure. Note that ethanol was used as solvent in the synthesis process.

C.4. X-ray diffraction (XRD) analysis for the residues of decomposition in air atmosphere of the biphenyl transition metal carboxylates

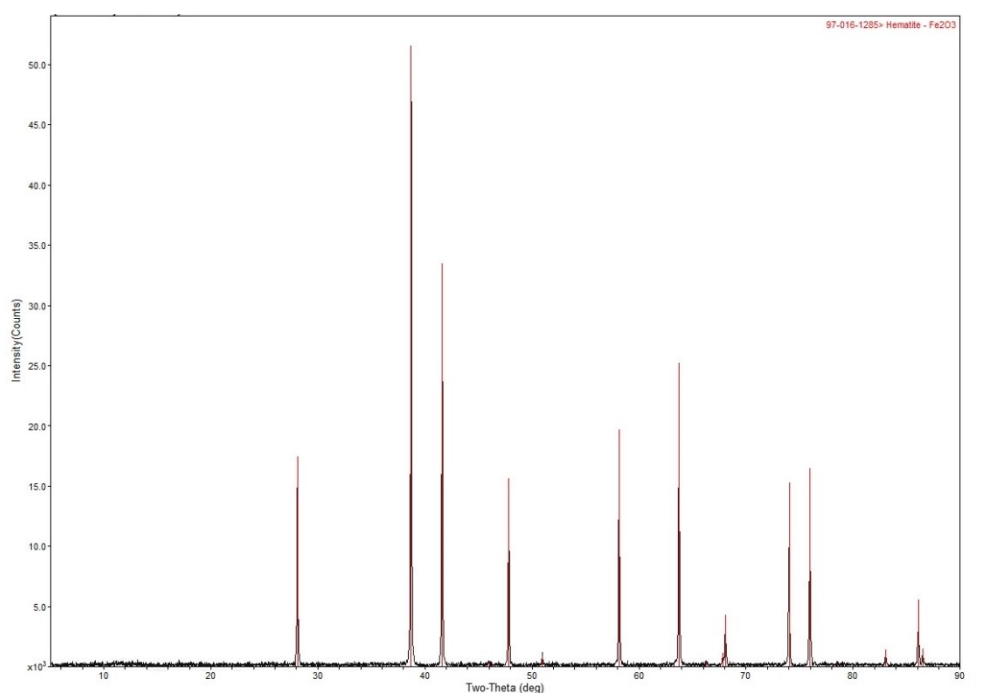
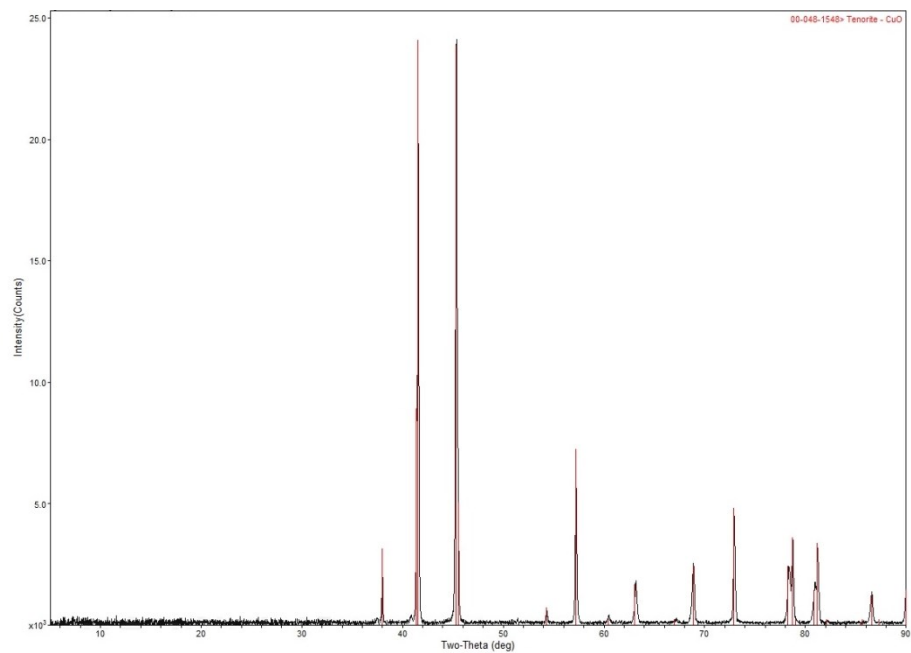
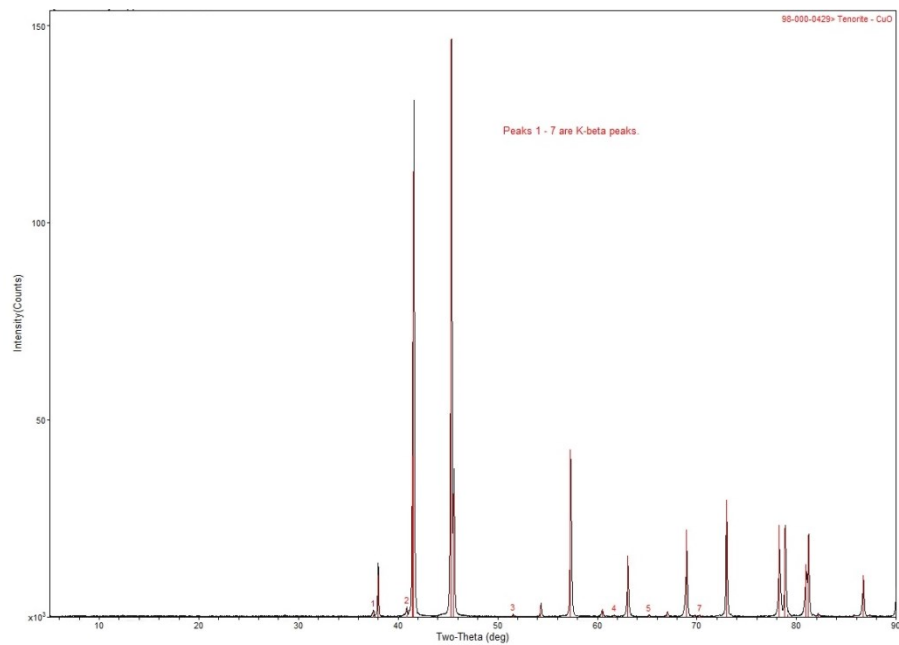


Figure C.9. XRD pattern of the residue of decomposition of the iron biphenyl-2,2'-dicarboxylate after heating in air atmosphere to 900 °C for 2 hours

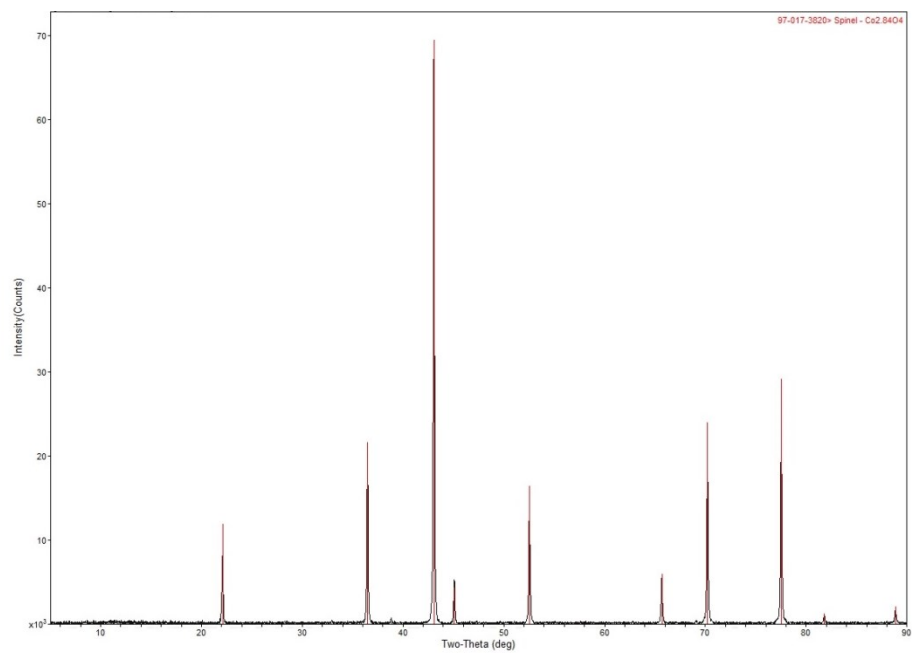


(a)

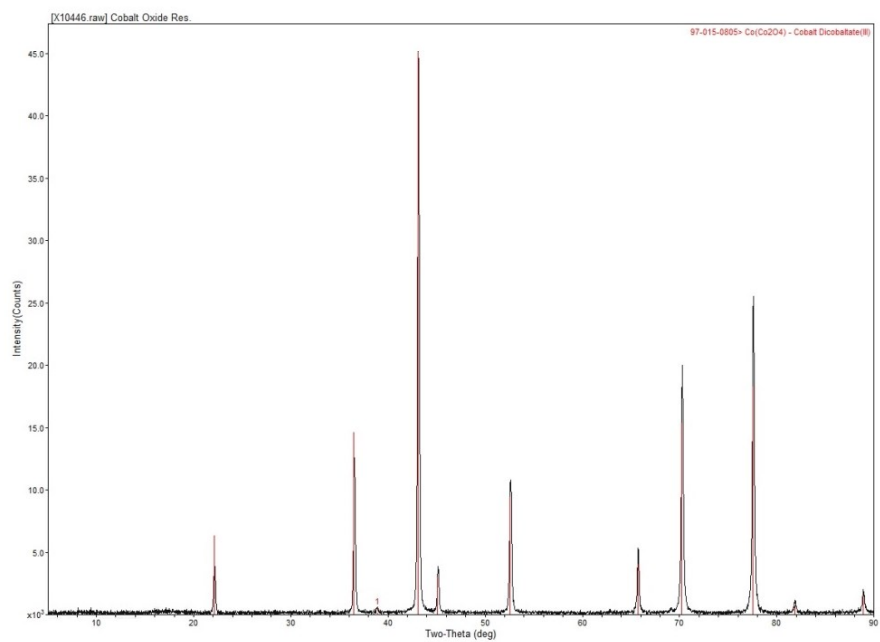


(b)

Figure C.10. XRD pattern of (a) the residue of decomposition of the copper biphenyl-2,2'-dicarboxylate after heating in air atmosphere to 900 °C for 2 hours (b) copper (II) oxide



(a)



(b)

Figure C.11. XRD pattern of (a) the residue of decomposition of the cobalt biphenyl-2,2'-dicarboxylate after heating in air atmosphere to 900 °C for 2 hours (b) Cobalt (II,III) oxide

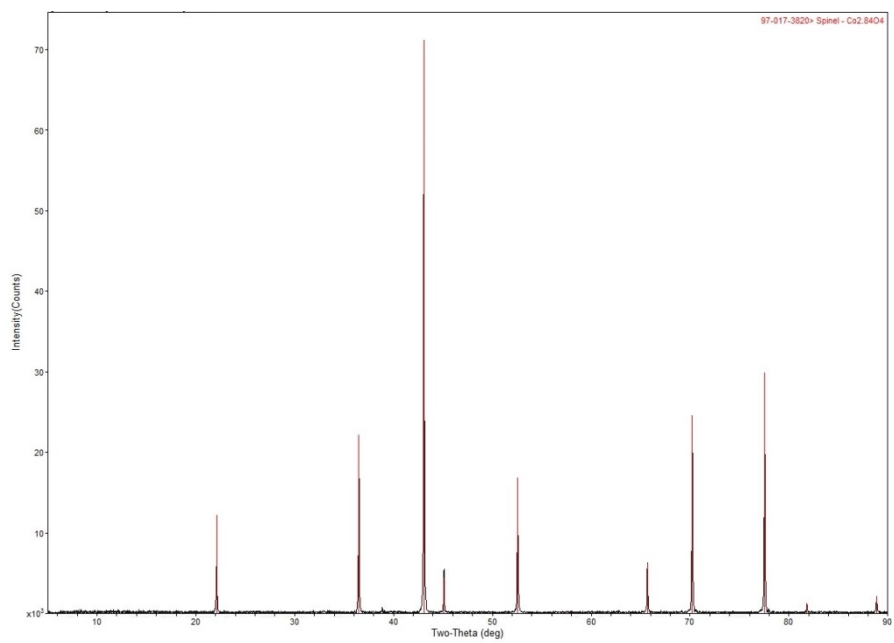


Figure C.12. XRD pattern of the residue of decomposition of the cobalt biphenyl-2-carboxylate after heating in air atmosphere to 900 °C for 2 hours

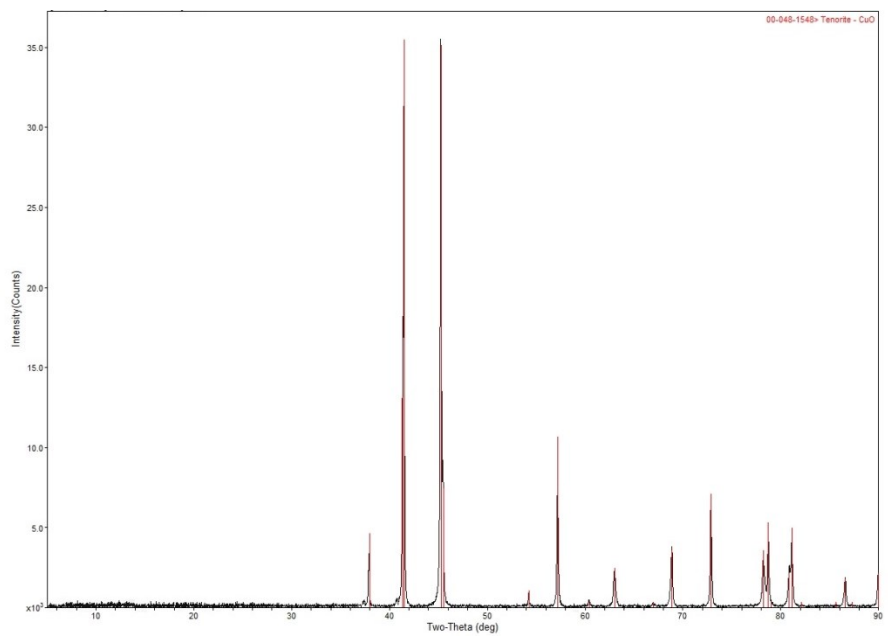


Figure C.13. XRD pattern of the residue of decomposition of the copper biphenyl-2-carboxylate after heating in air atmosphere to 900 °C for 2 hours

C.5. Infrared analysis of the gases evolved during thermal analysis of the synthesized metal carboxylates

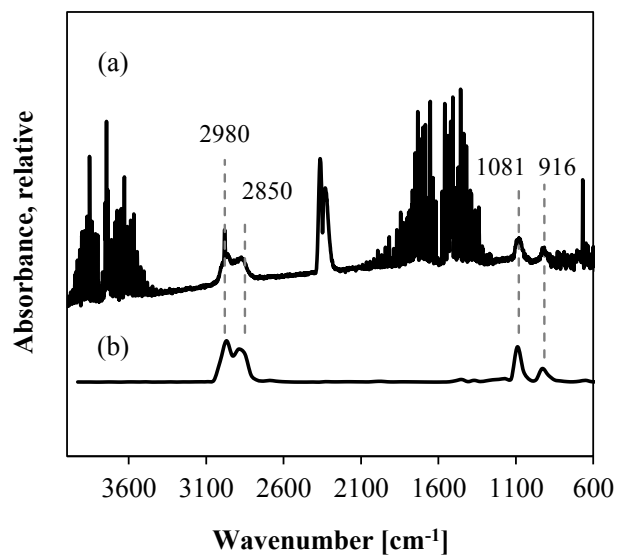


Figure C.14. Infrared spectra of (a) gases evolved during heating of the iron biphenyl-2,2'-dicarboxylate to 205 °C, and (b) gas phase tetrahydrofuran

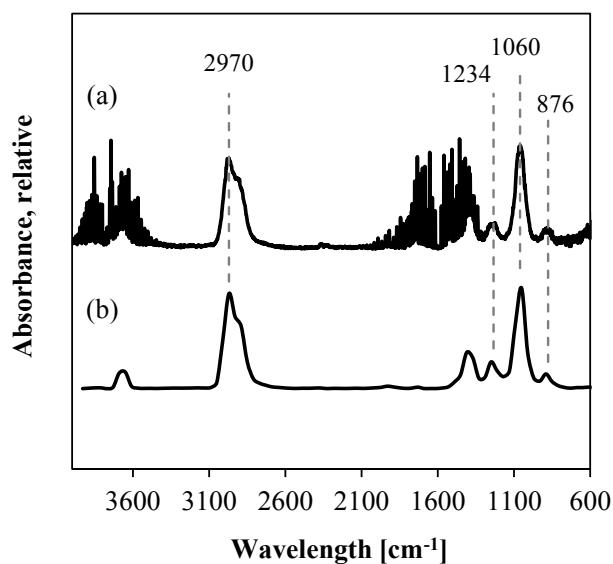


Figure C.15. Infrared spectra of (a) the gases evolved during heating of the copper (II) biphenyl-2,2'-dicarboxylate at 186 °C, and (b) gas phase ethanol

C.6. DSC-microscopy of cobalt biphenyl-2-carboxylate

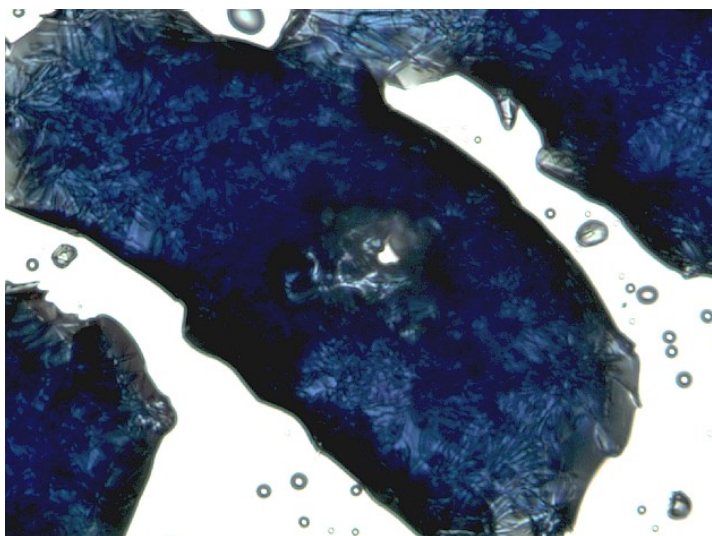


Figure C.16. DSC-microscopy of cobalt biphenyl-2-carboxylate to show transition *iii* after

Note: Picture was gamma-corrected to improve contrast